GPVI receptor spatial organisation and signalling in platelets

by

CHIARA PALLINI

A thesis submitted to the University of Birmingham

for the degree of DOCTOR OF PHILOSOPHY

Institute of Cardiovascular Sciences

College of Medical and Dental Sciences

University of Birmingham

September 2019

Abstract

Platelets are crucial players in many (patho)physiological processes including haemostasis, thrombosis and inflammation. The immunoreceptor tyrosine-based activation motif (ITAM)-containing receptor glycoprotein VI (GPVI) is the major platelet signalling receptor for collagen, which is exposed upon vascular injury. Once bound to collagen, multiple GPVI dimers cluster at the platelet surface increasing the avidity for collagen and regulating the signalling. In suspension, GPVI is cleaved by the metalloproteinases ADAM10/17 upon collagen activation. This thesis aimed to elucidate the signalling dynamics underlying GPVI clustering in platelets spread on collagen. Super-resolution microscopy and two-layer cluster analysis revealed that immobilised collagen induces long-term GPVI clustering and signalling in tandem with minimal shedding and low levels of GPVI/ADAM10 colocalisation. Conversely, GPVI is massively shed and the signalling rapidly downregulated in platelet suspensions stimulated with collagen. Syk, but not Src, kinase-dependent signalling is required to maintain clustering of the collagen integrin receptor α2β1, whilst neither is required for GPVI. This thesis proposes that GPVI clustering on immobilised collagen protects GPVI from shedding, thereby enabling longer-lasting Src and Syk-dependent signalling, integrin α2β1 activation and stable adhesion to collagen. Nanobodies targeting human GPVI have potential uses in many different biological applications from anti-platelet approaches to super-resolution imaging.

List of published papers

POULTER, N. S., KHAN, A. O., **PALLINI, C.** & THOMAS, S. G. 2018. Single-Molecule Localization and Structured Illumination Microscopy of Platelet Proteins. *Methods Mol Biol,* 1812**,** 33-54.

PIKE, J. A., KHAN, A. O., **PALLINI, C.**, THOMAS, S. G., MUND, M., RIES, J., POULTER, N. S. & STYLES, I. B. 2019. Topological data analysis quantifies biological nano-structure from single molecule localization microscopy. *Bioinformatics*.

ONSELAER, M. B., NAGY, M., **PALLINI, C.**, PIKE, J. A., PERRELLA, G., QUINTANILLA, L. G., EBLE, J. A., POULTER, N. S., HEEMSKERK, J. W. M. & WATSON, S. P. 2019. Comparison of the GPVI inhibitors losartan and honokiol. *Platelets***,** 1-11.

DUNSTER, J. L., UNSWORTH, A. J., BYE, A. P., HAINING, E. J., SOWA, M. A., DI, Y., SAGE, T., **PALLINI, C.**, PIKE, J. A., HARDY, A., NIESWANDT, B., GARCIA, A., WATSON, S. P., POULTER, N. S., GIBBINS, J. M. & POLLITT, A. Y. 2019. Interspecies differences in protein expression do not impact the spatiotemporal regulation of glycoprotein VI mediated activation. *J Thromb and Haemost.*

PALLINI, C., PIKE, J. A., O'SHEA, C., PROBERT, M., GARDINER, E. E., ANDREWS, R. K., WATSON, S. P. & POULTER, N. S. 2019. Immobilised collagen prevents shedding and induces sustained GPVI clustering and signalling in platelets. (Manuscript in preparation)

Acknowledgements

First, and most of all, I would like to express my infinite gratitude to my supervisor Natalie Poulter for believing in me and giving me the opportunity to do my PhD. Thank you for your immense patience, support and guidance throughout my PhD journey and for teaching me everything you know in Science. You have been a great scientific inspiration and a wonderful person to work with. I could not wish a better supervisor than you! A huge thanks go to my second supervisor Steve Watson for his continuous encouragements, unconditional help, positive attitude and innate scientific influence. Thank you also for giving me the chance to work an extra year in your lab and to attend many research conferences around the world. The success of the Birmingham Platelet Group is only thanks to you and as I always say I will never find another group like this worldwide. I would also like to thank the College for funding my 3-year PhD program and the COMPARE for financing the fourth year of my PhD. A particular acknowledgement goes to Jeremy for always being available for meetings and his precious technical help with the cluster analyses; Dee for managing the Imaging Suite and for fixing all the issues relating to *d*STORM and Sharmaine for being a good company outside the lab. A deserved thank to Christopher O'Shea for helping me with the calcium mobilisation analysis and his supervisor, Davor, for his friendship and for always losing the tan competitions. I would especially like to thank Mike Tomlinson for the interesting scientific discussions and all his lab members. In particular, Ally and Connie for always providing reagents and for the enjoyable chats. A fundamental thank to Elizabeth Gardiner for providing the anti-GPVI Fab without which I would not have been able to do most of the experiments. I have been extremely fortunate to be part of the Birmingham Platelet Group; so I would like to thank every single member past and present for making my PhD adventure easier and for gladdening my working days. Particularly, Gayle for being able to administrate a group of more than 30 people in a perfect way; the lab technicians Steph, Beata, Ying and Lourdes for taking care of the lab and for helping me every time with reagents, orders and experiments; Beata also for drawing the blood for me most of the times and Ying for being my 'partner in crime' in the initial nanobodies production; Yi and Ruben for providing data relating to the ELISA assay; Abs for being my 'pumbaa' and the friend you wish to have in your life; Chris for always helping me in the desperate moments and for disturbing me every time I was seriously concentrated on work; Annabel and Sam for being wonderful PhD colleagues; Pip for taking the blood samples for me and for his help with the aggregation

experiment and Amazon orders; Tom for choosing me as best friend in the lab; Malou for being a good deskmate; Zoltan for his genuine advices and for the hangover moments; Timo for being a sincere friend and for losing the six-pack challenge; Jun for generously sharing her time and scientific expertise and for her unique humor; Yotis and Alex for always being nice and supportive; Amanda, Gina and Ale for the fun lunch breaks; Alex S. for being a great and funny working partner and for helping me with the nanobodies generation and cloning during the last months of my PhD; Neil for his hilarious charm and for blood donations; MBO and Julie for the 'girlie moments'; Lizzie for drawing the blood and for calling me 'piccolina' all the time; Harlene for being my fashion mate; Pushpa for keeping me as a friend even after the end of the PhD and Zaher for the fitness advices and for being one of the best person I met in the life. This PhD also gave me away Giada who became one of my closest friend in a short time. My immense gratitude goes to you for brightening the first 2 years of my PhD, for being the perfect half of the 'dream team' and for our unforgettable moments which are impossible to list. I would do the PhD again only to meet you! A special thanks also go to Marco for being a pleasant distraction outside the lab, for his genuine disposition and for demonstrating that North and South of Italy can fuse in a wonderful friendship. This PhD would not have been achievable without the unconditional love, power and support of the most important people of my life, my mother, my father and my two brothers. Thank you for always believing in me and for all the sacrifices you have made for my happiness. All I am is thanks to you! Finally and most importantly a colossal thank you to Andrea for being at my side all the time, for never making me feel alone and for enlightening my dark days. I have no words to express my appreciation for what you have done for me…the dedication of this thesis is just a small gesture, but it comes from the deepest part of my heart!

“Sic itur ad astra”

Virgil (Aen. IX, 641)

Table of contents

CHAPTER 1

CHAPTER 3

CHAPTER 5

CHAPTER 6

List of figures

CHAPTER 1

CHAPTER 2

CHAPTER 3

CHAPTER 4

CHAPTER 5

CHAPTER 6

List of tables

CHAPTER 1

CHAPTER 2

Abbreviations

ADAM	A disintegrin and metalloproteinase
ADP	Adenosine diphosphate
BSA	Bovine serum albumin
CaM	Calmodulin
CBD	Collagen-binding domain
CDR	Complementarity-determining region
CLEC-2	C-type lectin-like receptor 2
CRP-XL	Cross-linked collagen-related peptide
CVX	Convulxin
DBSCAN	Density-Based Spatial Clustering of Applications with Noise
DIC	Differential interference contrast
*d*STORM	*Direct* STochastic Optical Reconstruction Microscopy
ECM	Extracellular matrix
FcR	Fc receptor
FOV	Field of view
FPLC	Fast protein liquid chromatography
GEF	Guanine nucleotide exchange factor
GP	Glycoprotein
GPCR	G protein-coupled receptor
Ig	Immunoglobulin
iPS	Induced pluripotent stem
ITAM	Immunoreceptor tyrosine-based activation motif
kDa	Kilodalton
LAT	Linker of activated T cells
LBD	Ligand-binding domain
MFI	Mean fluorescence intensity
MK	Megakaryocytes
MMP	Matrix metalloproteinase
MT	Microtubule
Nb	Nanobody
NEM	N-ethylmaleimide

PALM	PhotoActivated Localization Microscopy
PAR	Protease-activated receptor
PGI_2	Prostaglandin I_2
PI3K	Phosphatidylinositol 3-kinase
PK	Protein kinase
PLC	Phospholipase C
PM	Plasma membrane
PRD	Proline-rich domain
PRP	Platelet-rich plasma
PS	Phosphatidylserine
PTK	Protein tyrosine kinase
ROI	Region of interest
RT	Room temperature
SDS-PAGE	Sodium dodecyl sulfate-polyacrylamide gel electrophoresis
SEM	Standard error of the mean
SFK	Src family kinase
SH2 and 3	Src homology 2 and 3 domains
SIM	Structured Illumination Microscopy
SLP-76	SH2 domain-containing leukocyte phosphoprotein of 76 kDa
SMLM	Single Molecule Localisation Microscopy
SPR	Surface plasma resonance
Syk	Spleen tyrosine kinase
TCR	T cell receptor
TIRF	Total Internal Reflection Fluorescence
TPO	Thrombopoietin
TULA-2	T-cell ubiquitin ligand-2
TxA_2	Thromboxane A_2
VHH	Variable region of the heavy chain of ‘heavy-chain only’ antibody
vWF	Von Willebrand factor
WCL	Whole cell lysate

CHAPTER 1

General Introduction

1.1 Platelets

Platelets are abundant, small anucleate blood cells which are widely known for playing a pivotal role in haemostasis and thrombosis. Under physiological conditions, platelets remain in a quiescent, or resting, state within the circulatory system and are unable to interact with other cells, for example endothelial cells or other platelets. Platelets become activated at sites of endothelial lesions to rapidly form a platelet plug, thereby maintaining vascular integrity and restoring the blood flow. However, more recently it has been demonstrated that activated platelets also participate in the onset of other physiological or pathological states including atherosclerosis (Nording et al., 2015), inflammation (Ho-Tin-Noe et al., 2018), infection (Hottz et al., 2018) and cancer (Schlesinger, 2018) as well as vascular development (Bertozzi et al., 2010), angiogenesis (Walsh et al., 2015) and wound repair (Nurden et al., 2008).

Low platelet count leads to the generation of a condition known as thrombocytopenia which can be inherited or acquired as a consequence of a multisystem disorder. The thrombocytopenic state can result in severe, life-threatening bleeding which is usually resolved with the improvement of the primary pathological condition or via transfusions (Thachil and Warkentin, 2017).

Therefore, due to their wide repertoire of (patho)physiological roles, platelets represent an important topic of study for the development of different therapeutic approaches. The aim of antiplatelet therapies is to preserve the normal haemostasis while specifically targeting platelet mediators involved in the onset of different diseases. This Chapter will describe the main aspects of platelet biology with a particular focus on the regulatory mechanisms involved in platelet activation.

1.2 Platelet physiology

1.2.1 Platelet biogenesis

Platelets are derived from the cytoplasmic fragmentation of megakaryocytes (MKs) in the bone marrow (Machlus et al., 2014). Due to the ability of MKs to migrate, platelet formation has also been observed in the lung and peripheral blood. However, the function of this extramedullary platelet production remains unclear and controversial (Borges et al., 2017, Lefrancais et al., 2017). MKs are highly specialized precursor cells which descend from haematopoietic stem cells (HSCs) and undergo different phases of development to produce fully matured MKs (Woolthuis and Park, 2016). During the early stage of MK development, the pluripotent stem cells become committed to the myeloid lineage by differentiating into a common myeloid progenitor (CMP). The MK differentiation continues through the generation of different precursor cells, including burst-forming unit (BFU) and colony-forming unit (CFU)-MKs, which become increasingly committed to the MK lineage (Briddell et al., 1989). The terminal differentiation is characterised by the formation of immature MKs (promegakaryocytes) which undergo a process of endomitosis to evolve into mature polyploid MKs (Machlus et al., 2014). During the last stage, the MK cytoplasm reorganises into thin, branching processes, known as proplatelets, extending into the vessel lumen (Patel et al., 2005a). The cytoskeletal network represents the primary motor of proplatelet formation. In particular, continuous microtubule polymerisation and sliding highly contribute to proplatelet enlargement and elongation, respectively (Patel et al., 2005b). The platelet release is finally triggered by the high shear forces present in the circulatory system which shed the proplatelet ends (preplatelets) (Thon et al., 2010). The large preplatelets further divide within the circulation to ensure an average platelet count of 150-400 $\times 10^9$/L in humans (600-1,200 $\times 10^9$/L in mice) (Daly, 2011) (Fig. 1.1).

This orchestrated process is regulated by diverse factors including cytokines, extracellular matrix (ECM) components and stiffness, blood circulation and topographical surface features (e.g. spatial arrangement and orientation) (Leiva et al., 2018). Undoubtedly, the major regulator of platelet production is the cytokine thrombopoietin (TPO), although some *in vitro* experiments have suggested that TPO is not fundamental for proplatelet formation (Ito et al., 1996). TPO binds to its receptor c-Mpl on MKs and activates the JAK-STAT signalling cascade which ultimately regulates the gene expression necessary to induce MK differentiation and maturation and maintain the platelet pool at a constant level (Deutsch and Tomer, 2006). The life-span of circulating platelets is ~7-10 days in humans (~3-5 days in mice) before undergoing clearance into the reticuloendothelial system of spleen and liver. This limited life-span is strictly controlled by members of the Bcl-2 protein family which, through the regulation of the apoptotic cascade, act as a "molecular clock" to maintain a balanced rate of platelet genesis and clearance (McArthur et al., 2018).

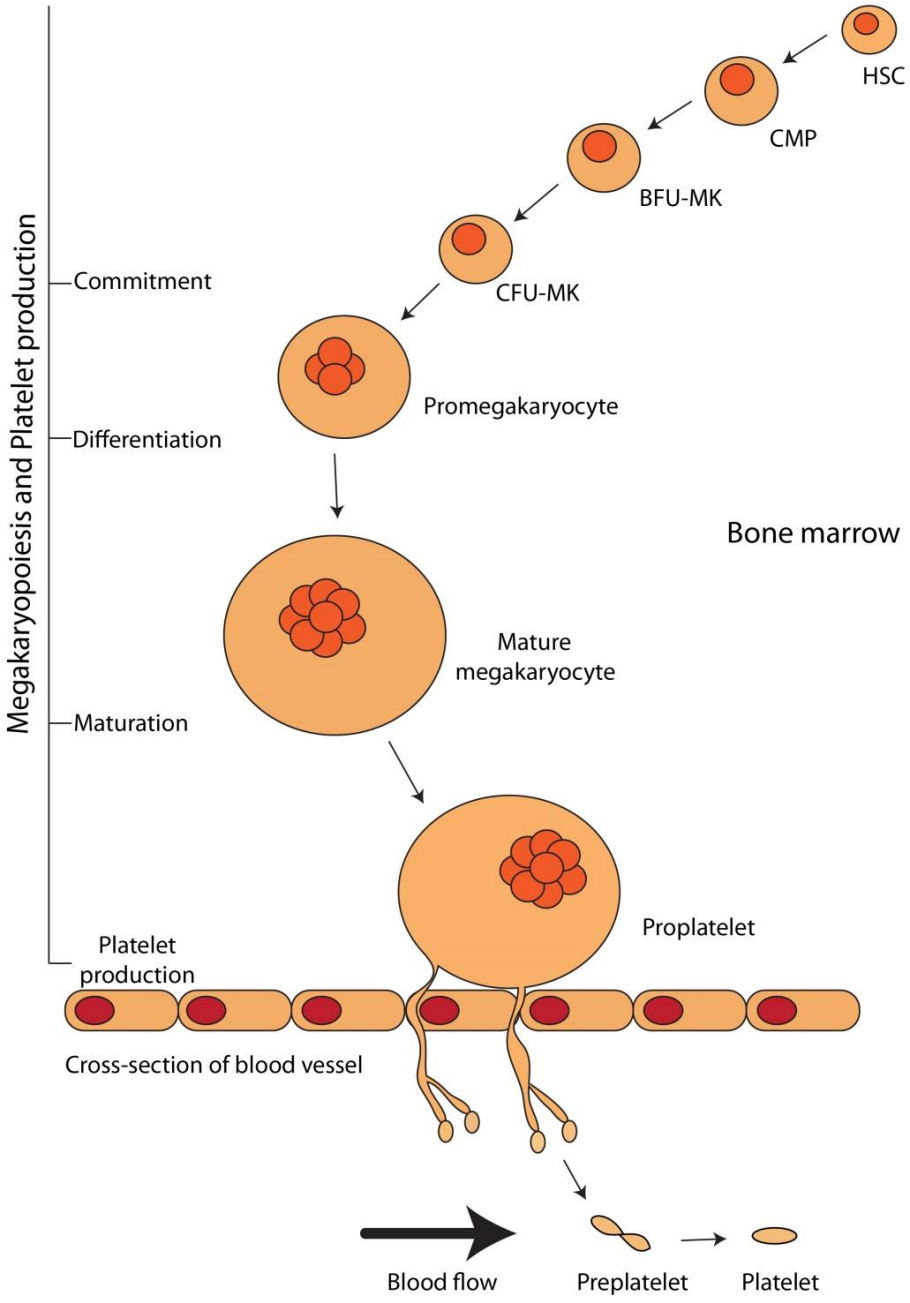

Figure 1.1. Different stages of platelet production from megakaryocytes. The megakaryocyte (MK) development in the bone marrow initiates with the commitment of haematopoietic stem cells (HSCs) to the myeloid lineage through the differentiation into a common myeloid progenitor (CMP) which in turn develops into different precursor cells such burst-forming unit (BFU) and colony-forming unit (CFU)-MKs. The MK differentiation culminates in the formation of immature cells (promegakaryocytes) which, via endomitosis, develop into mature polyploid MKs and extend pseudopodial protrusions (proplatelets) into the vessel lumen. The platelet shedding from proplatelet ends (preplatelets) is induced by blood shear stress. The preplatelets undergo further cellular division within the circulatory system to produce mature platelets.

1.2.2 Platelet structure

Despite the indubitable variability between different individuals, the platelet anatomy is characterised by numerous features which are well-conserved. Human platelets measure only 2-3 μm (mouse platelets only 0.5 μm) in diameter and exhibit a biconvex discoid shape in a resting state (Schmitt et al., 2001). Because platelets are cell fragments derived from MKs, they lack a nucleus but the entire set of organelles including mitochondria, endoplasmic reticulum, Golgi apparatus and lysosomes, is present (Hartwig, 2006). The platelet plasma membrane (PM) is characterised by numerous invaginations extending into the cytoplasm and forming the so-termed open canalicular system (OCS) (Behnke, 1967). The OCS functions as a duct for the granule release and supplements the PM with extra surface during platelet activation and spreading (Selvadurai and Hamilton, 2018). A dense tubular system (DTS) is also present in the membrane: it is the storage compartment of calcium (Ca^{2+}) (Brass, 1984) and the site of prostaglandin synthesis (Carey et al., 1982).

In addition, platelets have a prominent actin and microtubule (MT) cytoskeleton as well as a spectrin membrane skeleton. The actin cytoskeleton, consisting of dynamic actin polymers (F-actin) cross-linked by actin-binding proteins such as filamin and α-actinin, provides structural support to circulating platelets exposed to high blood shear stress (Boyles et al., 1985, Hartwig and DeSisto, 1991). The tetrameric network of spectrin, in combination with different binding proteins, anchors the actin cytoskeleton to the PM and integrins, forming a continuous framework to mechanically stabilise flowing platelets (Boyles et al., 1985, Hartwig and DeSisto, 1991). The disruption of the spectrin organisation results in the destabilisation of the membrane system as well as impairment of proplatelet formation and architecture (Patel-Hett et al., 2011). The primary function of the MT cytoskeleton, consisting of polymers of αβ tubulin, is to maintain the discoid conformation of quiescent platelets by

forming a rigid bundle beneath the PM surrounding the platelet perimeter (Patel-Hett et al., 2008, White and Rao, 1998). Platelet activation leads to the dismantling of the MT coil and extensive reorganisation of the actin cytoskeleton to allow the shape change during platelet spreading (Paknikar et al., 2019).

1.2.3 Platelet granules

Platelets contain three different types of secretory granules: alpha (α)-granules, dense (δ)-granules and lysosomes.

Being the largest (200-500 nm in diameter) and most abundant (40-80 per platelet) secretory vesicles, α-granules represent the repository of a variety of surface receptors and soluble proteins with different functions including integral membrane and adhesion proteins, coagulant and anticoagulant factors, chemokines and growth factors (Flaumenhaft and Sharda, 2019). Platelet activation triggers the discharge of the α-granule soluble contents, including fibrinogen, thrombospondin and von Willebrand factor (vWF) as well as the exposure of surface proteins, most importantly P-selectin (marker of platelet activation), to mediate platelet adhesion. α-granules also contain other membrane-associated proteins such as integrins, glycoprotein (GP)Ib-IX-V, GPVI and tetraspanin superfamily members which, contrarily to P-selectin, are constitutively located at the cell surface.

Fewer in number (4-8 per platelet) and smaller (150 nm in diameter), δ granules are so-called because of their electron-dense core. Exclusively found in platelets, they are highly enriched with divalent cations and phosphates as well as bioactive amines (serotonin and histamine) and nucleotides such as the second messenger adenosine diphosphate (ADP). Release of δ-granule components acts as positive feedback for the recruitment of additional platelets and formation of the platelet clot (Flaumenhaft and Sharda, 2019).

Platelet lysosomes share common features with those present in other cell types: they store acid hydrolases which catalyse the proteolytic degradation of proteins, carbohydrates and lipids and require a stronger stimulation than α- and δ-granules to induce the secretion (Flaumenhaft and Sharda, 2019).

1.3 Platelets in haemostasis and thrombosis

1.3.1 Platelet activation and thrombus formation

As the principal physiological role of platelets is to prevent bleeding and safeguard normal haemostasis, they must be competent at recognising and blocking any vascular damage without occluding the blood flow. When a vascular injury occurs, platelets switch from a resting to an activated form to immediately build a stable platelet plug and seal the damaged vessel wall, thereby preventing excessive bleeding and restoring haemostasis. This activatory transition is mediated by the interaction between platelet receptors, signalling mediators and soluble agonists with components of the ECM exposed after vascular injury. The resulting activation of the signalling machinery triggers a series of changes in the platelet conformation, fundamental for their rapid adhesion to the vessel wall and to other platelets to minimise blood loss (Lee, 2019). The multistep process of thrombus formation is described below and schematised in Fig. 1.2.

Initiation phase. The formation of a stable plug initiates with platelet tethering and rolling when ECM components (Collagen type I and III) are exposed to the bloodstream at sites of vascular injury. Soluble vWF present in the plasma is unable to tether circulating platelets. However, when it is trapped by the collagen structure, vWF becomes highly responsive towards moving platelets (Cruz et al., 1995, Pareti et al., 1987). This is caused by the shear stress which stretches its conformation and induces the exposure of the A1 binding domain

for the receptor GPIbα expressed at the platelet surface (Miura et al., 2000, Morales et al., 2006). As a consequence, platelets are tethered to vWF/collagen complexes and start to form a monolayer at the site of vessel breach (Kanaji et al., 2012, Reininger, 2008).

Stable adhesion phase. In the second step, the weak interaction between platelets and collagen is reinforced by the binding of the major signalling collagen receptor expressed at the platelet surface, the GPVI-Fc receptor γ-chain complex (GPVI-FcR-γ) (Nieswandt and Watson, 2003). GPVI-collagen interplay results in a strong platelet activation which triggers the conformational change of integrins αIIbβ3 and α2β1 from low to high-affinity state, in a process called 'inside-out signalling'. These coordinated signalling events enable firm platelet adhesion (Lecut et al., 2004).

Spreading phase. The spreading phase is triggered when platelets become fully adhered to the subendothelial ECM complex. It is characterised by sequential remodelling of the actin and MT cytoskeleton. Studies using LifeAct-GFP mouse platelets (Calaminus et al., 2008, Poulter et al., 2015b) or silicon-rhodamine (SiR) labelled actin and tubulin probes (Paknikar et al., 2019) have enabled live-cell visualisation of the cytoskeletal dynamics within spreading platelets. This process involves the initial formation of actin nodules (Calaminus et al., 2008, Poulter et al., 2015b) followed by the formation of finger-like protrusions, called filopodia. In the later stage of platelet spreading, filopodia are replaced by lamellipodia which expand the platelet surface area and reinforce the interaction with the ECM. In fully-spread platelets, the actin cytoskeleton organises into stress fibre-like structures which help to maintain the characteristic shape of spread platelets (Bearer et al., 2002). Inhibition of actin polymerisation by cytochalasin D or latrunculin A has been shown to prevent platelet spreading (Casella et al., 1981, Qiu et al., 2014). In addition, platelet spreading leads to disassembly of the MT ring via the contraction of actomyosin structures mediated by non-muscle myosin II. It has been

demonstrated that the simultaneous inhibition of MT polymerisation by nocodazole and myosin II function by blebbistatin does not disintegrate the MT ring and consequently abrogates platelet spreading (Paknikar et al., 2019).

Secretion and aggregation phase. At the site of a thrombus, platelet activation and spreading trigger the secretory machinery to release the granule contents which act as secondary mediators through the engagement of G protein-coupled receptors (GPCRs) (Golebiewska and Poole, 2015). In particular, once secreted, ADP binds to its specific receptors P2Y1 and P2Y12 whereas thromboxane A_2 (TxA_2) engages the thromboxane receptor (TP) (Woulfe, 2005). In addition, vWF and fibrinogen are discharged from α-granules and can bind to integrin αIIbβ3 to enhance the positive signalling feedback and induce the recruitment of additional platelets to form an aggregate (Bennett, 2005).

Thrombus formation phase. The onset of thrombus formation is characterised by the activation of the coagulation cascade. Following prolonged stimulation and sustained Ca^{2+} influx, a sub-population of platelets (procoagulant platelets) undergo ballooning, expose phosphatidylserine (PS) at the surface and recruit coagulation factors (most importantly FXa and FVa) to proteolytically convert prothrombin into the active form (Agbani and Poole, 2017, Fager et al., 2010). Indeed, the major actor of this phase is thrombin which, through the interaction with protease-activated receptors (PARs)1 and 4 in human (PAR3 and 4 in mouse) (Ofosu, 2003), induces a vigorous platelet activation as well as catalyses the conversion of fibrinogen into insoluble fibrin polymers (Monroe and Hoffman, 2006). Fibrin binds to integrin αIIbβ3 (Podolnikova et al., 2014) and creates a film at the thrombus core to facilitate its growth and stabilisation. Recent evidence has also shown that GPVI plays a critical role in the clot development, through its interaction with fibrin, which has been discovered to be a novel ligand for GPVI receptors in human and mouse platelets (Alshehri et al., 2015a,

Induruwa et al., 2018, Mammadova-Bach et al., 2015, Onselaer et al., 2017). Finally, the formed clot undergoes contraction induced by non-muscle myosin II to prevent excessive thrombus formation and therefore vessel obstruction (Lam et al., 2011).

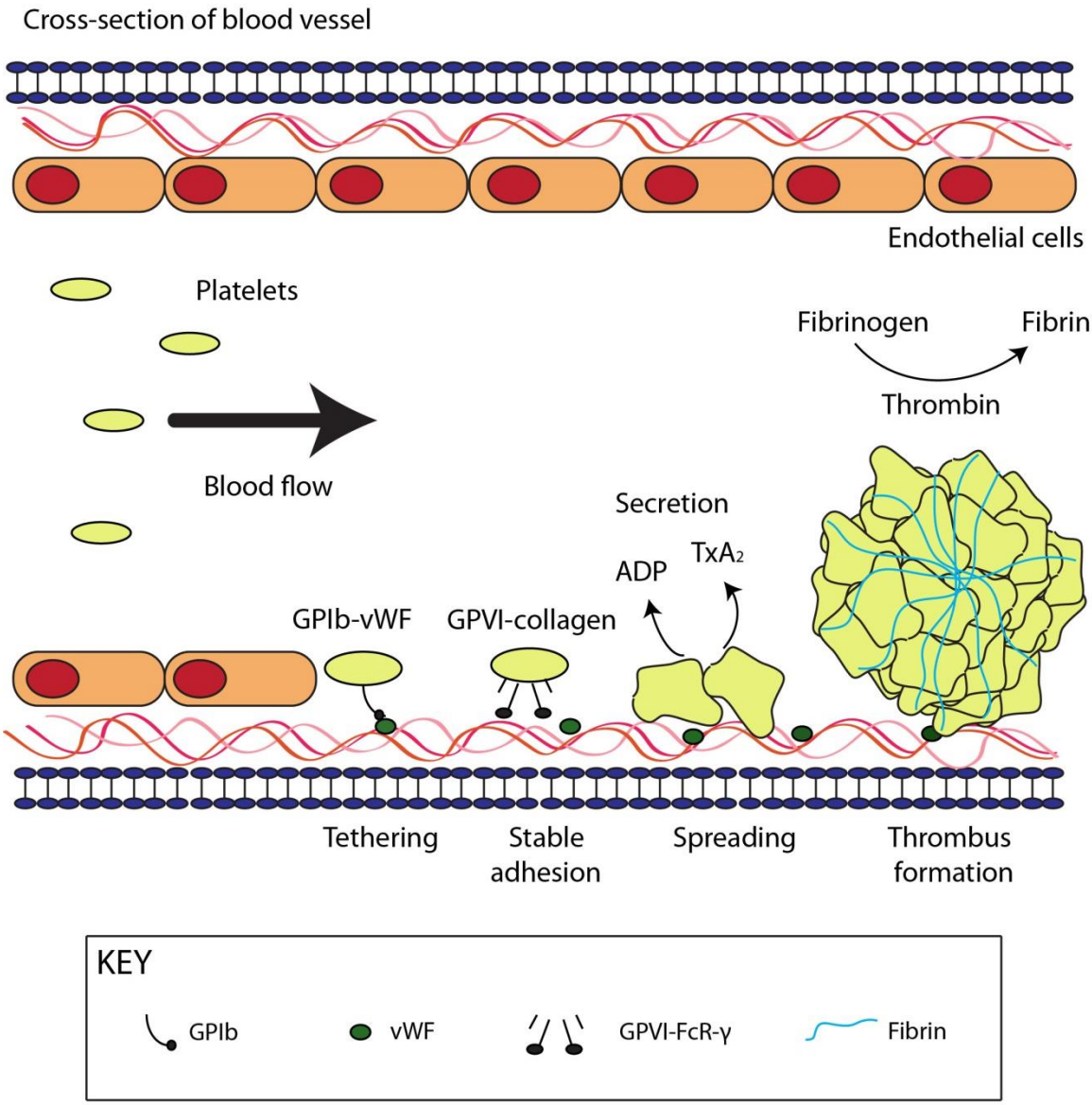

Figure 1.2. Main steps of platelet activation and thrombus formation. The process of platelet activation and thrombus formation at sites of vascular injury can be divided into five main steps: 1. Tethering and rolling induced by GPIb-vWF interaction; 2. Stable adhesion mediated by GPVI-collagen interplay followed by platelet activation and integrin 'inside-out' signalling; 3. Spreading which involves the cytoskeleton reorganisation to allow full adhesion of platelets to the ECM. 4. Secretion of granule contents such as ADP and TxA_2 which amplifies the activation and induces the recruitment of additional platelets to form a platelet aggregate. 5. Thrombus formation which is characterised by thrombin generation to reinforce platelet activation and convert fibrinogen to fibrin, thereby stabilising the platelet clot.

1.3.2 Platelet function in haemostasis, thrombosis and beyond

The initial anatomical and functional characterisation of platelets has been attributed to Giulio Bizzozero in 1882 (Bizzozero, 1882). In his elegant *in vivo* studies conducted via intravital microscopy in the mesentery of guinea pigs, Bizzozero discovered the presence of platelets with a disc-like structure in circulating blood and then demonstrated their primary role in haemostasis and experimental thrombosis. Although haemostasis and thrombosis are usually used to refer to the same mechanism, they are very different processes with heterogeneous consequences on human health. In classical haemostasis, formation of a platelet clot at sites of vessel damage aims to restore the blood flow. However, inappropriate platelet activation leads to life-threatening thrombi which are a major cause of different thrombotic conditions, including sepsis (Dewitte et al., 2017), atherosclerosis (Nording et al., 2015), heart attack (Chung and Lip, 2006) and stroke (Nieswandt et al., 2011). Indeed, at sites of vascular inflammatory lesions, such as atherosclerotic plaques, excessive thrombus formation leads to the blockage of the blood flow directly or through vessel embolism. The so-called 'atherothrombotic disease' can generate myocardial infarction and stroke which are the primary triggers of morbidity and mortality around the world (25% of worldwide deaths) (Kaplan and Jackson, 2011). Furthermore, recently a non-canonical role of platelets in maintaining vascular integrity at sites of inflamed vessels has emerged. This has been termed inflammatory haemostasis (Ho-Tin-Noe et al., 2018). The immune functions of platelets have also been characterised in the past few years: they are able to sense, phagocytize and kill pathogens (bacteria and viruses), directly eliminate them through the release of antimicrobial agents and recruit leukocytes at sites of infection enhancing the production of neutrophil extracellular traps (NETs) (Hottz et al., 2018). In addition, platelet-derived chemotactic factors facilitate wound healing and orchestrate tissue repair (Asai et al., 2016, Wichaiyo et

al., 2019). This is achieved through their ability to regulate the angiogenesis which also aids vascular development (Bénézech et al., 2014, Finney et al., 2012, Lowe et al., 2015a) as well as maintaining the blood/lymphatic vessel separation (Suzuki-Inoue et al., 2010). Conversely, platelet-induced angiogenesis has aberrant consequences in pathological conditions such as cancer (Janowska-Wieczorek et al., 2005), atherosclerosis (Burger and Wagner, 2003) and rheumatoid arthritis (Boilard et al., 2010). In particular, numerous studies have shown an important role of platelets in promoting cancer metastasis via the formation of a platelet monolayer which protects tumour cells from shear stress and the attack of immune cells. Subsequently, platelets release growth factors which help the metastatic dissemination of tumour cells to distant organs (Schlesinger, 2018). This diverse research has demonstrated that platelets are versatile cells. Therefore, understanding the signalling mechanisms involved in their activation will impact positively upon not only cardiovascular research but the entire medical field.

1.4 Platelet activation

As platelets circulate in the bloodstream in a resting state, in order to interact with their surroundings they must become 'activated'. This involves the engagement of numerous signalling and adhesive receptors which act at different stages of the platelet activation process. These signalling cascades all converge on a common pathway which leads to Ca^{2+} mobilisation from intracellular stores and platelet secretion. The large range of platelet activatory receptors can be divided into three main classes in accordance with their structures and functions: 1) protein tyrosine kinase (PTK)-linked receptors; 2) GPCRs and 3) immunoreceptor tyrosine-based activation motif (ITAM)-containing receptors (Clemetson and Clemetson, 2019).

1.4.1 PTK-linked receptors

This category includes the integrin superfamily and GPIb-IX-V complex whose function is fundamental for stable platelet adhesion and early activation. Platelets contain six different integrin heterodimers: α2β1, α5β1, α6β1, αLβ2, αIIbβ3 and α*v*β3 (Clemetson and Clemetson, 2019). However, only integrin α2β1 and αIIbβ3 will be discussed in this thesis for their relevance to platelet functions.

1.4.1.1 GPIb-IX-V

GPIb-IX-V complex is essential for platelet reactivity since its deficiency leads to the onset of the rare bleeding disorder, Bernard-Soulier syndrome (Savoia et al., 2014). Among the four subunits (GPIbα, GPIbβ, GPIX and GPV), GPIbα is the largest one and is fundamental for the interaction with different ligands. Indeed, its N-terminal leucine-rich domain represents the ligand-binding domain (LBD) for a variety of proteins, most importantly vWF, P-selectin, thrombin and the coagulation FXII (Li, 2019). In particular, GPIb-vWF interaction induces platelet aggregation under high shear stress (Reininger, 2008). GPIbα also regulates the actin cytoskeleton through a double interaction between its cytoplasmic tail, filamin-1 and the adaptor protein 14-3-3ζ (Chen et al., 2018). In addition, GPIbβ-14-3-3ζ binding contributes to the phosphorylation-dependent regulation of actin polymerisation to decelerate the rapid movement of platelets at the ECM during the first step of platelet adhesion (Chen et al., 2018). GPIb-IX binding to 14-3-3ζ is essential for vWF functions as it has been shown that the chemical or mutagenic disruption of this interplay impairs GPIb-IX-vWF interaction, platelet adhesion and aggregation (Dai et al., 2005).

1.4.1.2 Integrins αIIbβ3 and α2β1

With ~80,000 copies per cell (Burkhart et al., 2012), integrin αIIbβ3 is only expressed in platelets and its absence causes one of the most common bleeding disorder, Glanzmann thrombasthenia (Kannan et al., 2009). Integrin α2β1 is expressed at a much lower level than integrin αIIbβ3, only ~4,000 copies per platelet (Burkhart et al., 2012). In resting platelets, integrins are found at the cell surface in a low-affinity state. Upon activation, they switch to a high-affinity conformation capable of binding their ligands following 'inside-out' signalling. Activated integrins then initiate the 'outside-in' signalling which involves the same signalling kinases of the classical pathway mediated by ITAM-containing receptors (Kasirer-Friede et al., 2007).

Integrin αIIbβ3 contains the binding domain for numerous components of the ECM including fibrinogen, fibronectin, vitronectin, thrombospondin-1 and vWF (Bennett, 2005). Integrin α2β1 is well-known as the major adhesion receptor for collagen and it is believed to only weakly contributes to the activation signalling (Auger et al., 2005). Integrin α2β1 and GPVI bind to distinct amino acid sequences on collagen: GPVI binds to the three-residue repeat GPO (Glycine-Proline-Hydroxyproline) (Asselin et al., 1999) whereas the integrin binds to the six-residue sequence GFOGER (Glycine-Phenylalanine-Hydroxyproline-Glycine-Glutamate-Arginine) (Knight et al., 1998). Ligand binding of integrins mediates firm platelet adhesion to the ECM. In addition, the interaction of integrin αIIbβ3 with fibrinogen and vWF is required for the formation of a stable platelet aggregate (Bennett, 2005).

1.4.2 GPCRs

Upon activation and spreading, platelets produce and release soluble agonists, most importantly ADP, TxA_2 and thrombin which act as a positive feedback of thrombus formation through GPCR-dependent signalling (Lee, 2019). In particular, the second-wave messengers interact with their specific GPCRs: ADP with $P2Y_1$ (G_q-coupled) and $P2Y_{12}$ (G_{i2}-coupled) receptors and TxA_2 with TP (G_q-coupled) receptor. These interactions involve the activation of multiple signalling kinases and effectors leading to the increase of intracellular Ca^{2+} and reduction of the cytosolic cyclic adenosine monophosphate (cAMP) and converge in integrin αIIbβ3 activation through the 'inside-out' signalling (Woulfe, 2005). Proteolytically produced at the platelet surface, thrombin also potentiates thrombus growth and stabilisation through its interaction with members of the GPCR superfamily, PAR1 and 4 in human (PAR3 and 4 in mouse) (Ofosu, 2003). PAR1 (G_q and G_{13}-coupled) and 4 (G_q-coupled) are activated upon thrombin-mediated proteolytic cleavage of N-terminal recognition sequences, strengthening platelet activation as well as inducing cytoskeleton remodelling and shape change (Ofosu, 2003). Using specific inhibitors or blocking antibodies, it has been shown that PAR1 is more reactive than PAR4 which is dependent on higher doses of thrombin to induce platelet aggregation (Covic et al., 2000). Another, but less studied, platelet GPCR is the adrenergic receptor α_{2A} which mediates the signalling activation reducing intracellular cAMP. Table 1.1 shows the signalling mechanisms and relative effectors of GPCRs expressed in human platelets.

The importance of GPCRs in pathological conditions characterised by unregulated platelet activation such as myocardial infarction and ischemic stroke is demonstrated by the therapeutic use of antiplatelet drugs targeting GPCR signalling components and by the phenotype of patients and mice lacking a specific GPCR. Patients with congenital defects of

$P2Y_{12}$ receptor are affected by bleeding disorders and antagonists of this receptor such as clopidogrel are clinically effective anti-thrombotic drugs used in the prevention of cardiovascular diseases (Dorsam and Kunapuli, 2004). Mice deficient in TP receptor have reduced injury-induced platelet activation and retarded atherogenesis and inhibition of TxA_2 production via aspirin is the most common therapeutic approach used for the treatment of patients at high risk of cardiovascular events (Warner et al., 2011). PAR3 and 4-deficient mice have haemostatic defects and are completely protected against experimental thrombosis (Hamilton et al., 2004, Weiss et al., 2002). PARs represent alternative target candidates for the development of new anti-thrombotic drugs to reduce the bleeding risk associated with the current antiplatelet therapy (aspirin or aspirin and clopidogrel). In clinical studies, the PAR1 antagonist vorapaxar reduced the risk of cardiovascular events in patients with a previous history of myocardial infarction and peripheral arterial disease but failed to attenuate the bleeding risk associated with the standard therapy (Gryka et al., 2017).

Receptor	Ligand	G protein	Signalling
• $P2Y_1$ • TP • PAR1 • PAR4	• ADP • TxA2 Thrombin	G_q	↑ Phospholipase (PL)C ↑ Ca^{2+} release ↑ Protein kinase (PK)C ↓ **PLATELET ACTIVATION**
$P2Y_{12}$	ADP	G_{i2}	↓ Adenylate cyclase (AC) ↓ cAMP ↓ PKA ↑ Phosphatidylinositol 3-kinase (PI3K) ↙ **PLATELET ACTIVATION** ↓ RAP1-GAP, RASA3 ↑ Akt/PKB ↓ **INTEGRIN ACTIVATION**
PAR1	Thrombin	G_{13}	↑ Rho kinase ↓ **CYTOSKELETON REARRANGEMENT**
α_{2A} adrenergic	Epinephrine	G_z	↓ cAMP → **PLATELET ACTIVATION**

Table 1.1. Human platelet GPCRs and relative signalling dynamics. Adapted from (Woulfe, 2005).

1.4.3 ITAM-containing receptors

Despite the activatory role of PTK-linked receptors and GPCRs, vigorous and sustained platelet activation is mediated by three different receptors containing an ITAM motif. The FcR-γ, linked to GPVI, and FcγRIIA contain a dual ITAM conserved sequence (YxxI/LX6-12YxxI/L) (Gibbins et al., 1997, Huang et al., 1992) whereas the C-type lectin-like receptor 2 (CLEC-2) is considered as hemITAM receptor because of the presence of a single ITAM (YxxI/L) in its intracellular domain (Suzuki-Inoue et al., 2006). The consensus sequence within the ITAM motif is fundamental for initiating and transmitting the receptor signals through the docking of Src homology (SH)2 domain-containing proteins (Isakov, 1997). Being the main focus of my PhD, the GPVI-FcR-γ complex will be extensively explored in a separate section.

1.4.3.1 FcγRIIA

With a physiological role in haemostasis and thrombosis as well as the immune response to pathogens, FcγRIIA (also called CD32) is a low-affinity receptor for the constant (Fc) domain of monomeric Immunoglobulins (Igs) G. Its contains two extracellular Ig-like loops, a transmembrane domain and a cytoplasmic region harbouring two ITAM motifs. FcγRIIA shares a common signalling mode with the GPVI-FcR-γ complex involving the activation of Spleen tyrosine kinase (Syk) and the effector PLCγ2 (Clemetson and Clemetson, 2019). It is not expressed in mice; therefore the relevance of this platelet receptor in physiological/non-physiological thrombosis has been studied only in *in vitro* systems or transgenic mice. These experimental models have been pivotal in determining the important role of FcγRIIA in platelet interaction with bacteria and viruses as well as the contribution of platelets to the pathogenesis of immune-related diseases (Arman and Krauel, 2015, Arman et al., 2014, Boilard et al., 2014). FcγRIIA has also been shown to be a key player in the onset of heparin-

induced thrombocytopenia (HIT) via immune-complex-mediated platelet activation (Arman and Krauel, 2015, Reilly et al., 2001). Furthermore, it has been proposed an additional function of FcγRIIA in IgG-independent haemostasis as an amplifier of the αIIbβ3 'outside-in' signalling, although the experimental evidence of their physical interaction has not been reported (Boylan et al., 2008).

1.4.3.2 CLEC-2

CLEC-2 is a type II transmembrane receptor and member of C-type lectin superfamily of proteins. It is highly expressed in MKs and platelets; however lower levels are also present in B lymphocytes and myeloid cells (Lowe et al., 2015b, Suzuki-Inoue et al., 2006). Its structure is characterised by the presence of an extracellular C-terminal carbohydrate-like recognition domain (CRD), a transmembrane region and a cytoplasmic tail harbouring the hemITAM motif at the N-terminus (Weis et al., 1998). The link between CLEC-2 and platelet activation has been attributed by Suzuki-Inoue et al. (2006) with the discovery of the specific ligand for CLEC-2, the snake venom toxin rhodocytin (Suzuki-Inoue et al., 2006). A year later, the same group identified podoplanin as the physiological CLEC-2 agonist (Suzuki-Inoue et al., 2007). Podoplanin is expressed at the surface of a broad range of cells including glomerular podocytes, lymphatic endothelial cells, lung alveolar cells and cancerous cells (Ugorski et al., 2016). Surprisingly, podoplanin is not present in the blood vasculature, ruling out a critical role for CLEC-2 in the haemostatic process. Indeed, *in vitro* and *in vivo* studies by Hughes et al. (2010) have demonstrated that tail bleeding and platelet aggregation under flow do not change in CLEC-2 deficient mice (Hughes et al., 2010a) in contrast with previous observations by May et al. (2009) who proposed a critical role for CLEC-2 in haemostasis and thrombosis (May et al., 2009). In the same year, Suzuki-Inoue et al. (2010), using mice deficient in CLEC-2, confirmed the result of the tail bleeding assay. However, they found a

partial decrease in collagen-induced platelet aggregation under flow (Suzuki-Inoue et al., 2010), likely due to the differences in the experimental procedure. More recently, evidence has emerged for a possible blood-borne ligand or counter-receptor for CLEC-2 as mice expressing a novel knockin of a CLEC-2 receptor (Y7A KI), that can not signal through its hemITAM, still form stable platelet aggregates on collagen under flow (Haining et al., 2017a). The CLEC-2-podoplanin axis and its signalling cascade is also fundamental for maintaining separation of the blood and lymphatic vascular systems (Suzuki-Inoue et al., 2010), lymph node development and integrity of the brain vasculature (Bénézech et al., 2014, Finney et al., 2012, Lowe et al., 2015a) as well as promoting tissue repair (Suzuki-Inoue et al., 2018). Furthermore, recent evidence has shown that CLEC-2-podoplanin interplay mediates some of the non-canonical functions of platelets, most importantly in vascular integrity and thromboinflammation (Suzuki-Inoue et al., 2018).

The signalling mechanisms by which CLEC-2 mediates these functions have common features with the classical ITAM-mediated signalling (Fig. 1.3). It is expressed in a dimeric form in resting platelets (Hughes et al., 2010b) and, once bound to the ligand and further clustered, the dual hemITAM motif becomes phosphorylated upon interaction with Syk (Suzuki-Inoue et al., 2006). However, in contrast to the canonical ITAM-dependent signalling, Src family kinases (SFKs) signal downstream, contributing to the regulation of Syk and that of other effectors, most importantly PLCγ2 (Séverin et al., 2011). In addition, whereas the adapter protein Src homology 2 domain-containing leukocyte phosphoprotein of 76 kDa (SLP-76) and the Rho family guanine nucleotide exchange factors (GEFs) Vav1 and Vav3 play a critical role in GPVI signalling, platelets from mice deficient in these proteins can still fully aggregate in response to high concentrations of rhodocytin (Suzuki-Inoue et al., 2006). Ultimately, CLEC-2 signalling is also highly influenced by lipid rafts and actin

cytoskeleton reorganisation as well as the second-wave messengers ADP and TxA_2 (Pollitt et al., 2010).

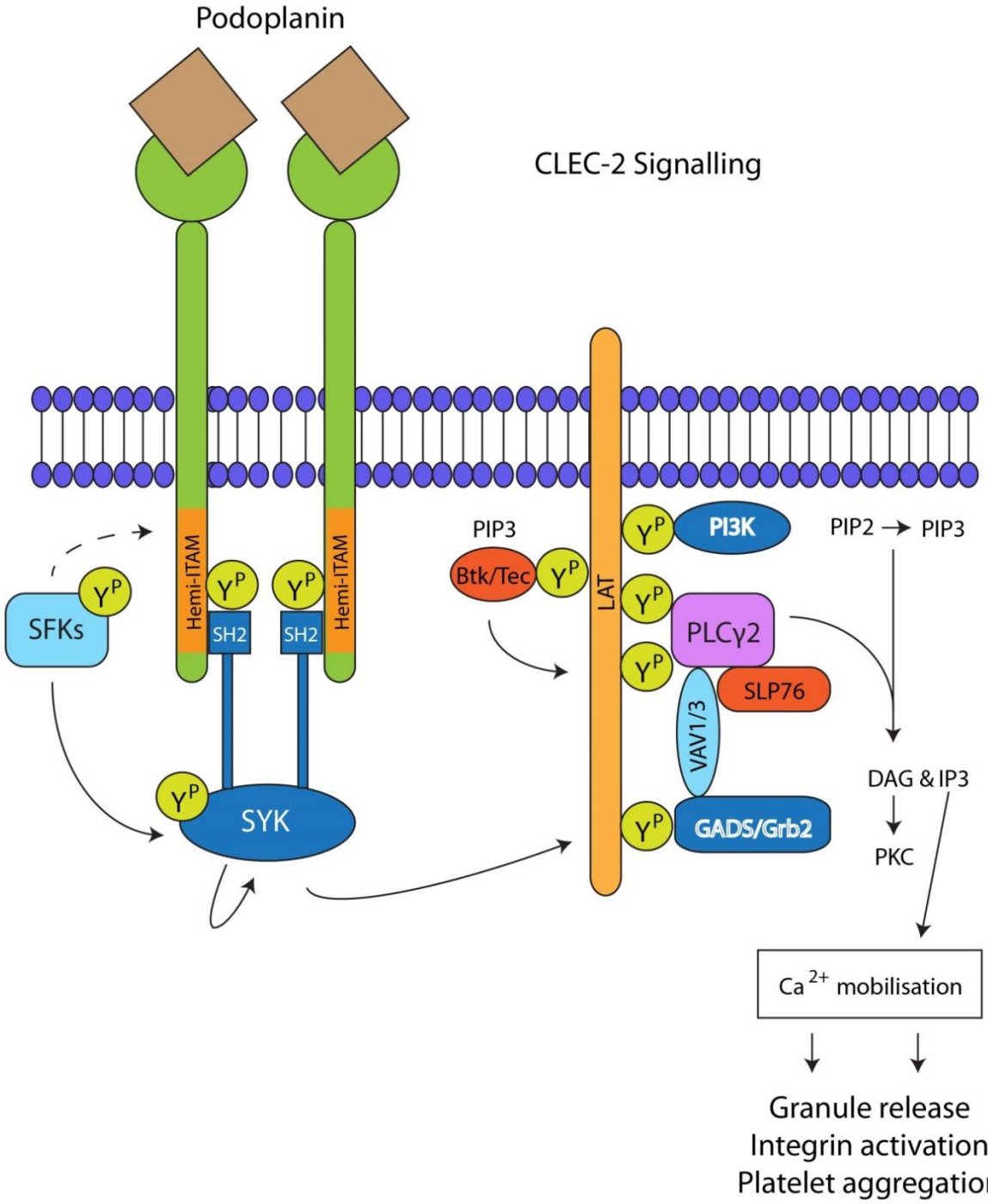

Figure 1.3. CLEC-2 signalling pathway. Upon ligand binding, the CLEC-2 signalling cascade initiates with the phosphorylation of the hemITAM motifs which allows binding of Syk. Syk engagement and activation, through auto-phosphorylation or SFKs-dependent phosphorylation, leads to the recruitment of the linker of activated T cells (LAT). Formation of the LAT-based signalosome involves the activation of a series of adaptor and effector molecules and culminates with the phosphorylation of PLCγ2. Activation of PKC and Ca^{2+} mobilisation from intracellular stores characterise the endpoint of the cascade leading to secretion of granule contents, integrin activation and platelet aggregation. Adapted from (Rayes et al., 2019).

1.5 Platelet GPVI receptor

Since its first discovery in a patient affected by autoimmune thrombocytopenic purpura (ITP) (Sugiyama et al., 1987), platelet GPVI receptor has been an attractive topic of study worldwide for nearly 30 years. This interest stems from the fact that platelets lacking GPVI exhibit only mild bleeding in both patients (Arai et al., 1995, Boylan et al., 2004, Dumont et al., 2009, Matus et al., 2013, Takahashi and Moroi, 2001) and mouse models (Kato et al., 2003, Lockyer et al., 2006, Nieswandt et al., 2000, Nieswandt et al., 2001b). Contrarily, the absence of GPVI provides protection from occlusive thrombus formation in experimental models of thrombosis (Bender et al., 2011, Cheli et al., 2008, Lockyer et al., 2006, Nieswandt et al., 2001b). The mechanism behind its divergent role in haemostasis and thrombosis is still unknown but it is the reason why GPVI is considered as an important target in anti-thrombotic therapy (Dütting et al., 2012). In addition, the limited expression of GPVI on MKs and platelets (Berlanga et al., 2000, Jandrot-Perrus et al., 2000, Lagrue-Lak-Hal et al., 2001) represents a further advantage for the development of novel anti-thrombotic drugs due to the limited off-target effects.

1.5.1 GPVI-FcR-γ structure

Cloned and purified in 1999 using a human bone marrow cDNA library, GPVI is a type 1 transmembrane receptor belonging to the Ig superfamily (Clemetson et al., 1999). Human GPVI gene, *GP6*, was mapped on the chromosome 19q13.4 and encodes a ~62 kDa protein made up by 339 amino acids (Ezumi et al., 2000). Only MKs and platelets express GPVI reaching up to ~9600 copies per human platelet (Burkhart et al., 2012). Lacking intrinsic catalytic activity, GPVI is expressed at the platelet surface associated with the disulphide-linked homodimer FcR-γ which exhibits one copy of the ITAM motif in its cytosolic region and is fundamental for GPVI expression and signalling transduction (Gibbins et al., 1997). As

an Ig, human GPVI extracellular domain is characterised by the presence of two Ig-C2-like loops, called D1 and D2, associated with a mucin-like stalk region enriched in sites for O-linked glycosylation (Fig. 1.4). It has been demonstrated that the D1 loop represents the major collagen-binding domain (CBD) of GPVI (Smethurst et al., 2004). The stalk domain, harbouring the cleavage site for members of the A disintegrin and metalloproteinase (ADAM) family of metalloproteinases, is involved in the receptor shedding from the platelet surface (Gardiner et al., 2007). It also connects the receptor extracellular and transmembrane domains. The arginine group (Arg^{273}) in the transmembrane domain represents the binding site for the FcR-γ (Berlanga et al., 2002, Nieswandt et al., 2000, Tsuji et al., 1997). The transmembrane domain converges in the cytosolic region (GPVI-tail) which has been shown to be fundamental for intracellular signalling through the interaction between a proline-rich domain (PRD) and the SH3 domain of SFKs (Ezumi et al., 1998, Schmaier et al., 2009, Suzuki-Inoue et al., 2002). GPVI tail also contains an important site for the binding of calmodulin (CaM). Indeed, CaM is constitutively bound to GPVI in platelets and it dissociates from the receptor tail upon cellular activation, although the function of this association is still unknown (Andrews et al., 2002). Murine GPVI receptor has a very similar structure and shares approximately 64% homology with the human amino acid sequence. However, its intracellular domain lacks the 23 amino acids located at the C-terminus of the human GPVI PRD and the experimental evidence of the functional relevance of this difference has not been reported until now (Jandrot-Perrus et al., 2000).

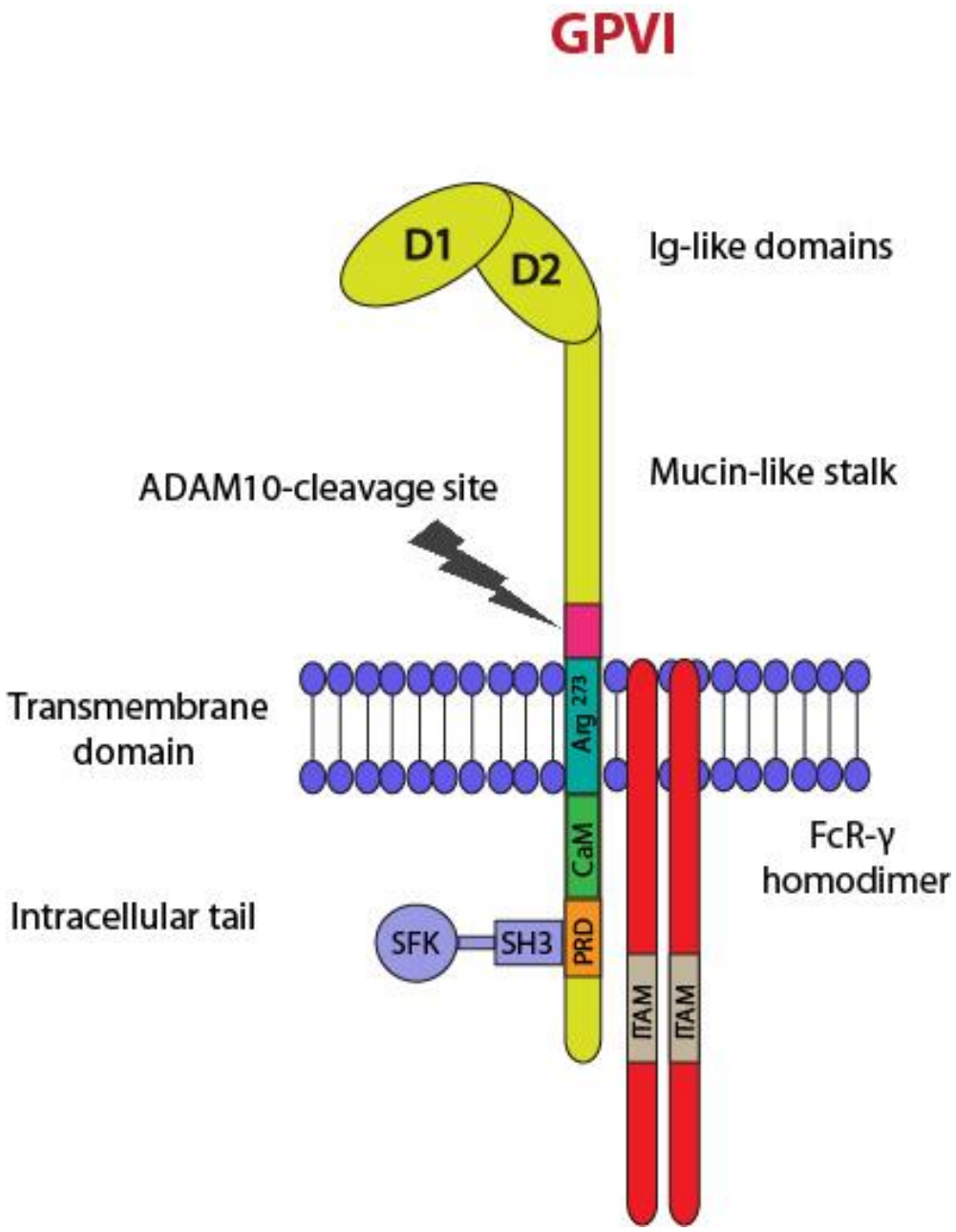

Figure 1.4. Structural domains of platelet GPVI receptor. Three different domains characterise the GPVI receptor structure: 1. the extracellular domain made up by two Ig-like domains D1 and D2 linked to a mucin-like stalk region containing the cleavage site for the sheddase ADAM10; 2. the transmembrane domain harbouring an arginine group (Arg^{273}) necessary for the association with the FcR-γ and 3. the cytosolic tail including the binding site for CaM and a PRD required for the interaction with the SH3 domain of SFKs.

1.5.2 GPVI dimerisation

GPVI is expressed at the platelet surface under two different conformations: the monomeric form which has no physiological affinity for fibrous collagen whereas the dimeric form is able to bind collagen with significantly higher affinity. This was demonstrated by measuring the binding of recombinant monomeric (GPVIex) and dimeric (GPVI-Fc_2) GPVI extracellular domains to immobilised collagen by enzyme-linked immunosorbent assay (ELISA) and surface plasma resonance (SPR) (Miura et al., 2002). Interestingly, they found that GPVI does not interact with soluble collagen and both monomeric and dimeric GPVI bind to CRP with the same affinity, highlighting the specificity of dimeric GPVI for the quaternary structure of fibrous collagen. The proof of concept was obtained in 2006 with the crystal structure of dimeric GPVI. The crystallographic data revealed the presence of an additional CBD located in the juncture region at the interface of the D2 domains when two receptor monomers bind each other to form a parallel, back-to-back dimer (Horii et al., 2006) (Fig. 1.5). In 2009, Jung et al. confirmed the presence of GPVI dimers at the surface of resting platelets, using a specific m-Fab-F against divalent GPVI (Jung et al., 2009). However, the controversial debate to determine the extent of receptor dimerisation in resting and activated platelets and its functional relevance is still unresolved. In 2012, Jung et al., using another specific Fab 204-11 against the dimeric conformation of GPVI, reported a constitutive expression of GPVI dimers in resting platelets: 29% which rises to 39% and 44% upon activation by CRP and thrombin, respectively (Jung et al., 2012). Both anti-dimeric GPVI Fabs, m-Fab-F and 204-11, blocked collagen-induced platelet aggregation, highlighting the critical role of receptor dimerisation for activation (Jung et al., 2009). Contrarily, several groups have detected the dimeric form of GPVI only upon platelet activation. Arthur et al. (2007) demonstrated the presence of disulphide-linked GPVI dimers in platelets activated with convulxin or other receptor

agonists, identifying the Cys-388 in the intracellular tail as the specific residue involved in the dimerisation. The appearance of dimers in activated platelets was independent of GPVI signalling and stabilised by the inhibition of receptor shedding (Arthur et al., 2007). Loyau et al. (2012), using an anti-GPVI monoclonal antibody 9E18 which binds specifically dimeric GPVI, showed that monomeric GPVI is predominant on resting platelets (only 14% of the dimeric form was detected) and dimerises upon platelet activation by vWF and other soluble agonists through a mechanism that involves the activation of the tyrosine phosphatase CD148 and low levels of cyclic nucleotides (Loyau et al., 2012). Although the homodimeric FcR-γ is required for GPVI expression at the platelet surface, it is not fundamental for receptor dimerisation as shown by the formation of a three-helix interface which would incorporate only a monovalent GPVI (Feng et al., 2005).

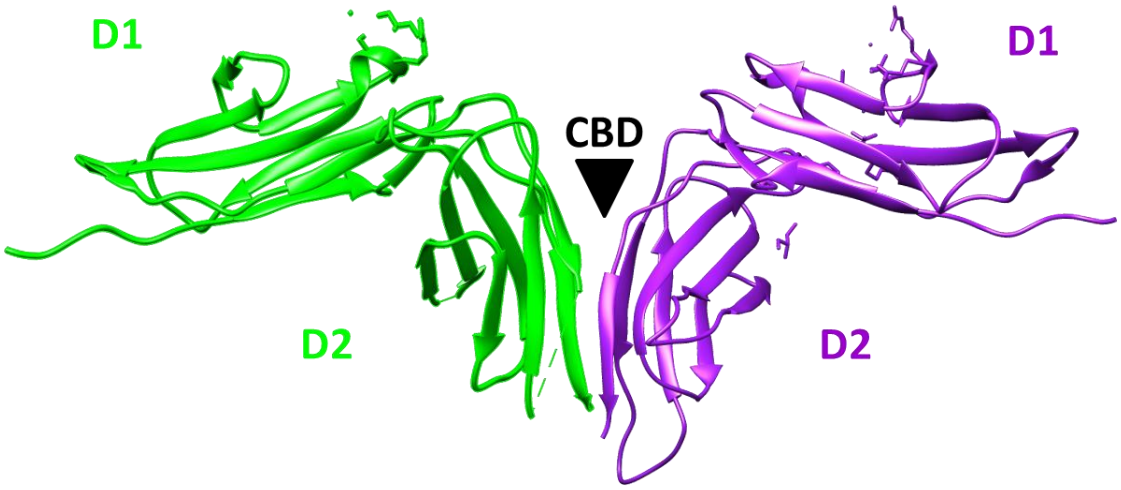

Figure 1.5. Crystal structure of dimeric GPVI. GPVI forms a parallel, back-to-back dimer in the crystal which contains an additional CBD (indicated by a black arrow) at the interface of the D2 domains of each monomer (highlighted in green and magenta). Figure generated with UCSF Chimera software (PDB accession number: 2GI7) (Horii et al., 2006).

1.5.3 GPVI ligands

GPVI was first proposed as a collagen receptor in the late 1980s with the discovery of the patient affected by auto-immune thrombocytopenia (Sugiyama et al., 1987). Since then numerous studies in GPVI-deficient patients (Arai et al., 1995, Boylan et al., 2004, Dumont et al., 2009, Matus et al., 2013, Takahashi and Moroi, 2001) and mouse models (Kato et al., 2003, Lockyer et al., 2006, Nieswandt et al., 2000, Nieswandt et al., 2001a, Nieswandt et al., 2001b) have demonstrated the critical role of GPVI-collagen interaction in mediating platelet activation. To date, GPVI is considered the major signalling collagen receptor expressed in platelets with integrin α2β1 contributing to the initial interaction (Auger et al., 2005). Collagen is the most abundant component of the ECM with fibrillar type I and III showing the highest affinity for GPVI among the nine types present in the vascular system (Jung et al., 2008). Using site-specific mutagenesis, it has been found that the D1 domain in the extracellular region of GPVI binds specifically to the three-residue repeat GPO (Glycine-Proline-Hydroxyproline) within the triple-helix of the collagen structure (Smethurst et al., 2004). As stated above, an additional CBD has been identified by crystallography studies only in the dimeric conformation of the receptor (Horii et al., 2006) and may explain the ~200-fold higher affinity of dimeric GPVI for collagen in comparison with the monomeric conformation (Jung et al., 2012). Synthetic ligands such as the collagen-related peptide (CRP), which contains multiple GPO triplets, have been developed to study GPVI-mediated platelet activation independently of integrin α2β1 (Asselin et al., 1997, Morton et al., 1995). Interestingly, only cross-linked CRP (CRP-XL) is able to induce efficient platelet activation, underlining that GPVI binds native fibrillar collagen at multiple sites. Snake venom toxins such as alborhagin, convulxin (CVX) and crotarhagin have also been described as non-physiological ligands of GPVI (Andrews et al., 2001, Polgár et al., 1997, Wijeyewickrema et

al., 2007). In particular, CVX binds to GPVI with higher affinity, faster association and slower dissociation rates than collagen and CRP. It forms a dimer of α4β4 rings in solution and can cluster up to eight copies of GPVI, indicating the presence of multiple binding sites (Horii et al., 2009). The CVX-binding sites are different from those of collagen and receptor dimerisation is not required for CVX binding (Miura et al., 2002). However, despite being a strong GPVI agonist, CVX induces a transient response whereas collagen stimulation results in a delayed but sustained activation as demonstrated in platelets and cell line models (Tomlinson et al., 2007). Diesel exhaust particles (DEP) and sulphated polysaccharides are also exogenous GPVI ligands which induce GPVI (and/or CLEC-2)-mediated platelet activation (Alshehri et al., 2015b). In addition to collagen, GPVI interacts with other ECM components (e.g. laminin) (Inoue et al., 2006) and the extracellular matrix metalloproteinase inducer (EMMPRIN) (Pennings et al., 2014) as well as the protein hormone adiponectin (Riba et al., 2008) and amyloid β (Aβ)42 (Elaskalani et al., 2018).

Recently, two proteins have been added to the list of physiological GPVI agonists, fibrinogen and fibrin. In 2015, Alshehri et al. and Mammadova-Bach et al. firstly discovered fibrin as a novel ligand for GPVI using GPVI-deficient patients and GPVI-deficient mice in a ferric chloride ($FeCl_3$) injury model, respectively (Alshehri et al., 2015a, Mammadova-Bach et al., 2015). In 2018, Induruwa et al. and Mangin et al. reported that fibrinogen supports platelet adhesion and activation through GPVI (Induruwa et al., 2018, Mangin et al., 2018). Whether these two novel ligands bind the monomeric and/or dimeric conformation of GPVI is controversial and represents a matter of current investigation in the platelet biology field (Slater et al., 2019). Mammadova-Bach et al. (2015) demonstrated binding of recombinant dimeric GPVI-Fc to polymerised fibrin but not fibrinogen which supported thrombin generation and recruitment of additional platelets to the thrombus surface (Mammadova-Bach

et al., 2015). In contrast, in the study by Alshehri et al. (2015), monomeric fibrin was able to induce platelet spreading whereas in solution only fibrin polymers induced GPVI activation, likely due to the formation of receptor clusters (Alshehri et al., 2015a). Recently, Onselaer et al. (2017) confirmed this finding and demonstrated that recombinant monomeric but not dimeric GPVI-Fc interacts with fibrin in the D-dimer region and the binding site is different from that of collagen (Onselaer et al., 2017). Lastly, only recombinant dimeric GPVI-Fc showed binding to immobilised fibrinogen and fibrin through their D-domains in the report from (Induruwa et al., 2018). Contrarily, Mangin et al. (2018) reported that immobilised fibrinogen activates human, but not mouse platelets, through monomeric GPVI (Mangin et al., 2018).

The physiological relevance of these interactions is not clear. It has been proposed that fibrin may support thrombus growth and stabilisation through its interaction with GPVI. Indeed, fibrin was found within the thrombus core in the revised model of thrombus formation (Stalker et al., 2014) which was later contradicted by another study showing that fibrin polymers cover also the shell of the thrombus (Macrae et al., 2018). The interaction between GPVI and fibrinogen leads to full platelet spreading and block of this interplay impaired platelet aggregation independently of collagen and fibrin (Mangin et al., 2018). Therefore, it is clear that GPVI may play multiple roles in haemostasis and thrombosis: it may contribute to thrombus growth and stabilisation through the interaction with fibrin whereas the binding to fibrinogen may support platelet spreading and aggregation. Only crystallography and cryo-electron microscopy studies will provide further insights into the exact conformation adopted by GPVI bound to fibrinogen and fibrin, allowing investigation of the physiological relevance of these interactions.

1.5.4 GPVI signalling transduction

Upon ligand binding, GPVI signalling initiates with Lyn, Fyn and Src-mediated phosphorylation of two conserved tyrosines within the ITAM motif of the co-receptor FcR-γ (Séverin et al., 2012). In particular, it has been shown that Lyn is the major SFK in priming GPVI-mediated signalling activation, being constitutively associated with GPVI-PRD in the cytosolic tail. On the contrary, Fyn is not linked to GPVI in resting platelets and it associates upon stimulation, contributing to sustained receptor activation (Schmaier et al., 2009). Phosphorylation of the FcR-γ ITAM motifs induces the engagement and following activation of the tyrosine kinase Syk, through auto-phosphorylation of tyrosines 525/526 (Y525/526 in human or Y519/520 in mouse) and SFKs-mediated phosphorylation of tyrosine 352 (Y352) (Speich et al., 2008). Syk contains tandem SH2 domains which allow binding to the phosphorylated ITAM motifs and the onset of a downstream signalling cascade involving several adapters and effectors. LAT represents one of the most important adaptor proteins of the GPVI signalling pathway, together with SLP-76 (Pasquet et al., 1999). Once phosphorylated by Syk on specific tyrosine residues, LAT forms a platform at the platelet PM in order to assemble the so-called 'LAT signalosome' which culminates in the phosphorylation and activation of the effector PLCγ2. Other adaptor proteins, with a minor role in mediating activation by GPVI, are recruited at the LAT signalosome such as the growth factor receptor-bound protein 2 (Grb2) and the Grb2 related adaptor (Gads) (Asazuma et al., 2000). In addition, the Rho family GEFs Vav1 and Vav3 contribute to GPVI-mediated PLCγ2 activation in a redundant way as demonstrated by *in vivo* studies using double knock-out mice (Pearce et al., 2004). The translocation of the protein/lipid kinase PI3K to the signalosome followed by the generation of phosphatidylinositol 3,4,5-trisphosphate (PIP_3) is another important step involved in PLCγ2 activation (Gibbins et al., 1998), with Btk/Tec

kinases also contributing (Atkinson et al., 2003). Upon activation, PLCγ2 liberates the second messengers inositol 1,4,5-trisphosphate (IP_3) and 1,2-diacylglycerol (DAG), which in turn induce the Ca^{2+} movement from intracellular compartments and activation of PKC, respectively. The final events of this orchestrated signalling cascade (Fig. 1.6) are characterised by granule release, activation of integrin αIIbβ3 through 'inside-out' signalling and platelet aggregation (Nieswandt and Watson, 2003).

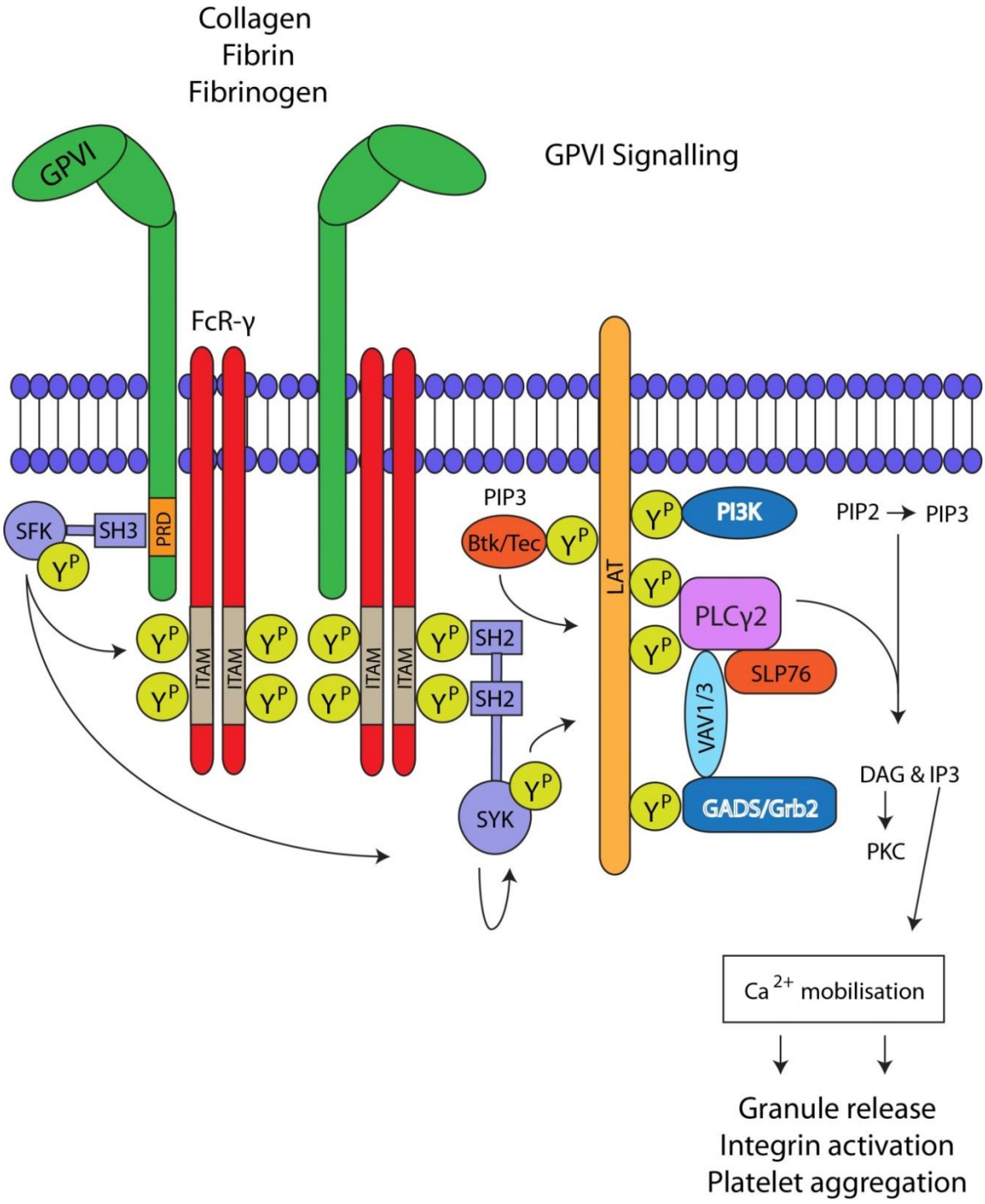

Figure 1.6. GPVI signalling pathway. Upon ligand engagement, the GPVI signalling cascade initiates with the SFKs-mediated phosphorylation of FcR-γ in its ITAM motifs and the subsequent recruitment and activation of the tyrosine kinase Syk. Syk, in turn, induces the phosphorylation of LAT which forms a platform at the PM for the recruitment of a variety of adaptors and effectors, most importantly PLCγ2. The final events are characterised by the activation of PKC and Ca^{2+} influx from intracellular compartments which lead to granule release, integrin activation and platelet aggregation. Adapted from (Rayes et al., 2019).

1.6 Regulation of GPVI spatial organisation and signalling transduction

In order to coordinate platelet responses and prevent unregulated platelet activation, GPVI signalling and surface expression are tightly regulated by a variety of inhibitory mechanisms. For example, prostacyclin (prostaglandin I_2, PGI_2) and nitric oxide (NO), which are released by endothelial cells, play a critical role in maintaining platelets in a deactivated state within the circulation and prevent their accumulation at sites of vascular damage (Nagy and Smolenski, 2018). Platelet inhibition is also mediated by the activation of inhibitory receptors containing an immunoreceptor tyrosine-based inhibitory motif (ITIM) which are able to dephosphorylate key proteins of ITAM-signalling pathways via the action of SH2 domain-containing phosphatases 1 and 2 (SHIP1 and 2) (Coxon et al., 2017). In addition to the endogenous and exogenous inhibitory mechanisms, GPVI signalling and distribution require further levels of control to mediate platelet sensitivity. These cooperative regulatory factors include components of the PM such as lipid rafts, the tetraspanin-enriched microdomains and the actin cytoskeleton. GPVI clustering and shedding as mechanisms to enhance and limit platelet reactivity will also be discussed in this section.

1.6.1 Role of lipid rafts in GPVI distribution and signalling

Exactly how GPVI organisation and clustering mediates the spatio-temporal regulation of the signalling transduction in platelets is still under investigation, but a number of studies have demonstrated that specialised membranous areas, called lipid rafts, play a critical role. Glycosphingolipids, saturated or non-saturated phospholipids, and arrayed cholesterol are the major components of lipid rafts, resulting in liquid-ordered and tightly packed structures (~20-50 nm in diameter) floating in the PM bilayer (Bodin et al., 2003). Found also in T cells and B cells, lipid rafts function as organising centres for the recruitment and assembly of receptor oligomers and signalling mediators at the PM, necessary for the onset of immune-

receptor signalling transduction (Dykstra et al., 2003). The hypothesis of lipid rafts in platelet is highly controversial due to the limitation of the experimental procedure used for isolating and characterising these membranous domains. Lipid rafts are commonly isolated by sucrose gradients and defined as being the fractions insoluble into nonionic detergents but enriched in GM1 ganglioside and LAT. The latter are used as markers to determine the association of a specific protein with lipid rafts. Using this classical method of isolation, a variety of studies have highlighted the importance of these microdomains in platelet activation, especially mediated by ITAM-containing receptors (Bodin et al., 2003). The first observation of their involvement in GPVI-mediated platelet activation came from Boesze-Battaglia et al. (1996) who found a change in the cholesterol distribution upon collagen stimulation (Boesze-Battaglia et al., 1996), which was confirmed many years later by different groups. In 2002, Locke et al. showed that GPVI is not associated with lipid rafts in resting platelets but it translocates to these membranous domains upon platelet activation (Locke et al., 2002). However, in the same year, Wonerow et al. reported that platelet activation induces no major change in GPVI localisation within the lipid rafts (Wonerow et al., 2002). This discrepancy is likely due to the different detergent used for the lipid rafts isolation (Triton X-100 vs Brij 58) which can affect the detection of GPVI. In accordance with Wonerow et al., Ezumi et al. (2002) demonstrated that GPVI-FcR-γ complex is constitutively and functionally associated with membrane rafts wherein SFKs and LAT are also present (Ezumi et al., 2002). Lipid rafts may also facilitate the interaction of GPVI with other receptors as it has been shown for GPIb-IX-V (Arthur et al., 2005) and the inhibitory receptor platelet endothelial adhesion molecule-1 (PECAM-1) (Lee et al., 2006) with further consequences on the signalling transduction. Finally, a proteomic comparative study reported that the lipid rafts composition changes upon activation mediated by GPVI or CLEC-2 with loss of numerous cytoskeletal

proteins (Izquierdo et al., 2019). This raises the question of whether the high abundance of signalling proteins within the lipid rafts of activated platelets is due to their translocation or cytoskeleton reorganisation. Only the adoption of cutting-edge microscopy techniques and development of specific probes will confirm the lipid rafts hypothesis and clarify the contribution of these highly-organised PM domains to GPVI clustering and signalling as well as platelet activation and reactivity.

1.6.2 Tetraspanin microdomains as organisers of GPVI localisation and signalling

In addition to the lipid rafts, GPVI is also compartmentalised into specific tetraspanin-enriched microdomains at the platelet PM (Protty et al., 2009). Tetraspanins are a family of 33 proteins with four transmembrane domains which are able to modulate the intracellular maturation and trafficking as well as mobility and oligomerisation of specific partner proteins (Charrin et al., 2014). The importance of tetraspanins in platelet function has been demonstrated by the mild bleeding phenotypes of mice deficient in CD151 or Tspan32 attributed to the altered 'outside-in' signalling mediated by integrin αIIbβ3 (Goschnick et al., 2006, Orlowski et al., 2009). Since then, lots of studies have been undertaken to identify new platelet tetraspanins and their involvement in haemostasis and thrombosis. In 2009, Tspan9 was identified as a novel component of the platelet tetraspanin microdomains where GPVI is specifically compartmentalised (Protty et al., 2009). The functional relevance of this interaction was revealed with the generation of a Tspan9-deficient mouse (Haining et al., 2017b). In the absence of Tspan9, they found a mild but specific impairment of GPVI-induced platelet aggregation and secretion as well as GPVI signalling but not platelet adhesion to collagen under flow, haemostasis and arterial thrombosis. Furthermore, GPVI-Tspan9 association was not essential for GPVI cluster formation but single-particle tracking of GPVI

revealed that the absence of Tspan9 adversely affected GPVI lateral diffusion within the PM. This advanced the hypothesis that Tspan9, like other uncharacterised platelet tetraspanins, may facilitate the movement of GPVI receptors within the PM to allow the 'fine-tuning' of GPVI signalling.

The GPVI specific sheddase ADAM10 is also compartmentalised into tetraspanin microdomains. Different studies have demonstrated that members of the TspanC8 subfamily, so called because of the presence of eight cysteine residues within the extracellular domain, are involved in ADAM10 maturation and trafficking (Dornier et al., 2012, Haining et al., 2012, Prox et al., 2012). Furthermore, the specific TspanC8 tetraspanin, Tspan14 has been shown to inhibit ADAM10-mediated GPVI shedding in a cell line model, proposing a possible involvement of the tetraspanin partner in the regulation of the specificity of the ADAM10 target (Noy et al., 2016). Such regulation may also take place in platelets where the association of GPVI and ADAM10 with different tetraspanins may induce or prevent the receptor cleavage. This is a current matter of investigation in Tomlinson laboratory (University of Birmingham, UK).

1.6.3 Actin cytoskeleton regulates GPVI organisation and signalling

As stated in the previous sections, the actin cytoskeleton plays a fundamental role in maintaining platelet morphology, promoting the rapid shape change upon platelet activation and contributing to thrombus stability and retraction. Like in other cells, a dynamic actin cytoskeleton also regulates receptor conformation and movement within the platelet membrane as well as facilitates their clustering required for the initiation of the signalling transduction (Jaqaman and Grinstein, 2012). GPVI-mediated platelet activation results in the reorganisation of the actin cytoskeleton to allow platelets to become fully spread. This process

is controlled by members of the Rho family of small GTPases, most importantly RhoA, Cdc42 and Rac1 which, through the activation of specific effectors, play important roles in platelet aggregation, secretion, spreading and thrombus formation (Aslan and McCarty, 2013). In particular, RhoA and Cdc42 modulate platelet contractility and secretion whereas Rac1 is required for platelet spreading and aggregation. Interestingly, Rac1 has emerged as a regulator of the pathway downstream of GPVI. Notably, platelets from Rac1-deficient mice exhibited impairment in GPVI-mediated PLCγ2 activation and Ca^{2+} mobilisation (Pleines et al., 2009). Furthermore, in human platelets, Rac1 inhibition reduced platelet aggregation in response to CRP in a dose-dependent fashion (Pollitt et al., 2010). Transient deletion of Cdc42 in a conditional knockout mouse model also impaired GPVI-mediated platelet responses including filopodia formation, secretion of ATP and platelet aggregation in response to CRP (Akbar et al., 2011). In accordance with this, another study showed that the pharmacological inhibition of p21 activated kinase (PAK), a Rho GTPases effector, blocks platelet lamellipodia formation, secretion and aggregation in response to GPVI (Aslan et al., 2013). Whether inhibition of Rho GTPases affects GPVI signalling via an effect on receptor clustering in human and mouse platelets is still unknown and it is a matter of investigation in the Watson laboratory (University of Birmingham, UK). Dependence of GPVI dimerisation and clustering on the actin dynamics has only been demonstrated through the use of different blockers of the actin polymerisation such as cytochalasin D and latrunculin A. In addition to the impairment of platelet spreading, both drugs were able to decrease GPVI dimerisation in resting platelets and CRP- or thrombin-activated platelets as well as depress cluster formation on CRP and different collagenous substrates (Poulter et al., 2017). However, in another study, they did not abolish GPVI signalling or maximal platelet aggregation in response to GPVI

agonists (Pollitt et al., 2010). Therefore, more investigation is required to better understand the correlation between GPVI signalling, clustering and the actin dynamics.

1.6.4 Receptor clustering

The signalling transduction initiated by cell-surface receptors is an orchestrated and coordinated mechanism involving a series of signalling kinases, adaptor and effector proteins which converges in the modulation of the final cellular response. A growing body of evidence suggests that the receptor organisation itself can regulate the signalling intensity and duration through the formation of higher-order clusters (Bethani et al., 2010). These tightly packed multimeric complexes could affect signalling through a number of mechanisms, including: 1) limiting the lateral diffusion of individual receptor monomers and potentially incorporating other signalling proteins; 2) concentrating secondary mediators and 3) preventing the access of negative regulators such as sheddases or phosphatases, ultimately leading to the amplification of the signalling transduction. Receptor oligomerisation has been reported for different categories of receptors and in a variety of cell types, including GPVI in platelets.

1.6.4.1 GPVI clustering

As mentioned in the 'GPVI dimerisation' section above, resting platelets contain up to ~29% of GPVI as a dimer, suggesting that an additional level of regulation is expected to occur at the platelet surface for GPVI signalling to take place. Indeed, different groups have suggested the existence of a higher-order clustering of receptors which may play a critical role in the potentiation of ligand avidity and signalling strength. Investigating the structural basis of GPVI-collagen interaction, Horii et al. (2006) hypothesized a model in which a single GPVI dimer is not able to trigger the signalling transduction due to the length of the stalk region. Contrarily, numerous GPVI receptors would place the chains in proximity to induce platelet

activation (Horii et al., 2006). This model was supported by Smethurst et al. (2007) who showed that CRP-XL, which contains four GPO triplets able to bind two GPVI receptors simultaneously, triggers platelet aggregation (Smethurst et al., 2007). Consistent with this, all the bivalent Fabs, but not the monovalent m-Fab-F, developed by Jung et al. (2009) were able to induce platelet aggregation, suggesting that a single GPVI dimer is not sufficient to trigger the signalling and a further level of receptor organisation is required to induce activation (Jung et al., 2009). Furthermore, the ability of GPVI to form tight complexes at the platelet surface was demonstrated by chemical cross-linking (Berlanga et al., 2007). Only the adoption of advanced microscopy techniques such as Single Molecule Localisation Microscopy (SMLM) in combination with quantitative algorithms allowed the first visualisation and characterisation of dimeric GPVI clusters at the surface of platelets adhered to different substrates (Poulter et al., 2017). These clusters colocalised with platelet areas enriched in tyrosine-phosphorylated proteins (markers of signalling activation), although the specific signalling mediators involved in the process have not been investigated. The intrinsic features of different GPVI ligands determined the formation of a variety of cluster templates which may influence the strength and duration of signalling as well as ligand avidity. In this context, the ability of CVX to cluster up to eight copies of GPVI may explain the reason why it induces robust platelet activation (Horii et al., 2009). Indeed, it has previously been shown that GPVI mediates both signalling and adhesion of platelets to collagen in a density-dependent manner (Chen et al., 2002). Lastly, the contribution of fibrinogen and fibrin to GPVI clustering is unclear because of the contrasting findings relative to the conformation adopted by GPVI in the interaction with the two ligands (Slater et al., 2019). SMLM showed the presence of GPVI clusters in platelets adhered to an immobilised fibrinogen-coated surface (Poulter et al., 2017) whereas cluster formation on fibrin has not been investigated.

Polymerised fibrin would likely induce GPVI multimerisation and strengthen the initial signalling mediated by GPVI-collagen interplay, a topic for future investigation.

Receptor clustering, as a mechanism to control cellular signalling, is known to occur in many cell types, for example with the T cell receptor (TCR) in T cells (Goyette et al., 2019). In platelets, in addition to GPVI, receptor clustering has been associated with the other two (hem)ITAM-containing receptors, FcγRIIA (Chacko et al., 1994) and CLEC-2 (Pollitt et al., 2014) as well as the GPIb-IX-V complex (Arya et al., 2003). In particular, live-cell imaging has shown that upon podoplanin engagement, CLEC-2 coalesces to form clusters, which in turn induces the oligomerisation of podoplanin itself, facilitating the interaction between platelets and lymphatic endothelial cells. It has been proposed that this mechanism is critical for the development of the lymphatic vasculature (Pollitt et al., 2014).

1.6.5 Downregulation of platelet signalling

In addition to the inhibitory function of endothelial mediators and ITIM receptors mentioned above, platelet reactivity can also be limited by receptor removal from the cell surface. This can be achieved in a number of ways including receptor endocytosis and receptor shedding. Endocytosis of receptors removes them from the cell surface but does not necessarily destroy the receptors as they can be recycled back to the cell membrane. There is some evidence that both GPVI (Takayama et al., 2008) and CLEC-2 (Lorenz et al., 2015, May et al., 2009) can be endocytosed in platelets. Receptor shedding represents the extracellular proteolysis of receptors expressed at the cell surface which leads to the irreversible downregulation of the receptor itself in order to limit cell activation. This regulatory mechanism is active in platelets with the receptors GPIb, GPV and GPVI being affected (Montague et al., 2018a). Activation of platelet receptor cleavage results in the decrease of surface receptor density and ligand

binding with negative consequences on platelet signalling and activation and the generation of soluble fragments which can be used as markers of platelet activation as well as associated pathological conditions such as coronary artery disease, ischaemic stroke, thermal injury, sepsis and inflammatory bowel disease (IBD) (Montague et al., 2018a).

1.6.5.1 GPVI shedding

In light of the multiple roles played by GPVI in platelet activation and thrombus formation, lots of studies have been undertaken to understand the mechanisms underlying the receptor shedding and its role in physiology and pathology. The dynamics by which GPVI shedding occurs depend on the specific trigger (Fig. 1.7). In human platelets, ligand engagement induces GPVI shedding from the platelet surface, predominantly by ADAM10 which belongs to the ADAM family of metalloproteinases (Gardiner et al., 2004). In murine platelets, the major GPVI sheddase has not been identified, with ADAM10, ADAM17 and likely other metalloproteinases playing a role in the receptor cleavage (Bender et al., 2010). The ADAM10 cleavage site (P^{260}AR∧QYY) was mapped in the stalk region of both human and mouse GPVI (Gardiner et al., 2007). Once shed, the ~55 kDa soluble extracellular domain (sGPVI) is released in the plasma whereas the ~10 kDa fragment (GPVI-tail) remains anchored to the membrane. To induce shedding, ligand engagement also requires the activation of the signalling cascade since inhibitors of key signalling kinases such as SFKs and Syk abrogated GPVI shedding (Gardiner et al., 2004). In addition, like receptor clustering, the intrinsic characteristics of different agonists determine the extent and kinetics of GPVI shedding, with CVX representing a stronger and faster stimulus than collagen and CRP (Andrews et al., 2007). GPVI signalling and therefore shedding also involves the dissociation of CaM from the intracellular tail (Andrews et al., 2002). Indeed, ADAM10-mediated GPVI shedding *in vitro* can be induced by non-physiological stimuli such as the

CaM inhibitor W7 which stimulates the CaM release from the cytoplasmic tail (Gardiner et al., 2004). However, both CVX and W7-induced shedding are independent of integrin αIIbβ3 signalling. Moreover, carbonyl cyanide m-chlorophenylhydrazone (CCCP), which causes mitochondrial injury, triggers GPVI cleavage through ADAM17 in murine platelets (Bergmeier et al., 2004). Alternatively, the thiol-modifying reagent N-ethylmaleimide (NEM) directly activates ADAM10 and other metalloproteinases, representing a strong trigger for GPVI shedding (Gardiner et al., 2007). Unlike ligand engagement, these stimuli do not require activation of GPVI signalling.

In addition to GPVI agonists and synthetic compounds, other physiological/non-physiological stimuli can downregulate GPVI expression through the activation of receptor shedding (Fig. 1.7). The coagulation factor FXa is fundamental to downregulate GPVI under procoagulant conditions (Al-Tamimi et al., 2011b). Pathophysiological shear stress also promotes GPVI cleavage in the absence of GPVI ligand, proposing a possible implication in thrombus stability (Al-Tamimi et al., 2012). Moreover, other (hem)ITAM-containing receptors engagement such as CLEC-2 (Gitz et al., 2014) and FcRγIIA (Gardiner et al., 2008), but not GPCRs activation (Montague et al., 2018b), downregulates GPVI through this mechanism. GPVI shedding can also be induced *in vivo* through the administration of anti-GPVI monoclonal antibodies, leading to a long-term anti-thrombotic effect (Nieswandt et al., 2001b, Schulte et al., 2003). This antibody-induced shedding was further described in patients affected by immune thrombocytopenia who developed autoantibodies against GPVI (Boylan et al., 2004, Sugiyama et al., 1987, Takahashi and Moroi, 2001) and in human platelets after injection into a non-obese diabetic/severe combined immunodeficiency (NOD/SCID) mouse and treatment with anti-human GPVI antibodies (Boylan et al., 2006).

As stated before, ADAM10 is the essential metalloproteinase to induce loss of GPVI from the platelet surface. Expressed at the surface of a variety of cell types including platelets, ADAM10 is a type I transmembrane protease made up by an N-terminal prodomain followed by a catalytic domain, a region containing the disintegrin/cysteine motif, a transmembrane domain and the intracellular tail. Exposure to a variety of stimuli induces the proteolytic removal of the prodomain and the activation of the metalloproteinase domain (Anders et al., 2001). Recently, ADAM10 activity has been monitored real-time using a new GPVI-based fluorescence resonance energy transfer (FRET) sensor in resting and activated platelets (Facey et al., 2016). Interestingly, quiescent platelets expressed mature ADAM10 on their surface but very little GPVI shedding occurred whilst exposure to shear and treatment with NEM dramatically increased the level of its activity and GPVI shedding rate. On the contrary, GPVI activation by collagen, CRP or CVX did not induce any change in ADAM10 activity but GPVI shedding increased, suggesting that different stimuli are able to trigger GPVI shedding via different mechanisms.

In resting platelets, GPVI copy number is maintained at a steady level by a minimal degree of receptor shedding (Gardiner et al., 2007). Ligand-induced shedding decreases platelet responsiveness to collagen (Chen et al., 2002) which may be functional in conditions characterised by unregulated and excessive platelet activation such as occlusive thrombi. Therefore, sGPVI may be used as a specific biomarker of platelet activation for the detection of thrombotic/non-thrombotic disorders. Indeed, elevated levels of sGPVI have been recorded in the plasma of patients affected by coronary artery disease, ischaemic stroke (Al-Tamimi et al., 2011a, Bigalke et al., 2010) as well as inflammatory conditions such as thermal injury, sepsis and inflammatory bowel disease (IBD) (Montague et al., 2018b). In the latter three diseases, GPVI shedding was proposed to be triggered by fibrin engagement.

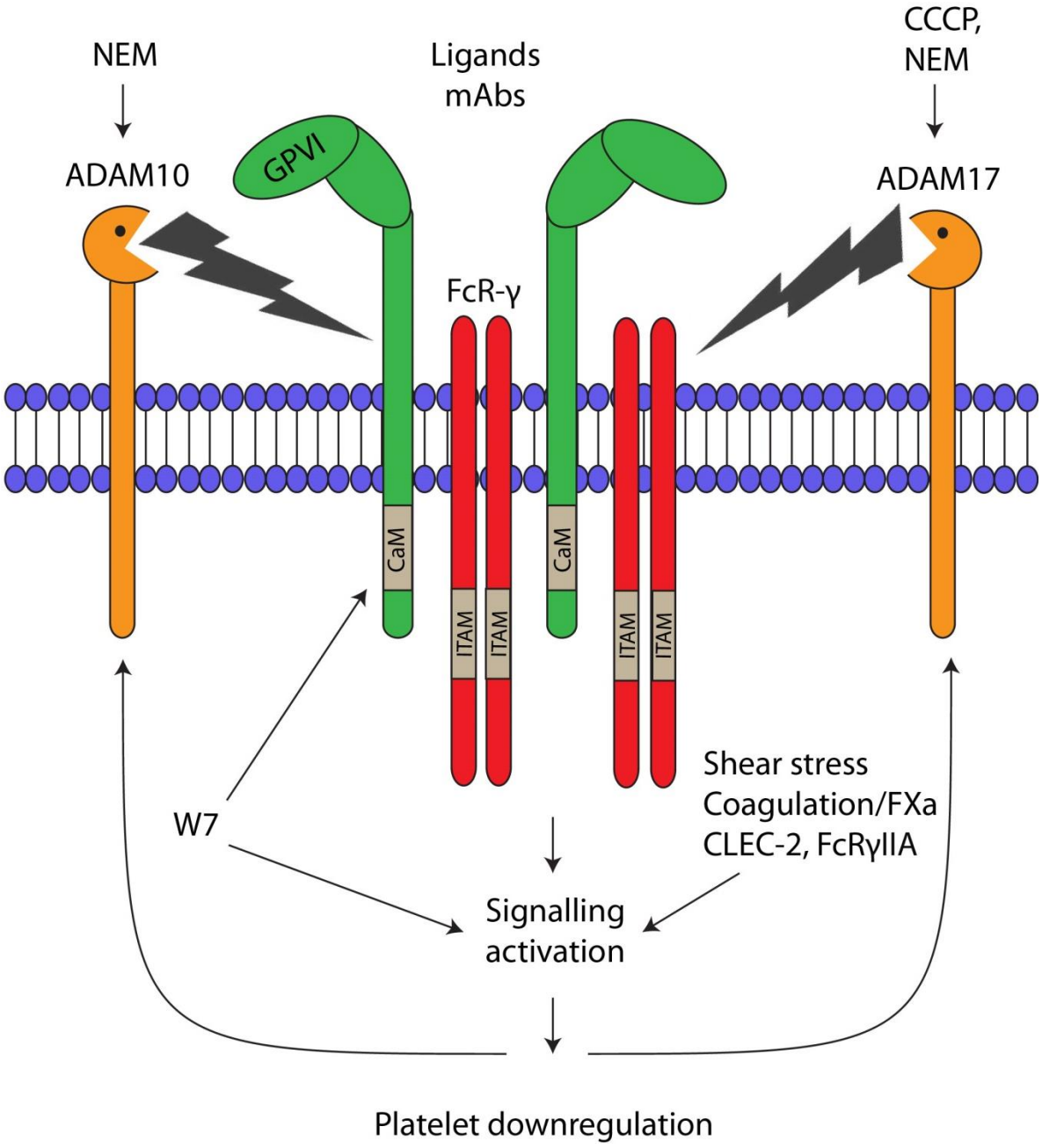

Figure 1.7. Different mechanisms of GPVI shedding. A variety of physiological/non-physiological stimuli induce GPVI shedding via different mechanisms. The CaM inhibitor W7 induces GPVI shedding through ADAM10 whereas CCCP, which damages the mitochondrial metabolism, triggers ADAM17-dependent cleavage. The general activator of metalloproteinases NEM leads to a robust GPVI proteolysis. The antibody-mediated GPVI shedding occurs *in vivo* but the specific protease implicated in this process is still unknown. Ligand engagement, exposure to shear stress and coagulation factors as well as activation of other (hem)ITAM-containing receptors represent other important stimuli involved in GPVI downregulation through the metalloproteinase-dependent proteolytic cleavage. Adapted from (Newman, 2010).

1.7 GPVI function in physiology and pathology

In light of its multitasking properties, the role of GPVI has been investigated in most of the canonical and newly-discovered platelet functions in both physiological and pathological processes. This section will provide an overview of the main regulatory functions of GPVI in haemostasis, thrombosis and beyond as well as the current anti-thrombotic approaches undertaken to target GPVI.

1.7.1 GPVI function in haemostasis and thrombosis

Although considered as a potent receptor activator in platelets from *in vitro* studies, deficiency of GPVI in human patients induced by genetic mutations (Arai et al., 1995, Dumont et al., 2009, Matus et al., 2013) or autoimmune processes (Boylan et al., 2004, Sugiyama et al., 1987, Takahashi and Moroi, 2001) results in a mild bleeding diathesis. The scarcity of clinical defects is reflected in different GPVI-deficient mouse models which exhibit only a moderate increase of time in tail bleeding assays. These include GPVI knockout mice (Kato et al., 2003, Lockyer et al., 2006), mice lacking GPVI due to FcR-γ deficiency (Nieswandt et al., 2000) and mice treated with antibodies against GPVI to induce the receptor immunodepletion (Nieswandt et al., 2001b). This discrepancy between *in vitro* and *in vivo* studies may be due to the redundant role of different platelet-activating pathways such as thrombin-mediated PAR4 activation. Indeed, GPVI and PAR4 double knockout mice exhibited a pronounced haemostatic defect (Bynagari-Settipalli et al., 2014). The same phenotype was found in mice lacking both GPVI and CLEC-2, highlighting the redundancy between the two receptors in the haemostatic process (Bender et al., 2013). In contrast, it is now accepted worldwide that GPVI is a crucial player in arterial thrombosis as demonstrated by *in vivo* models of experimental thrombosis. Loss of GPVI protects against occlusive thrombus formation in mechanical and $FeCl_3$ injury models (Bender et al., 2011, Cheli et al.,

2008) as well as experimentally induced pulmonary thromboembolism (Lockyer et al., 2006, Nieswandt et al., 2001b). On the contrary, thrombin but not GPVI has been proposed as a key player in thrombus formation in laser-induced vascular injury (Dubois et al., 2006, Mangin et al., 2006). Interestingly, the *in vivo* studies of experimental thrombosis suggested a predominant role for GPVI in thrombus growth and stabilisation, in accordance with the identification of fibrinogen and fibrin, which are involved in both stages of clot formation, as novel GPVI agonists (Bender et al., 2011, Onselaer et al., 2017). A role for GPVI has also been demonstrated in occlusive thrombus formation associated with the rupture of atherosclerotic plaques. In this context, GPVI is believed to be fundamental in the initial phase of clot development since it is the major receptor for collagen which is highly abundant in the atherosclerotic plaques (Kuijpers et al., 2009, Penz et al., 2005).

1.7.2 GPVI as a target for anti-thrombotic therapy

For its negligible role in haemostasis and restricted expression to MKs and platelets, GPVI is considered as a promising and safe target in anti-thrombotic therapy (Dütting et al., 2012). Different anti-platelet strategies, which target GPVI, are being investigated *in vitro* and *in vivo*, in order to evaluate benefits and drawbacks. One approach aims to inhibit GPVI-collagen interaction using fusion proteins (GPVI-Fc) which occupy the same collagen-binding site as GPVI. Revacept (under phase II clinical trial) is an example of this strategy. *In vivo* studies showed that Revacept successfully reduced arterial thrombosis without significant bleeding as well as improved the cerebral infarction size after ischaemic stroke (Goebel et al., 2013, Massberg et al., 2004). A similar, but possibly more powerful, procedure to block GPVI-collagen interaction relies on the use of anti-GPVI Fab fragments which irreversibly saturate the collagen-binding site on GPVI. The successful outcome of this approach is represented by the Fab fragment of the anti-GPVI monoclonal antibody OM4 which showed

in vivo anti-thrombotic protection without bleeding complications in rats (Li et al., 2007). This was corroborated by *ex vivo* studies conducted in cynomolgus monkeys using the Fab of the monoclonal antibody 9012.2 against human GPVI (Ohlmann et al., 2008) and the humanized anti-GPVI Fab ACT017 (Lebozec et al., 2017). An additional tactic implicates the use of inhibitors of key signalling kinases, such as SFKs, Syk or Btk in order to block GPVI-induced platelet activation (Busygina et al., 2018, Gratacap et al., 2009, Nicolson et al., 2018) but the major drawback of this strategy is the lack of specificity, since these kinases are also involved in immune cell signal transduction.

1.7.3 Roles of GPVI beyond haemostasis and thrombosis

Beyond its crucial role in thrombosis, GPVI is also involved in maintaining vascular integrity during inflammation. The importance of platelets in vascular integrity was first described by Goerge et al. (2008) when he observed severe bleeding in the skin, brain and lung of thrombocytopenic mice submitted to inflammatory stimulation (Goerge et al., 2008). Only a later study demonstrated that vascular integrity in the inflamed skin and lung requires GPVI as well as CLEC-2 (Boulaftali et al., 2013). This non-canonical haemostasis, also called 'inflammatory haemostasis', does not culminate in thrombus formation and does not require integrin αIIbβ3 signalling. Instead, it has been revealed that GPVI mediates the interaction of single platelets with collagen exposed at sites of neutrophil-inflicted vascular damage to seal the vessel and prevent haemorrhage in inflamed skin (Gros et al., 2015). In addition, GPVI-mediated vascular integrity is organ- and stimulus-dependent since its protection from inflammatory bleeding has been detected in the skin but not in the lung of mice with normal platelet count (Rayes et al., 2018). GPVI also plays a fundamental role in thromboinflammatory conditions such as ischaemic stroke as demonstrated by the elevated levels of sGPVI in the plasma of patients affected by this disease (Al-Tamimi et al., 2011a).

Experimental strategies using GPVI blocking antibodies or fusion proteins (e.g. Revacept) have been shown to successfully reduce the infarct size and improve the functional outcome in mouse models of ischaemic-reperfusion injury inflicted by middle cerebral artery occlusion (MCAO) (Goebel et al., 2013, Kleinschnitz et al., 2007). A recent study has shown that GPVI is also a key player in preventing bleeding during infection. GPVI knockout or immunodepleted mice, submitted to *Klebsiella pneumoniae*-driven sepsis, exhibited bacterial proliferation in the lung and in distant organs as well as reduction of platelet numbers, activation and platelet-leukocyte complex formation within the circulation (Claushuis et al., 2018). The beneficial function of GPVI in local host defence may be due to the enhanced recruitment and activation of leukocytes as it has been found in immune complex-mediated inflammation (Gros et al., 2015). On the contrary, GPVI has been reported to be the platelet target for the *Hepatitis C virus* (HCV) acting as a transporter of the virus to the lung (Zahn et al., 2006). Finally, the involvement of GPVI in experimental cancer metastasis has been shown only in one study where they found a reduction of ~50% of tumour foci in the lung carcinoma or melanoma cells of GPVI-deficient mice (Jain et al., 2009). Taking these data together, it is clear that GPVI represents one of the principal platelet mediators in a variety of pathological conditions and could be considered as a potential anti-platelet target in disorders beyond thrombosis such as inflammation and infection.

1.8 Application of super-resolution microscopy to the platelet biology

In the past few years, the advent of super-resolution microscopy has allowed the investigation of cellular ultrastructures and receptor organisation in a variety of biological systems, including platelets, with a resolution up to 10-fold higher over the conventional fluorescence microscopy (Poulter et al., 2018). In this section, we will provide an overview of the advantages and limitations of super-resolution microscopy to the platelet field with a

particular focus on *direct* STochastic Optical Reconstruction Microscopy (*d*STORM), since it has been widely employed in this PhD project.

1.8.1 Super-resolution microscopy

Due to their small size, lack of nucleus and complex ultrastructure, high-quality imaging in platelets has been a big challenge for many years. Electron Microscopy (EM) has been a powerful tool for the structural study of platelet cytoskeleton (Hartwig et al., 1999) and secretory granules (tot Pannerden et al., 2010). However, it does not provide any dynamic information and is also limited by the laborious sample processing. The advance of fluorescence microscopy has provided numerous benefits over EM, becoming the gold-standard microscopy technique in the platelet field due to the simple sample preparation and the ability to track the dynamics of multiple proteins in real-time (Renz, 2013). However, the diffraction limit of light represents a significant drawback of the fluorescence microscopy which restricts the imaging resolution to approximately 200-300 nm in *xy* and ~500 nm in *z*, interfering with the visualisation of nanoscopic cellular components, such as actin filaments and microtubules (~10 and ~25 nm in diameter, respectively) as well as lipid rafts (~20-50 nm in diameter). Discovered by the physicist Ernst Abbe in 1873, the diffraction barrier of light under an optical microscope does not permit resolution of two objects whose distance is less than half of the wavelength of the light (Abbe, 1873). This represents an important inconvenience in the study of platelet biology since fundamental spatial features underlie the diffraction limit. However, recently there has been a revolution in the microscopy field with the introduction of sub-diffraction imaging methodologies, also called super-resolution microscopy techniques, which have allowed the diffraction barrier of light to be overcome (Huang et al., 2010) and the nanoscale organisation of platelet receptors, signalling proteins and sub-cellular structures to be investigated (Poulter et al., 2018). SMLM (discussed in the

next section) and Structured Illumination Microscopy (SIM) are two of the most widely used super-resolution microscopy methodologies. Application of these advanced microscopy techniques has enabled the characterisation of the structure of actin nodules in human and mouse platelets, providing novel insights into the cytoskeletal dynamics during platelet spreading (Poulter et al., 2015b). Furthermore, they have proved to be powerful tools for the interrogation of receptors organisation within the platelet PM (Pollitt et al., 2014, Poulter et al., 2017) and for the diagnosis of platelet granule disorders (Westmoreland et al., 2016). Further applications of SMLM to the platelet biology will be discussed in the next section.

1.8.2 Single Molecule Localisation Microscopy

In conventional fluorescence microscopy, the entire set of fluorophores mapping a specific protein within the sample is excited and imaged at the same time, allowing the detection of a dense accumulation of molecules and resulting in a final poorly resolved image due to the resolution limit of light (Renz, 2013). SMLM techniques bypass the diffraction barrier of light by localising proteins of interest at the single molecule level via the temporal separation of dense fluorophores (Allen et al., 2013). This is achieved by exploiting the photochemical properties of a single fluorophore which is switched from a dark ("off") to a light ("on") state using high laser power and an oxidising and reducing buffer, allowing the 'blinking' performance to take place. At any one time, the majority of the fluorophores are in the dark state and only a small and sparse subset of them will enter the fluorescent state in a stochastic fashion. This way the centroid position of individual fluorescent emitter can be localised at each image frame with high precision by statistically fitting them to a point spread function (PSF) model, usually a two-dimensional (2D) Gaussian function. The repetitive iteration of activation, localisation and deactivation ('blinking' events) of single fluorophores over many thousands of frames results in a list of localisations to build up the final reconstructed image

with the highest resolution achievable, usually ~10-20 nm in the lateral dimensions (Fig. 1.8) (Allen et al., 2013). A critical parameter in SMLM is how precise the position of individual fluorescent emitter can be estimated, which highly affects the final image resolution. The localisation precision primarily depends on the photoswitching properties of the fluorescent probes (Dempsey et al., 2011). High photon yield per switching cycle allows determining the fluorophore position with high precision. Contrarily, high on/off duty cycle (the time frame a fluorophore remains in the light state) adversely affect the localisation precision. The switching performance of a specific fluorophore, in turn, is highly dependent on the imaging buffer composition and light intensity which need to be adapted in accordance with the photochemical properties of the probe (Dempsey et al., 2011). These and other factors such as the microscope setup (e.g. objective and optics) and the sample preparation (e.g. labelling density) are crucial determinants of the achievable spatial resolution.

STORM (Bates et al., 2007, Huang et al., 2008, Xu et al., 2017) and PhotoActivated Localisation Microscopy (PALM) (Betzig et al., 2006) are the first two SMLM techniques that have been developed and they differ in the labelling method for the protein of interest. STORM uses fluorescent dyes conjugated to antibodies whereas PALM relies on fluorescent proteins which also permit live-cell imaging. Among the different sub-types, *d*STORM is the most commonly used for its numerous advantages. It relies on commercial antibodies to label the epitope of interest in fixed samples and uses high laser power and an oxidising and reducing buffer to allow the photoswitching performance (Dempsey et al., 2011, Metcalf et al., 2013). It also enables three-dimensional (3D) (Huang et al., 2008) and multicolour imaging (Bates et al., 2007) as well as visualisation of intracellular proteins by cell permeabilisation or surface expressed receptors when combined with Total Internal Reflection Fluorescence Microscopy (TIRFM) (Huang et al., 2008, Poulter et al., 2017). In particular,

using an evanescent wave to illuminate and excite only the fluorescent molecules in a restricted sample area close to the interface between the liquid medium of the sample and the glass coverslip, TIRFM enables the selective imaging of fluorescently labelled proteins within the PM with high signal-to-noise ratio (Poulter et al., 2015a).

In the last few years, *d*STORM has been revealed to be a powerful spatio-temporal quantitative tool to extract important numerical information such as size and density, elucidating the protein patterning, topography or clustering in a range of biological systems (Nicovich et al., 2017). However, this potential suffers from significant caveats such as the unknown labelling ratio and the exact identification of 'single molecules' during the switching cycles (Annibale et al., 2011, van de Linde et al., 2010). High-quality antibodies and an optimised switching buffer can improve the imaging performance as well as reconstruction and quantification of the final images. These limitations restrict investigations in platelets to relative quantitative comparisons rather than absolute numbers since they are anucleate cells and therefore unable to be transfected with PALM photoswitchable tags characterised by a defined labelling stoichiometry (Betzig et al., 2006). However, recent work from Khan et al. (2017) has demonstrated the benefits provided by CRISPR-Cas9 in tagging PALM fluorophores at the cellular endogenous level without encountering the issues relating to the transfection (Khan et al., 2017). This genome tagging technology, in combination with the development of *in vivo* models or *ex vivo* platelet production from induced pluripotent stem cells (iPSC) (Thon et al., 2017), will significantly advance the field of high-resolution live-cell imaging in platelets.

Despite these limitations, numerous studies have demonstrated the benefits provided by *d*STORM imaging in the functional investigation of platelet structures and proteins. In

particular, Poulter et al. (2015) mapped the localisation of integrin αIIbβ3 and phosphorylated proteins at the platelet actin nodules employing *d*STORM imaging (Poulter et al., 2015b). In this way, they provided new insights into the structure of these actin foci, identifying phosphoprotein enriched-areas and integrin-depleted zones at the core of the nodule. Furthermore, Pollitt et al. (2014) and Poulter et al. (2017) demonstrated the importance of clustering for CLEC-2 and GPVI signalling exploiting the quantitative essence of *d*STORM (Pollitt et al., 2014, Poulter et al., 2017). In 2018, Mayr et al. and Lickert et al. characterised the actin cytoskeleton morphology in human platelets adopting this technology (Lickert et al., 2018, Mayr et al., 2018). Notably, Lickert et al. (2018) highlighted the diagnostic potential of *d*STORM imaging investigating the actin morphological changes in patients affected by bleeding disorders.

Ultimately, the highest *d*STORM performance, in terms of spatial resolution, would be achieved with the use of fluorescently conjugated single-domain antibodies, also called nanobodies, which are much smaller (15 kDa, ~2-4 nm) than conventional antibodies (150 kDa, ~15 nm) and Fabs (50 kDa, ~9 nm). This would place the fluorophore, which is what is localised in *d*STORM, closer to the protein/structure of interest thereby obtaining the best estimation of the true size and position of ultrastructures and signalling molecules in a variety of biological processes (Manglik et al., 2017, Pleiner et al., 2015, Traenkle and Rothbauer, 2017, Virant et al., 2018).

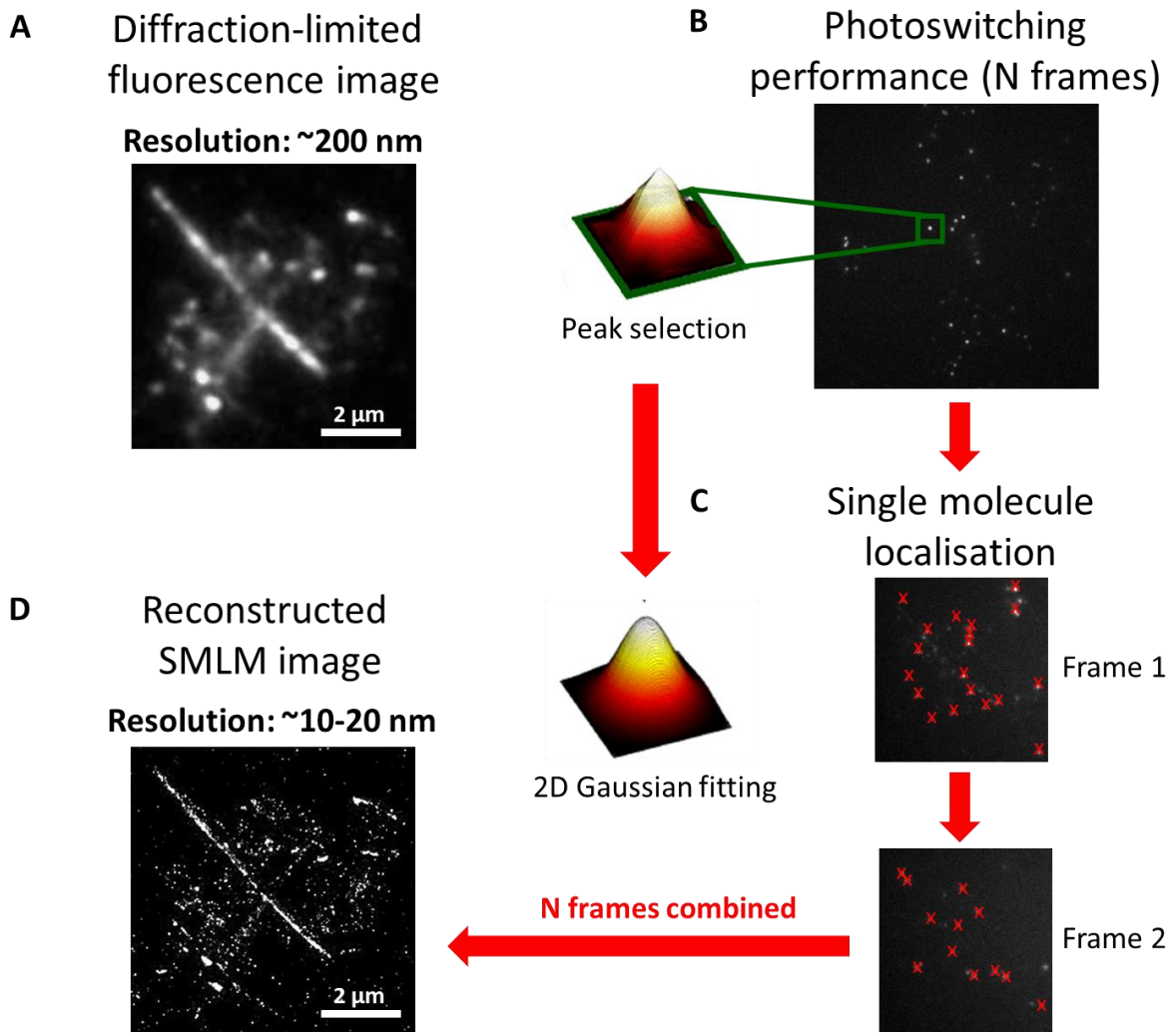

Figure 1.8. The basic principle of Single Molecule Localisation Microscopy. Diffraction-limited fluorescence image (resolution: ~200 nm) of GPVI (labelled with 1G5-Fab) in platelets spread on collagen and secondary labelled with anti-mouse Alexa Fluor 647 conjugated (A). Intense laser excitation and an oxidising and reducing buffer drive the majority of fluorophores to an "off" state, from which only a small and sparse subgroup of them stochastically become fluorescent in each frame (photoswitching performance, B). Single fluorophore positions are localised at each frame with high precision by fitting the point spread function (PSF) to a two-dimensional (2D) Gaussian model (C). Repetitive cycles of photoswitching events over a large number of frames allow to build up a final super-resolved image (resolution: ~10-20 nm, D).

1.9 Hypothesis and aims of the thesis

GPVI clustering at the platelet surface has been proposed as a key regulatory mechanism of platelet signalling and activation in response to collagen. While the advent of super-resolution microscopy techniques has allowed us to construct a detailed map of GPVI distribution at the platelet surface, we still have a rudimentary understanding of how these spatial events modulate platelet signalling. The hypothesis behind this thesis is that GPVI clustering mediates the strength and duration of signalling through the recruitment and incorporation of downstream signalling mediators, concentration of second messengers and exclusion of negative regulators. This hypothesis was tested following three main research lines:

1) Map the location of GPVI within the human platelet PM and explore receptor clustering employing current cluster analysis algorithms and developing further data analysis methods for the *d*STORM data of receptor localisation.
2) Investigate and correlate the mechanisms of GPVI clustering, signalling and shedding in platelets spread on an immobilised collagen monolayer.
3) Generate and validate nanobodies targeting human GPVI for use in super-resolution imaging.

CHAPTER 2

Materials and Methods

2.1 Materials for platelet function and nanobody studies

2.1.1 Antibodies and reagents

Tables 2.1 and 2.2 contain the detailed list of primary and secondary antibodies used for immunofluorescence and western blot. All the platelet agonists and inhibitors are listed in Tables 2.3 and 2.4, respectively. If unstated, the rest of the reagents used within this thesis derived from Sigma (Poole, UK).

Table 2.1. Primary antibodies

Primary antibody	Host species	Use	Source
1G5-Fab (Pan-GPVI)	Mouse	I: 2 µg ml^{-1}	Dr E. Gardiner (Canberra, Australia)
ADAM10 (11G2)-Alexa Fluor 647 mAb	Mouse	I: 0.5 µg ml^{-1}	Abcam (Cambridge, UK) and Alexa647-conjugated by Dr M. G. Tomlinson (Birmingham, UK)
α-GPVI cytoplasmic tail	Rabbit	I: 5 µg ml^{-1} WB: 1 µg ml^{-1}	Dr E. Gardiner (Canberra, Australia)
α-LAT polyclonal antibody (pAb)	Rabbit	I: 5 µg ml^{-1} WB: 2 µg ml^{-1}	Millipore Merck (Abingdon, UK)
α-phosphotyrosine (4G10) mAb and 4G10-Alexa Fluor 647	Mouse	I: 5 µg ml^{-1} WB: 1 µg ml^{-1}	Millipore Merck (Abingdon, UK)
α-tubulin mAb	Mouse	WB: 1 µg ml^{-1}	Sigma-Aldrich (Poole, UK)
CD49b (integrin α2β1) mAb	Mouse	I: 5 µg ml^{-1}	abD Serotec (Oxford, UK)
LAT pY200 pAb	Rabbit	I: 5 µg ml^{-1} WB: 2 µg ml^{-1}	Abcam (Cambridge, UK)
PE human CD62-P (P-selectin)	Mouse	FC: 1/40	BioLegend (San Diego, CA, USA
PLCγ2 (Q-20) pAb	Rabbit	WB: 5 µg ml^{-1}	Santa Cruz Biotechnology (Dallas, USA)
PLCγ2 pY1217 pAb	Rabbit	WB: 4 µg ml^{-1}	Cell Signalling Technology (Hitchin, UK)

Syk (4D10) mAb	Mouse	WB: 5 µg ml^{-1}	Santa Cruz Biotechnology (Dallas, USA)
Syk (N-19) pAb	Rabbit	I: 5 µg ml^{-1} WB: 5 µg ml^{-1}	Santa Cruz Biotechnology (Dallas, USA)
Syk pY525/526 pAb	Rabbit	I: 5 µg ml^{-1} WB: 4 µg ml^{-1}	Cell Signalling Technology (Hitchin, UK)
Syk pY525/526-Alexa Fluor 647 mAb	Rabbit	I: 5 µg ml^{-1}	Cell Signalling Technology (Hitchin, UK)

I, immunofluorescence; WB, western blot; FC, flow cytometry

Table 2.2. Secondary antibodies

Secondary antibody	Host species	Use	Source
His_6 and HA HRP conjugated	Rabbit	WB, E: 1/2000	Bethyl Laboratories, Montgomery, TX, USA)
His_6 HRP conjugated	Mouse	FC: 1/500	BioLegend (San Diego, CA, USA)
His_6 Alexa Fluor 647 conjugated	Mouse	FC: 1/80 I: 1/300	Thermo Fisher Scientific (Waltham, MA, USA)
HA Alexa Fluor 647 conjugated	Mouse	FC: 1/20	R&D Systems (Abingdon, UK)
Mouse IgG HRP conjugated	Sheep	WB: 1/10,000	GE Healthcare (Bucks, UK)
Rabbit IgG HRP conjugated	Donkey	WB: 1/10,000	GE Healthcare (Bucks, UK)
Mouse and Rabbit IgG IRDye 800CW conjugated	Goat	WB: 1/10,000	antibodies-online GmbH (Aachen, Germany)
Mouse and Rabbit IgG Alexa Fluor 647 or 488 conjugated	Goat	I: 1/300	Thermo Fisher Scientific (Waltham, MA, USA)

I, immunofluorescence; WB, western blot; E, ELISA; FC, flow cytometry

Table 2.3. Agonists

Agonist	Target receptor	Source
Collagen (Horm)	GPVI, α2β1	Takeda (Linz, Austria)
Collagen-related peptide-cross linked (CRP-XL)	GPVI	Dr R.W. Farndale (Cambridge, UK)
Fibrinogen (FIB 3; plasminogen-, vWF- and fibronectin-depleted)	αIIbβ3	Enzyme Research Laboratories (Swansea, UK)
Fibrinogen-Alexa 488	αIIbβ3	Invitrogen (Life Technologies, Paisley, UK)
PAR1 peptide	PAR1	Alta Bioscience (Birmingham, UK)
Thrombin	PAR1, PAR4	Sigma-Aldrich (Poole, UK)

Table 2.4. Inhibitors

Inhibitor	Target	Use	Source
AEBSF	Serine proteases	2 mM	Calbiochem (San Diego, USA)
Aprotinin	Serine proteases	10 μg ml^{-1}	Sigma-Aldrich (Poole, UK)
Apyrase	ATP	2 U ml^{-1}	Sigma-Aldrich (Poole, UK)
GI254023	ADAM10 inhibitor	2 μM	Scientific Laboratory Supplies (Nottingham, UK)
GM6001	Broad MMP inhibitor	100 μM	Millipore Merck (Abingdon, UK)
Indomethacin	Cycloxygenase	10 μM	Sigma-Aldrich (Poole, UK)
Integrilin	αIIbβ3	9 μM	QE Hospital (Birmingham, UK)

Leupeptin	Cysteine, serine and threonine proteases	10 µg ml^{-1}	Enzo Life Sciences (Exeter, UK)
Pepstatin	Aspartyl proteases	1 µg ml^{-1}	Sigma-Aldrich (Poole, UK)
PP2	Src-family tyrosine kinases (SFKs)	20 µg ml^{-1}	TOCRIS (Abingdon, UK)
PPACK	Thrombin	20 µM	Cambridge Biosciences (Cambridge, UK)
Prostacyclin (PGI_2)	Platelets	0.1 µg ml^{-1}	Cayman Chemicals (Cambridge, UK)
PRT-060318	Syk kinase	10 µg ml^{-1}	Caltag Medsystems (Buckingham, UK)
Sodium Orthovanadate (Na_3VO_4)	Tyrosine phosphatases	5 mM	Sigma-Aldrich (Poole, UK)

2.2 Human platelet isolation

Human washed platelets were prepared from blood samples donated by healthy, consenting volunteers under the following licence: ERN_11-0175 'The regulation of activation of platelets' (University of Birmingham). Blood was drawn via venipuncture into the anticoagulant sodium citrate and then acid/citrate/dextrose (ACD: 97 mM sodium citrate, 111 mM glucose and 71 mM citric acid) added to 10% (v:v). Blood was centrifuged at 200 × g for 20 min at room temperature (RT). Platelet-rich plasma (PRP) was collected and centrifuged at 1,000 × g for 10 min in the presence of 0.1 μg ml^{-1} PGI_2. Plasma was removed and the platelet pellet was resuspended in modified Tyrode's-HEPES buffer (129 mM NaCl, 0.34 mM Na_2HPO_4, 2.9 mM KCl, 12 mM $NaHCO_3$, 20 mM HEPES, 5 mM glucose, 1 mM $MgCl_2$; pH 7.3) containing ACD and 0.1 μg ml^{-1} PGI_2 before centrifugation at 1,000 × g for 10 min. The washed platelet pellet was resuspended in modified Tyrode's-HEPES buffer and left to rest for 30 min at RT. The platelet count was measured using the Coulter Z_2 Particle Count and Size Analyzer (Beckman Coulter Ltd, High Wycombe, UK). The platelet concentration was then adjusted in accordance with the experimental procedure. All the studies described in this thesis were performed on human platelets.

2.3 Platelet function assays

2.3.1 Light transmission aggregometry (LTA)

After adding to a glass aggregometer cuvette with a stirrer bar, washed platelets (2×10^8 cells ml^{-1}) were pre-warmed at 37 °C for 2 min in a Chrono-log 700 Lumi-Aggregometer (Havertown, PA, USA). An additional glass vial with the same volume of modified Tyrode's-HEPES buffer was used as a blank. Warmed platelets were then stirred at 1200 rpm for 1 min. The function of kinases inhibitors (PP2 and PRT-060318) was tested by pre-incubating

platelets with increasing concentrations of each drug for 5 min. To induce platelet aggregation, Horm collagen at 10 μg ml^{-1} was added and the response was monitored for 5 min under constant stirring conditions (1200 rpm). The area under the curve (AUC) was measured using the AGGRO/LINK8 software (Chrono-Log, Havertown, PA, USA).

In the nanobody study, collagen (3 μg ml^{-1})-induced platelet aggregation after nanobody treatment (5 min at 10 μg ml^{-1}) was monitored using Chrono-Log Optical Aggregometer (Labmedics, Manchester, United Kingdom), following the protocol described above.

2.3.2 Platelet spreading and staining

For confocal and epifluorescence imaging, 13 mm #1.5 glass coverslips (VWK, UK) were coated with 10 μg ml^{-1} Horm collagen diluted in a manufacturer-supplied diluent. For *d*STORM imaging, glass bottomed dishes (MatTek Corporation, Ashland, MA, USA) were also coated with 10 μg ml^{-1} CRP-XL or 100 μg ml^{-1} fibrinogen diluted in phosphate-buffered saline (PBS). Fibrin coating of the dish was achieved as described below. Substrate-coated coverslips and dishes were left overnight at 4°C, before being blocked in 5 mg ml^{-1} heat-inactivated fatty acid-free bovine serum albumin (BSA) for 1 hour at RT. Washed and rested platelets were diluted to 2×10^7 cells ml^{-1} in modified Tyrode's-HEPES buffer and allowed to spread on the substrate-coated surfaces for different time points at 37 °C. When required, washed platelets were labelled with 2 μg ml^{-1} 1G5-Fab against Pan-GPVI (Al-Tamimi et al., 2009) for 10 min at 37 °C before spreading. Where stated, platelets were also incubated with inhibitors or the control vehicle before or after spreading. To evaluate the effect of the nanobodies on collagen-induced platelet spreading, platelets were pre-treated with 10 μg ml^{-1} nanobodies for 10 min at 37 °C. Adhered cells were PBS-washed and fixed with 10% neutral buffered Formalin solution for 10 min at RT. To allow imaging of actin cytoskeleton and

intracellular proteins, spread platelets were also permeabilised with 0.1% Triton X-100 in PBS for 5 min, prior to blocking with 1% BSA + 2% Goat serum (in PBS) for at least 30 min. As stated, F-actin and platelet proteins were labelled with Alexa Fluor 488® phalloidin (1/300, Invitrogen, Life Technologies, Paisley, UK) and specific fluorescently-conjugated primary antibodies or primary + fluorescent secondary antibodies, respectively. For confocal and epifluorescence imaging, samples were mounted on glass slides using Hydromount solution (National Diagnostics, Atlanta, USA), and stored at RT. Samples for *d*STORM imaging were stored in PBS at RT until imaged.

2.3.3 Fibrin generation

*d*STORM MatTek dishes were incubated with 100 μg ml^{-1} fibrinogen for 30 min at RT. To allow fibrin generation, 1 U ml^{-1} thrombin was added to fibrinogen-coated dishes and incubated for an additional 15 min before being stored at 4°C overnight. Thrombin was then neutralised by addition of 20 μM PPACK diluted in 5 mg ml^{-1} heat-denatured BSA for 1 hour at RT. After PBS-washes, fibrin-coated dishes were left at RT, ready for platelet spreading and immunostaining. In another study, to confirm fibrin production by fluorescent imaging, glass coverslips were coated with 100 μg ml^{-1} fibrinogen-Alexa 488 and the above procedure carried out.

2.3.4 Protein phosphorylation and receptor shedding assays

2.3.4.1 Protein lysate preparation from platelets in solution

Washed platelets were diluted to 5×10^8 cells ml^{-1} in modified Tyrode's-HEPES buffer and pre-treated with 9 μM integrilin to prevent platelet aggregation. In GPVI shedding experiments, platelets were supplemented with 2 mM $CaCl_2$. Platelets were left to warm in the aggregometer vials for 1 min at 37 °C using the Chrono-Log Optical Aggregometer

(Labmedics, Manchester, United Kingdom). Warmed platelets were then stirred at 1200 rpm for 1 min prior to agonist stimulation. 30 μg ml^{-1} Horm collagen was added to the platelet suspension and stimulated for 90 sec, 15 min, 30 min, 1 hour and 3 hours. Unstimulated samples were treated with collagen diluent (vehicle) for the same times. For GPVI cleavage studies, platelets were stimulated with the thiol-modifying reagent NEM (2mM, Millipore Merck, Abingdon, UK) under the same stirring conditions for 1 hour. To investigate whether nanobodies induced GPVI-shedding, platelets were stimulated with 4 μg ml^{-1} nanobodies or PBS (vehicle) for 1 hour before lysis. Activation was stopped by the addition of of 2x lysis buffer (300 mM NaCl, 20 mM Tris, 2 mM EGTA, 2 mM EDTA, and 2% NP-40 detergent), pH 7.4 supplemented with protease inhibitors [2 mM Na_3VO_4, 2 mM 4-(2-Aminoethyl) benzenesulfonyl fluoride hydrochloride (AEBSF), 10 μg ml^{-1} leupeptin, 10 μg ml^{-1} aprotinin and 1 μg ml^{-1} pepstatin]. Whole-cell lysates (WCLs) were resuspended in 5x reducing sodium dodecyl sulfate (SDS) sample buffer (10 mg ml^{-1} SDS, 25% 2-mercaptoethanol, 50% glycerol, 25% Stacking buffer, small amount of Brilliant Blue). Platelet lysates were stored at -20°C until tested.

2.3.4.2 Protein lysate preparation from spread platelets

6-well plates were coated overnight at 4°C with 10 μg ml^{-1} Horm collagen and then blocked in 5 mg ml^{-1} heat-denatured BSA for 1 hour at RT. Washed platelets, diluted to 5×10^8 cells ml^{-1} in modified Tyrode's-HEPES buffer and pre-incubated with 2 mM $CaCl_2$ for receptor shedding assays, were spread on the collagen-coated surface for 15 min, 30 min, 1 hour and 3 hours at 37 °C. Where indicated, inhibitors or the control vehicle were added to the platelets before or after spreading. Non-adhered platelets were removed and lysed with 2x lysis buffer. Adhered and spread platelets were PBS-washed and then lysed with 1x lysis buffer. The concentration of both lysates was measured using a Protein Assay kit (Bio-Rad,

Hemel Hempstead, UK). Once diluted to the same concentration in lysis buffer, platelet lysates were supplemented with an adequate volume of 5x reducing sample buffer and stored at -20°C until used.

2.3.4.3 SDS-PAGE and Western blotting

Platelet lysate samples were denatured at 95°C for 10 min and centrifuged at 13000 × rpm for 5 min at 4°C to pellet insoluble material. Pre-cast polyacrylamide gels, Bolt or NuPAGE 4-12% Bis-Tris Plus (Invitrogen, Life Technologies, Paisley, UK) were used to run samples. Proteins resolved by sodium dodecyl sulfate-polyacrylamide gel electrophoresis (SDS-PAGE) were transferred to a low-autofluorescence polyvinylidene difluoride (PVDF) membrane (Trans-Blot Turbo RTA Midi LF PVDF transfer kit, Bio-Rad, Hemel Hempstead, UK) using a Bio-Rad semi-dry Turbo transfer system. The broad range (11-245 kDa) colour prestained protein standard was used to evaluate the molecular weight (MW) (New England BioLabs/NEB, Hitchin, UK). After transfer, the membrane was blocked for 1 hour at RT in blocking buffer [3% BSA (w:v), 0.1% sodium azide (w:v) and 0.1% (v:v) Tween-20 Tris-buffered saline (TBS-T, 200 mM Tris, 1.37 M NaCl, 0.1% Tween-20, pH 7.6)]. The blocked membrane was then incubated with specific primary antibodies diluted in 3% BSA blocking buffer overnight at 4°C. Membrane washing (3 x 10 min) to remove unbound primary antibodies was executed in TBS-T before incubating with fluorophore 800 or horseradish peroxidase (HRP) conjugated secondary antibodies (1/10,000 in TBS-T) for 1 h at RT as indicated. To remove unbound secondary antibodies, the TBS-T washing (3 x 10 min) was repeated. For the chemiluminescence-based detection of proteins, the immunoblotted membrane was then revealed using the enhanced chemiluminescence (ECL) substrate (Thermo Fisher Scientific, Waltham, MA, USA). Both chemiluminescent and fluorescent blots were scanned using the Odyssey Fc System (LI-COR Biosciences, Cambridge, UK).

When stated, autoradiographic film was used for the chemiluminescence visualisation. Quantification of the band intensities was performed using LI-COR Image Studio v5.2.

For loading control, the TBS-T-washed membrane was incubated in Stripping buffer (TBS-T + 2% SDS) supplemented with 1% β-mercaptoethanol for 15 min at 80°C followed by another β-mercaptoethanol-free stripping cycle (15 min at 80°C). To remove the remnant stripping buffer, the membrane was washed in TBS-T (3 x 10 min), blocked in 3% BSA and incubated with loading control antibodies overnight at 4°C as above.

2.4 Imaging

2.4.1 Epifluorescence imaging

Single-colour phalloidin-Alexa 488-stained F-actin and dual-colour imaging of Alexa 488 and 647-labelled platelets spread on collagen were performed using a Zeiss Axio Observer 7 Epifluorescent microscope equipped with a 63 × 1.4 NA oil immersion lens, Colibri 7 LED light source, Zeiss Filter sets 38 and 50 for GFP/FITC and Cy5/647, respectively and Hamamatsu ORCA Flash 4 LT sCMOS camera for the image acquisition. Differential interference contrast (DIC) images were also taken (intensity = 7.0 V and exposure time = 100 ms) to visualise the collagen distribution. For each condition, 5 separate fields of view (FOVs) were imaged (intensity = 20% and 25% and exposure time = 200 ms and 100 ms for 488 and 647, respectively) within the Zen Pro v2.3 software and then analysed in Fiji v1.52 (Schindelin et al., 2012).

2.4.2 Confocal imaging

2.4.2.1 Leica TCS SP2

Spread platelets mounted on glass slides were imaged using a Leica TCS SP2 confocal system with an HCX Plan Apo Lbd.BL 63 × 1.4 NA oil immersion objective lens. The Leica

confocal software version 2.61 Build 1537 was implemented to acquire 5 random z-stacks (step size 0.25 µm) for each condition at a resolution of 1024 x 1024 pixels and zoom of 4. Phalloidin-Alexa 488-labelled platelets were imaged with the 488 nm line of the Argon laser whereas Alexa-647-stained platelets with the 633 nm line of the HeNe laser. Dual-colour labelled platelets were imaged simultaneously. Single-plane reflection images were also taken to monitor the location of collagen fibres. The images were then processed using ImageJ v1.48 (NIH, Bethesda, USA).

2.4.2.2 Zeiss LSM880 with Airyscan Fast

Dual-colour imaging of platelets adhered to collagen and stained with Alexa-647 for GPVI and Alexa-488 for phosphotyrosine proteins was carried out using a Zeiss LSM 880 confocal microscope with Airyscan Fast detector equipped with a Plan Apo 63 × 1.2 NA water immersion objective lens, a 25-mW multiline Argon 458, 488, 514-nm laser and a 5-mW HeNe 633-nm laser for 488 and 647 excitation, respectively. At least 5 z-stacks with a step size 0.2 µm were randomly taken within the coverslip with simultaneous imaging of the two channels. The format size of the images was set to 512 x 512 pixels whereas the zoom was adjusted to 3. Collagen distribution was followed using the transmitted light T-PMT. Image acquisition and processing were executed within the Zen Pro v2.3 software.

2.4.3 *d*STORM imaging

Super-resolution imaging of GPVI receptors was performed using a Nikon N-STORM system in TIRF and *d*STORM mode with a 100 × 1.49 NA TIRF objective lens. The system includes a Ti-E microscope stand with Perfect Focus, an Agilent Ultra High Power Dual Output Laser bed with 170-mW 647-nm and 20-mW 405-nm lasers for the fluorophore excitation and an Andor IXON Ultra 897 EMCCD camera for the image capture. DIC and TIRF images were

acquired on random FOVs containing both platelets and collagen fibres. An oxidizing and reducing buffer (100 mM MEA, 50 μg ml^{-1} glucose oxidase and 1 μg ml^{-1} catalase diluted in PBS, pH 7.5) was used to allow the photoswitching performance (Metcalf et al., 2013). The N-STORM emission cube, combined with the gradual increase of the 405 laser power (5% every 30 sec) to restore the appropriate number of blinking cycles, allowed the single-colour (Alexa647) imaging of labelled GPVI. Simultaneous dual-colour (Alexa647 and Alexa488) imaging was carried out using the Nikon Quad Cube. For each FOV and each colour, 20,000 frames were acquired in Nikon NIS Elements v4.5 software using an exposure time of 9.2 (*Chapter 3*) or 20 ms (*Chapter 4*), gain 300 and conversion gain 3. To generate the final super-resolved images, the Nikon STORM analysis module v3.2 was implemented, with the application of the drift correction and Gaussian rendering (*Chapter 3*). To remove poorly localised detections, a photon count filtering (>500 photons) was applied to the reconstructed images before further processing. Where indicated, the ThunderSTORM plugin for Fiji (Ovesný et al., 2014) was adopted to reconstruct the final images with the application of the Gaussian PSF model and the maximum likelihood estimator to fit the position of the fluorescent molecules. Drift correction and photon intensity filtering (>1000 photons) were applied within ThunderSTORM to post-process the reconstructed images. To minimise the 'multiblinking' artifacts, detections within 75nm of another detection either in the same or subsequent frames were merged. The pointillistic datasets, which contain the spatial coordinates for each detected fluorescent blink, were finally exported as text files before being analysed with different cluster algorithms (described below).

2.5 Image analyses

2.5.1 Platelet spreading data analysis

The confocal and epifluorescence images of platelets spread on collagen were assessed for platelet count and surface area using the open-source KNIME software (Berthold et al., 2009) where an Ilastik (Sommer et al., 2011) pixel classifier was implemented to construct a binary cell segmentation. The centre of each single platelet was set manually to divide attached cells. The coordinates of the cell centre positions were then used to generate the final segmentation employing a watershed-based transformation algorithm. Only objects with a size > 1 μm^2 were included in the final analysis. This is a validated data analysis for platelet spreading within the Birmingham Platelet Group.

2.5.2 Colocalisation analysis

Qualitative and quantitative colocalisation analyses of GPVI and phospho-proteins were performed using Fiji v1.52 (Schindelin et al., 2012). For the qualitative colocalisation analysis, the maximum intensity projections of z-stacks of the two individual colours were thresholded using the Fiji Default method and multiplied obtaining the colocalisation mask which shows only the colocalising pixels. For the quantitative colocalisation analysis, regions of interest (ROIs) were drawn around single platelet or group of platelets randomly chosen within the FOV and the Plugin Coloc2 was implemented to measure the degree of colocalisation using the Pearson's correlation coefficient.

2.5.3 Ca^{2+} mobilisation analysis

For Ca^{2+} mobilisation analysis, washed platelets, diluted to 2×10^8 cells ml^{-1} in modified Tyrode's-HEPES buffer, were incubated for 45 min at 37°C with 1 μM Oregon green-488 BAPTA-1-AM (Invitrogen, Life Technologies, Paisley, UK) and spun at 1000 × g for 10 min

in the presence of 2.8 μM PGI_2 and ACD. The platelet pellet was then resuspended in the same volume of modified Tyrode's-HEPES buffer and left to rest for at least 30 min before diluting to 2×10^7 cells ml^{-1} for spreading. Rested platelets were then exposed to collagen-coated MatTek dishes, prepared as previously described, allowing adhesion and spreading. Live-cell imaging of Ca^{2+} mobilisation was tracked using a Zeiss Axio Observer 7 Epifluorescent microscope previously described. Where indicated, the SFK inhibitor PP2 (20 μM) and the Syk inhibitor PRT-060318 (10 μM) or the vehicle (DMSO) were added to the platelets after 45 min of spreading. Images were then acquired every 1 sec for 2 min using Zen Pro v2.3 software. Once processed in Fiji v1.52 (Schindelin et al., 2012), the percentage of spiking platelets, number of spikes per platelet, amplitude and peak duration were measured using a custom-made algorithm in MATLAB (Mathworks, Inc., Natick, MA) in each single platelet within one representative FOV (~150 cells) for each condition. Signals were baseline-corrected by application of a linear top-hat filter. A threshold of 20 fluorescence units was set for identification of spikes and the duration of a spike was defined as the time for fluorescence to reduce to below this threshold. The MATLAB code was written by Christopher O'Shea (University of Birmingham, UK) and can be found in Appendix I.

2.5.4 Cluster analyses

2.5.4.1 Ripley's K-function-based cluster analysis

Cluster analysis of GPVI was performed on the STORM images in MATLAB using a custom-made algorithm based on Ripley's K-function., as described by (Owen et al., 2010) with the adjustments detailed in (Pollitt et al., 2014). For each image, ROIs were selected within platelets and on and off collagen fibres. In the MATLAB code, the ROI size (2 x 2 μm^2), cluster size (radius = 25, 50 or 100 nm) and threshold [L(r) = 50, 100 or 150] were

selected. After running the MATLAB code on the reconstructed image data, a cluster heat map, a binary map of clusters and an Excel file, containing quantitative information such as the number of clusters, number of localisations in clusters, percentage of localisations in clusters and cluster area, were obtained (Fig. 2.1). The threshold value was applied to the cluster heat map to create a binary map of clusters. Areas of the cluster heat map below the threshold were described as holes whilst areas above the threshold were identified as clusters. For GPVI clustering quantification, at least 50 ROIs on and off collagen fibres for each condition were analysed, discounting the clusters with a number of localisations <3.

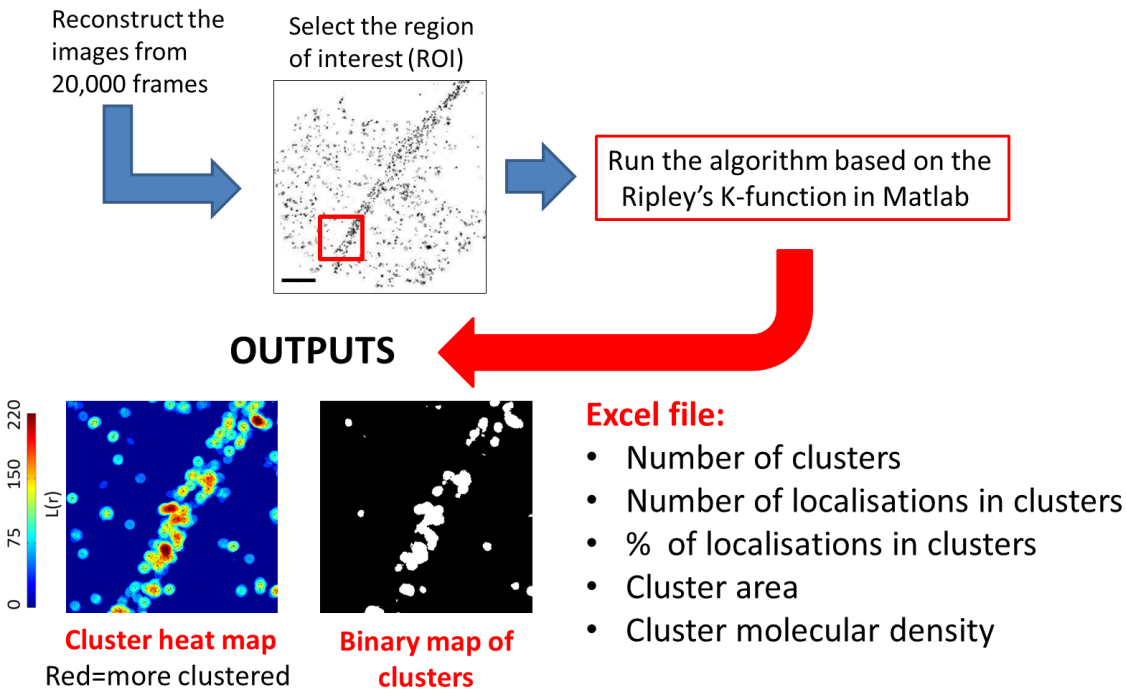

Figure 2.1. Ripley's K-function-based cluster analysis workflow. 2 x 2 μm^2 ROIs were placed on the reconstructed *d*STORM images in regions along visible collagen fibres and areas outside the fibres within the boundaries of the platelets. The clustering parameters (ROIs size, radius and threshold) were set within the MATLAB code before running the algorithm on the *d*STORM pointillistic datasets. The cluster analysis generated the following outputs: 1) a cluster heat map showing the degree of clustering L(r) where red represents highly clustered localisations; 2) a binary map highlighting the clusters as defined by the threshold and 3) an Excel file containing quantitative information relative to the detected clusters.

2.5.4.2 One-level and two-level DBSCAN-based cluster analyses

The single-level cluster analysis of GPVI was carried out on the *d*STORM pointillistic datasets by grouping individual detected localisations, including those on the edges, into clusters applying the Density-Based Spatial Clustering of Applications with Noise (DBSCAN) (Ester et al., 1996). This analysis was implemented using the R library RSMLM (Pike et al., 2019) and KNIME (Berthold et al., 2009) (workflow available in Appendix II). In the clustering settings, the radius of the neighbouring localisations was set to 50 nm and the minimum number of reachable detections was adjusted to 10 unless otherwise stated. Clusters with <10 points were discarded within the analysis. GPVI clustering on Horm collagen was also executed at two spatial layers using different parameter values within the KNIME workflow (available in Appendix II). The two-level cluster analysis was performed by first isolating large clusters, corresponding to the collagen fibres (Level I), and then segmenting these large clusters into nanoclusters using different clustering parameters (Level II). The radii of the neighbouring localisations were set to 75nm and 30nm for Level I and II, respectively and the minimum number of reachable detections was adjusted to either 3 or 10 for the different levels. Clusters with less than either 100 (Level I) or 10 (Level II) detections were removed. For the single-level and two-level analyses, the union of circular regions (radius = 30 nm) positioned around each point in a cluster was used to measure the cluster area applying a grid of 5 nm pixels and image-based dilation. The clustering analyses were carried out on the whole FOV and the outputs were exported as Excel files. This analysis was designed and implemented in collaboration with Dr Jeremy Pike, COMPARE Imaging Analyst, University of Birmingham, UK.

2.5.4.3 Voronoï tessellation

Clustering of GPVI was assessed on the localisation-based datasets employing the free software SR-Tesseler based on the Voronoï tessellation (Levet et al., 2015). The Voronoï diagram was computed on whole FOVs within the platform in order to assign each point to a polygonal area. The first level of segmentation created 'objects' after setting a density factor δ of 2 and a minimum area of 1µm x 1µm. In the study of GPVI clustering on collagen, these settings were chosen to isolate only the localisations aligned along visible collagen fibres. In the second level of segmentation, the density factor δ was set to 0.5 and a minimum number of points was adjusted to 10 in order to generate clusters within the detected objects. Quantitative information relative to objects and clusters were outputted into an Excel file.

2.6 Generation of nanobodies targeting human GPVI

2.6.1 Nanobody library construction and phage display selection

The generation of nanobodies raised against human GPVI was contracted out to the company VIB Nanobody Core (Brussel, Belgium). A brief outline of the method they used is detailed here. We provided VIB with recombinant human GPVI fused to human IgA Fc (Fcα) with a His_6 tag at the C-terminus [kindly made by Andrew B. Herr's lab, Cincinnati Children's Hospital, USA and detailed in (Horii et al., 2009)] which was used for the immunization of two llamas. A control protein containing the same Fc region was also supplied to allow for negative screening and the selection of GPVI-specific clones. Using the phagemid vector pMECS, a VHH library was constructed from each llama to screen for the presence of antigen-specific nanobodies. In total, 190 colonies from two rounds of pannings were randomly selected and analysed by ELISA for the presence of GPVI-specific nanobodies in their periplasmic extracts. Out of these, 86 colonies scored positive in the ELISA assay.

Based on sequence data of the positive colonies, 54 different full-length nanobodies were distinguished, belonging to 33 different complementarity-determining region (CDR)3 groups. VIB provided us with *E. coli* TG1 strains harbouring the recombinant phagemid pMECS containing the 54 nanobody genes ready for their production and characterisation in our assays. The main steps of nanobodies production are schematized in Fig. 2.2.

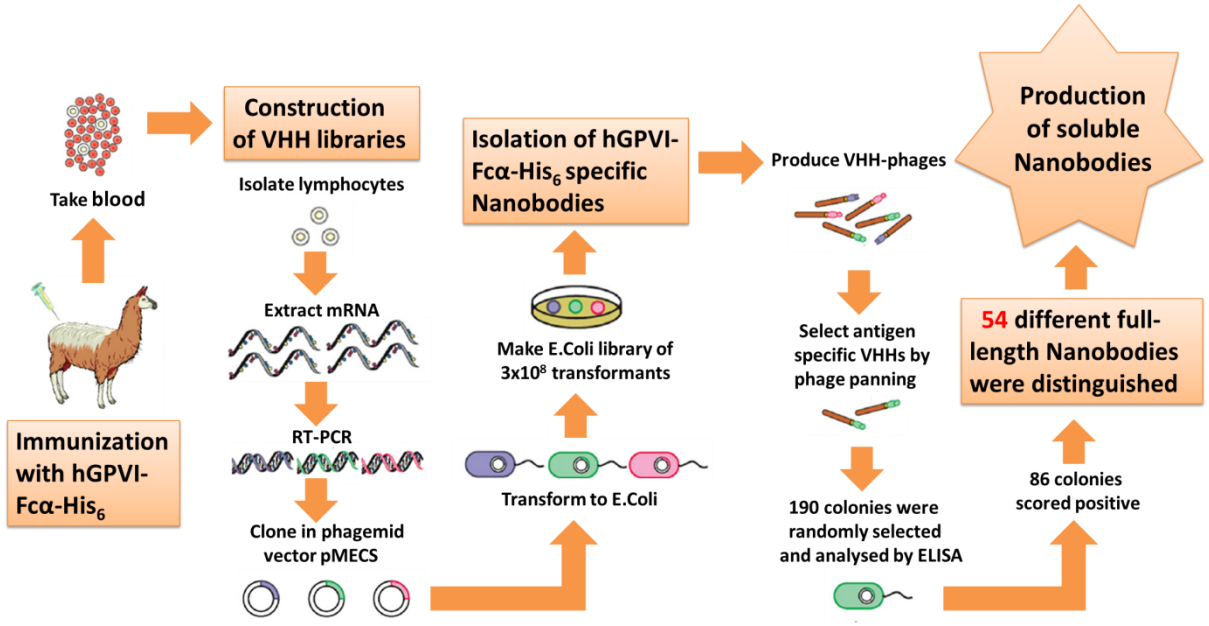

Figure 2.2. Overview of anti-GPVI nanobody generation. The production of nanobodies targeting human GPVI can be divided into three main steps: 1) immunization: two llamas were immunized with recombinant human GPVI fused to IgA Fc and His_6 tag (hGPVI-Fcα-His_6); 2) construction of VHH libraries: the RNA extracted from the lymphocytes of each llama was transformed into complementary DNA (cDNA) and amplified via reverse transcriptase-polymerase chain reaction (RT-PCR). The nanobody encoding sequences were then cloned into the PstI and NotI sites of the phagemid vector pMECS which was used to transform *E. coli* strains. Two VHH libraries were generated, each consisting of 3 x 10^8 transformants; 3) isolation of nanobodies: phage display was carried out for the selection of antigen-specific phages of which 190 colonies were randomly selected and further analysed by ELISA. From this assay, 86 colonies scored positive for the presence of antigen-specific nanobodies. In total, 54 different full-length nanobodies were identified and further purified from the periplasm of *E. coli* strains. Adapted from (Schoonooghe et al., 2012).

2.6.2 Nanobody expression and purification in TG1 *E. coli* strain

In the first 2 rounds, 20 nanobodies, belonging to different CDR3 groups, were expressed and purified in TG1 *E.coli* strain. The remaining 34 nanobodies were kindly generated by the research technician Ying Di (University of Birmingham, UK). The nanobody genes cloned in pMECS vector contain a PelB signal sequence at the N-terminus which directs the nanobody to the periplasmic space of the *E.coli.* pMECS vector also codes for Ampicillin resistance (AmpR) and adds a C-terminal AAA linker, an HA tag and a His_6 tag to the nanobody sequences which were used for their detection. In addition, in pMECS vector, the His_6 tag is followed by an amber stop codon (TAG) which separates the His_6 tag from the gene III of M13 phage (Fig. 2.3). In the suppressor TG1 *E. coli* strain, the amber stop codon is sometimes read as glutamine and therefore the nanobodies were expressed as a mixed population of pure nanobodies and nanobodies fused with the protein III of the phage.

A 10 ml TG1 *E. coli* pre-culture [Luria-Bertani (LB) medium (10 gr L^{-1} NaCl, 10 gr L^{-1} Tryptone, 5 gr L^{-1} Yeast extract) containing 100 μg ml^{-1} Ampicillin and 1% glucose] was incubated at 37 °C overnight with shaking at 200-250 rpm. 1.5 ml of the pre-culture was added to 390 ml Terrific Broth (TB) medium (2.3 g L^{-1} KH_2PO_4, 12.5 g L^{-1} K_2HPO_4, 12 g L^{-1} Tryptone, 24 g L^{-1} Yeast extract, 4 ml L^{-1} 100% glycerol) supplemented with 100 μg ml^{-1} Ampicillin, 2 mM $MgCl_2$ and 0.1% glucose and grown at 37 °C with shaking (200-250 rpm) until an optical density $(OD)_{600}$ of 0.6-0.9 was reached. The nanobody expression was induced by addition of 1 mM IPTG at 28 °C overnight (~16-18 hours) with shaking. Once it reached an OD_{600} of ~25-30, the overnight induced culture was centrifuged at 4,000 × g for 20 min. The cell pellet from 390 ml culture was then lysed in 5 ml TES buffer (0.2 M Tris pH 8.0, 0.5 mM EDTA, 0.5 M sucrose) and incubated at 4 °C for 1 hour with shaking. Additional 7.5 ml TES/4 buffer was added to each 5 ml TES used and incubated again at 4 °C for 1 hour with

shaking. The lysed bacterial suspension was supplemented with 1.25 ml 2M $MgCl_2$ and spun down at 10,000 × g for 30 min at 4 °C. The supernatant, which contains proteins extracted from the periplasmic space of *E. coli*, was supplemented with 5 mM imidazole solution (in PBS). The nanobody purification was carried out by immobilised metal affinity chromatography (IMAC) using HisPur Ni-NTA Superflow Agarose beads (Thermo Fisher Scientific, Waltham, MA, USA). His-nickel resins were prepared by PBS washing and low-speed centrifugation (700 × g for 3 min, 3x) before the overnight incubation with the periplasmic extract (at 4 °C with shaking). Once PBS-washed (3x), the beads were resuspended in 0.5 ml PBS and loaded into 0.5 ml Zeba Spin Desalting columns (cut-off 7 kDa, Thermo Fisher Scientific, Waltham, MA, USA). The bound nanobodies were eluted 3 times, each time by the addition of an equal volume of 0.5 M imidazole (in PBS) and centrifuged at 10,000 × g for 2 min. The final nanobodies were collected and the concentration was measured by Nanodrop (Nanodrop ND-1000 Spectrophotometer, Geneflow, Lichfield, UK). To remove the imidazole, nanobodies were dialysed at 4 °C against PBS (Slide-A-Lyzer MINI Dialysis Devices, cut-off 3.5 kDa, Thermo Fisher Scientific, Waltham, MA, USA). To ensure efficient dialysis, the buffer (PBS) was changed 3 times and then the concentration was recorded again before further characterisation.

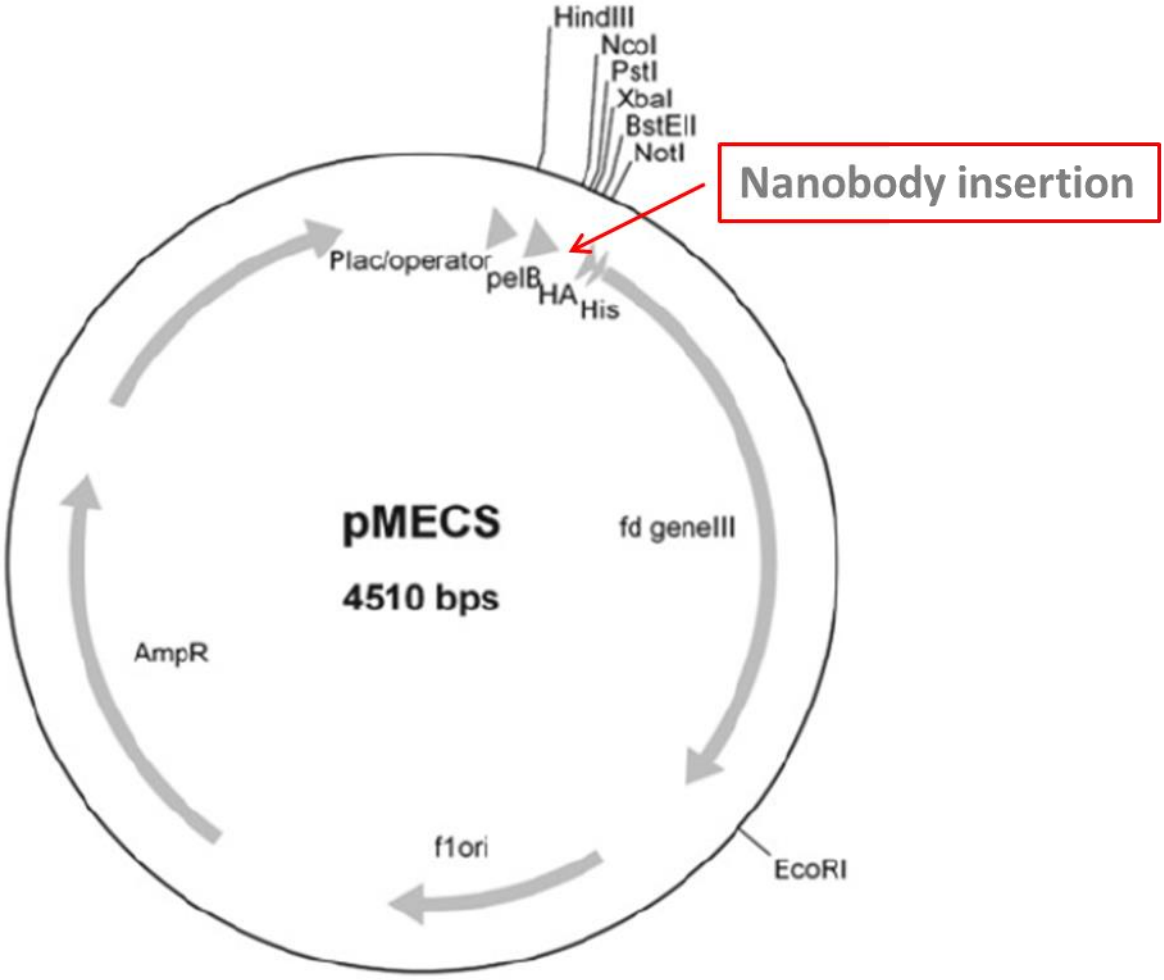

Figure 2.3. Map of the phagemid vector pMECS (4510 bps) used for nanobody cloning. The different nanobodies were cloned into the PstI and NotI sites of the pMECS vector. The lac promoter/operator (Plac) and the PelB signal sequence are located at the N-terminus whereas the HA tag, His_6 tag and the gene III of M13 phage lie at the C-terminus of the nanobody genes. Image taken from (Vincke et al., 2012).

2.6.3 Nanobody expression and purification in WK6 *E. coli* strain

The initial screening of all 54 nanobodies purified in TG1 *E. coli* strain was carried out by the research technician Ying Di. Based on her screening using flow cytometry, collagen-adhesion assay, GPVI-binding assay, NFAT assay with collagen stimulation conducted in either human platelets or the GPVI-EGFP DT40 cell line, three nanobodies were selected, expressed and purified from WK6 *E. coli* strain and further characterised in my PhD project. Nanobodies #14 (family 29) and #27 (family 1) were identified as good candidates for imaging and nanobody #21 (family 9) as a blocking nanobody. In non-suppressor WK6 *E. coli* strain (provided by VIB Nanobody Core), the amber stop codon which follows the His_6 tag in the pMECS vector is read as a stop codon. Therefore the resulting nanobodies are not fused to protein III of the phage creating a pure preparation of nanobodies for further analysis.

2.6.3.1 Generation of WK6 *E. coli* competent cells

In order to transform WK6 *E. coli* with recombinant pMECS vector, the chemical ($CaCl_2$) generation of competent bacteria cells was executed. Under sterile conditions, a 5 ml *E. coli* WK6 pre-culture (LB medium, no antibiotics) was prepared and incubated at 37 °C overnight with shaking at 200-250 rpm. 2 ml of the overnight culture was subcultured into 100 ml LB and incubated at 37 °C with shaking until an OD_{600} of 0.4 was reached. The culture was then incubated on ice for 5 min and centrifuged at 2,000 × g for 5 min at 4 °C. The bacterial pellet was resuspended with 20 ml ice-cold 75 mM $CaCl_2$ containing 15% glycerol and incubated on ice for 5 min. The $CaCl_2$ washing was repeated twice before the final resuspension in 4 ml ice-cold 75 mM $CaCl_2$ (15% glycerol). 100 µl of competent bacterial cells were aliquoted into microcentrifuge tubes and snap-frozen using the isopropanol bath.

2.6.3.2 Transformation of competent WK6 *E. coli* cells with recombinant pMECS vector

In order to express the nanobodies cloned in pMECS vector into WK6 *E. coli* strain, the plasmid DNA was extracted from TG1 *E. coli* using the GeneElute Plasmid Miniprep kit under the manufacturer guidelines. Under sterile conditions, 1 µl of PMECS plasmid DNA was added into 100 µl of competent WK6 *E. coli* cells and incubated on ice for 30 min. The transformation by heat-shock was carried out by placing the tube into a 42 °C water bath for 45 sec and then directly on ice for 2 min. Transformed cells were allowed to grow by adding 400 µl of pre-warmed LB medium and incubating for 1 hour at 37 °C with shaking. WK6 *E. coli* harbouring the recombinant pMECS vector were plated on Ampicillin agar plates and incubated at 37 °C overnight before colony picking and pre-culture for nanobody expression and purification (as described above in TG1 *E. coli* strain). To increase the nanobody yield, 1 L culture was prepared and the volumes of all the reagents were proportionally adjusted. In addition, 5 ml HisTrap HP (GE Healthcare, Bucks, UK) instead of 0.5 ml Zeba Spin Desalting columns were used for the nanobody elution.

2.7 Nanobodies characterisation

The purity of nanobodies was checked by Coomassie staining (InstantBlue Protein Stain, Expedeon, Cambridge, UK) of SDS-PAGE gel under reducing conditions. Western blot and anti-His_6 tag secondary antibody confirmed the presence of nanobodies.

In this section, only ELISA and flow cytometry will be described. The other assays used (Western blot, platelet aggregation, spreading and GPVI shedding) followed the protocols described above.

2.7.1 Enzyme-linked immunosorbent assay (ELISA)

Binding of nanobodies #14, #21 and #27 (from WK6 *E. coli*) to recombinant monomeric and dimeric GPVI was tested using ELISA. The recombinant proteins used were: dimeric GPVI which corresponds to human GPVI D1, D2 domains, residues 21-203 fused to the Fc domain of IgG (GPVI-Fc) and monomeric GPVI which corresponds to the same residues as dimeric GPVI but is not fused to the Fc (mGPVI). The Fc domain was used as a negative control. All the recombinant proteins were provided by Dr Alex Slater (University of Birmingham, UK). Nunc MaxiSorp® micro-titer 96 well plates (Thermo Fisher Scientific, Waltham, MA, USA) were coated with 0.1 μM recombinant GPVI-Fc, mGPVI and Fc domain at 4 °C overnight. After 3x washing in PBS + 0.05% Tween (PBS-T), plates were blocked with filtered 3% BSA (in PBS) for 1 hour at RT. An extra well was coated with 3% BSA and was used as an additional negative control. 1 μM of each of the nanobodies, diluted in diluent blocking buffer (0.1 % BSA + 0.05% Tween), was then added to each well after being washed in PBS-T (3x). Following incubation with the nanobodies for 1 hour at RT with shaking, plates were washed again (5x) before adding the anti-His_6 HRP conjugated (1/10,000) for the nanobody detection. The secondary antibody was left to incubate for 1 hour at RT with shaking followed by PBS-T washing (5x) and addition of the 3,3′,5,5′-Tetramethylbenzidine (TMB) Liquid Supersensitive ELISA Substrate for the visualisation of nanobody binding. The chemiluminescence reaction was stopped by the addition of 1 M H_2SO_4 and absorbance was measured at 405 nm with VersaMax microplate reader (Molecular Devices LLC, California, USA).

To test nanobody binding, the ELISA assay was also performed on other recombinant GPVI constructs by Dr Ruben Barroso and Dr Yi Sun (University of Birmingham, UK): the monomeric full-length of GPVI ectodomain (GPVI FL), the D1 domain (GPVI D1, Ser22-

Thr108) and the D2 domain (GPVI D2, Pro114-Thr203) of GPVI. The recombinant proteins contain a signal peptide, the GPVI sequence (full-length or truncated), followed by a CD4 region and a His_6 tag. The same construct, with the substitution of GPVI with another unrelated protein (CD200), was used as a negative control. The nanobodies were used at 300 nM and then 1:3 serial dilution. Bound nanobodies were detected using anti-HA HRP conjugated secondary antibody (1/10,000).

2.7.2 Flow cytometry

Binding of nanobodies #14, #21 and #27 to GPVI in resting or CRP-XL and PAR1-activated platelets was evaluated using flow cytometry (BD Accuri C6 Flow Cytometer, BD Biosciences, New Jersey, USA). 2×10^8 cells ml^{-1} washed and rested platelets were diluted 1/10 in PBS and simulated with 200 μM PAR1 peptide or 10 μg ml^{-1} CRP-XL when required. After incubated with agonists for 3 min, unstimulated and activated platelets were aliquoted (50 μl) and incubated with 1 μl of nanobodies (0.4 mg ml^{-1} = stock concentration of nanobody #14) for 30 min at RT. Firstly, all the nanobodies were diluted to the same concentration (0.4 μg ml^{-1}). To explain the lack of binding of nanobodies #21 and #27, 1 μl of the stock concentration of both nanobodies (1.9 mg ml^{-1} and 3.1 mg ml^{-1} for #21 and #27, respectively) was then added to 50 μl of platelets. Platelet activation was monitored by P-selectin exposure: unstimulated and stimulated platelets were incubated with 10 μl PE anti-human CD62-P (P-selectin) antibody (1/40) for 20 min at RT in the dark. Detection of nanobodies was carried out using anti-His_6 Alexa Fluor 647 conjugated (1/80) in both unstimulated and activated platelets. The secondary antibody was also used alone in unstimulated samples as the negative control. Following incubation (15 min, RT, in the dark), 500 μl of PBS was added to each sample and run by flow cytometry. Samples were gated and the positive fluorescence for P-selectin and nanobodies was detected in the FL-2 and FL-4 channels, respectively.

In the initial screening study of 20 nanobodies, anti-His_6 HRP conjugated (1/500) and anti-Mouse IgG Alexa Fluor 647 conjugated (1/500) were used for the detection of nanobodies, due to the lack of anti-His_6 Alexa Fluor 647 conjugated. In addition, nanobodies were diluted at the final concentration of 1 μg ml^{-1} and GPVI binding was not investigated in PAR1-activated platelets.

2.8 Generation of Alexa Fluor 647 conjugated SNAP-tagged nanobody #14

2.8.1 Cloning

To reclone the nanobody #14 gene from pMECS to the SNAP-tag vector, the restriction sites BamHI and Xhol were inserted at the ends of the nanobody sequence. In the first round, the BamHI site (GGATCC) was inserted at the N-terminus of the nanobody gene using BamHI Forward and Reverse primers (annealing temperature 72 °C, Table 2.5) and Q5 site-directed mutagenesis kit (NEB, Hitchin, UK) under the manufacturer guidelines. 5 colonies of transformed 5-alpha competent *E.coli* cells (NEB, Hitchin, UK) were picked for DNA isolation (GeneElute Plasmid Miniprep kit) and verification by Sanger sequencing (Source Bioscience, Nottingham, UK) using BamHI Reverse primer. This first step was carried out by Dr Alex Slater (University of Birmingham, UK). Once confirmed as the right insertion, the nanobody #14 with BamHI site at the N-terminal was used as a template for the insertion of the Xhol site (CTCGAG) at the C-terminal using Xhol Forward and Reverse primers (annealing temperature 59 °C, Table 2.5) and Q5 site-directed mutagenesis kit. Upon sequencing validation using BamHI Forward primer, both nanobody #14 gene (1 μg), containing BamHI and Xhol restriction sites, and pSNAP-tag (T7)-2 vector (1 μg, NEB, Hitchin, UK) were digested with 1 μl of BamHI and Xhol restriction enzymes (NEB, Hitchin, UK) simultaneously (double-digestion) using 5 μl of Cutsmart buffer (NEB, Hitchin, UK) for 1 hour at 37 °C. The digested products were then run on 1% agarose gel for DNA extraction

using the GeneJet Gel Extraction kit (Thermo Fisher Scientific, Waltham, MA, USA). Once purified, the nanobody #14 and SNAP-tag vector were ligated using T4 DNA ligase (Promega, Madison, WI, USA) with 1:3 vector:insert ratio. The reaction was incubated for 10 min at RT and overnight at 4 °C and then used to transform competent XLIB *E. coli* cells. The DNA was extracted from 5 different colonies and sent off for Sanger sequencing using the T7F primer provided by Source Bioscience (Nottingham, UK). 2 colonies resulted to contain the right insertion of the nanobody #14 into the SNAP-tag vector.

Table 2.5. Primers

Primers	Forward	Reverse
BamHI	5'-GGATCCCAGGTGCA GCTGCAGGAGTCTGG-3'	5'-GGCCATGGCCGGCTGGGC-3'
Xhol	5'-CTCGAGACTGTTGAA AGTTGTTTAGC-3'	5'-CTAGTGATGGTGATGGTG-3'

2.8.2 Expression and purification of SNAP-tagged nanobody #14

In the SNAP-tagged nanobody #14 cloning, the N-terminal PelB leader, which is used for the purification of the nanobody from the periplasm of *E. coli*, was deleted whereas the His_6 tag, used for the detection, was maintained. Therefore, the procedure used for the nanobody expression and purification is slightly different.

Briefly, each positive colony was grown in 20 ml LB medium supplemented with 100 μg ml^{-1} Ampicillin at 37 °C overnight with shaking at 200-250 rpm. 20 ml of the pre-culture was then added to 1 L LB medium and incubated at 37 °C for 2-5 hours with shaking until an OD_{600} of 0.6 was reached. The culture was induced by the addition of 1 mM IPTG at 30 °C for 5 hours with shaking and then centrifuged at 3,000 × g for 20 min. The bacterial cell pellet obtained was resuspended in 25 ml PBS + 1mM DTT. Bacteria were then sonicated (7 x 10 sec) to induce cell lysis, centrifuged at 15,000 × g for 30 min and the supernatant, which contains the pool of proteins, was filtered and run through a fast protein liquid chromatography system (FPLC, ÄKTA Start chromatography, GE Healthcare, Bucks, UK) for the nanobody purification (with the technical help of Dr Alex Slater, University of Birmingham, UK). The proteins were loaded onto a 5 ml HisTrap HP (GE Healthcare, Bucks, UK) and the SNAP-tagged nanobody was eluted by applying a gradient of 0-500 mM imidazole. Samples of the cell lysate for total protein and flow-through liquid were collected to verify that the SNAP-tagged nanobody did bind to the beads and did not flow through the column. The purity of the SNAP-tagged nanobody #14 was checked by Coomassie staining of SDS-PAGE gel. The fractions 7 and 8 of the eluent, which showed the highest purity, were further dialysed at 4 °C against PBS or PBS + 1 mM DTT (Slide-A-Lyzer MINI Dialysis Devices, cut-off 3.5 kDa, Thermo Fisher Scientific, Waltham, MA, USA) to remove the imidazole. The SNAP-tagged nanobody #14 was then concentrated (Amicon Ultra-0.5 ml Centrifugal Filter Units, cut-off

30 kDa) up to 50 μM for direct labelling of the SNAP-tag with Alexa Fluor 647 *in vitro* (SNAP-Surface Alexa Fluor 647 labelling kit, NEB, Hitchin, UK). Briefly, 50 μM SNAP-tagged nanobody #14 was incubated with 250 μM SNAP-tag substrate (dissolved in DMSO) and PBS + DTT (50 mM) in the dark for 30 min at 37 °C. The fluorescently labelled nanobody was then run on an SDS-PAGE gel and detected using the Odyssey fluorescence detection system. The rest of the sample was stored at -20 °C.

2.9 Statistical analysis

All the data presented in this thesis were expressed as means ± standard error of the mean (SEM). Data were analysed using GraphPad Prism 8 software (GraphPad Software, Inc., La Jolla, CA, USA). Significant differences were determined using unpaired two-tailed Student's *t*-test or one-way Analysis of variance (ANOVA) with Tukey's post-hoc test for multiple comparisons. The significance was set at $p \leq 0.05$.

CHAPTER 3

Platelet GPVI receptor organisation: comparison of different clustering methods for the analysis of *d*STORM imaging data

3.1 Aims

The main aim of this Chapter was to map the localisation and assess the clustering of GPVI in the human PM in platelets adhered to an immobilised substrate monolayer using a combination of *d*STORM imaging and cluster analysis. To explore this, we compared the most widely used clustering methods to identify and develop the appropriate analysis for the quantitation of clusters on fibrous structures such as collagen or globular clusters such as those induced by CRP-XL, fibrinogen and fibrin. This is relevant since different cluster methods may generate different results, restricting the validity of the biological findings to the specific analysis used.

3.2 Introduction

GPVI spatial organisation is tightly regulated at the platelet plasma membrane to orchestrate the signalling transduction and prevent improper activation. Higher-order clustering has been proposed as a putative mechanism to facilitate and intensify the signalling required for platelet activation (Horii et al., 2006, Jung et al., 2009, Poulter et al., 2017, Smethurst et al., 2007). While wide-field and confocal microscopy techniques enable us to map the location of surface receptors and obtain information relative to the colocalisation with other signalling mediators, visualisation by conventional microscopy of receptor clusters has been hindered by the diffraction limit of light which restricts the resolution to ~200 nm. The SMLM technique *d*STORM allows up to 10x increased resolution (10-30 nm in xy) over conventional microscopy, providing new insights into the structure of multi-molecular signalling complexes at the single molecule level (Owen et al., 2010, Pollitt et al., 2014, Poulter et al., 2017). Despite numerous advantages due to the relatively easy setup and the use of conventional fluorescent probes to label the target protein (Dempsey et al., 2011, Heilemann et al., 2008), *d*STORM is characterised by many challenges in terms of sample preparation,

acquisition and reconstruction of the final super-resolved image. In addition, whereas conventional fluorescence microscopy generates a series of pixels reflecting the localisation of fluorophores, a *d*STORM image is essentially a high-density map containing the spatial localisation of all the detected molecules within the specimen, with the precision of the localisation varying depending on several factors such as fluorophore brightness. Indeed, the further level of complication of a *d*STORM imaging experiment is represented by the complex and time-consuming data analysis. A number of quantitative algorithms have been applied to the pointillistic datasets to extract valuable details relative to the pattern, topography or oligomerisation of super-resolved cellular components, including membrane-bound proteins (Nicovich et al., 2017). These algorithms, usually referred to as cluster analyses, aim to identify the presence of clusters based on the statistics of the spatial localisation datasets (Owen et al., 2010, Pageon et al., 2016, Sengupta et al., 2011). Alternatively, they allow to extract quantitative cluster information once the optimal free parameter settings, which are chosen by the user (e.g. density threshold and distance/radius), have been applied (Levet et al., 2015, Owen et al., 2010, Pageon et al., 2016). Ripley's K-function (Ripley, 1977), DBSCAN (Ester et al., 1996) and Voronoï tessellation (Andronov et al., 2016, Levet et al., 2015) are the most commonly used clustering approaches applied to the analysis of SMLM data (Endesfelder et al., 2013, Nan et al., 2013, Owen et al., 2010, Pageon et al., 2016, Rossy et al., 2013, Scarselli et al., 2012, Williamson et al., 2011). All these cluster analyses rely on the local point density and combine individual localisations, with an above-threshold density and within a specific search radius, into clusters. However, despite being similar in principle, they diverge in many aspects. Ripley's K-function is a spatial statistical algorithm which compares the point pattern distribution of interest with a random distribution to determine whether it is clustered, dispersed or randomly distributed within a

given distance (Ripley, 1977). DBSCAN and Voronoï tessellation are density-based algorithms which differ in some ways. DBSCAN uses a single length scale to estimate the local density (Ester et al., 1996) whereas the tessellation relies on the polygonal areas (multiple distance scales) of the Voronoï diagram to do so (Andronov et al., 2016, Levet et al., 2015). In addition, only last year a clustering method based on Voronoï tessellation was developed for the analysis of 3D SMLM data (Andronov et al., 2018). Ripley's K-function, like DBSCAN, uses a single length scale when clustering but is limited by the assumption of cluster size and shape (circular). Instead, DBSCAN does not suffer from this limitation and may be better than Ripley's K-function at separating close clusters with uniform density and low background noise (Deschout et al., 2014a).

However, all the clustering methods described are limited by user-specified parameters such as density threshold and distance, which are difficult to be defined especially when analysing heterogeneous samples. A model-based Bayesian method, which takes into account the localisation precision, has been validated for the automatic selection of the free parameters (Rubin-Delanchy et al., 2015). However, this model is limited by several assumptions which are not suitable for many *d*STORM datasets. Otherwise, to avoid user bias, automatic thresholding can be defined by the average density (Levet et al., 2015) or Monte-Carlo simulations (Andronov et al., 2016). In addition, putative multiblinking artifacts represent another factor to consider which, if not corrected, can interfere with the reliability of the quantitative analysis outcomes (Annibale et al., 2011, van de Linde et al., 2010). Therefore, it is clear that, despite being valuable quantitative instruments, cluster analyses are characterised by substantial limitations and differences between each other which need to be considered in accordance with the specific point spatial distribution of interest.

Application of Ripley's K-function-based cluster analysis in platelets has been demonstrated by Pollitt et al. (2014) and Poulter et al. (2017) in the characterisation of CLEC-2 and GPVI clusters at the plasma membrane (Pollitt et al., 2014, Poulter et al., 2017). In particular, Poulter et al. (2017) proposed the existence of different degrees of GPVI clustering induced by different collagenous substrates and fibrinogen, giving rise to the question as to whether Ripley's K-function is the appropriate method to analyse different shapes of clusters (Poulter et al., 2017). DBSCAN was implemented in the investigation of the role of GPVI inhibitors on receptor clustering induced by platelet adhesion to CRP-XL (Onselaer et al., 2019). Furthermore, DBSCAN allowed determination of whether the inhibitory effect of the adenosine receptor A_{2A} on collagen-induced platelet activation was dependent on the impairment of GPVI clustering in platelets (Clark et al., 2019). To our knowledge, the application of Voronoï tessellation has not been reported in platelets.

In this Chapter, a head-to-head comparison of Ripley's K-function, DBSCAN and tessellation-based cluster analyses has been carried out to explore GPVI cluster formation in platelets adhered to fibrous collagen at different time points. In collaboration with the image analyst Dr Jeremy Pike (University of Birmingham, UK), we then developed a custom-made two-layer DBSCAN-based cluster analysis for the assessment of GPVI nanoclusters only along the fibrous structure of collagen. A single-layer DBSCAN was finally employed to compare the collagen-induced clustering degree with that elicited by other GPVI ligands such as CRP-XL, fibrinogen and fibrin.

3.3 Results

3.3.1 *d*STORM imaging allows visualisation of GPVI cluster formation in platelets interacting with different immobilised substrates

We have investigated the spatial distribution of GPVI receptors in platelets that have been spread on Horm collagen (fibrillar type I collagen), CRP-XL, fibrinogen and fibrin using a combination of TIRFM and *d*STORM imaging. Washed platelets, labelled for F-actin and Pan-GPVI, were allowed to adhere and spread on the immobilised substrates for 1 h and platelet spreading and cluster formation were visualised by TIRFM (Fig. 3.1i, ii). All the substrates were able to support platelet spreading (Fig. 3.1i). The diffraction-limited imaging showed the presence of GPVI clusters on all the substrates investigated, although it is not sensitive enough to detect small changes in clustering. Indeed, non-clustered GPVI or small clusters appeared to be poorly resolved (Fig. 3.1ii). With a lateral optical resolution of ~20 nm (Nicovich et al., 2017), *d*STORM enabled mapping the nanoscopic organisation of GPVI in platelets adhered to the different substrates. GPVI coalesced to form different types of clusters in accordance with the nature of the substrates (Fig. 3.1ii, iii). The TIRFM images show how GPVI lined up along Horm collagen fibres (Fig. 3.1Aii) whereas the reconstructed *d*STORM images allowed us to super-resolve the receptor clustering on fibrous collagen and highlight the presence of small clusters in platelet areas where there are no visible collagen fibres (Fig. 3.1Aiii, iv). Discrete clusters were also detected in platelets spread on CRP-XL, the GPVI-specific ligand, and appeared to be round oligomers with no specific distribution pattern over the platelet surface (Fig. 3.1Bii). *d*STORM enabled the visualisation of a mixed population of small and big clusters of GPVI receptors bound to CRP-XL (Fig. 3.1Biii, iv). Fibrinogen also induced the formation of globular clusters which appear to be similar to those found on CRP-XL (Fig. 3.1Ciii, iv). They seem to be characterised by a homogeneous shape whereas fibrin-

induced clusters appear to be a mixture of circular and slightly elongated oligomers (Fig. 3.1Diii, iv). Therefore, it became clear that quantitative methods were needed to extract key clustering information from the *d*STORM images to describe GPVI organisation at the platelet surface induced by the different substrates.

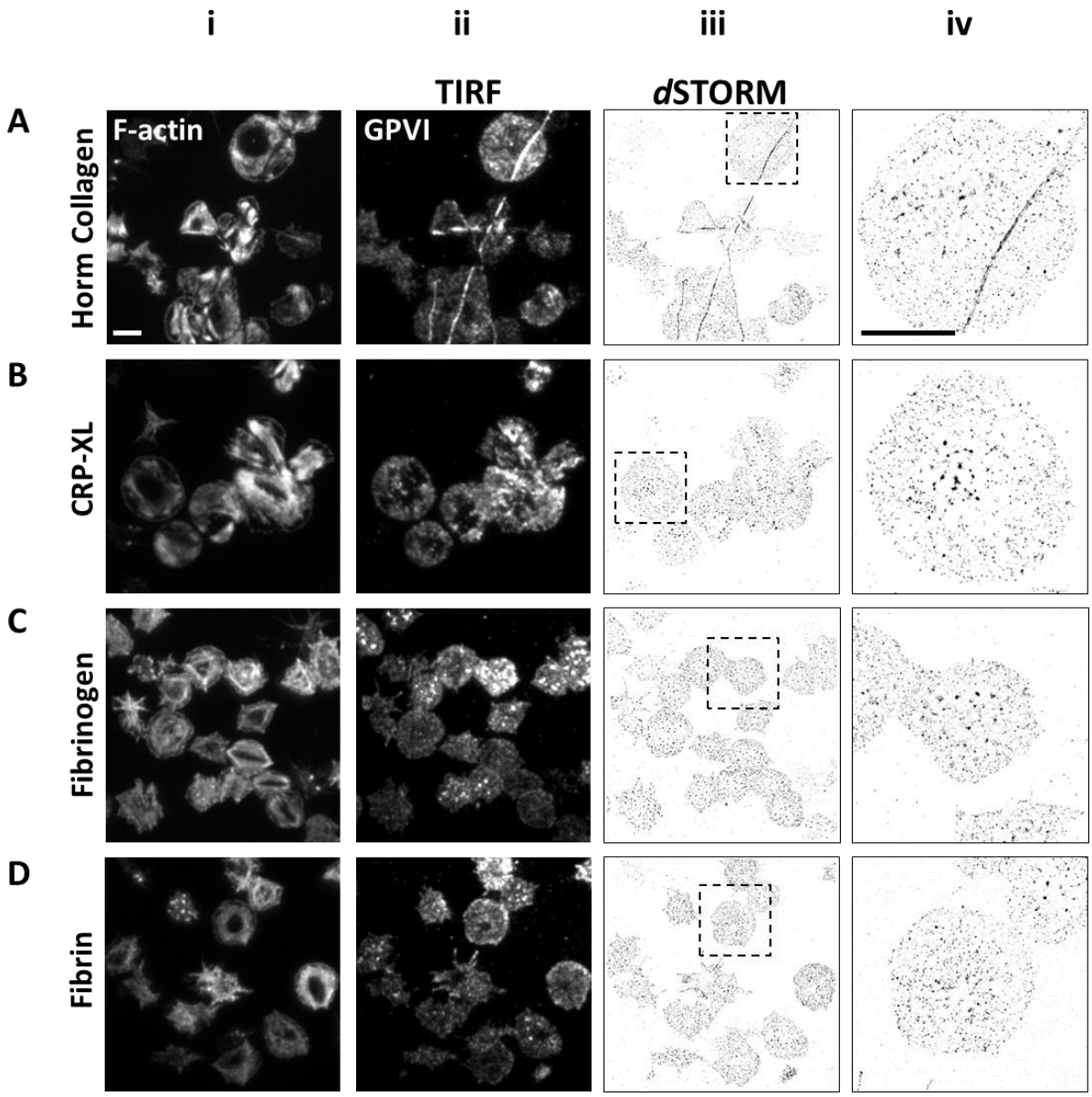

Figure 3.1. TIRFM and *d*STORM imaging of GPVI in platelets adhering to immobilised Horm collagen, CRP-XL, fibrinogen and fibrin. Human washed platelets, pre-labelled with 1G5-Fab (2 μg ml^{-1}) for Pan-GPVI, were spread on a Horm collagen (A, 10 μg ml^{-1}), CRP-XL (B, 10 μg ml^{-1}), fibrinogen (C, 100 μg ml^{-1}) and fibrin (D, generated as described in *Materials and Methods*) monolayers for 1 h at 37 °C and secondary stained with anti-mouse Alexa Fluor 647 conjugated. F-actin was labelled with Alexa Fluor 488 phalloidin. GPVI distribution was assessed by TIRFM and cluster formation was visualised by *d*STORM. The whole FOV (i, ii, iii) and single platelet (iv) images are representative of three independent experiments. In total, 12 FOVs for each condition were acquired. Scale bar: 5 μm.

3.3.2 GPVI clustering increases along collagen fibres in spread platelets

Although *d*STORM imaging provided evidence of the ability of GPVI to form oligomers specifically along collagen fibres, only quantitative analysis enabled comparison of receptor clustering on and off fibrous collagen and investigate whether it is sustained over time. TIRFM and *d*STORM imaging showed the same organisation of GPVI at the platelet surface as that visualised in the previous images after 1 h and 3 h of spreading (Fig. 3.2Ai, ii). Here, we adopted a custom-made algorithm based on the Ripley's K-function run in MATLAB (Owen et al., 2010) to quantitatively assess GPVI clustering over time. 2 x 2 μm^2 non-overlapping ROIs were placed within the boundary of the platelet either in areas where the collagen fibre was visible or regions where there was no observable fibre. For each ROI, indicated by the red box area (Fig. 3.2Aii), the cluster analysis was performed and is represented by the two-dimensional (2D)-cluster heat map of individual spots (Fig. 3.2Aiii). Setting a radius of 50 nm within the MATLAB code, each molecule was given a value based on its degree of clustering, calculated by the unitless measure of clustering L(r) where red indicates high levels [L(r)>150] of clustering and blue no clustering [L(r)=0] (Fig. 3.2Aiii). Clusters are shown in the binary image as defined by the threshold L(r)=100 (Fig. 3.2Aiv). Collagen induced a higher degree of GPVI clustering along the fibres than that expected from a random distribution. These clusters showed sustained size, number of localisations per cluster, number of clusters and density within clusters over time (Fig. 3.2B, C, D, E). Cluster formation was also detected in off-collagen areas, although they were 27% smaller and contained more than 50% fewer localisations per cluster than those aligned along the fibres (Fig. 3.2B, C). The number of clusters out of the collagen-rich areas were 29% higher than on collagen after 3h of spreading (Fig. 3.2D), likely due to fibrinogen released from the granules of activated platelets which can also bind GPVI (Induruwa et al., 2018, Mangin et al., 2018).

In addition, the number of clusters did not change, something which might have been predicted as there is a limited number of GPVI binding sites on collagen. However, cluster density also increased along fibrillar collagen over time, although this was not statistically significant, probably due to the high variability between different donors and the minimum number of replicates.

To confirm the robustness of our data and conclusion, we have run the cluster analysis on a small dataset (10 ROIs) changing different parameters such as the cluster size (radius=25 nm and 100 nm) and the threshold (50 and 150) within the MATLAB code to verify whether they can influence the outcome. The cluster density was used to evaluate the putative change in clustering. Setting the radius to 25 nm or 100 nm, GPVI cluster density still increased along collagen fibres and over time (Fig. 3.3A, B, C, D). In the same way, maintaining a 50 nm radius, but adjusting the threshold value to 50 or 150 did not change the result (Fig. 3.3E, F, G, H). Therefore, despite the absolute values being different due to the different settings in the MATLAB code, the trend in the GPVI cluster density on and off collagen fibres was maintained. Overall, these data suggest that, independently of the clustering scale applied, Horm collagen causes specific oligomerisation of GPVI along the fibres characterised by sustained size and density with no additional recruitment of clusters over time.

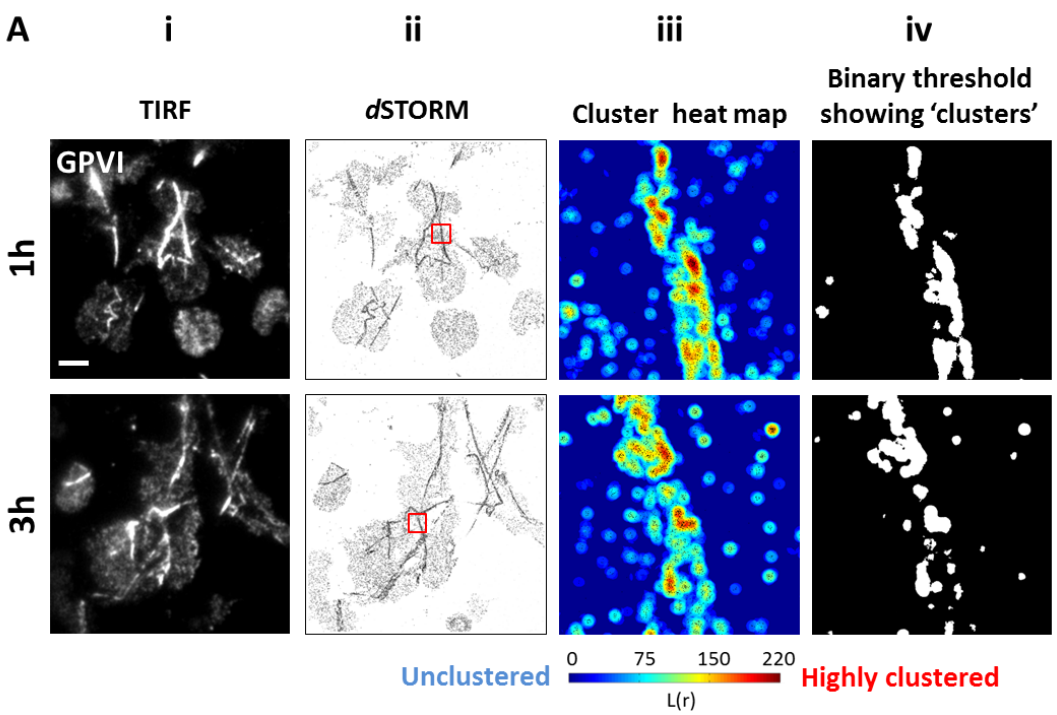
A
i
ii
iii
iv
TIRF
dSTORM
Cluster heat map
Binary threshold showing 'clusters'
GPVI
1h
3h
0
75
150
220
Unclustered
Highly clustered
L(r)

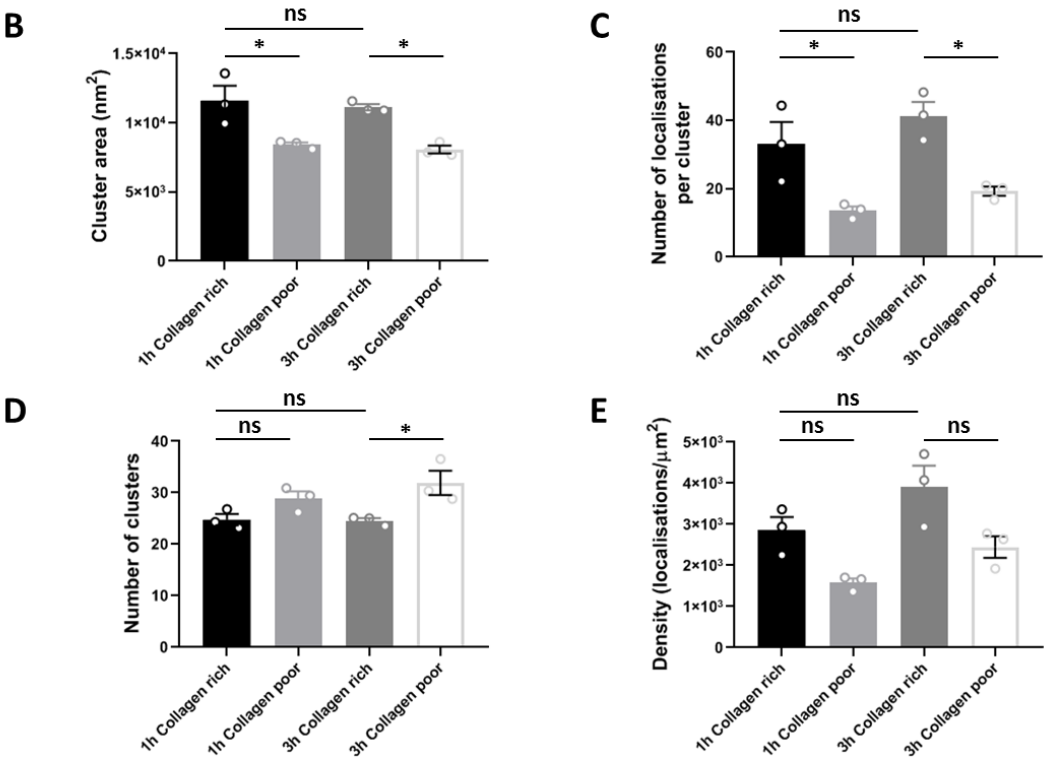
B
C
D
E
Cluster area (nm²)
Number of localisations per cluster
Number of clusters
Density (localisations/μm²)
ns
*
1h Collagen rich
1h Collagen poor
3h Collagen rich
3h Collagen poor

Figure 3.2. Ripley's K-function-based cluster analysis of GPVI *d*STORM imaging in platelets spread on Horm collagen for 1 h and 3 h. Human washed platelets spread on a Horm collagen (10 µg ml^{-1})-coated surface for 1 h and 3 h were pre-incubated with 1G5-Fab (2 µg ml^{-1}) for GPVI labelling, secondary stained with anti-mouse Alexa Fluor 647 conjugated and imaged by TIRFM (Ai). The *d*STORM images of the same cells illustrate the increased resolution obtained by this cutting-edge technique (Aii). The first panel of images refers to the immunolocalisation of GPVI after 1h of spreading whereas the distribution of GPVI in platelets spread for 3 h is shown in the second set of images. 2 x 2 μm^2 square ROIs were taken inside platelets and on and off collagen fibres. Heat maps of the clusters (radius= 50 nm) in the ROI (red box area) are shown in the images Aiii. Binary maps of the clusters following thresholding [L(r)=100] of the heat map show clustering of GPVI along the collagen fibres (Aiv). Quantification of GPVI clustering on and off collagen fibres is reported in the histograms, with each point corresponding to the mean ± SEM from three independent experiments: cluster area (B), number of localisations per cluster (C), number of clusters (D) and density within clusters (E). In total, 48 and 43 ROIs were analysed on and off collagen fibres after 1 h of spreading (9 FOVs) whereas 61 and 59 ROIs were measured on and off collagen fibres after 3 h of spreading (10 FOVs), respectively. Significance was measured using one-way ANOVA with Tukey's multiple comparisons: a significance of $P < 0.05$ is denoted by * whereas non-significant difference is indicated by ns. Scale bar: 5 µm.

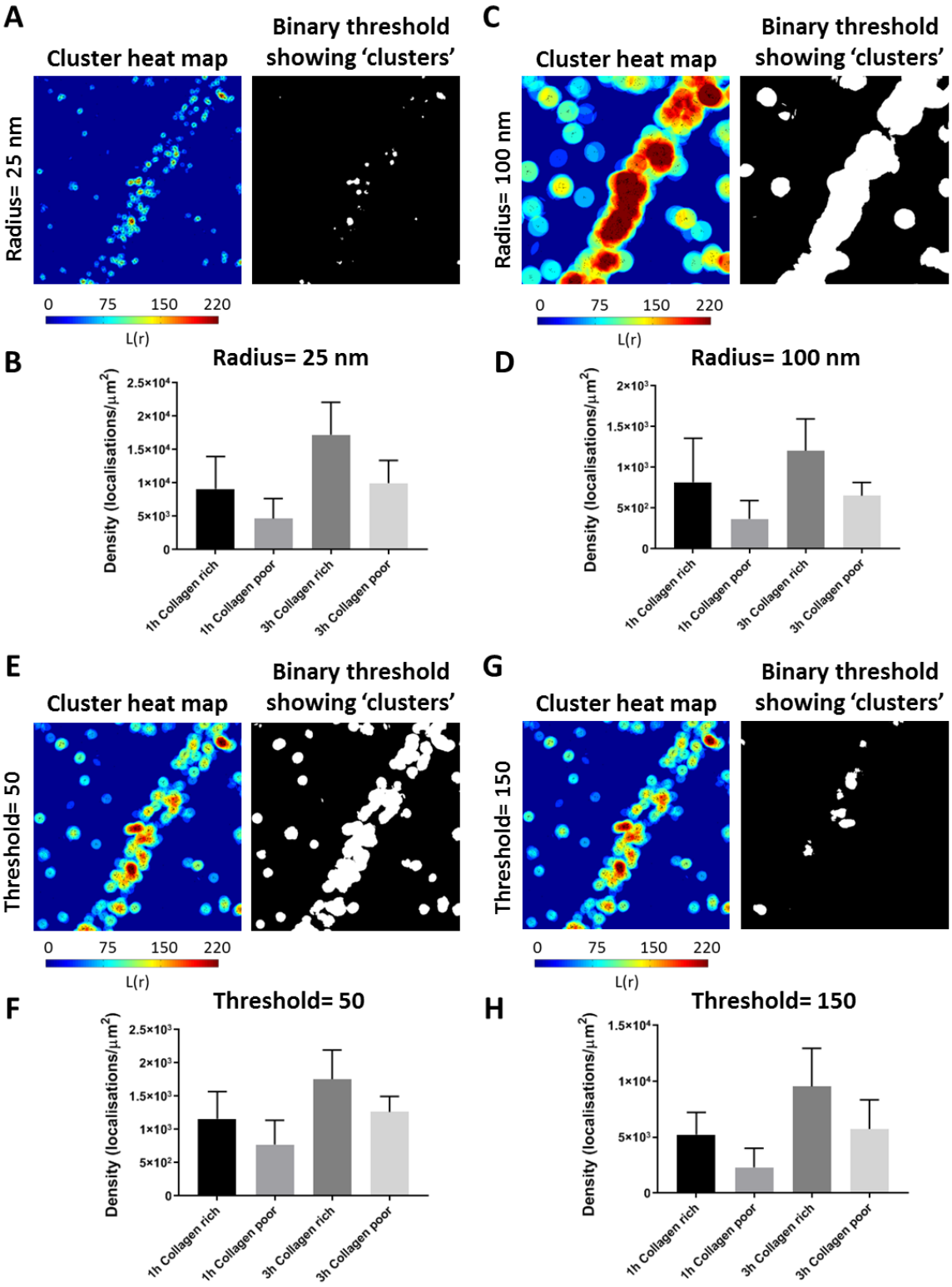
A
Cluster heat map
Binary threshold showing 'clusters'
Radius= 25 nm
0 75 150 220
L(r)
C
Cluster heat map
Binary threshold showing 'clusters'
Radius= 100 nm
0 75 150 220
L(r)
B
Radius= 25 nm
Density (localisations/μm²)
2.5×10⁴
2×10⁴
1.5×10⁴
1×10⁴
5×10³
0
1h Collagen rich
1h Collagen poor
3h Collagen rich
3h Collagen poor
D
Radius= 100 nm
Density (localisations/μm²)
2×10³
1.5×10³
1×10³
5×10²
0
1h Collagen rich
1h Collagen poor
3h Collagen rich
3h Collagen poor
E
Cluster heat map
Binary threshold showing 'clusters'
Threshold= 50
0 75 150 220
L(r)
G
Cluster heat map
Binary threshold showing 'clusters'
Threshold= 150
0 75 150 220
L(r)
F
Threshold= 50
Density (localisations/μm²)
2.5×10³
2×10³
1.5×10³
1×10³
5×10²
0
1h Collagen rich
1h Collagen poor
3h Collagen rich
3h Collagen poor
H
Threshold= 150
Density (localisations/μm²)
1.5×10⁴
1×10⁴
5×10³
0
1h Collagen rich
1h Collagen poor
3h Collagen rich
3h Collagen poor

Figure 3.3. Comparison between different radii and thresholds within Ripley's K-function-based cluster analysis applied to GPVI *d*STORM datasets. A small GPVI *d*STORM dataset (10 ROIs) was used to test different clustering parameters within the Ripley's K-function algorithm. The cluster heat maps of a representative ROI along collagen fibres, with different cluster size (radius= 25 and 100 nm) selected in the MATLAB code, show the degree of clustering where red represents the highest value (A, C). Binary images of the clusters, obtained applying a threshold of L(r)=100 to the heat maps, illustrate the GPVI oligomers along fibrous collagen (A, C). GPVI cluster analysis, with a standard cluster size (radius=50 nm) and a lower and higher value of threshold [L(r)=50 and 150] than the standard one [L(r)=100] is shown in E, G. The quantitative analysis of GPVI *d*STORM images shows that the receptor cluster density rises along collagen fibres and over time, independently of the clustering parameters selected in the MATLAB code (B, D, F, H). No statistical analysis was performed due to the small size of the dataset (2 FOVs from n=1 experiment).

3.3.3 Comparison between Ripley's K-function and SR-Tesseler for the study of GPVI clustering on fibrous collagen

Ripley's K-function-based cluster analysis has been demonstrated to be powerful in quantifying cluster parameters in other cell types, particularly T cells (Owen et al., 2010, Rossy et al., 2013, Williamson et al., 2011) and above in discriminating GPVI receptor organisation on and off collagen fibres. However, quantitation of receptor clustering along the fibrous structure of the Horm collagen was limited by the adoption of square ROIs, which also included the localisations not in direct contact with visible fibres in the final quantitative analysis. To overcome this limitation, we applied a modified approach based on the previous Ripley's K-function cluster analysis to the same *d*STORM dataset. GPVI clusters only along visible and obvious collagen fibres within each ROI were manually selected in the binary map and only those were further analysed in Excel (highlighted in red in Fig. 3.4Aiv). This allowed us to assess GPVI oligomerisation specifically localised along collagen fibres and verify whether the clustering changed in accordance with the spreading duration. The exclusion of localisations off-collagen fibres within each ROI did not affect GPVI cluster area and density values (Fig. 3.4B, C) in comparison with the previous result. This approach also confirmed the trend followed by GPVI clustering over time: the cluster area and density were maintained over the 3 h time frame studied (Fig. 3.4B, C). Notably, the density within clusters showed an upward trend over time, but again this result was not statistically significant due to the variability between the different replicates.

A further assessment of GPVI clustering aligned along collagen fibres was obtained employing SR-Tesseler (Levet et al., 2015). The Voronoï diagram computed on the *d*STORM GPVI images shows the segmentation of the data points into separate polygons (Fig. 3.4Di) whereas the high molecular density of GPVI along collagen is highlighted by a different

colour-code in the density map (Fig. 3.4Dii). GPVI data points along visible collagen fibres were first isolated within the whole FOVs using a density factor δ of 2 and a minimum area of 1μm x 1μm to generate distinct objects (Fig. 3.4Diii). The detected objects were then thresholded by density factor δ of 0.5 and minimum number of points of 10 to group the isolated points into individual clusters (Fig. 3.4Div). These parameters were deemed to be the most suitable for the segmentation and clustering of GPVI on Horm collagen after running different density factors δ on a small dataset (δ = 1, 1.5 and 2 for the I level and δ = 0.125, 0.25 and 0.5 for the II level). In accordance with the Ripley's K-function analysis, SR-Tesseler showed sustained GPVI cluster density along collagen over the 3 h time frame investigated (Fig. 3.4E). In contrast to Ripley's K-function, the cluster area was slightly lower at 3 h comparing to 1 h, however, this difference was not statistically significant. Overall, as two different cluster algorithms have produced comparable results although being different in the absolute values, we can deduce that GPVI clustering on collagen fibres is maintained at a steady state over the time frame of 3 h investigated here.

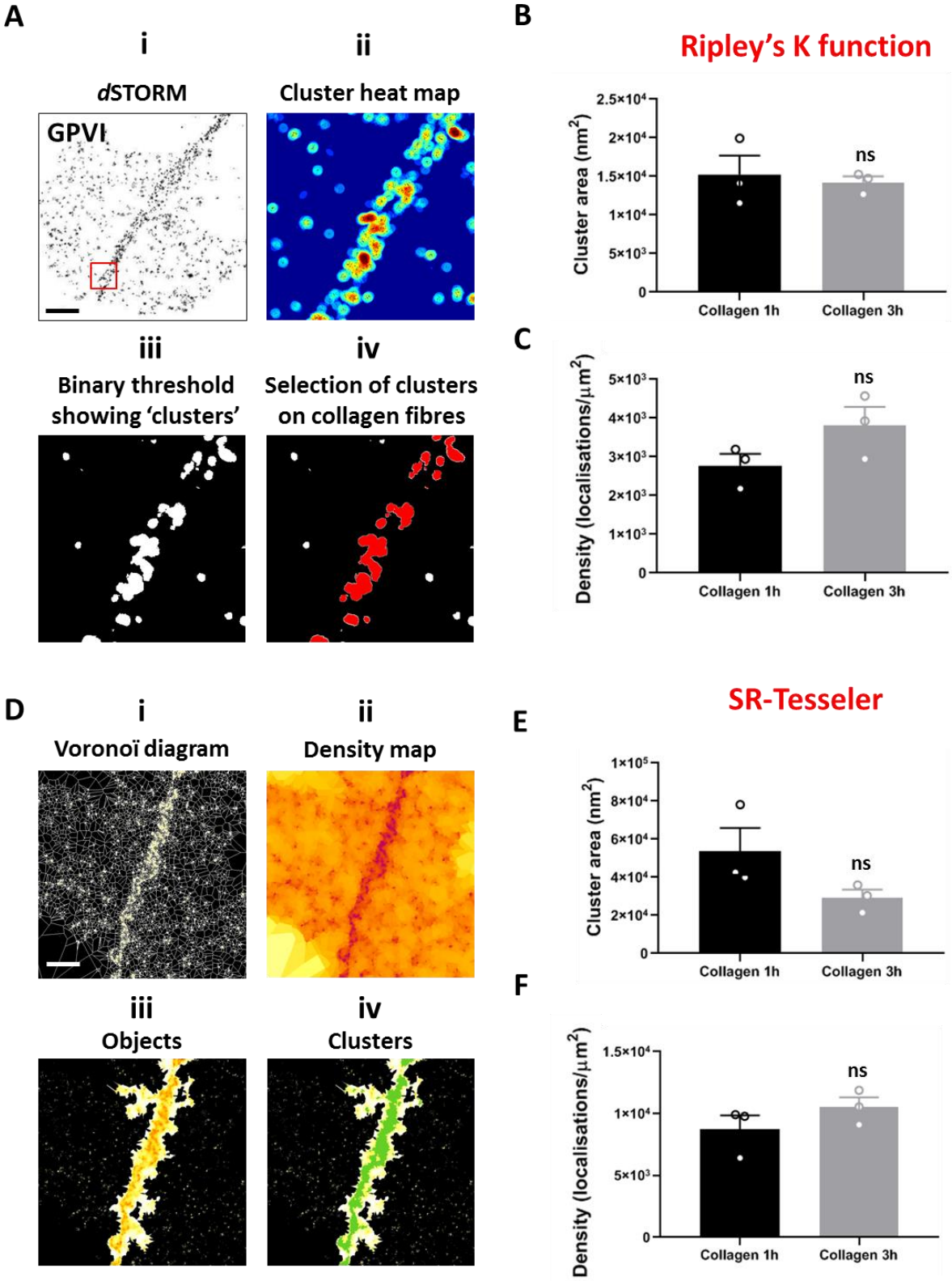
A
i
ii
dSTORM
Cluster heat map
GPVI
iii
iv
Binary threshold showing 'clusters'
Selection of clusters on collagen fibres
B
Ripley's K function
Cluster area (nm²)
2.5×10⁴
2×10⁴
1.5×10⁴
1×10⁴
5×10³
0
ns
Collagen 1h
Collagen 3h
C
Density (localisations/μm²)
5×10³
4×10³
3×10³
2×10³
1×10³
0
ns
Collagen 1h
Collagen 3h
D
i
ii
Voronoï diagram
Density map
iii
iv
Objects
Clusters
E
SR-Tesseler
Cluster area (nm²)
1×10⁵
8×10⁴
6×10⁴
4×10⁴
2×10⁴
0
ns
Collagen 1h
Collagen 3h
F
Density (localisations/μm²)
1.5×10⁴
1×10⁴
5×10³
0
ns
Collagen 1h
Collagen 3h

Figure 3.4. Cluster analysis of GPVI *d*STORM imaging comparing Ripley's K-function and SR-Tesseler. The same *d*STORM datasets of previous experiments were analysed using the custom-made algorithm based on the Ripley's K-function. A representative *d*STORM image of a single platelet is shown in Ai. The cluster heat map of the ROI highlights the high degree of clustering along collagen (indicated in red, Aii). In the MATLAB code, the radius and threshold were set to 50 nm and 100, respectively. The clusters are shown in the binary image (Aiii) after thresholded the cluster heat map. Only clusters distributed along visible collagen fibres (highlighted in red, Aiv) were selected and analysed within each ROI. The quantitative analysis shows no significant difference in GPVI cluster area and density over time (B, C). *d*STORM images of GPVI (whole FOVs) were processed using SR-Tesseler software. The Voronoï diagram shows the segmentation of the data points into polygonal regions (Di) whereas the molecular densities are represented by different colour-coded tiles in the density map (Dii). A density factor δ of 2 and minimum area of 1μm x 1μm were used for the object isolation (GPVI on collagen fibres, Diii) and density factor δ of 0.5 and minimum number of spots of 10 for the cluster segmentation (Div). The cluster area and density quantitation are reported in E and F. All the bars in the histograms represent the mean ± SEM from three individual experiments. In total, 9 and 10 FOVs for 1 h and 3 h of spreading, respectively, were analysed. Significance was measured using unpaired two-tailed t-test ($P < 0.05$): non-significant difference is indicated by ns. Scale bar: 1 μm.

3.3.4 DBSCAN confirms sustained collagen-induced GPVI clustering over time

To further validate our data, the DBSCAN algorithm (Ester et al., 1996) was employed to investigate GPVI cluster formation in platelets spread on fibrillar collagen for 1 h and 3 h. In contrast to SR-Tesseler, DBSCAN only considers a single length scale when grouping individual data points into clusters based on the local density. Here, to identify collagen-induced GPVI clusters, the local density was defined by the search radius of 50 nm and minimum number of points of 10. These settings were chosen to sufficiently separate the prominent clusters on collagen fibres and limit the background noise. In the DBSCAN map, individual clusters are represented by different colours (Fig. 3.5Aii). DBSCAN-based cluster analysis demonstrated that GPVI cluster area and density remain constant after 3 h of spreading (Fig. 3.5B, C, D), in agreement with Ripley's K-function and SR-Tesseler analyses. The cluster area and number of detections per cluster showed a tendency to rise proportionally with the spreading duration, but the variability between different platelet donors did not make the result statistically significant. In addition, the absolute values of cluster area and number of localisations per cluster appeared to be comparable to those extracted from the Ripley's K-function cluster analysis (Fig. 3.2B, C and 3.4B). Therefore, DBSCAN further supports the result obtained with Ripley's K-function and SR-Tesseler quantitative analyses.

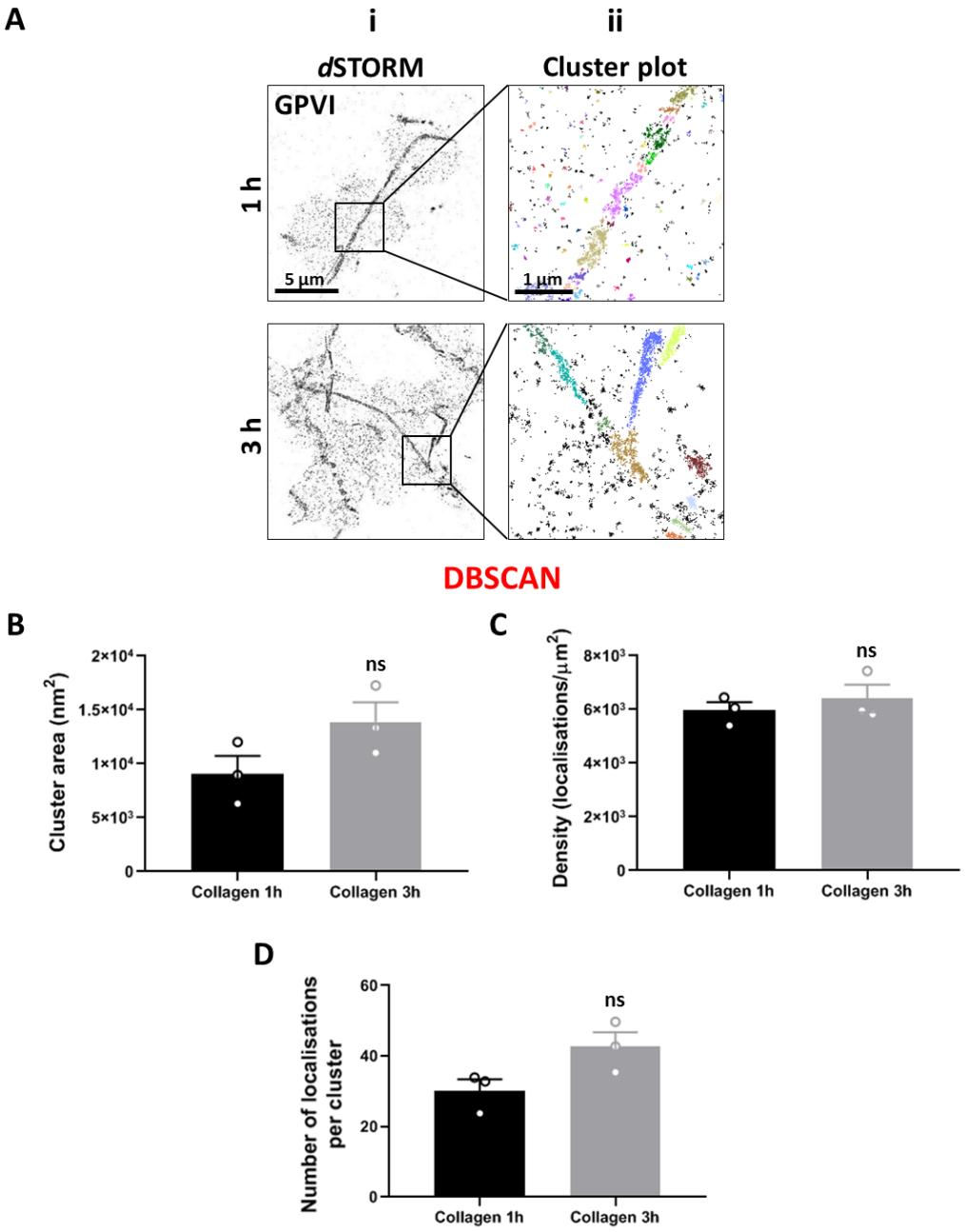

Figure 3.5. DBSCAN-based cluster analysis of GPVI *d*STORM imaging in platelets spread on Horm collagen for 1 h and 3 h. The GPVI *d*STORM localised detections within whole FOVs (Ai) were grouped into individual clusters (represented by different colours in Aii) by applying a single-level DBSCAN clustering method in KNIME setting a search radius of 50 nm and a minimum number of points of 10. The background spots are highlighted in black and are detected as non-clustered localisations by DBSCAN. The histograms show no significant difference in cluster area (B), density within clusters (C) and number of detections per cluster (D) over time. Each dot represents the mean ± SEM from three independent experiments. In total 10 and 11 FOVs for 1 h and 3 h of spreading, respectively, were analysed. Significance was calculated using unpaired two-tailed t-test ($P < 0.05$) with ns indicating non-significant difference. Scale bar: 5 µm (*d*STORM images) and 1 µm (cluster plots).

3.3.5 Two-layer DBSCAN cluster analysis permits the evaluation of GPVI nanoclustering formation on collagen fibres

The DBSCAN-based cluster analysis employed previously allowed the overall GPVI clustering level in platelets adhered to immobilised collagen to be assessed, independently of the colocalisation with the fibres. To explore the nanoscale spatial organisation of GPVI receptors specifically distributed along visible collagen fibres, a custom-made 2-level cluster analysis based on DBSCAN (Ester et al., 1996) was implemented to first identify and isolate large clusters of GPVI on collagen (Level I; Fig. 3.6Aii) and then take those clusters and subdivide them into nanoclusters (Level II; Fig. 3.6Aiii). This approach allowed us to assess only GPVI nanoclusters associated with the visible collagen fibres, to identify any differences between the platelets spread for different durations. Before performing the cluster analysis, the acquired images were reconstructed in ThunderSTORM plugin for Fiji (Ovesný et al., 2014) instead of the Nikon STORM analysis software used previously and post-corrected for multiblinking artifacts. The algorithm groups the localised data points into individual clusters (Level I) and nanoclusters (Level II), based on parameters relating to cluster radius (75 and 30 nm for Level I and II, respectively) and points number (3 and 10 for Level I and II, respectively), with different clusters being represented by different colours (Fig. 3.6Aii, iiii). Quantitative analysis of the clusters showed no significant difference in cluster area between 1 h and 3 h of spreading at either Level I or Level II clustering (Fig. 3.6B, C). Cluster density also remained constant over time (Fig. 3.6D, E). Notably, the area of nanoclusters aligned along collagen fibres (Level II clustering) appeared to be similar to the one extracted from the single-layer DBSCAN (Fig. 3.5B) and Ripley's K-function analyses (Fig. 3.2B and 3.4B). Therefore, this finding further suggests that GPVI receptor-collagen interaction remains constant regardless of the platelet spreading time, also at the nanocluster level.

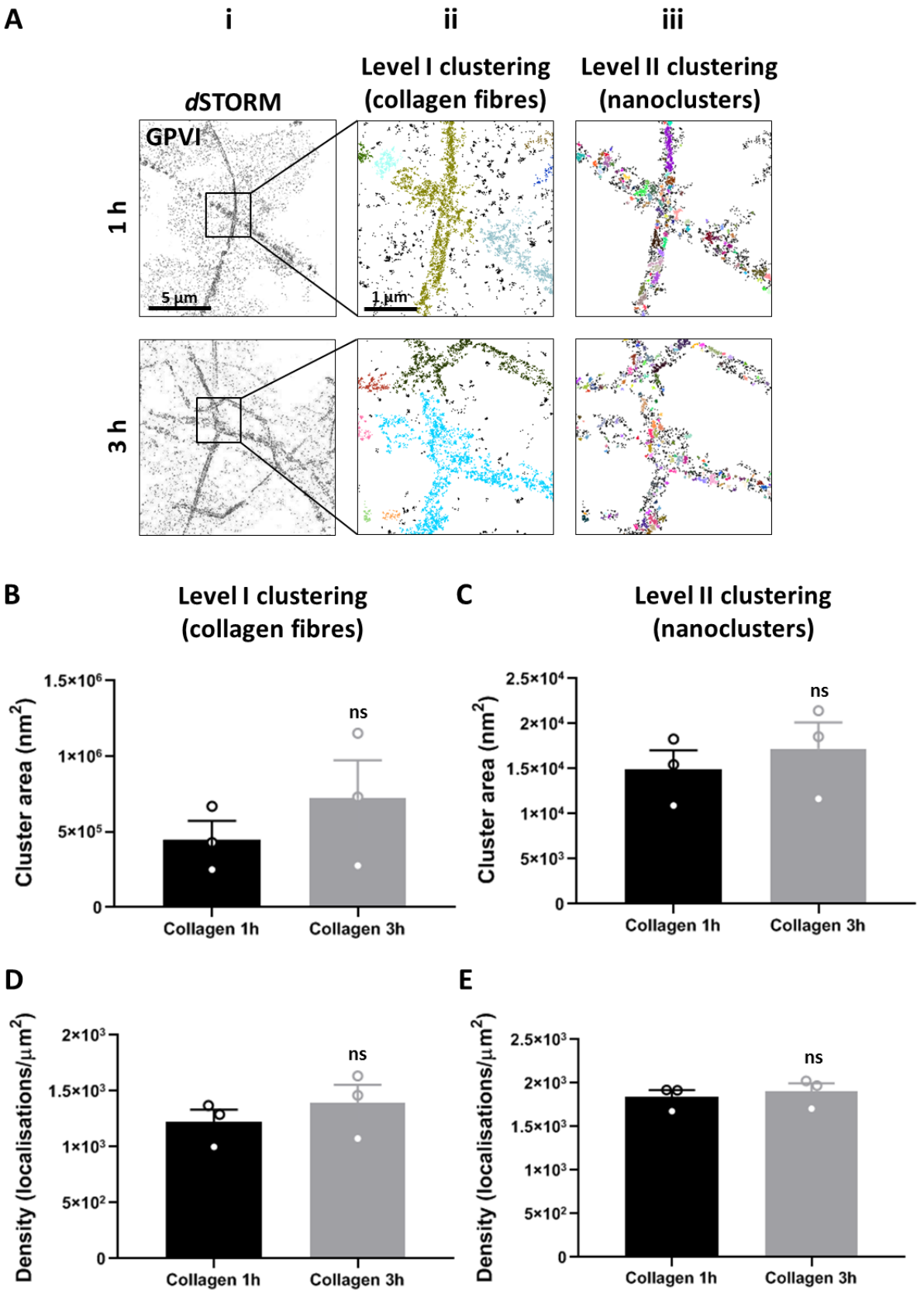
A
i
ii
iii
Level I clustering
(collagen fibres)
Level II clustering
(nanoclusters)
dSTORM
GPVI
1 h
3 h
5 µm
1 µm
B
Level I clustering
(collagen fibres)
Cluster area (nm²)
1.5×10⁶
1×10⁶
5×10⁵
0
ns
Collagen 1h
Collagen 3h
C
Level II clustering
(nanoclusters)
Cluster area (nm²)
2.5×10⁴
2×10⁴
1.5×10⁴
1×10⁴
5×10³
0
ns
Collagen 1h
Collagen 3h
D
Density (localisations/µm²)
2×10³
1.5×10³
1×10³
5×10²
0
ns
Collagen 1h
Collagen 3h
E
Density (localisations/µm²)
2.5×10³
2×10³
1.5×10³
1×10³
5×10²
0
ns
Collagen 1h
Collagen 3h

Figure 3.6. Two-level DBSCAN cluster analysis of GPVI *d*STORM imaging in platelets spread on collagen for 1 h and 3 h. The acquired GPVI *d*STORM images in platelets spread on collagen for 1 h and 3 h were reconstructed in ThunderSTORM plugin for Fiji and post-correction was applied to minimise multiblinking artifacts (Ai). The localised data points were grouped into clusters using a 2-level cluster analysis based on DBSCAN (Aii, iii). In the Level I clustering, the large clusters corresponding to collagen fibres were segmented using a search radius of 75 nm and a minimum number of reachable detections of 3 (Aii). In the Level II clustering, these clusters were isolated and divided in nanoclusters using as search radius and minimum number of points of 30 and 10, respectively (Aiii). For both scales, quantitative analysis of GPVI *d*STORM images shows the area and density of individual clusters within the whole FOV (B, C). Bars in the histograms represent mean ± SEM from three independent experiments. In total, 12 and 13 FOVs for 1 h and 3 h of spreading, respectively, were analysed. Significance was measured using unpaired two-tailed t-test $P < 0.05$: ns indicates non-significant difference. Scale bar: 5 μm (*d*STORM images) and 1 μm (Level I and II cluster plots). The two-level analysis was designed and implemented by Dr Jeremy Pike, University of Birmingham, UK.

3.3.6 GPVI clusters to the same extent on Horm collagen and CRP-XL in spread platelets

To investigate whether the total extent of GPVI cluster formation induced by Horm collagen was independent of the other collagen receptor integrin α2β1, GPVI oligomerisation was quantitatively compared in platelets adhered to fibrous collagen and non-fibrous CRP-XL. The synthetic triple-helical peptide CRP-XL contains multiple and continuous GPO triplets, the specific GPVI-binding motif, enabling it to bind different GPVI receptors simultaneously and induce receptor clustering (Asselin et al., 1997, Morton et al., 1995). Platelets labelled for GPVI were allowed to spread on immobilised Horm collagen and CRP-XL for 1 h and cluster formation was monitored by *d*STORM. As previously shown in Fig. 3.1, these two ligands induced different receptor organisations and clustering patterns, making the choice of the cluster analysis to adopt challenging. Since Ripley's K-function was limited by the use of ROIs and objects on CRP-XL were difficult to be defined in SR-Tesseler due to their homogeneous distribution, single-layer DBSCAN turned out to be the best method to analyse the globular GPVI clusters formed on CRP-XL and compare them with those on Horm collagen. The local density, defined by the same search radius and number of points used previously (radius = 50 nm and minimum number of points = 10), allowed the segmentation of GPVI localisations into clusters marked by different colours (Fig. 3.7Aii). Quantification showed that GPVI oligomers induced by CRP-XL have the same properties of those triggered by platelet-collagen binding (Fig. 3.7B, C, D). The unchanged cluster area, density and number of localisations per clusters suggest that the contribution of integrin α2β1 to GPVI cluster formation on fibrous collagen is negligible.

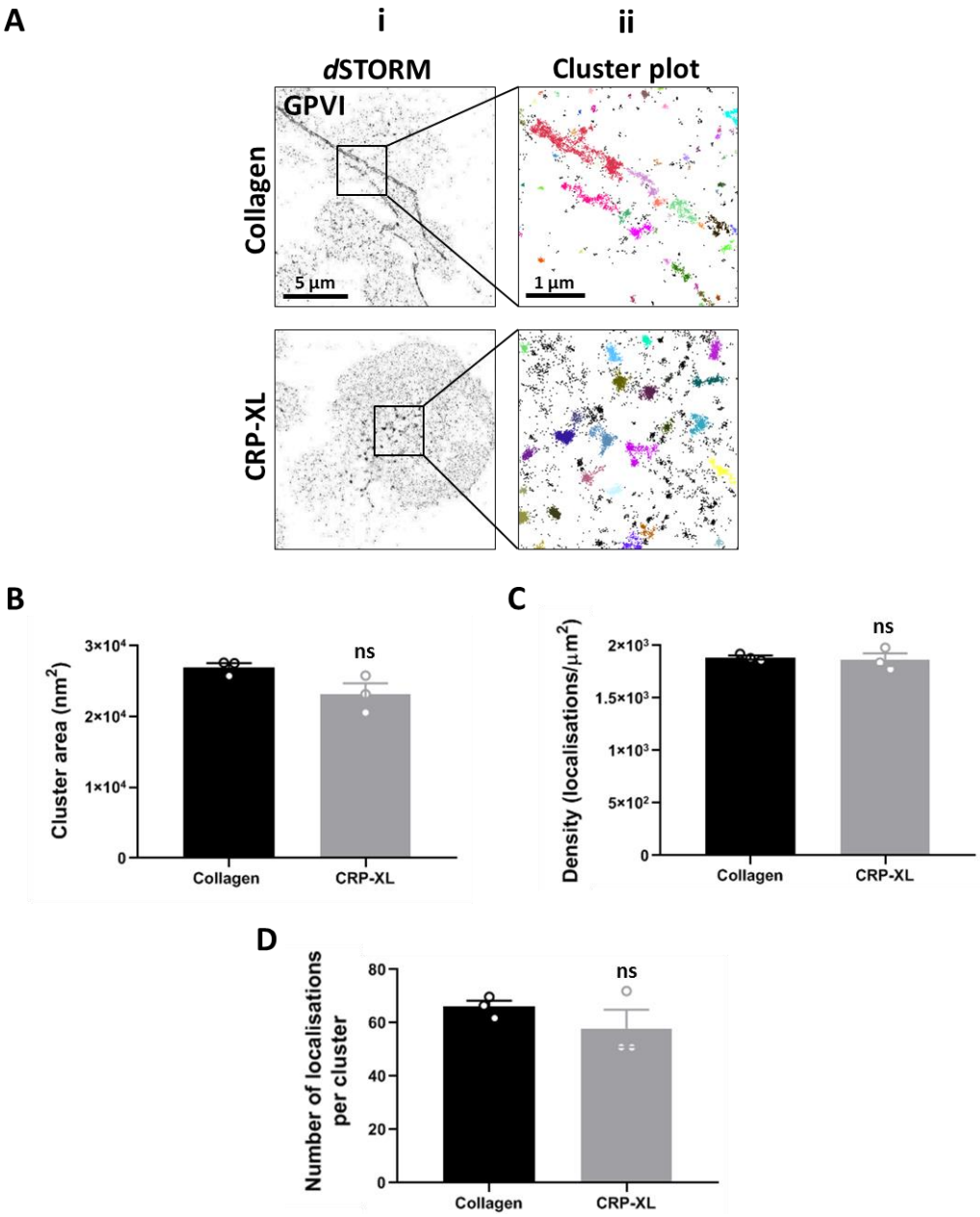

Figure 3.7. Single-layer DBSCAN cluster analysis of GPVI *d*STORM imaging in platelets spread on Horm collagen and CRP-XL. Human washed platelets spread on Horm collagen (10 µg ml^{-1}) and CRP-XL (10 µg ml^{-1}) monolayers for 1 h were labelled for GPVI using 1G5-Fab (2 µg ml^{-1}) before spreading and secondary stained with anti-mouse Alexa Fluor 647 conjugated. GPVI organisation was visualised by *d*STORM in TIRF mode (Ai). Clustering was assessed by a single-layer DBSCAN cluster analysis where the search radius and the minimum number of detections were adjusted to 50 nm and 10, respectively. The clusters are highlighted in different colours and the background points in black (Aii). The mean ± SEM cluster area, density and number of localisations per clusters are reported in the histograms (B, C, D). In total, 12 FOVs for each condition from n=3 individual experiments were analysed. Unpaired two-tailed t-test was used to calculate the significance ($P < 0.05$): ns indicates non-significant difference. Scale bar: 5 µm (*d*STORM images) and 1 µm (cluster plots).

3.3.7 Comparison of GPVI clustering in platelets adhered to immobilised collagen, fibrinogen and fibrin

Fibrinogen and its proteolytic product, fibrin, have recently been discovered to be novel ligands for GPVI (Alshehri et al., 2015a, Induruwa et al., 2018, Mammadova-Bach et al., 2015, Mangin et al., 2018, Onselaer et al., 2017). Since GPVI clusters were also found at the platelet surface not in direct contact with visible collagen fibres, we hypothesized that soluble granule contents, including fibrinogen, released by adherent platelets may contribute to receptor oligomerisation through the 'outside-in' signalling. To address the question as to whether other GPVI ligands induce the receptor clustering to the same extent as collagen, we compared the nanoscopic GPVI organisation in platelets spread on immobilised Horm collagen, fibrinogen and fibrin. To verify the successful generation of fibrin (as described in *Materials and Methods*), platelets were allowed to adhere to a fibrinogen and fibrin-Alexa 488-coated surfaces. The fibrinogen and fibrin monolayers (Fig. 3.8A, E) were then visualised by confocal microscopy to compare their localisation with that of adherent platelets (Fig. 3.8C, G) and GPVI receptors (Fig. 3.8B, F). Fibrinogen inhomogeneously distributed throughout the surface due to the presence of aggregates within the fibrinogen preparation (Fig. 3.8A) which seem to overlap with the platelet surface and GPVI (Fig. 3.8B, C, D). Contrarily, fibrin formed well-defined polymeric structures (Fig. 3.8E) touching the platelet edges and therefore GPVI receptors (Fig. 3.8H).

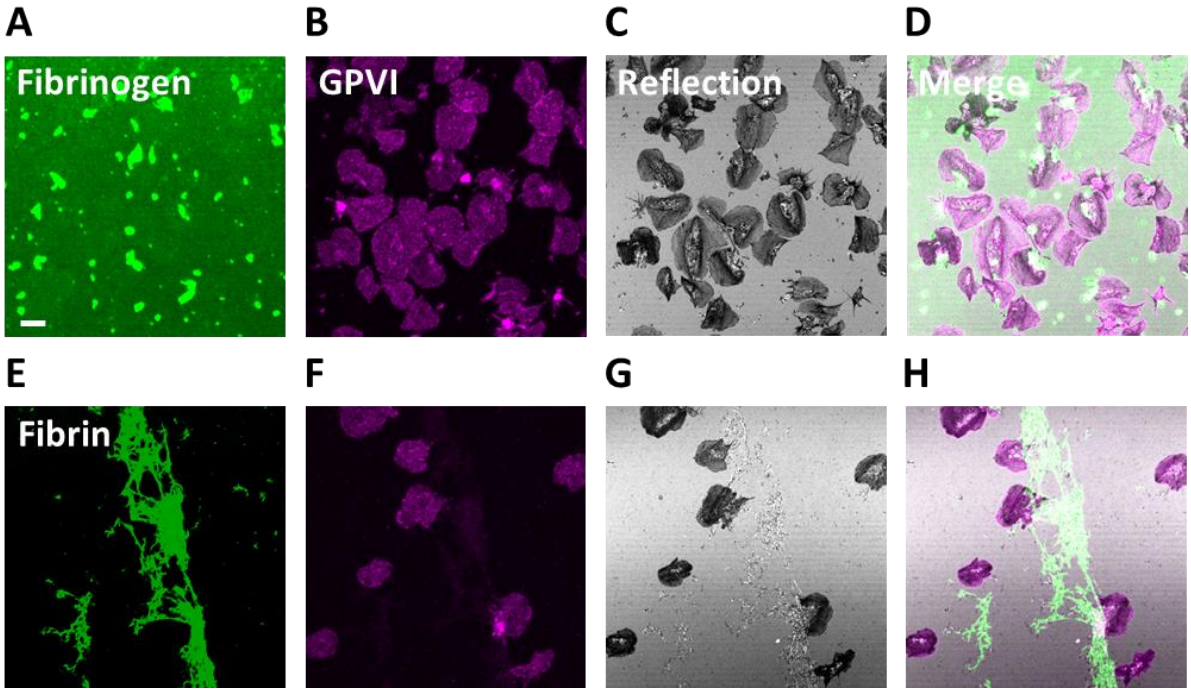

Figure 3.8. Confocal imaging of platelets adhered to fibrinogen and fibrin. Human washed platelets, pre-labelled with 1G5-Fab (2 μg ml^{-1}) for GPVI, were allowed to spread on fibrinogen-Alexa 488 (100 μg ml^{-1}) and fibrin-Alexa 488 (generated as described in *Materials and Methods*) monolayers for 1 h, secondary stained with anti-mouse Alexa Fluor 647 conjugated and imaged by confocal microscopy. Fibrinogen and fibrin monolayers are shown in A and E whereas GPVI distribution is illustrated in B and F. The Reflection images demonstrate the presence of platelets (C, G). The Merge images highlight the localisation of platelets and GPVI expressed at the cell surface relative to the fibrinogen/fibrin monolayers (D, H). For each condition, 5 random FOVs were acquired using confocal microscopy. The images are representative of a single experiment. Scale bar: 5 μm.

*d*STORM combined with a single-layer DBSCAN-based clustering method enabled the visualisation and quantitation of the different types of clusters (indicated by different colours) induced by Horm collagen, fibrinogen and fibrin (Fig. 3.9Ai, ii). The clusters formed on fibrinogen were characterised by a circular shape (Fig. 3.9Aii, first panel); on fibrin there was a mixture of circular and some slightly elongated clusters (indicated by arrows in Fig. 3.9Aii, second panel) whereas on the Horm collagen there were continuous clusters colocalising with visible collagen fibres and round clusters outside of the fibres (Fig. 3.9Aii, third panel). In addition to the shape, clusters formed on Horm collagen also slightly differed in size from those induced by fibrinogen: in platelets adhered to collagen, GPVI clusters (which include clusters both on and off visible collagen fibres) were 20% smaller overall than those in platelets spread on fibrinogen (Fig. 3.9B). In addition, fibrinogen caused the fusion of larger clusters than fibrin (40% increased cluster area, Fig. 3.9B) characterised by ~60% more localisations per cluster (Fig. 3.9D). No significant difference between clustering induced by Horm collagen and fibrin was found (Fig. 3.9B, C, D). In addition, the density within clusters did not change in platelets spread on all the substrates investigated (Fig. 3.9C). Taken together these data suggest that, when analysed using DBSCAN at one length scale, fibrinogen induces the formation of the largest clusters, however, cluster density remains the same for all the substrates.

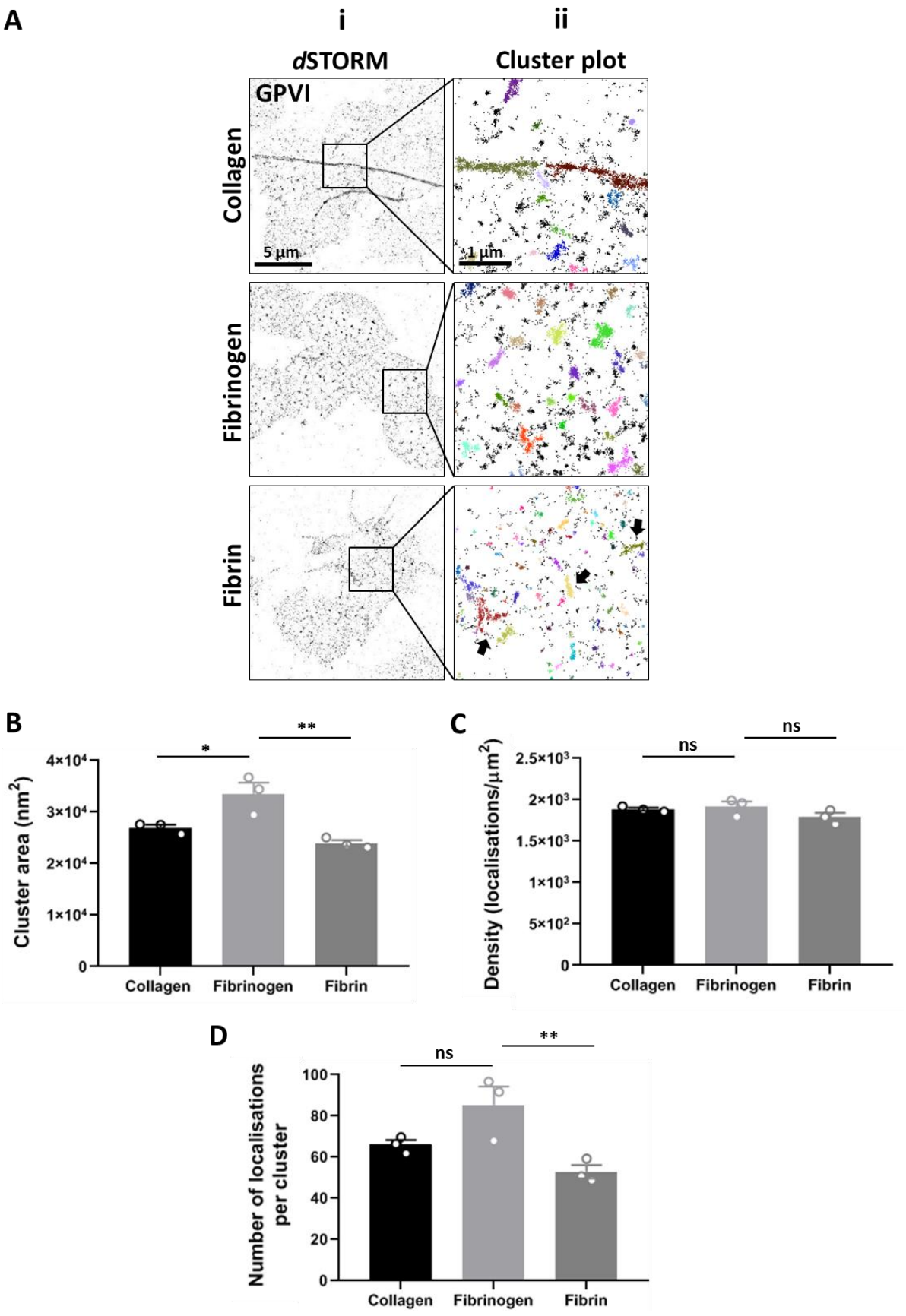
A
i
ii
dSTORM
Cluster plot
GPVI
Collagen
Fibrinogen
Fibrin
5 µm
1 µm
B
Cluster area (nm²)
4×10⁴
3×10⁴
2×10⁴
1×10⁴
0
*
**
Collagen
Fibrinogen
Fibrin
C
Density (localisations/µm²)
2.5×10³
2×10³
1.5×10³
1×10³
5×10²
0
ns
ns
Collagen
Fibrinogen
Fibrin
D
Number of localisations per cluster
100
80
60
40
20
0
ns
**
Collagen
Fibrinogen
Fibrin

Figure 3.9. Single-level DBSCAN cluster analysis of GPVI *d*STORM imaging in platelets adhered to Horm collagen, fibrinogen and fibrin. Human washed platelets were spread on a Horm collagen (10 µg ml^{-1}), fibrinogen (100 µg ml^{-1}) and fibrin (generated as described in *Materials and Methods*) monolayers for 1 h, labelled for GPVI (using 1G5-Fab, 2 µg ml^{-1}) and secondary stained with anti-mouse Alexa Fluor 647 conjugated. A single-level DBSCAN cluster analysis was applied to the reconstructed *d*STORM images (Ai) to evaluate cluster formation on different substrates. Representative cluster plots are shown in Aii: individual clusters are identified by different colours whereas the background is highlighted in black using a search radius of 50 nm and a minimum number of spots of 10 within the analysis. Elongated clusters formed on fibrin are indicated by black arrows (Aii, third panel). Quantitative cluster analysis of GPVI on Horm collagen, fibrinogen and fibrin is shown in the histograms (B, C, D) with each point representing the mean ± SEM from three individual experiments. In total, 12 FOVs for each condition were analysed. Statistical analysis was performed using one-way ANOVA with Tukey's multiple comparisons, setting the significance to $P < 0.05$. Non-significant difference is indicated by ns. Scale bar: 5 µm (*d*STORM images) and 1 µm (cluster plots).

3.4 Discussion

GPVI is the most important signalling collagen receptor expressed at the surface of platelets. It has been proposed that clustering of GPVI dimers offers a second level of control for GPVI signalling by increasing avidity for collagen and bringing signalling molecules into close proximity (Poulter et al., 2017). Furthermore, the recent discovery of additional agonists for GPVI such as fibrinogen and fibrin (Alshehri et al., 2015a, Induruwa et al., 2018, Mammadova-Bach et al., 2015, Mangin et al., 2018, Onselaer et al., 2017) suggests that receptor oligomerisation may be not restricted to the collagen stimulus. Therefore, it appears evident that receptor clustering may represent a critical target mechanism to modulate GPVI-mediated platelet responses and understanding GPVI clustering at the nanoscale will be useful in directing the potential mode of action of future therapies.

In this Chapter, a combination of TIRFM and *d*STORM imaging techniques has allowed us to explore the nanoscale organisation of GPVI receptors at the platelet surface using 1G5-Fab which binds both monomeric and dimeric GPVI (Al-Tamimi et al., 2009). TIRFM highlighted the presence of continuous clusters along collagen fibres but failed to resolve small clusters or clusters which appeared more randomly distributed such as those formed on non-fibrous CRP-XL, fibrinogen and fibrin. With its high spatial resolution (~10-30 nm in *xy*), *d*STORM is able to localise single molecules and, in combination with cluster analysis, extract quantitative information (e.g. cluster size and molecular density). There has been substantial recent work investigating different types of cluster analysis for SMLM (Nicovich et al., 2017) and it has become clear that different algorithms may generate different results. Therefore it is important to verify the clustering of GPVI using different approaches to determine the robustness of our data and conclusions. This has also allowed us to identify the advantages and limitations of each method and dictate the selection of the quantitative approach to

employ in accordance with the specific cluster structures in our future work. Ripley's K-function-based analysis, firstly described by (Owen et al., 2010), has previously been applied to platelet receptors by (Pollitt et al., 2014) and (Poulter et al., 2017). This cluster analysis permits the relative quantitative comparison of receptor cluster size, density, number of localisations per cluster and number of clusters. However, it is restricted to square ROIs placed by the user in platelet areas containing both collagen fibres and random surface regions outside the fibres. The use of ROIs introduces the problem of user bias in terms of where the ROIs are placed as well as restricts the analysis towards the centre of the cell. ROIs must be completely contained within the boundaries of the cell so not to introduce cluster bias and as platelets tend to be round when spread, areas towards the periphery of the cell are not able to be analysed. Nevertheless, using this method we demonstrated that the receptor cluster area, density and number of localisations per cluster all increase along collagen fibres in comparison with platelet areas where the collagen is not visibly present. This is in line with the ultra-structure of the triple-helical collagen which would potentially induce the binding of multiple GPVI receptors to consecutive molecules of tropocollagen and facilitate receptor clustering (Herr and Farndale, 2009). Although the cluster density increased along collagen fibres, this result was not statistically significant. This may be due to the high variability between platelets from the three different donors and suggests that the number of replicates may need to be increased to address this.

All the clustering parameters investigated (size, density, number of clusters and number of localisations per cluster) were sustained over time, suggesting that, once GPVI is bound to collagen and clustering is induced, no additional receptors are recruited or lost after the initial spreading has taken place. Round clusters were also found randomly dispersed throughout the platelet surface, although they were smaller, less dense and with a lower number of

localisations per clusters in comparison with the receptor clusters colocalising with the collagen fibres. These small clusters may represent GPVI receptors which have bound to very small fibrils or non-fibrous collagen not visible by light microscopy as Horm collagen is prepared from equine tendons and, although it is predominantly type I fibrils (95%), it may contain traces of other collagens e.g. type III collagen (5%) (Favaloro, 2000). They could also be GPVI clusters on fibrinogen released from the granules of activated platelets. Alternatively, they could represent receptors that are not bound to ligand but may appear as small clusters due to the repeated blinking of the fluorescent dye during imaging, a process which can be influenced by the buffer used to image the sample (Annibale et al., 2011, van de Linde et al., 2010).

However, the limitation of this analysis method is based on two different aspects: the adoption of user-specified parameters such as radius and threshold and user-defined square ROIs which do not adapt to the elongated structure of collagen fibrils and would also include localisations outside the fibres. Running the cluster analysis on the single-molecule datasets using different radii and thresholds confirmed the increase in GPVI clustering induced by fibrous collagen. The second point was addressed by selecting and analysing only GPVI clusters distributed along collagen fibres and comparing them at different spreading times. This allowed us to more accurately investigate whether collagen-induced GPVI clustering is sustained over time, based on the hypothesis that it may contribute to the maintenance of signalling required for platelet activation (Poulter et al., 2017). This approach confirmed the previous finding, demonstrating that GPVI cluster area and density remains steady over the 3 h time period studied.

Ripley's K-function has been shown to be a powerful clustering method in a variety of biological models (Muranyi et al., 2013, Owen et al., 2010, Scarselli et al., 2012). However,

Ripley's K-function would not be the ideal cluster analysis for the assessment of elongated clusters induced by collagen fibres, since it is based on the assumption of cluster size/shape (circular clusters) and homogeneous point pattern distribution (Ripley, 1977). Indeed, extensions of the function have been developed for the detection of spatial molecular complexes in inhomogeneous populations (Baddeley et al., 2000). In light of these considerations, alternative algorithms such as Voronoï tessellation (Levet et al., 2015) and DBSCAN (Ester et al., 1996), which do not take into account the molecular organisation, were explored. Both clustering methods generated comparable results with Ripley's K-function. Voronoï tessellation allowed the isolation and quantification of GPVI clusters only along collagen fibres. However, the same free parameters successfully selected GPVI clusters in some images but failed in others. This may be the reason for the reduced cluster area in platelets spread on collagen for 3 h in comparison with the earlier time point investigated, although the difference was not statistically significant. Ripley's K-function and DBSCAN, using a single length scale instead of polygonal 'cells', were better than Voronoï tessellation in separating tight clusters such as those formed on collagen fibres. Indeed, the absolute values of cluster size calculated by Ripley's K-function and DBSCAN were similar but much lower than those generated by SR-Tesseler.

However, when the DBSCAN-based analysis was extended to the whole FOV it was not ideal for the quantitation of GPVI clusters only along collagen fibres. To address this, a two-step DBSCAN-based cluster analysis was developed and then validated on all the GPVI *d*STORM datasets. This method successfully marginalised all the large clusters formed on collagen fibres and then segmented the selected clusters into nanoclusters, allowing accurate quantitative comparisons at the nanoscale level. Multiblinking artifacts can result in the appearance of false clusters which will be counted within the quantitative analysis, resulting

in unreliable results (Annibale et al., 2011, van de Linde et al., 2010). To face this drawback, the *d*STORM images were post-corrected for multiblinking artifacts before performing the two-layer analysis. This method demonstrated that the area and density of GPVI nanoclusters do not change over time, confirming the outcome of the previous methods investigated. In addition, these nanoclusters measured ~1.5×10^4 nm^2 in size which is comparable to the absolute values of cluster area extracted by Ripley's K-function and one-layer DBSCAN. This validated cluster analysis for fibrous structures will be employed to answer a variety of biological questions in *Chapter 4*.

GPVI formed circular clusters in platelets adhered to CRP-XL, fibrinogen and fibrin. To compare these circular clusters with the elongated ones induced by collagen and extract clustering information, we used one-step DBSCAN analysis. We found that CRP-XL induces the same clustering degree of that triggered by collagen, suggesting that the adhesive receptor integrin α2β1, which also binds to collagen in close proximity to GPVI (Herr and Farndale, 2009), does not significantly contribute to GPVI clustering. This is in accordance with Poulter et al. (2017) who demonstrated that the blocking anti-α2β1 antibody Gi9 did not impair platelet spreading and dimeric GPVI cluster formation on Horm collagen (Poulter et al., 2017).

Immobilised fibrinogen and fibrin were also able to support GPVI clustering in line with recent findings showing that both ligands bind to and activate GPVI in human platelets (Alshehri et al., 2015a, Induruwa et al., 2018, Mammadova-Bach et al., 2015, Mangin et al., 2018, Onselaer et al., 2017). This suggests that receptor clustering may be a critical activatory mechanism in all the steps of thrombus formation from the initial platelet adhesion to thrombus growth and stabilisation. Furthermore, fibrinogen and fibrin may strengthen the initial clustering induced by GPVI-collagen interaction. While GPVI clusters formed on

Horm collagen, fibrinogen and fibrin were similar in density, surprisingly the largest clusters with the highest number of localisations per cluster were detected in platelets adhered to fibrinogen. The reason may be attributed to the inhomogeneous distribution of fibrinogen throughout the glass surface and accumulation in small areas which could also be enhanced by soluble fibrinogen released from the α-granules of adherent platelets which has been shown to help extend platelet spreading (Sakurai et al., 2015). In addition, the analysis was performed on whole FOVs, taking into account the entire set of GPVI localisations, independently of their colocalisation with the fibres, leading to the underestimation of the collagen-induced clustering. Lastly, how GPVI binds to fibrin(ogen) is still controversial, since different groups have reported contrasting results about the exact receptor conformation required for ligand binding (Induruwa et al., 2018, Mangin et al., 2018). Poulter et al. (2017) showed that fibrinogen induced the formation of smaller but more numerous GPVI clusters than Horm collagen (Poulter et al., 2017). The differences in our findings and those reported by Poulter et al. (2017) may be due to the different cluster analysis adopted and the use of a specific Fab 204-11 which detects only the dimeric conformation of GPVI. Whether GPVI clusters are pre-formed and are made up by monomeric and/or dimeric receptors remains to be understood.

Findings from this Chapter highlight the complexity of the clustering field and underline the concept that the intrinsic structural properties of the input data drive the selection of the appropriate analysis for the quantitative interrogation of proteins in a variety of biological systems. We propose a novel two-layer cluster analysis based on DBSCAN for the specific assessment of receptor clustering on fibrous structures whereas one-layer DBSCAN has been shown to be suitable for the quantitative analysis of circular clusters or a mixture of cluster

shapes. Future work is needed to integrate these algorithms with simulation methods for the selection of the free parameters to allow automated segmentation and avoid user bias.

CHAPTER 4

Immobilised collagen prevents shedding and induces sustained GPVI signalling in platelets

4.1 Aims

The first aim of this Chapter was to investigate whether immobilised collagen is able to induce the release of GPVI receptors from the platelet surface through the mechanism of ectodomain shedding, thereby limiting platelet activation. The underlying hypothesis was that receptor clustering may protect from ADAM10-mediated cleavage, allowing the signalling to be maintained over time. The second goal was to evaluate the contribution of secondary mediators and signalling kinases on GPVI clustering and signalling in platelets interacting with collagen. For these purposes, using a combination of biochemical and advanced imaging approaches, we have correlated GPVI signalling, clustering and shedding to elucidate the events characterising the first step of thrombus formation, namely platelet-collagen interaction.

4.2 Introduction

Collagen, one of the major components of the ECM, is a potent activator of platelets acting through its interaction with the platelet receptor GPVI. The GPVI-FcR-γ complex is a signalling rather than an adhesive receptor complex as activation of integrins through inside-out signalling is required for stable platelet adhesion under flow (Pugh et al., 2017). Collagen engagement of GPVI triggers Src family kinase-dependent phosphorylation of the conserved tyrosines in the ITAM motif within the associated FcR-γ and binding of the tyrosine kinase Syk via its tandem SH2 domains. Activation of Syk, by Src-dependent phosphorylation and autophosphorylation, initiates the formation of a LAT-based signalosome that culminates in the activation of PLCγ2, intracellular Ca^{2+} increase, integrin activation and full platelet activation (Watson et al., 2010). A critical event involved in platelet activation is the secretion of secondary mediators, ADP and TxA_2, which represents a positive feedback loop to support platelet activation, aggregation and thrombus development (Bye et al., 2016). In particular,

second messenger have been shown to be fundamental for the tyrosine phosphorylation of the related hemITAM receptor CLEC-2 as well as platelet aggregation in response to rhodocytin, its non-physiological ligand (Pollitt et al., 2010).

GPVI is found at the platelet surface primarily as a monomer but up to ~29% of the total GPVI has been detected in a dimeric state in resting platelets (Jung et al., 2012). Upon platelet activation by collagen, the levels of dimeric GPVI receptors increase with the subsequent fusion into larger clusters at the platelet surface (Jung et al., 2009, Jung et al., 2012, Loyau et al., 2012, Miura et al., 2002, Poulter et al., 2017). Therefore, receptor dimerisation and clustering tightly modulate the local density of the GPVI receptor at the platelet surface. It has been proposed that GPVI signalling may be influenced by receptor density as decreased GPVI levels result in a severe impairment of platelet adhesion to collagen under flow (Sarratt et al., 2005). In addition, a study conducted in RBL-2H3 cells expressing GPVI at a lower or similar density of that found in human platelets has demonstrated that the receptor density modulates both platelet adhesion and signalling in response to collagen (Chen et al., 2002). Collagen also induces slow but sustained signalling whereas the non-physiological ligand CVX causes rapid but transient signalling in platelet suspensions (Tomlinson et al., 2007) and this may be due to the difference in spatial distribution of the receptor and its interacting proteins. We have shown that GPVI clustering is sustained over time (*Chapter 3*) and this could represent the underlying mechanism involved in maintaining the active signalling required to support platelet adhesion to collagen.

GPVI surface density, and therefore platelet reactivity to collagen, is regulated by ADAM10 and ADAM17-mediated ectodomain shedding in human and mouse platelets (Bender et al., 2010, Bergmeier et al., 2004, Facey et al., 2016, Gardiner et al., 2007). In suspension, activation of human platelets by collagen and other ligands leads to shedding of GPVI,

thereby limiting activation (Gardiner et al., 2004). This paradoxically could lead to the unwanted embolisation of platelets from an immobilised surface. To date, shedding of GPVI in platelets adhered to and spreading on an immobilised collagen substrate, which would represent the first step of thrombus formation or adhesion of platelets to the ECM in a blood vessel with compromised integrity, has not been investigated.

In this Chapter, we have used biochemical methods combined with cutting-edge microscopy techniques to elucidate the dynamics of GPVI signalling and shedding in platelets spreading on fibrillar collagen and compare with those observed in platelets stimulated in suspension. A broad investigation of GPVI localisation was then undertaken to understand whether the receptor colocalises with downstream signalling mediators and/or the metalloproteinase ADAM10. In addition, we have interrogated the putative role of secondary mediators, ADP and TXA_2, in GPVI cluster forming and whether sustained Src-family and Syk kinases activation represents a positive feedback loop acting on GPVI oligomerisation in response to collagen.

4.3 Results

4.3.1 GPVI signalling is sustained over time in platelets adhering to immobilised collagen

In vitro studies in platelets and cell lines activated with receptor agonists in suspension have demonstrated that fibrillar collagen triggers slow but sustained GPVI signalling (Tomlinson et al., 2007) in tandem with shedding of the receptor (Gardiner et al., 2004). This raises the question of whether this is also the case on an immobilised surface where shedding might lead to loss of adhesion to collagen. In Fig. 4.1A, confocal imaging of F-actin shows that the stress fibres are already formed after 15 min of spreading and the fully-spread state is maintained for up to 3 h. Reflection images illustrate how spread platelets distribute along the collagen fibres. As expected, there was a steady increase in the number of platelets coming into contact with the fibres over time, however no change in the platelet surface area was observed (Fig. 4.1B, C).

To assess platelet signalling in these cells, whole-cell tyrosine phosphorylation and specific phosphorylation sites on two key signalling mediators, Syk and LAT, which are positioned at the centre of the GPVI signalling pathway, were measured by Western blot (Fig. 4.2A). Total phospho-tyrosine levels, detected by the antibody clone 4G10, increased in adhered platelets relative to cells in suspension (non-adhered, NA) and remain sustained over time (Fig. 4.2A). Site-specific tyrosine phosphorylation of both Syk (Y525/526) and LAT (Y200), residues associated with activation and docking, respectively, was maintained, with no significant change over 3 h (Fig. 4.2A, B, C).

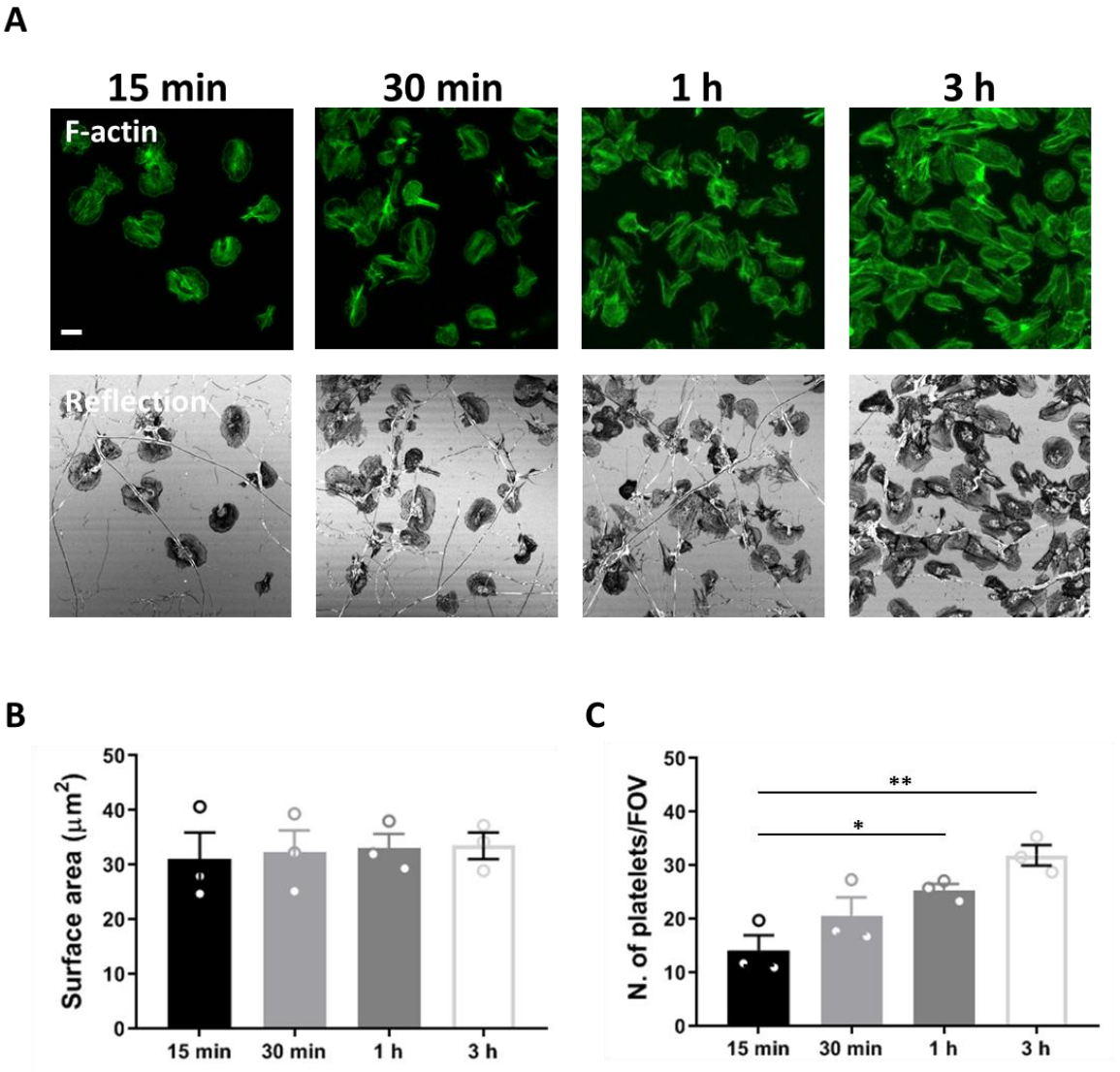

Figure 4.1. Time course of platelets spreading on a collagen monolayer. Human washed platelets were spread on a Horm collagen-coated surface (10 µg ml^{-1}) for the indicated times, labelled with Alexa Fluor 488 phalloidin (F-actin) and imaged by confocal microscopy. Platelet spreading at different time points is illustrated in the confocal images of the actin cytoskeleton (A, first panel) whereas the reflection images show how platelets localise along the collagen fibres (A, second panel). Mean ± SEM platelet surface area (B) and platelet number (C) were measured in KNIME integrated with Ilastik pixel classifier to segment individual cells. In total, 15 FOVs for each condition from three representative experiments were analysed. Significance ($P < 0.05$) was measured using one-way ANOVA with Tukey's multiple comparisons. Scale bar: 5 µm.

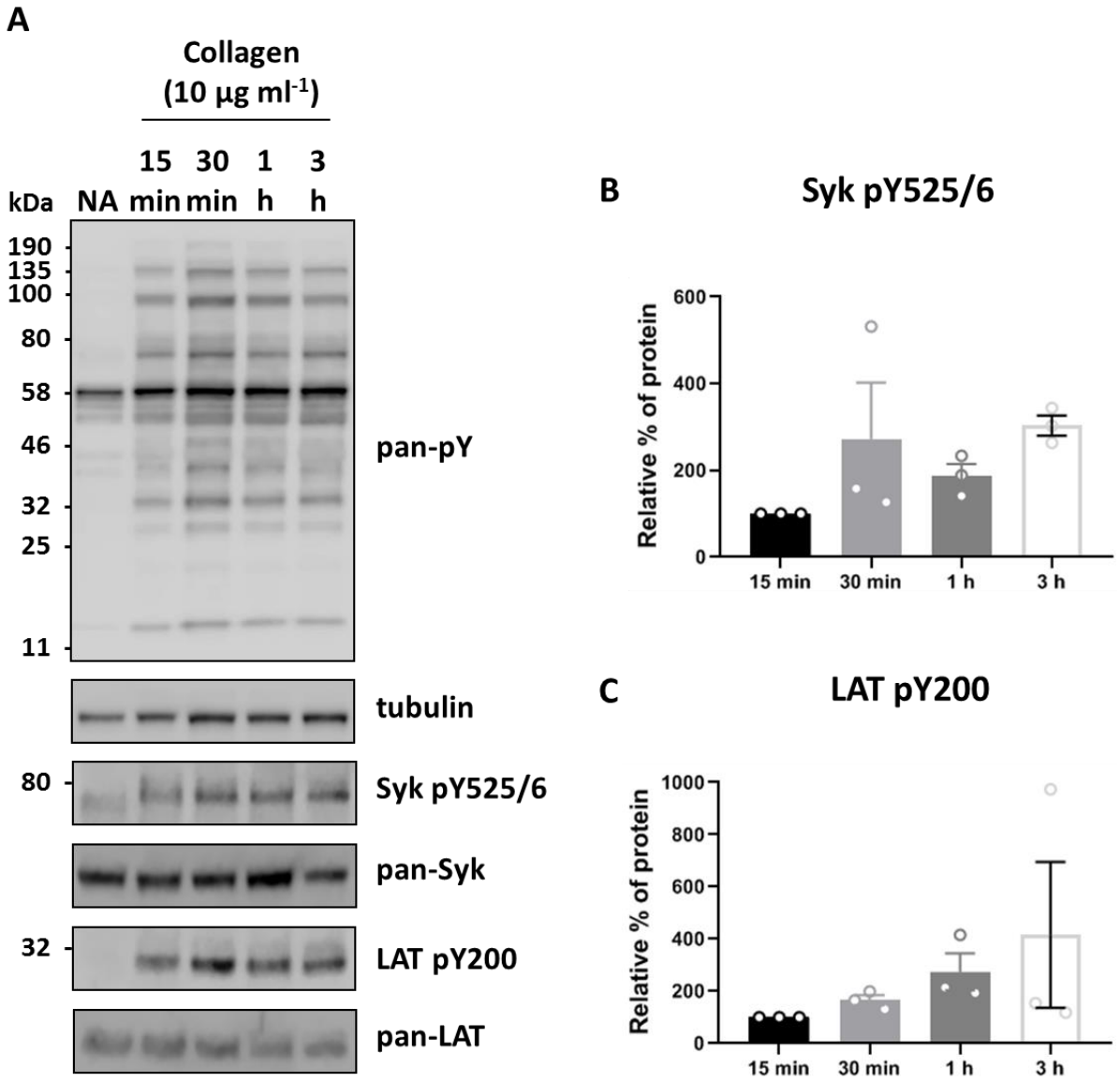

Figure 4.2. Whole-cell tyrosine phosphorylation and site-specific phosphorylation of Syk and LAT are sustained over time in platelets adhered to collagen. Human washed platelets were spread on a collagen (10 µg ml^{-1})-coated surface at 37 °C for the indicated times. Spread and non-adherent (NA) platelets were gathered, lysed, separated by SDS-PAGE and immunoblotted with the phosphotyrosine antibody (4G10) and antibodies specific for phosphorylated Syk (Y525/6) and LAT (Y200) (A). The antibodies against α-tubulin, pan-Syk and pan-LAT were used as loading controls for total phosphotyrosines, phospho-Syk and phospho-LAT, respectively (A). The secondary labelling was carried out using HRP conjugated secondary antibody (for 4G10) and IRDye 800CW conjugated secondary antibodies (for Syk pY525/6 and LAT pY200). The detection of the bands was performed using the Odyssey Fc system (LI-COR) with Syk and LAT appearing at ~72 kDa and ~35 kDa, respectively (A). Normalized quantification of band intensities against the pan signals is shown in B and C as mean ± SEM relative % of protein (the start point was set at 100%) from three independent experiments.

The last step of GPVI signalling transduction is represented by Ca^{2+} movement from intracellular compartments upon activation of PLCγ2 (Nieswandt and Watson, 2003). Therefore, we monitored the Ca^{2+} spiking in platelets labelled with the Ca^{2+} dye Oregon green 488 BAPTA-1-AM that had been spread on immobilised collagen for different time periods: 15 min, 30 min, 1 h and 3 h (Fig. 4.3). From the single-cell analysis, conducted in MATLAB, we were able to extract important features such as percentage of spiking platelets, number of Ca^{2+} spikes per platelet, amplitude and the peak duration. The analysis clearly shows that the percentage of spiking platelets spread on collagen for 3 h remained constant (Fig. 4.3A) and these were still able to spike with the same frequency (Fig. 4.3B), although the amplitude and peak duration slightly declined (Fig. 4.3C, D). Overall, immobilised collagen supports platelet spreading via GPVI signalling for at least 3 h.

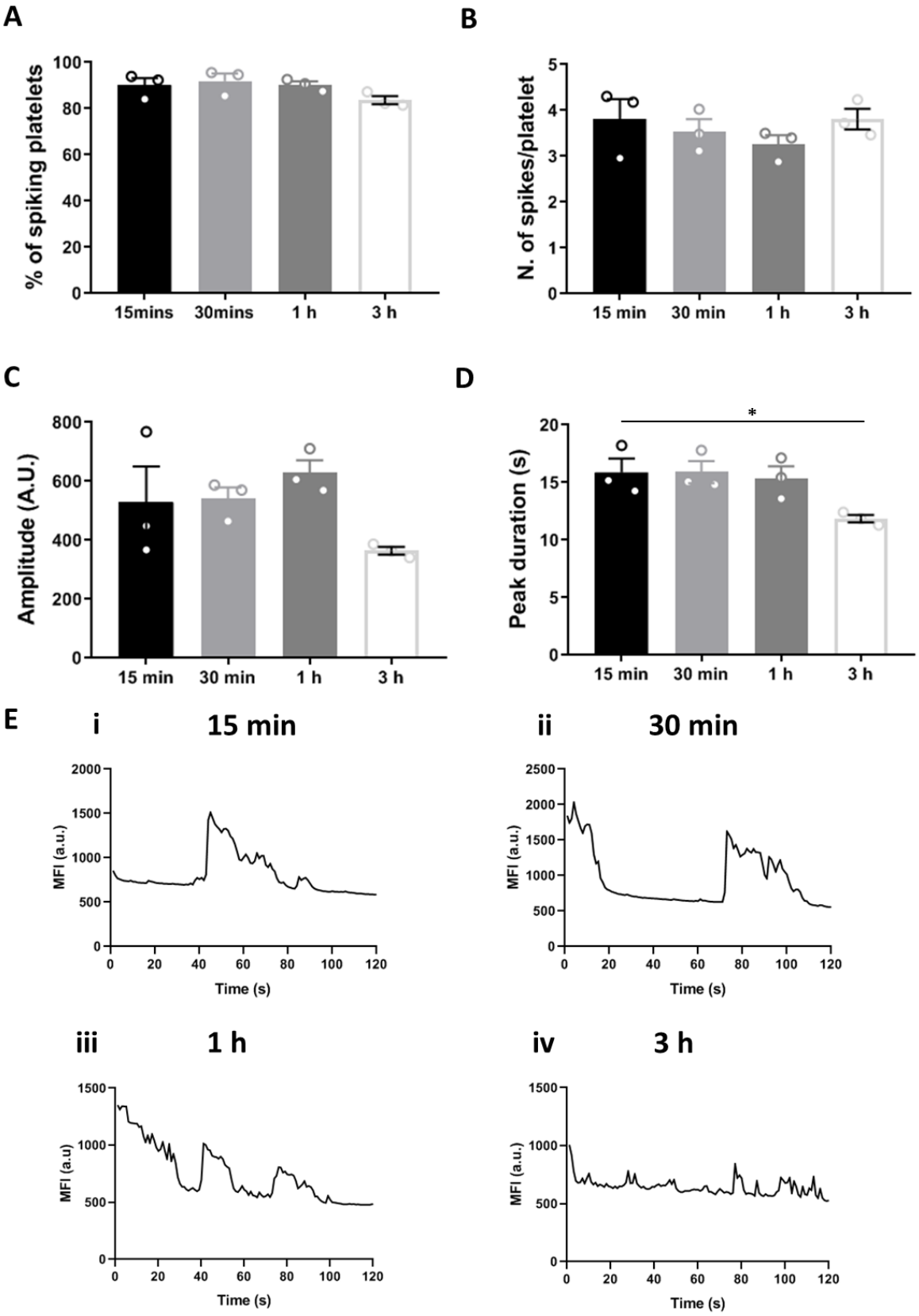
A
% of spiking platelets
100
80
60
40
20
0
15mins
30mins
1 h
3 h
B
N. of spikes/platelet
5
4
3
2
1
0
15 min
30 min
1 h
3 h
C
Amplitude (A.U.)
800
600
400
200
0
15 min
30 min
1 h
3 h
D
Peak duration (s)
*
20
15
10
5
0
15 min
30 min
1 h
3 h
E
i
15 min
ii
30 min
MFI (a.u.)
Time (s)
iii
1 h
iv
3 h
MFI (a.u)

Figure 4.3. Collagen-induced Ca^{2+} mobilisation remains constant in platelets spread for 3 h. Live-cell imaging of Ca^{2+} mobilisation in platelets labelled with Oregon green-488 BAPTA-1-AM Ca^{2+} dye and spread on a collagen (10 µg ml^{-1}) monolayer at 37 °C for the indicated time points. The Ca^{2+} influx was recorded by epifluorescence microscopy and images captured every 1 sec for 2 min (1 or 2 movies for each condition were acquired). Using a threshold of 20 fluorescent unit, the percentage of spiking platelets (A), number of spikes per platelet (B), amplitude (C) and peak duration (D) were measured in MATLAB on three representative FOVs for each time point (~150 platelets in each FOV) from three independent experiments. Data are expressed as mean ± SEM. Significance was calculated using one-way ANOVA with Tukey's multiple comparisons test: a significance of $P < 0.05$ is indicated by *. For each time point, representative Ca^{2+} traces in a single cell are shown in Ei, ii, iii, iv. The MATLAB coding and data analysis were kindly carried out by Christopher O'Shea, University of Birmingham, UK. The MATLAB code used can be found in Appendix I.

4.3.2 GPVI signalling declines over time in platelets stimulated with collagen in suspension

To investigate whether the signalling dynamics underlying GPVI pathway are different in non-static conditions, platelets were stimulated with collagen in suspension for 90 sec, 15 min, 30 min, 1 h and 3 h in the presence of integrilin to prevent integrin αIIbβ3 signalling and therefore platelet aggregation. The site-specific phosphorylation of Syk and LAT, central mediators of GPVI signalling activation, was followed over time by Western blot. Both Syk and LAT were not phosphorylated in unstimulated platelets (Fig. 4.4A). Collagen induced a strong and rapid phosphorylation of the signalling proteins after 90 sec of stimulation but the signalling activation appeared to decrease over time (Fig. 4.4A, B, C). The drop in tyrosine phosphorylation was detected after 15 min of collagen stimulation and the downregulation remained steady for up to 3 h (Fig. 4.4A, B, C). From these data we conclude that, unlike platelets adhered to a static monolayer, following an initial spike in phosphorylation, collagen induces a decay in GPVI signalling over time in platelets stimulated in suspension.

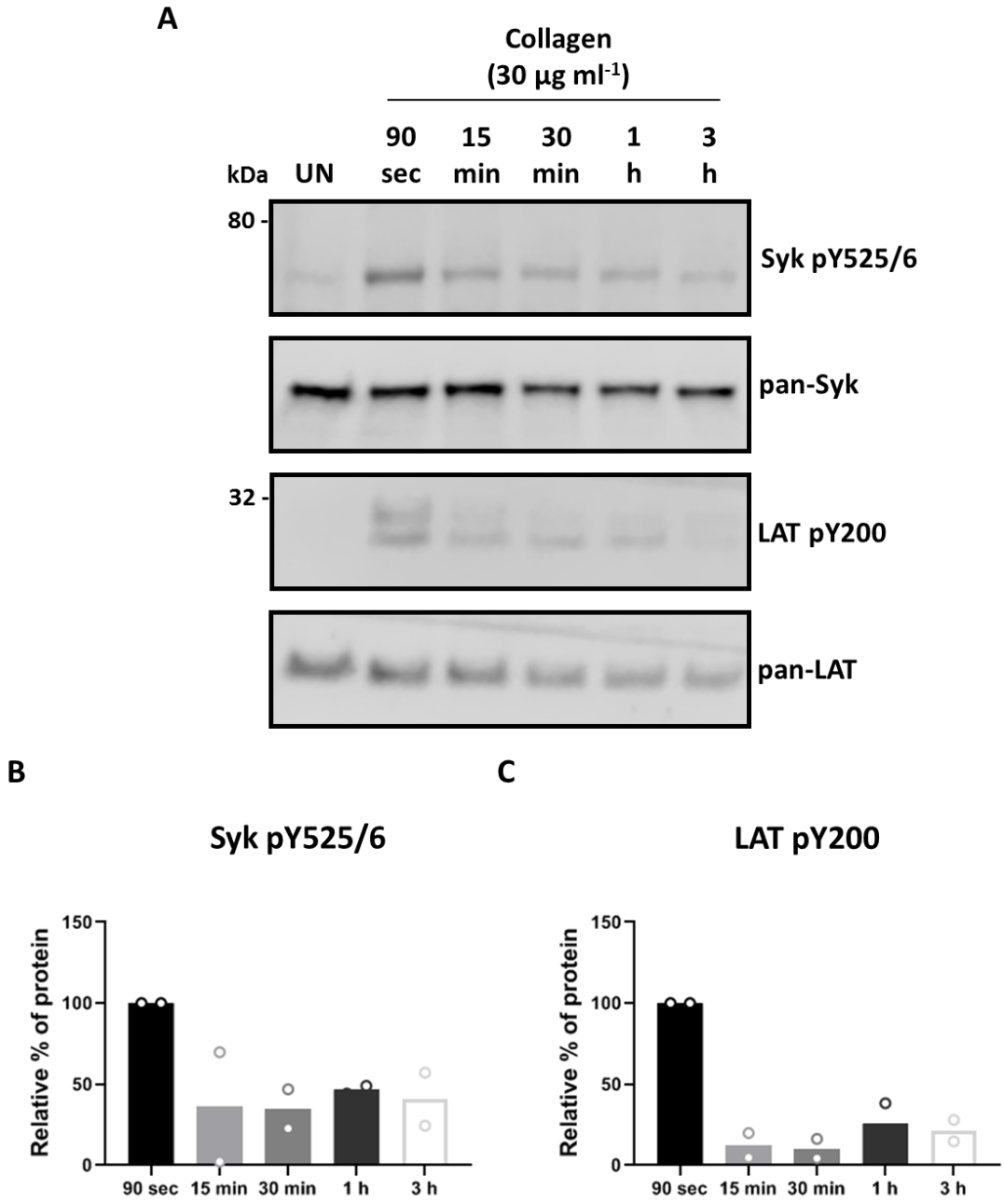

Figure 4.4. Site-specific phosphorylation of Syk and LAT decreases over time in platelets stimulated with collagen in suspension. Human washed platelets were stimulated with collagen (30 µg ml^{-1}) and collagen diluent (unstimulated, UN), in the presence of 9 µM integrilin, under stirring conditions at 37 °C for the indicated time course. Stimulated and non-stimulated platelets were collected, lysed, separated by SDS-PAGE and Western blotted for phospho-Syk (Y525/6) and phospho-LAT (Y200) (A). Pan-Syk and pan-LAT antibodies were used to verify the loading. The secondary labelling was carried out using IRDye 800CW conjugated secondary antibodies. The fluorescent detection of the phospho-proteins was undertaken using the Odyssey Fc system (LI-COR) in the 800 nm channel (A). The signal intensities were quantified, normalized against the pan signals and plotted as mean % relative of protein (the start point was set at 100%) from two independent experiments (B, C).

4.3.3 Sustained signalling colocalises with GPVI on collagen in spread platelets

Western blot analysis gives an overview of the signalling events taking place in the whole platelet but it does not give any spatial information about where these events are taking place. To visualise areas where the signalling is occurring, platelets spread on immobilised collagen for 1 h were labelled for GPVI using 1G5-Fab and phospho-tyrosines using the antibody clone 4G10. High-resolution confocal imaging shows that phosphorylated proteins (magenta) are specifically organised along collagen fibres where GPVI (cyan) is abundantly present (Fig. 4.5), which is in agreement with similar experiments carried out by (Poulter et al., 2017). The 4G10 antibody labels all phosphorylated tyrosines, some of which may represent negative regulation of the protein. To identify the activated signalling proteins lined up along fibrous collagen, spread platelets were labelled for phospho-Syk (Y525/6) and phospho-LAT (Y200) and imaged by confocal microscopy. The images in Fig. 4.6A illustrate that, despite the different distribution pattern of the two proteins, both pSyk Y525/6 (Fig. 4.6Aii) and pLAT Y200 (Fig. 4.6Aiv) are concentrated along collagen (indicated by red arrows) in comparison with the lower density of phospho-proteins detected in areas where there are no visible collagen fibres. Total (pan) Syk and LAT, used as controls, cover most of the platelet surface, resulting in a more homogenous distribution (Fig. 4.6Ai,iii). Dual-colour confocal imaging of GPVI and phosphorylated signalling mediators was carried out to assess their location in platelets spread on collagen (Fig. 4.6B). A combination of qualitative (colocalisation mask, showing pixels which contain both GPVI and phospho-proteins, Fig. 4.6Biv) and quantitative (Pearson's correlation coefficient, Fig. 4.6C) analyses demonstrates that there is a high degree of colocalisation between the phosphorylated signalling proteins and GPVI along collagen after 1 h of spreading (~50%) and the colocalisation is sustained for

up to at least 3 h. Taken together, these data suggest that fibrous collagen represents the site of signalling activation where GPVI highly colocalises with phosphorylated signalling mediators to sustain platelet activation over time.

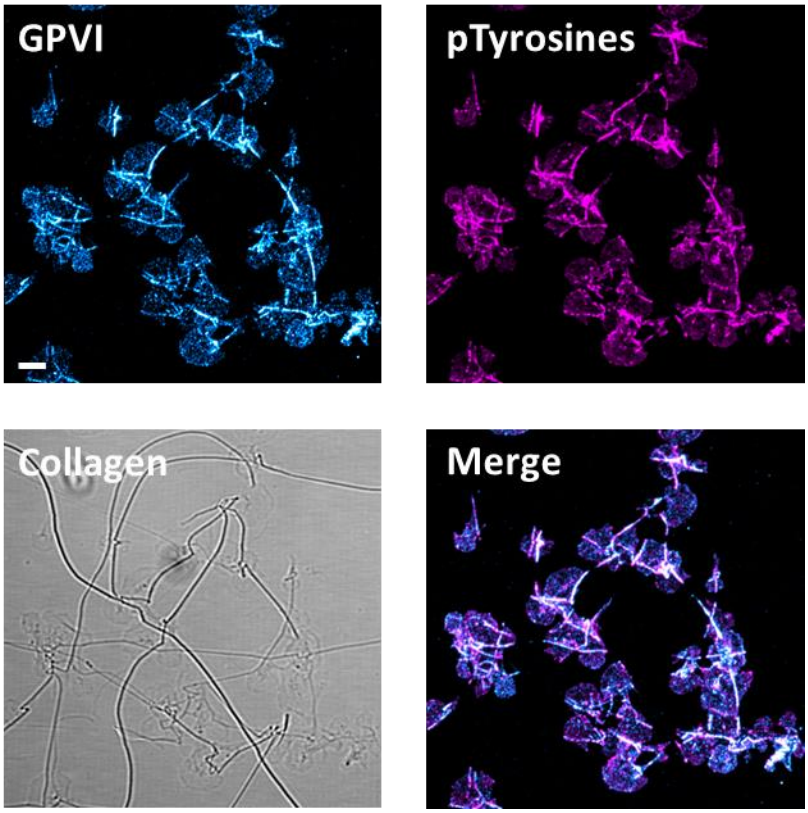

Figure 4.5. Phospho-tyrosines are concentrated along collagen fibres in spread platelets. Human washed platelets, spread on a collagen (10 µg ml^{-1}) monolayer for 1 h, were labelled with 1G5-Fab for GPVI (Cyan) and 4G10 Alexa Fluor 647 conjugated for phospho-tyrosines (magenta). Samples, secondary stained with anti-mouse Alexa Fluor 488 conjugated for GPVI, were imaged via Zeiss LSM 880 with Airyscan Fast. Images are maximum intensity projections of confocal z-stacks. The Merge image highlights the colocalisation of GPVI and phosphorylated proteins along collagen fibres (indicated by white colour). Visualisation of the collagen distribution was carried out using the transmitted light. In total, 12 FOVs from three independent experiments were acquired. Scale bar: 5 µm.

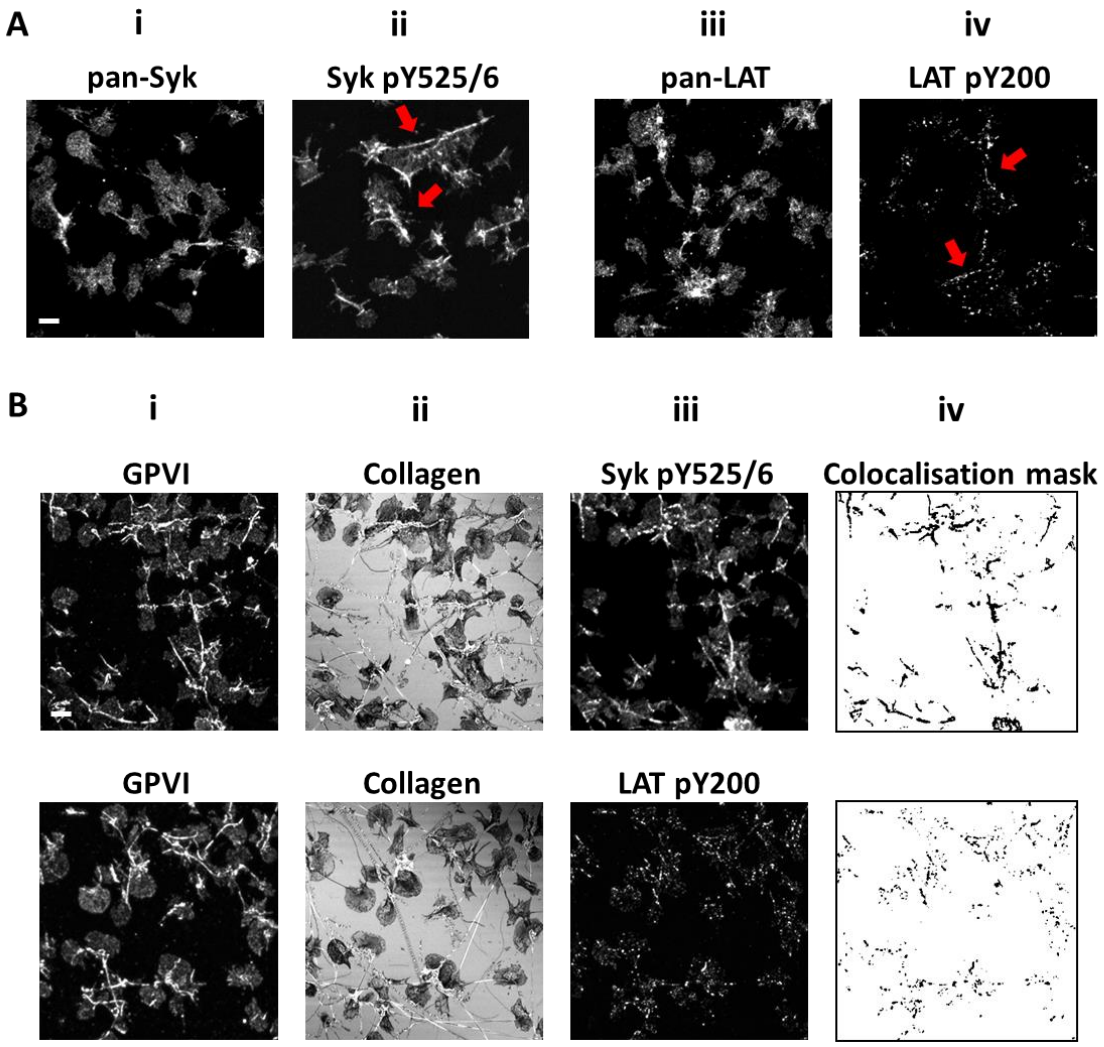
A
i
ii
iii
iv
pan-Syk
Syk pY525/6
pan-LAT
LAT pY200
B
i
ii
iii
iv
GPVI
Collagen
Syk pY525/6
Colocalisation mask
GPVI
Collagen
LAT pY200
C
Pearson's correlation coefficient
1.0
0.8
0.6
0.4
0.2
0.0
*
GPVI-Syk pY525/6 1h
GPVI-Syk pY525/6 3h
GPVI-LAT pY200 1h
GPVI-LAT pY200 3h

Figure 4.6. Phosphorylated Syk and LAT colocalise with GPVI along collagen fibres. Confocal microscopy imaging of human washed platelets spread on collagen (10 µg ml^{-1}) for 1 h, labelled for (Ai) Pan-Syk, (Aiii) Pan-LAT, LAT pY200 (Aiv) and secondary stained with anti-rabbit Alexa Fluor 488 conjugated. Platelets were also labelled for pSyk Y525/6 (Aii) using the conjugated antibody Syk pY525/6-Alexa Fluor 647. The enrichment of Syk pY525/6 and LAT pY200 along fibrous collagen is indicated by red arrows (Aii, iv). Dual-colour confocal imaging of platelets, pre-incubated for Pan-GPVI using 1G5-Fab (Bi, first panel), spread on collagen for 1 h and 3 h, post-labelled with Syk pY525/6 Alexa Fluor 647 conjugated and secondary stained with anti-mouse Alexa Fluor 488 conjugated for GPVI (Biii, first panel). Platelets, pre-incubated with 1G5-Fab for GPVI (Bi, second panel), were also post-labelled for LAT pY200 (Biii, second panel) and secondary stained with anti-mouse Alexa Fluor 647 conjugated (for GPVI) and anti-rabbit Alexa Fluor 488 conjugated (for LAT pY200). Only the confocal images relative to 1 h of spreading are shown (B). Reflection images display the presence of platelets seeded on collagen (Bii). In total, 15 FOVs for each condition from three independent experiments were acquired. The qualitative and quantitative colocalisation analyses were performed in Fiji. The colocalisation mask shows only the colocalising pixels of GPVI and phospho-proteins in the representative FOV (Biv). Scatter plot represents mean ± SEM of Pearson's correlation coefficient measured on n=30 platelets from three independent experiments (C). Significance, set to $P < 0.05$, was measured using unpaired two-tailed t-test. Scale bar: 5µm.

4.3.4 GPVI shedding is minimal in platelets spreading on collagen

We hypothesized that GPVI shedding from the platelet surface may regulate the duration of the signalling. In human platelets, GPVI is cleaved upon stimulation in suspension with different agonists, predominantly through ADAM10 (Gardiner et al., 2004). However, whether GPVI is cleaved in platelets that have been spread on an immobile ligand is still unknown. Here, we have used an antibody which is specific for the cytosolic tail of GPVI to assess the degree of GPVI shedding that is occurring in platelets spread for different time periods on collagen. Intact GPVI has a molecular weight of ~65 kDa but, when the extracellular domain is shed, the cytosolic tail that remains bound to the platelet is ~10 kDa. First, we investigated GPVI shedding in platelets stimulated with collagen in suspension to confirm the findings reported in the literature. Platelets, pre-treated with $CaCl_2$ to induce Ca^{2+}-dependent metalloproteinases activation, were stimulated with collagen under stirring conditions for different time points and GPVI shedding was assessed over time. Western blot showed that, in unstimulated platelets, GPVI remains intact whereas it is cleaved upon collagen stimulation, with the decrease in the amount of the receptor full-length and the appearance of the membrane-bound tail detected (Fig. 4.7A). The extent of GPVI cleavage rose proportionally with the time of stimulation, reaching ~70% of GPVI shed after 3 h of stimulation (Fig. 4.7B). As a positive control, platelets were also stimulated with the thiol-modifying reagent NEM, which triggers activation of human platelet metalloproteinases. NEM induced ~100% of GPVI shedding (Fig. 4.7A, B). On the contrary, in platelets adhered to a static collagen monolayer, only a minimal amount of GPVI shedding was detected, with ~15% shed after 3 h of spreading (Fig. 4.7C, D). In platelets that have not come into contact with collagen (non-adhered, NA, Fig. 4.7C, D), no GPVI shedding was detected, indicating that GPVI is only cleaved upon platelet activation.

To complement the Western blot data we carried out two-colour immunolocalisation of the intracellular tail of GPVI (using the anti-GPVI-tail antibody) and the extracellular domain (using 1G5-Fab) to get spatial information on the intact receptor. Epifluorescence imaging reveals a strong overlap of the two receptor domains, which was particularly prevalent along the collagen fibres, as highlighted in the colocalisation mask (Fig. 4.8A). Dual-colour *d*STORM imaging confirmed the high degree of colocalisation between the extracellular and intracellular domains of GPVI clusters along collagen fibres, indicated in white in the Merge image (Fig. 4.8B). This indicates that this pool of GPVI has not been shed from the platelets in this 3 h timeframe, in accordance with the biochemical data.

To further support our hypothesis that GPVI shedding is not occurring in platelets spread on collagen we investigated the location of the GPVI sheddase ADAM10 in relation to that of GPVI oligomers in spread platelets using two-colour epifluorescence (Fig. 4.8C) and *d*STORM (Fig. 4.8D) imaging. The images highlight the different distribution of the two proteins, with no visible enrichment of ADAM10 at collagen fibres as is seen for GPVI (Fig. 4.8C). Dual-colour *d*STORM imaging enabled us to assess the nanoscale organisation of the collagen receptor and the sheddase at the single molecule level (Fig. 4.8D). ADAM10 appeared to be uniformly distributed at the platelet surface and most of the ADAM10 localisations do not colocalise with the tightly packed GPVI clusters, suggesting that the metalloproteinase may be excluded from the receptor clusters, preventing shedding and allowing signalling to continue.

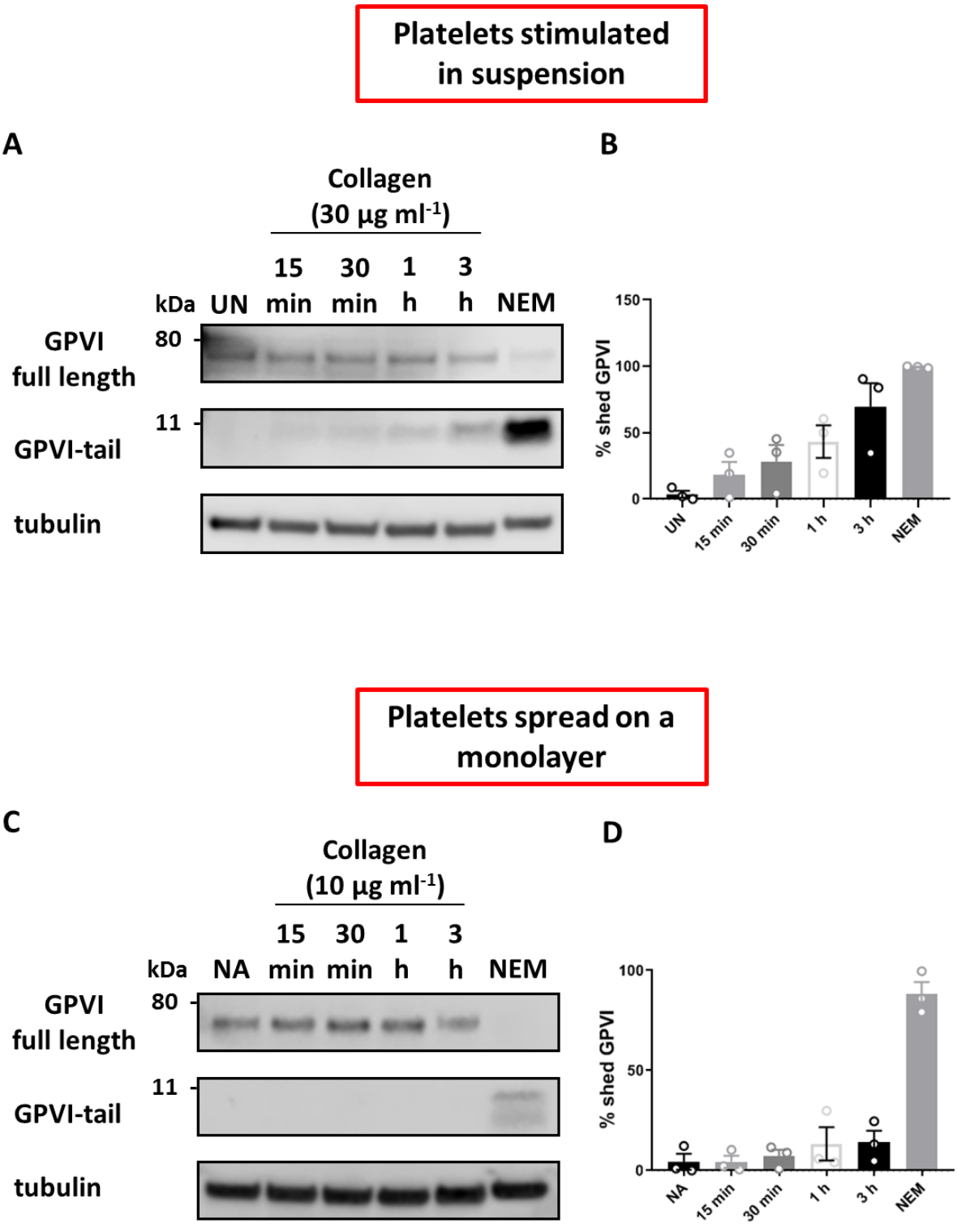
Platelets stimulated in suspension
A
Collagen (30 µg ml-1)
15 min
30 min
1 h
3 h
kDa
UN
NEM
GPVI full length
80
11
GPVI-tail
tubulin
B
% shed GPVI
150
100
50
0
UN
15 min
30 min
1 h
3 h
NEM
Platelets spread on a monolayer
C
Collagen (10 µg ml-1)
15 min
30 min
1 h
3 h
kDa
NA
NEM
GPVI full length
80
11
GPVI-tail
tubulin
D
% shed GPVI
100
50
0
NA
15 min
30 min
1 h
3 h
NEM

Figure 4.7. GPVI is shed in platelets stimulated in suspension but not in those spread on a monolayer. Human washed platelets, pre-treated with 2 mM $CaCl_2$, were stimulated with collagen (30 µg ml^{-1}) or collagen diluent (unstimulated, UN) for 15 min, 30 min, 1 h and 3 h under stirring conditions. Platelets were also treated with 2 mM NEM for 1 h and used as a positive control of shedding (A). For the analysis of GPVI shedding on a monolayer, platelets were allowed to spread on a collagen (10 µg ml^{-1})-coated surface for the same time points. The supernatant represents the fraction of non-adhered (NA) platelets. The positive control NEM (2 mM) was added for 30 min to platelets that have been spread on collagen for 2 and a half h (C). Stimulated/adhered and unstimulated/non-adhered platelets were lysed, separated by SDS-PAGE and immunoblotted with anti-GPVI-tail antibody. The α-tubulin antibody was used as a loading control The secondary labelling was carried out using IRDye 800CW conjugated secondary antibodies. Full-length GPVI and GPVI-tail were detected at ~62 kDa and ~10 kDa, respectively, using the Odyssey Fc system (LI-COR) (A, C). The band intensities were measured using Image Studio: percentage of shedding was calculated as: (shed GPVI/full-length GPVI + shed GPVI) *100 (B,D). Bars in the histograms represent the mean ± SEM from three separate experiments.

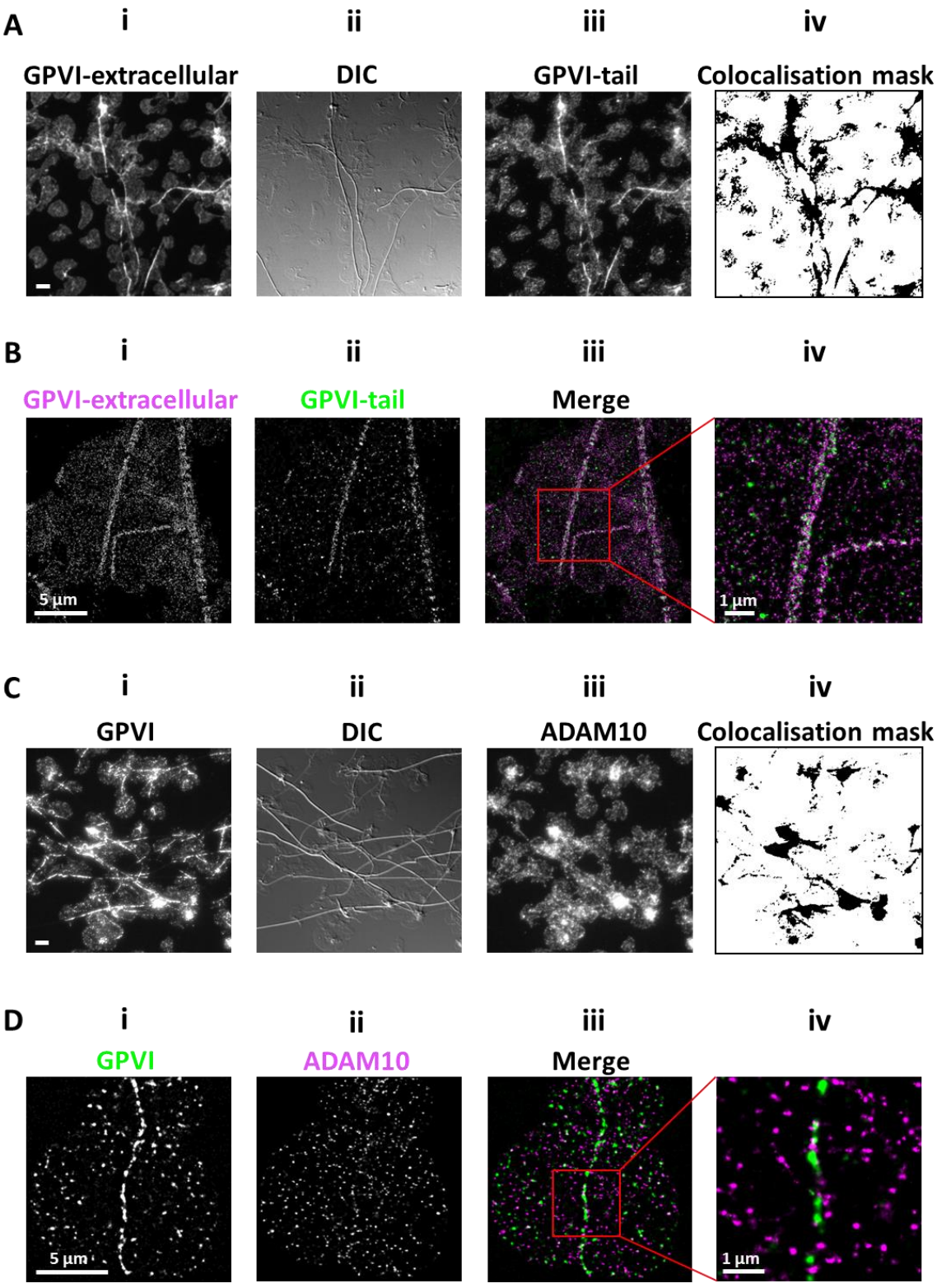
A
i
ii
iii
iv
GPVI-extracellular
DIC
GPVI-tail
Colocalisation mask
B
i
ii
iii
iv
GPVI-extracellular
GPVI-tail
Merge
5 µm
1 µm
C
i
ii
iii
iv
GPVI
DIC
ADAM10
Colocalisation mask
D
i
ii
iii
iv
GPVI
ADAM10
Merge
5 µm
1 µm

Figure 4.8. GPVI extracellular domain colocalise with the intracellular tail but not ADAM10 in platelets spread on collagen. Dual-colour epifluorescence imaging of spread platelets labelled for GPVI extracellular domain (pre-incubation with 1G5-Fab, Ai) and intracellular tail (post-incubation with anti-GPVI-tail, Aiii) and secondary labelled with anti-mouse Alexa Fluor 647 and anti-rabbit Alexa Fluor 488 conjugated, respectively. The distribution of fibrous collagen is shown in the DIC image (Aii). The high level of colocalisation between the two GPVI domains along collagen fibres is highlighted in the colocalization mask (Aiv). In total, 15 FOVs from three independent experiments were acquired. Two-colour *d*STORM imaging illustrates the colocalising clusters of extracellular (Bi) and intracellular (Bii) GPVI on collagen, highlighted in white in the Merge image and magnification of the boxed area (Biii, iv). In total, 7 FOVs from two separate experiments were acquired. Dual-colour epifluorescence imaging of spread platelets pre-labelled with 1G5-Fab for Pan-GPVI (Ci) and post-stained with Alexa Fluor 647 conjugated ADAM10 [11G2] antibody (Ciii). Secondary labelling of GPVI was carried out using anti-mouse Alexa Fluor 488 conjugated. Platelet adhesion to collagen is shown in the DIC image (Cii) whereas the overlapping pixels are selected in the colocalization mask (Civ). In total, 15 FOVs from three independent experiments were acquired. Two-colour *d*STORM imaging of the same platelets allows to visualise the distribution of ADAM10 (Dii) relative to that of GPVI (Di) at the single-molecule level (as shown in the Merge image, Diii, iv). In total, 13 FOVs from three independent experiments were acquired. Scale bar: 5 μm (whole FOVs and single platelet images) and 1 μm (magnified sections inside the boxed regions).

4.3.5 Effect of metalloproteinases inhibition and activation on GPVI cluster formation

To further investigate whether GPVI remains intact and clustered at the cell surface, *d*STORM imaging and two-level DBSCAN cluster analysis was carried out in the presence of the broad-spectrum metalloproteinase inhibitor GM6001, the ADAM10-specific inhibitor GI254023 (pre-spreading) or the generic activator of metalloproteinases NEM (post-spreading) to block or induce receptor shedding, respectively. The concentrations used have previously been shown to block/activate GPVI shedding in platelets (Facey et al., 2016, Gardiner et al., 2004, Gardiner et al., 2007). If GPVI shedding is occurring in spread platelets then we would expect to see an increase in the cluster parameters we are measuring when the metalloproteinase inhibitors are present. NEM is a positive control to show that shedding can occur in spread platelets if stimulated to do so. Both metalloproteinase inhibitors have no effect on platelet spreading (Fig. 4.9A, B). Notably, unlike GM6001, the ADAM10-specific inhibitor GI254023 induced a change in the actin cytoskeleton as shown by the stretching of stress fibres along collagen, likely due to the generation of actin-defined confinement regions for the accumulation of GPVI (Fig. 4.9A). NEM significantly impaired the ability of platelets to bind to collagen showing a significant reduction in the surface area in comparison to the control (Fig. 4.9A, B). No effect on cell count was found in platelets treated with all the compounds (Fig. 4.9B).

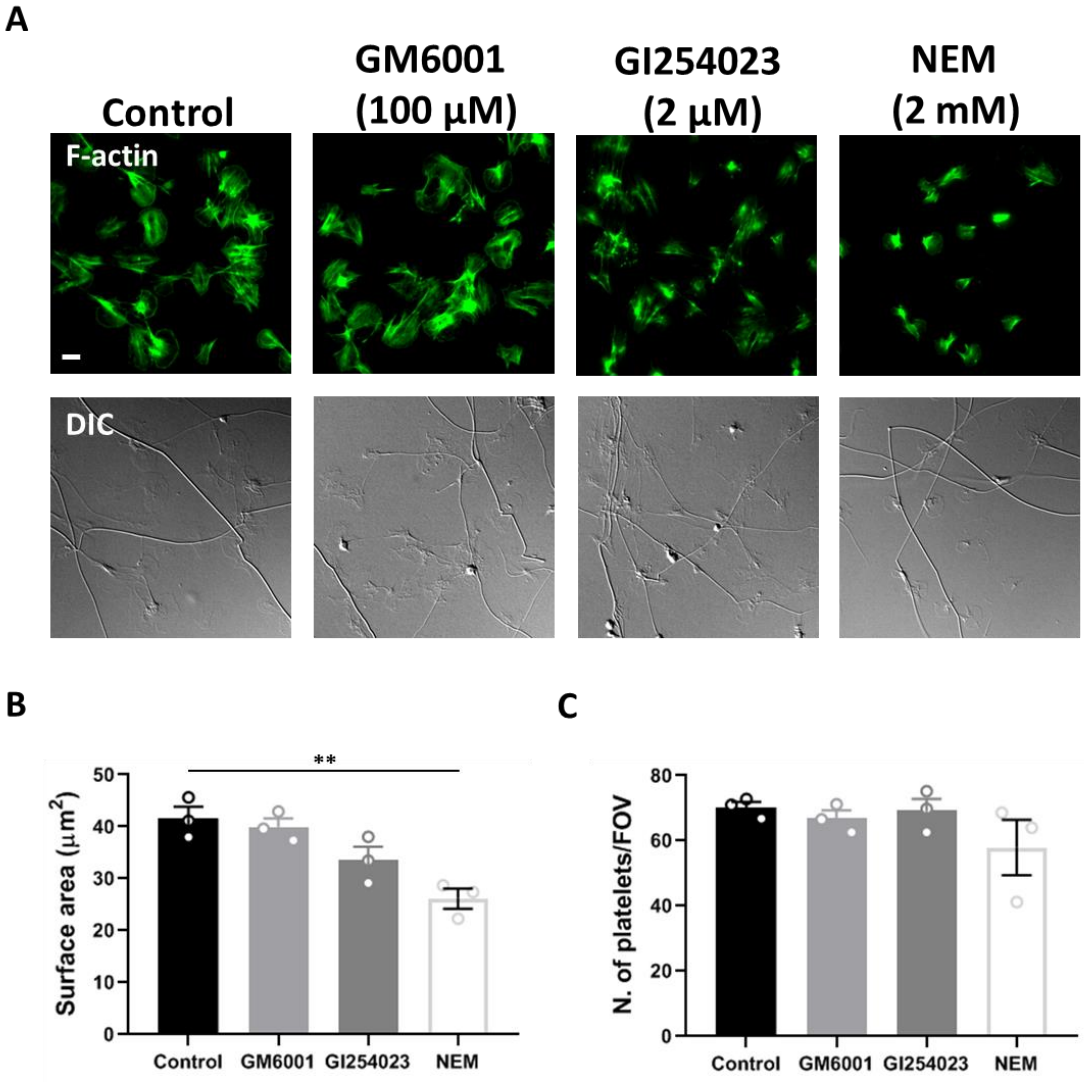

Figure 4.9. Effect of metalloproteinase inhibitors and NEM on platelet spreading. Human washed platelets were treated with GM6001(100 µM) or GI254023 (2 µM) before spreading on a collagen (10 µg ml^{-1}) monolayer for 1 h. NEM (2 mM) was added after spreading and left at 37 °C for 30 min. Control platelets were pre-treated with DMSO (vehicle for metalloproteinases inhibitors), spread on collagen and post-incubated with ethanol (vehicle for NEM) for 30 min. F-actin was labelled with Alexa Fluor 488 phalloidin and imaged by epifluorescence microscopy (A, first panel). The DIC images (A, second panel) illustrate the distribution of platelets on collagen fibres. Quantification of platelet surface area (B) and platelet number (C) in control and treated platelets was performed in KNIME on 15 FOVs for each condition from three independent experiments. Each dot represents the mean of each of the replicates with the overall mean ± SEM shown in the histograms. The significance ($P < 0.05$) was calculated using one-way ANOVA with Tukey's multiple comparisons. Scale bar: 5 µm.

In accordance with this finding, TIRFM and *d*STORM imaging allowed the visualisation of discrete GPVI clusters along collagen in platelets treated with each of the metalloproteinase inhibitors (Fig. 4.10Ai, ii). The DBSCAN-based two-layer cluster analysis enabled the isolation of these large and continuous oligomers colocalising with collagen fibres (Level I clustering, Fig. 4.10Aiii) and further segmentation into nanoclusters (Level II clustering, Fig. 4.10Aiv) in both control and treated platelets. The detected GPVI clusters and nanoclusters along collagen fibres in GM6001 and GI254023-treated platelets were not significantly different from those formed in control platelets in terms of area and density at both clustering levels (Fig. 4.10B, C, D, E). Contrarily, NEM-activating ADAM10 triggered the release of ~90% of GPVI localisations from the human plasma membrane with very few clusters detected (Fig. 4.10F) making the two-level cluster analysis impossible to perform. This again supports the hypothesis that significant GPVI shedding does not occur in platelets spread on collagen.

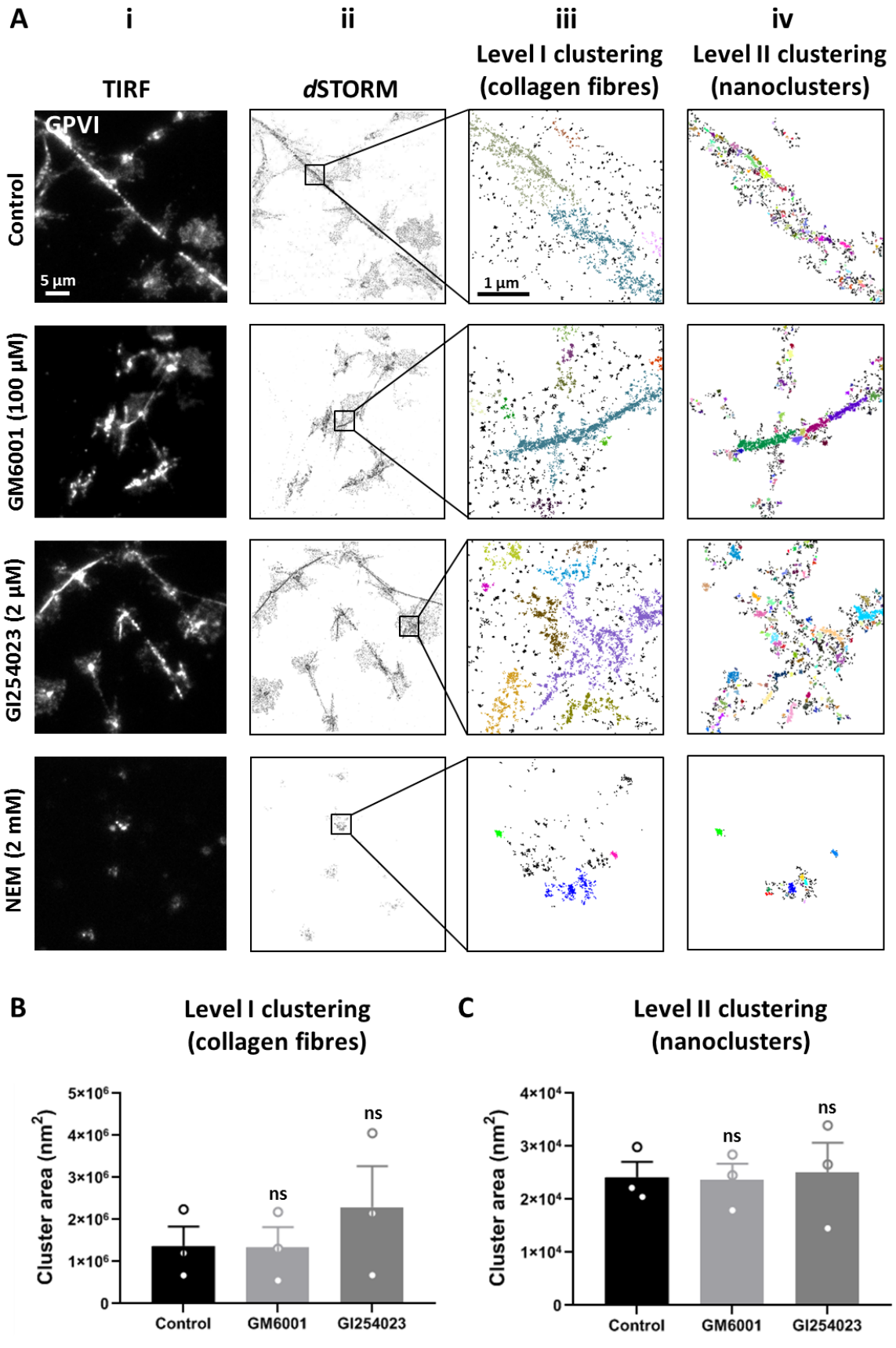
A
i
ii
iii
iv
TIRF
dSTORM
Level I clustering (collagen fibres)
Level II clustering (nanoclusters)
GPVI
Control
GM6001 (100 µM)
GI254023 (2 µM)
NEM (2 mM)
5 µm
1 µm
B
Level I clustering (collagen fibres)
Cluster area (nm²)
5×10⁶
4×10⁶
3×10⁶
2×10⁶
1×10⁶
0
ns
ns
Control
GM6001
GI254023
C
Level II clustering (nanoclusters)
Cluster area (nm²)
4×10⁴
3×10⁴
2×10⁴
1×10⁴
0
ns
ns
Control
GM6001
GI254023

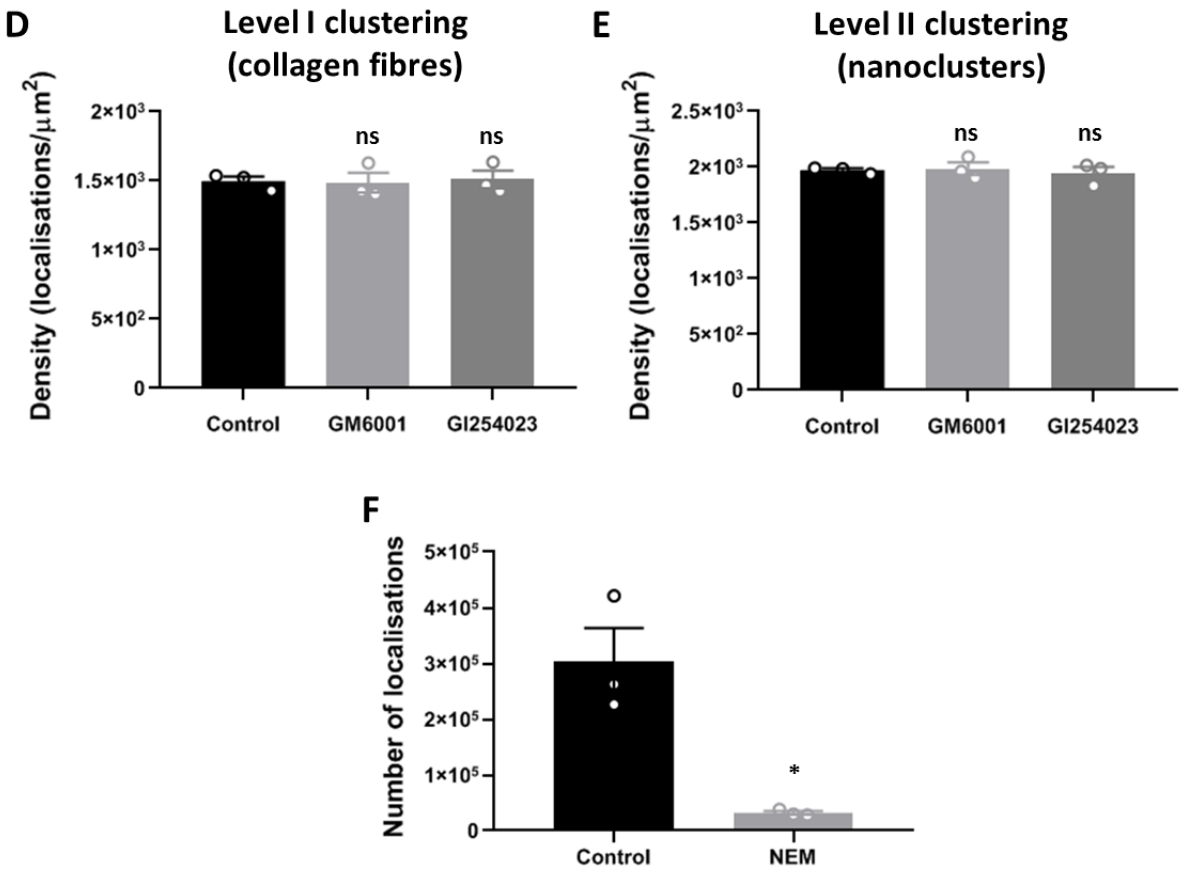

Figure 4.10. Effect of metalloproteinase inhibitors and NEM on GPVI clustering. Human washed platelets, treated with GM6001, GI254023 and NEM as described before, were pre-incubated with 1G5-Fab (2 μg ml^{-1}) for Pan-GPVI, spread on a collagen (10 μg ml^{-1}) monolayer and secondary labelled with anti-mouse Alexa Fluor 647 conjugated to allow GPVI visualisation. Receptor distribution was assessed using *d*STORM imaging in TIRF mode in both control and treated platelets (Ai, ii). GPVI clustering (Level I clustering) and nanoclustering (Level II clustering) along collagen fibres were quantified using two-level DBSCAN-based cluster analysis (Aiii, iv) as described in *Chapter 3* with the same parameters and threshold values. In total, 14 or 15 FOVs were analysed for the control, GM6001and GI254023-treated platelets whereas only 8 FOVs for the NEM-treated platelets. Quantitative analysis relative to GPVI cluster area and density at both clustering levels is reported in B, C, D, E as mean ± SEM from three independent experiments. One-way ANOVA with Tukey's multiple comparisons ($P < 0.05$) shows non-significant (ns) difference in the cluster and nanocluster area and density between the control and platelets treated with metalloproteinase inhibitors. Only a few clusters were detected in platelets incubated with NEM: the histogram in F shows a significantly lower number of localisations in comparison with the control ($P < 0.05$ using unpaired two-tailed t-test). Scale bar: 5 μm (*d*STORM images) and 1 μm (Level I and II cluster plots). The two-level DBSCAN was designed and implemented by Dr Jeremy Pike, University of Birmingham, UK.

4.3.6 Effect of secondary mediators inhibition on platelet spreading, GPVI signalling and clustering on collagen

The secondary mediators, TxA_2 and ADP, enhance the integrin activation on adherent platelets and induce the thrombus development through the recruitment and activation of additional platelets. We, therefore, wanted to test whether secondary mediators have any effect on platelet spreading on collagen as well as collagen-mediated GPVI signalling and oligomerisation. Platelets were pre-incubated with the ADP scavenger apyrase and the cyclooxygenase inhibitor indomethacin at concentrations able to block collagen-induced platelet aggregation (Atkinson et al., 2001), prior to spreading on collagen. Inhibition of secondary mediators did not prevent platelet spreading on collagen as the surface area and count were not affected (Fig. 4.11A, B, C).

The effect of ablation of the secondary mediators pathway on downstream GPVI signalling was then investigated by measuring the total level of tyrosine phosphorylation and the site-specific phosphorylation of Syk and LAT using Western blot. The combined treatment of platelets with indomethacin and apyrase did not have a major effect on whole-cell phosphotyrosines and tyrosine phosphorylation of Syk (Y525/6) and LAT (Y200) in platelets spread on collagen (Fig. 4.12A, B, C), suggesting that secondary mediators are not critical for signalling events downstream of GPVI-collagen interplay in these spreading platelets.

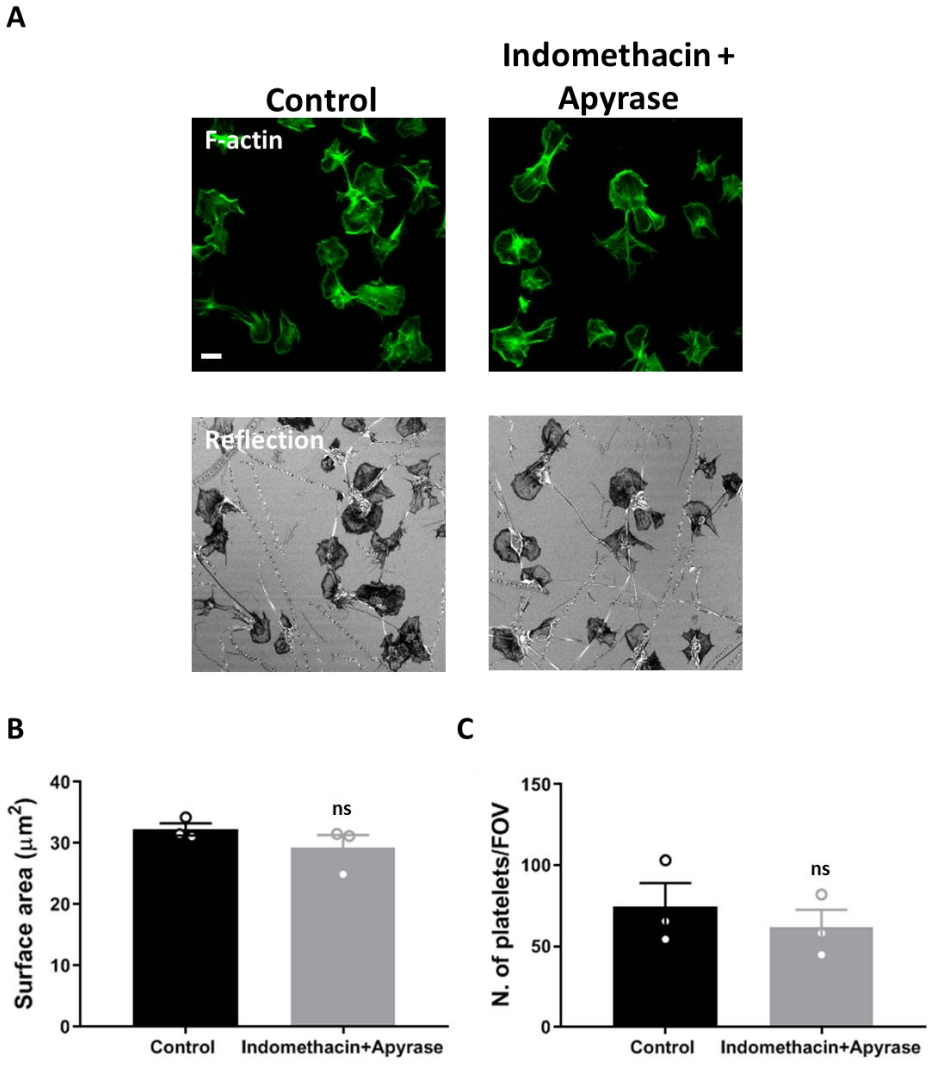

Figure 4.11. Platelet spreading on immobilised collagen occurs independently of secondary mediators signalling. Human washed platelets, pre-incubated with indomethacin (10 µM) and apyrase (2 U/ml) or DMSO (vehicle control) for 10 min, were allowed to spread on a collagen (10 µg ml^{-1})-coated surface for 1 h, stained with Alexa Fluor 488 phalloidin for actin and imaged by confocal microscopy. The effect of secondary mediators inhibitors on platelet actin cytoskeleton (F-actin images, first panel) and platelet adhesion to collagen (Reflection images, second panel) is shown in A. Measurement of platelet surface area and count, conducted in KNIME on 15 FOVs for each condition from three independent experiments, shows non-significant difference between control and treated platelets (B, C). Significance was measured using unpaired two-tailed t-test with $P < 0.05$. Scale bar: 5 µm.

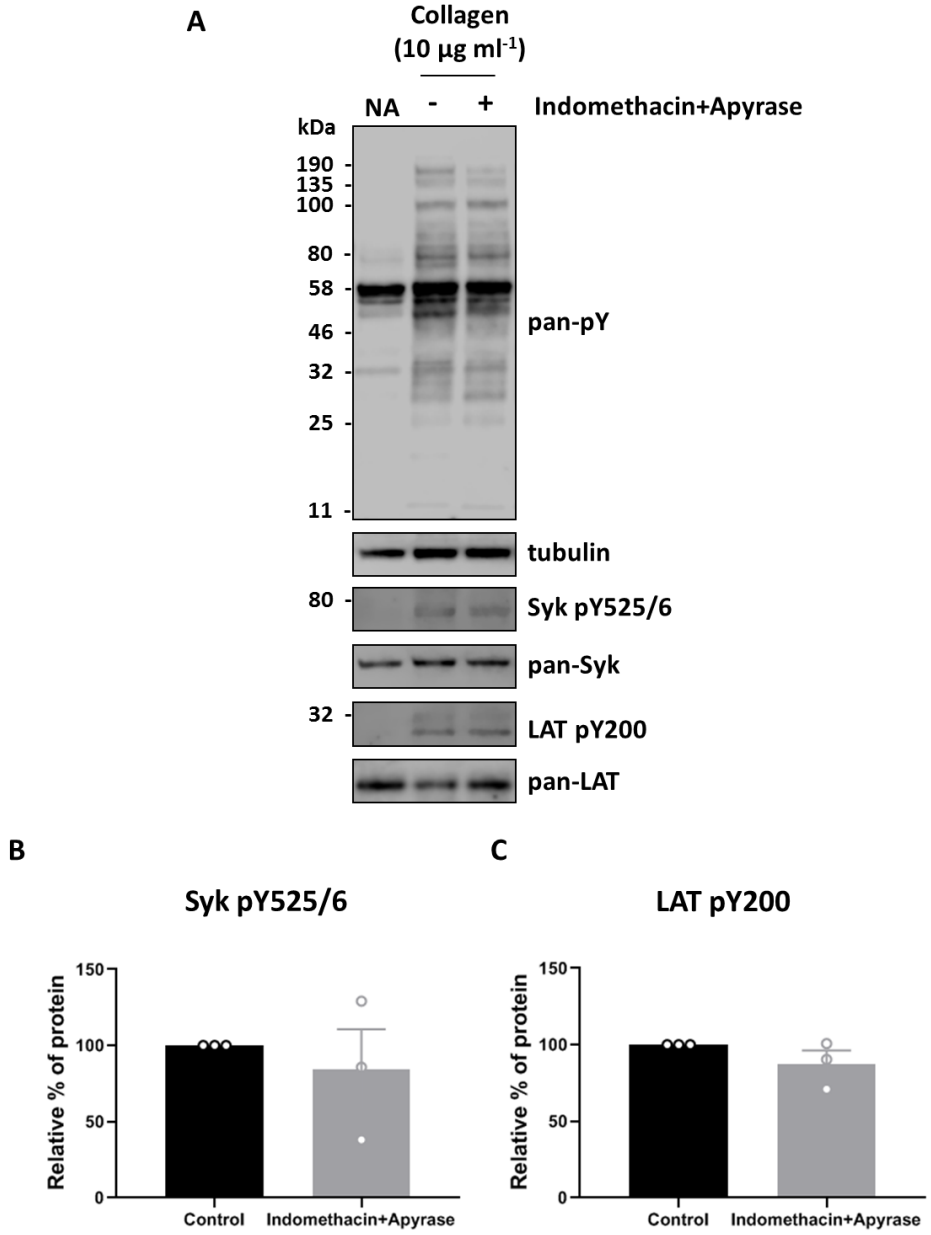

Figure 4.12. Total phosphotyrosines and site-specific phospho-Syk and phospho-LAT levels in platelets spread on collagen in the presence of secondary mediators inhibitors. Human washed platelets, in the presence of indomethacin and apyrase or DMSO (vehicle control), were spread on a collagen (10 µg ml^{-1}) monolayer for 1 h before being lysed. Lysates from non-adhered (NA) and spread platelets were separated by SDS-PAGE and Western blotted using the phosphotyrosine antibody 4G10 and the phospho-specific antibodies against pSyk Y525/6 and pLAT Y200 (A). Antibodies detecting tubulin, pan-Syk and pan-LAT were used as loading controls. The secondary labelling was carried out using HRP conjugated secondary antibody (for 4G10) and IRDye 800CW conjugated secondary antibodies (for Syk pY525/6 and LAT pY200). The detection of the bands was performed using the Odyssey Fc system (LI-COR) (A). The normalized quantification against the pan signals is represented as mean ± SEM relative % of protein (the control was set at 100%) from three independent experiments (B, C).

As we hypothesized that GPVI clustering on collagen is a mechanism to sustain and potentiate the signalling transduction, we expected no effect of ADP and TxA_2 blockers on the ability of GPVI to coalesce in clusters at the cell surface. Indeed, GPVI spatial organisation and oligomerisation in platelets adhered to collagen was not perturbed by the abolishment of secondary mediators activity as shown in the TIRFM and *d*STORM images (Fig. 4.13Ai, ii). The two-layer DBSCAN clustering method was still able to isolate large and dense clusters along collagen in treated platelets (Level I clustering, Fig. 4.13Aiii, B, D). The quantitative analysis also shows that secondary mediators inhibitors did not alter GPVI nanoclusters with unchanged cluster area and density in comparison with the control (Level II clustering, Fig. 4.13Aiv, C, E).

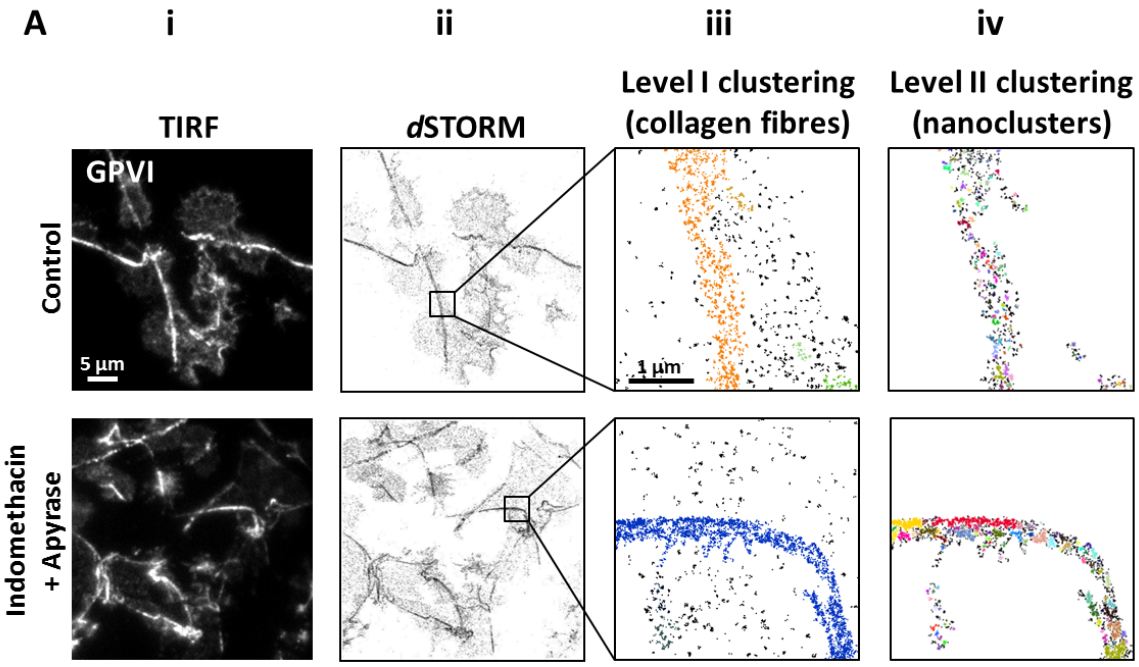
A
i
ii
iii
iv
TIRF
dSTORM
Level I clustering (collagen fibres)
Level II clustering (nanoclusters)
GPVI
Control
Indomethacin + Apyrase
5 µm
1 µm

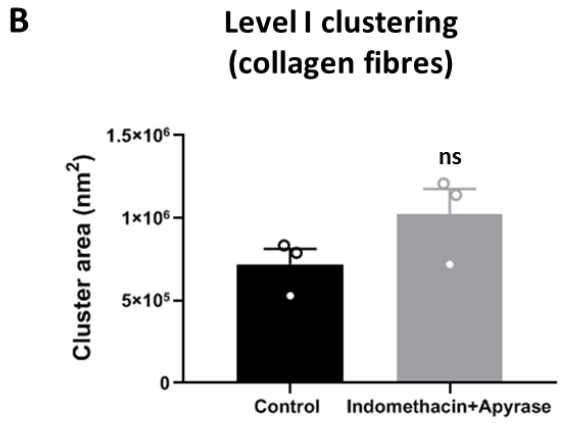
B
Level I clustering (collagen fibres)
Cluster area (nm2)
1.5×10^6
1×10^6
5×10^5
0
ns
Control
Indomethacin+Apyrase

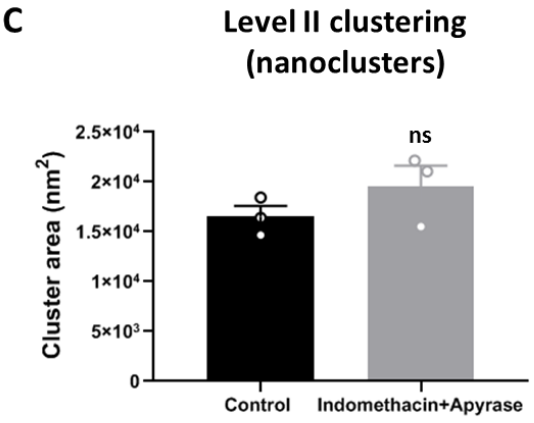
C
Level II clustering (nanoclusters)
Cluster area (nm2)
2.5×10^4
2×10^4
1.5×10^4
1×10^4
5×10^3
0
ns
Control
Indomethacin+Apyrase

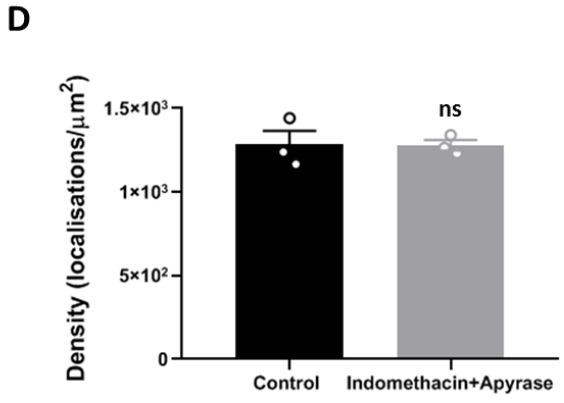
D
Density (localisations/µm2)
1.5×10^3
1×10^3
5×10^2
0
ns
Control
Indomethacin+Apyrase

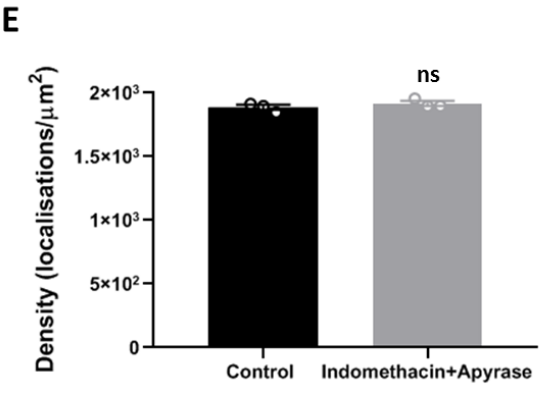
E
Density (localisations/µm2)
2×10^3
1.5×10^3
1×10^3
5×10^2
0
ns
Control
Indomethacin+Apyrase

Figure 4.13. Inhibition of secondary mediators does not perturb GPVI cluster formation in platelets spread on collagen. Human washed platelets, pre-treated with secondary mediators inhibitors or DMSO (vehicle control) and pre-labelled with 1G5-Fab (2 μg ml^{-1}) for GPVI, were spread on a collagen (10 μg ml^{-1})-coated surface for 1 h. Secondary labelling of spread platelets was carried out using anti-mouse Alexa Fluor 647 conjugated before being imaged by *d*STORM in TIRF mode. The diffraction-limited images show the effect of indomethacin and apyrase on GPVI organisation (Ai) whereas *d*STORM allows visualisation of their contribution to GPVI cluster formation on collagen (Aii). GPVI clustering and nanoclustering were assessed using the two-level clustering tool based on DBSCAN (Aiii, iv) with the same parameters and filtering setting applied in the previously described experiment (A). A total of at least 13 FOVs for each condition from three independent experiments were analysed. The histograms show non-significant (ns) difference in the area and density of clusters (B, D) and nanoclusters (C, E) between the control and treatment, calculated using one-way ANOVA with Tukey's multiple comparisons ($P < 0.05$). Data are presented as mean ± SEM from three independent experiments. Scale bar: 5 μm (*d*STORM images) and 1 μm (Level I and II cluster plots). Raw *d*STORM image data was collected by Mark Probert, undergraduate student at University of Birmingham.

4.3.7 Effect of inhibiting Src-family and Syk kinases on platelet spreading on collagen

Our results show that immobilised collagen supports platelet spreading for at least 3 h. To investigate whether Src-family and Syk kinases, fundamental for the initiation of GPVI signalling cascade, are required to maintain platelet spreading downstream of the platelet-collagen interaction, we interrupted the signalling using either the Src-family kinase inhibitor PP2 or the Syk kinase inhibitor PRT-060318 (PRT). To test the efficacy of both compounds, collagen-induced platelet aggregation was carried out in the presence of increasing concentrations of PP2 (10, 20 and 50 μM) and PRT (5, 10 and 20 μM) or DMSO (vehicle). Fig. 4.14 shows that collagen at 10 μg ml^{-1} stimulated ~70% of the maximal aggregation in a 5 min time frame. PP2 and PRT completely blocked platelet aggregation in response to collagen at all the concentrations tested (Fig. 4.14A, B). Therefore, we decided to use concentrations already reported in the literature for further experiments: 20 μM PP2 (Mangin et al., 2018, Spalton et al., 2009) and 10 μM PRT (Montague et al., 2018b, Onselaer et al., 2017).

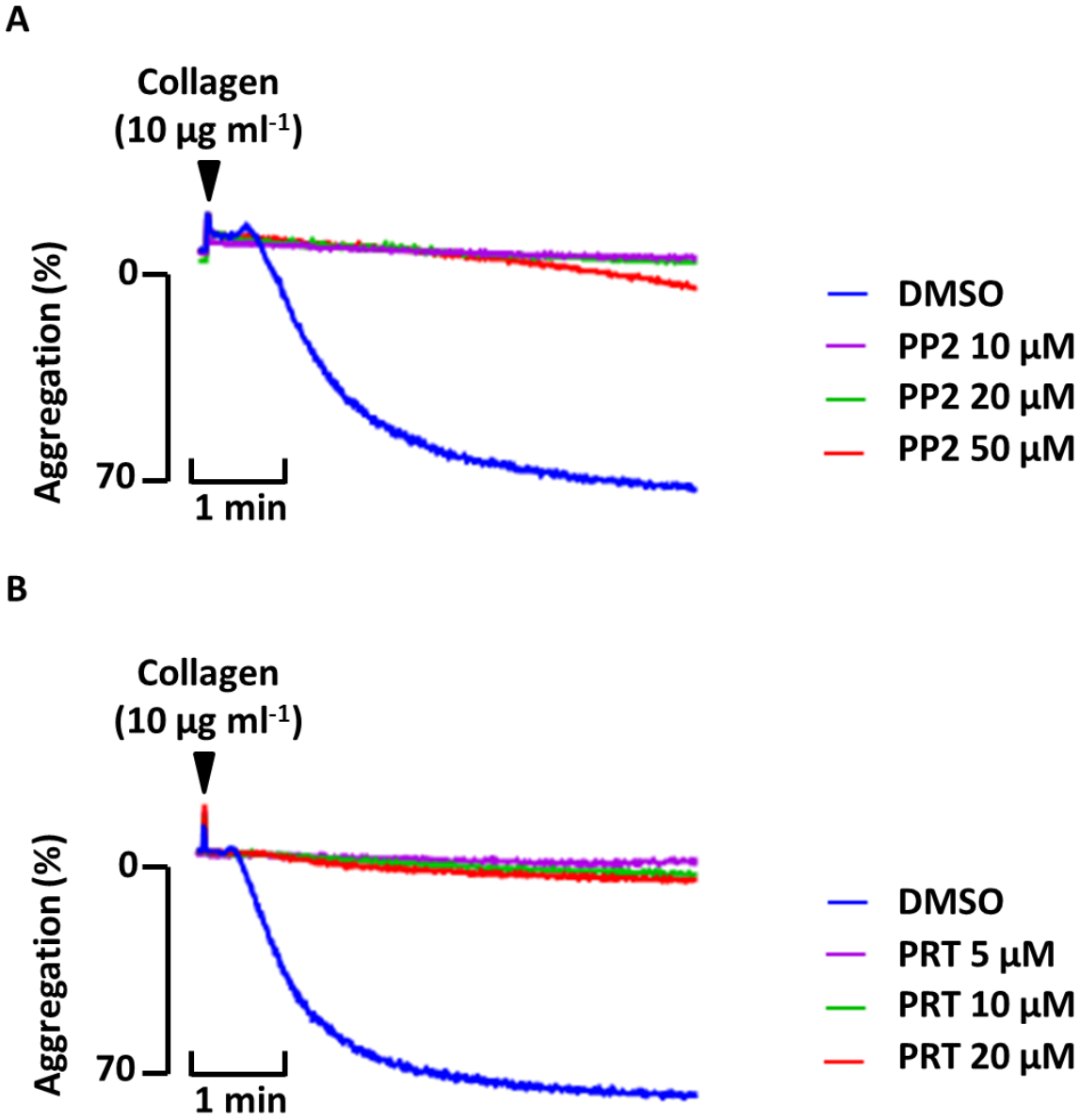

Figure 4.14. Test of increasing concentrations of PP2 and PRT on collagen-induced platelet aggregation. The effect of different concentrations of (A) PP2 (10, 20, 50 µM) or (B) PRT (5, 10, 20 µM) or DMSO (vehicle control) on collagen (10 µg ml^{-1})-induced platelet aggregation was recorded by light transmission aggregometry at 37 °C under constant stirring conditions (1200 rpm) for 5 min. The aggregation traces (representative of n=1 experiment) show that PP2 and PRT at all the concentrations tested block platelet aggregation in response to collagen. Data kindly provided by Dr Pip Nicolson, University of Birmingham, UK.

In accordance with previous results (Poulter et al., 2017), pre-incubation of platelets with either PP2 or PRT significantly reduced the extent of platelet spreading on collagen (Fig. 4.15A). The platelet surface area was diminished by ~40% in the presence of PP2 whereas PRT had a more marked effect (~78% reduction) with a complete abolishment of platelet lamellipodia, filopodia and stress fibres formation (Fig. 4.15A, B, D). The number of platelets coming into contact with collagen did not change in the presence of PP2 and PRT (Fig. 4.15A, C, E).

To investigate whether both kinases are necessary to maintain platelet adhesion to collagen once the spreading has already occurred, we post-treated fully spread platelets for 15 min with each of the inhibitors or the vehicle control. We found that sustained spreading did not require Src-family kinase signalling as demonstrated by the lack of an effect of PP2 on platelet surface area and count (Fig. 4.16A, B, C). On the contrary, PRT-treatment slightly reduced platelet surface area but not platelet number (Fig. 4.16D, E). PRT also had a dramatic effect on the cortical actin cytoskeleton with depolymerisation of stress fibres and the appearance of actin nodule-like structures (white arrows in Fig. 4.16A), suggesting that Syk kinase activity may play a role in the maintenance of platelet morphology. Despite PRT slightly decreasing the platelet surface area in all the three experiments performed on different donors, this result was not significantly different from the control, indicating that a higher number of replicates may be needed to reduce the inter-experimental variability caused by different donors. Overall, these results show that Src-family and Syk kinases are fundamental for the initial interaction of platelet with collagen and propose that Syk, but not Src, may play an important function in supporting the actin cytoskeleton reorganisation during platelet spreading on collagen.

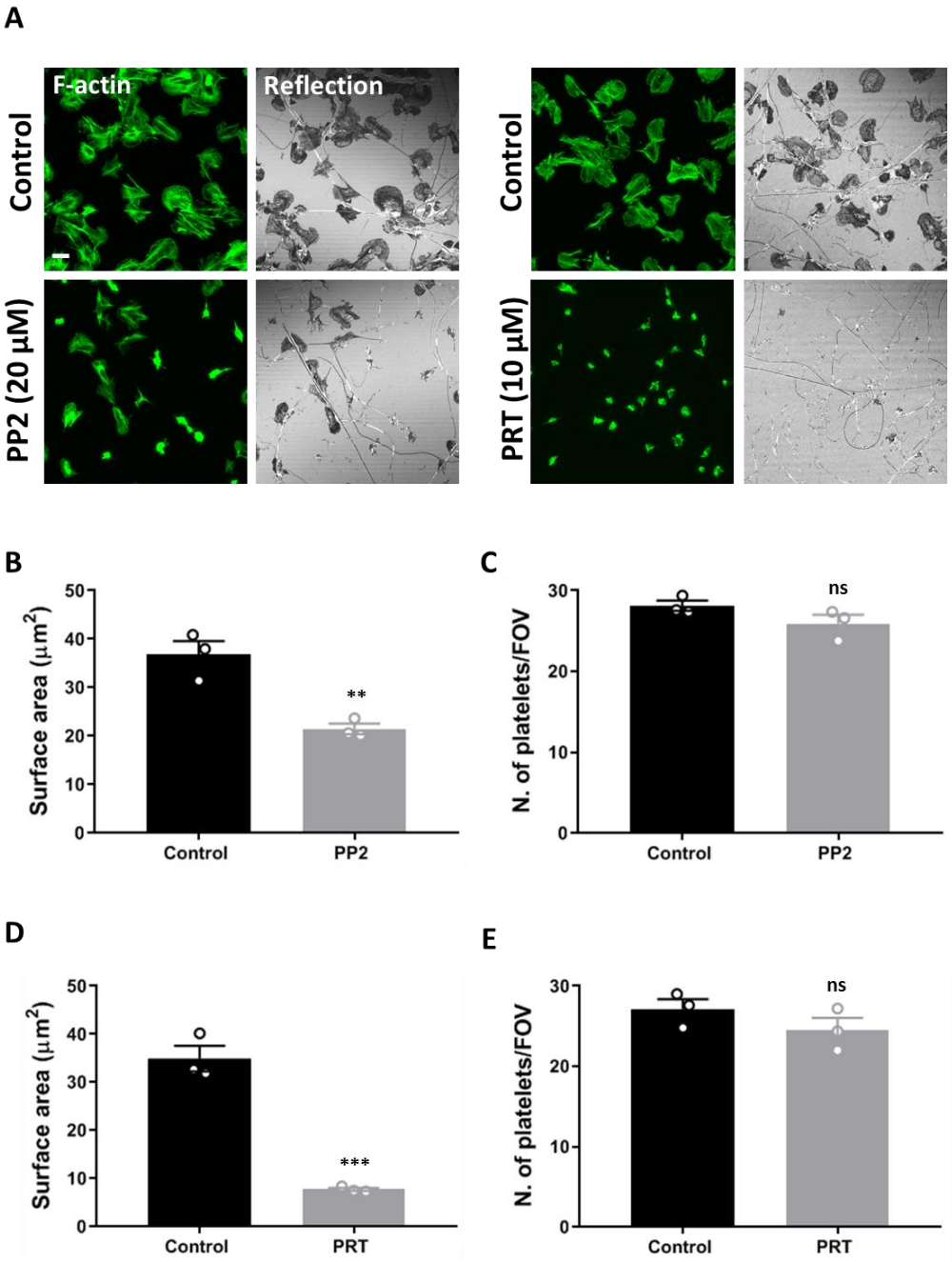

Figure 4.15. Pre-incubation of platelets with PP2 and PRT decreases platelet spreading on collagen. Human washed platelets were pre-incubated with PP2 (20 µM) or PRT (10 µM) or DMSO (vehicle control) for 10 min prior to spreading on a collagen (10 µg ml^{-1})-coated surface for 1 h. The effect of PP2 and PRT on F-actin cytoskeleton (labelled with Alexa Fluor 488 phalloidin) and platelet distribution on collagen (Reflection) is illustrated in the confocal images (A). Quantitative analysis of platelet spreading conducted in KNIME shows a significant reduction in the surface area, but not adhesion, of platelets treated with PP2 or PRT in comparison with DMSO (B, C, D, E). The analysis, performed on 15 FOVs for each condition from three independent experiments, is reported as mean ± SEM. The significance was measured using unpaired two-tailed t-test with $P < 0.05$. Scale bar: 5 µm.

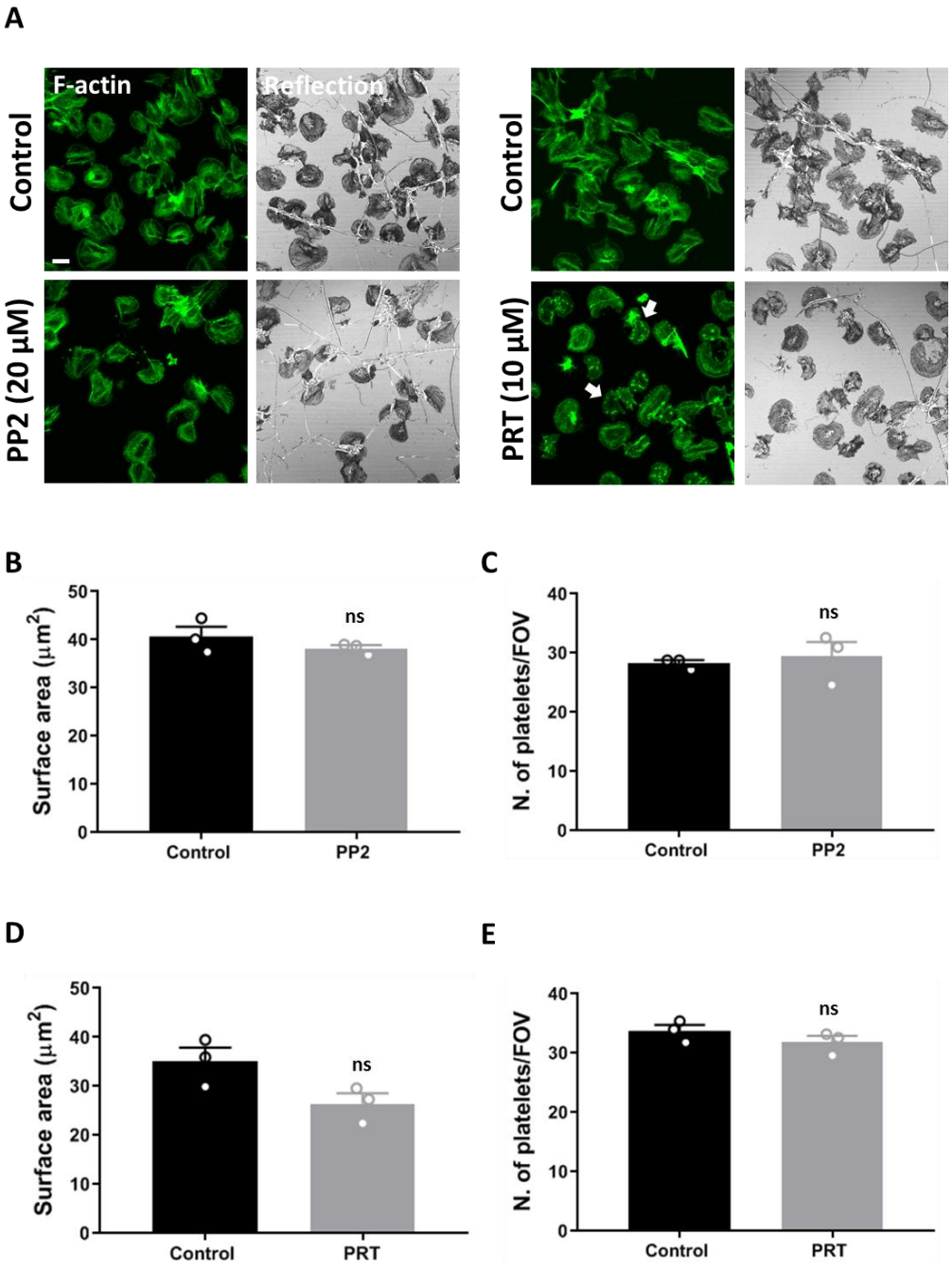

Figure 4.16. Effect of PP2 and PRT post-treatment on platelet spreading on collagen. Human washed platelets spread on collagen (10 µg ml^{-1}) for 45 min were post-incubated with PP2 (20 µM) or PRT (10 µM) or DMSO (vehicle control) for 15 min, labelled with Alexa Fluor 488 phalloidin for actin and imaged by confocal microscopy (A). The effect of PRT on the actin cytoskeleton is indicated by white arrows. The collagen distribution on the surface is illustrated in the Reflection images (A). The quantification of platelet surface area and number of platelets per FOV was performed in KNIME (B, C, D, E) on 15 separate confocal images for each condition from three independent experiments. The significance was measured using unpaired two-tailed t-test where $P < 0.05$. The data are reported as mean ± SEM. Scale bar: 5 µm.

4.3.8 Effect of Src-family and Syk kinases inhibition on collagen-induced GPVI signalling in spread platelets

As GPVI signalling is sustained in spread platelets, with Syk and LAT maintaining tyrosine phosphorylation on their activation and docking sites and Ca^{2+} spiking still active after 3 h of spreading, we sort to investigate whether Src-family and Syk kinases are required to maintain collagen-induced GPVI activation. Spread platelets were post-treated with PP2 and PRT as described above and the signalling events were analysed by Western blot using phospho-specific antibodies against members of early (Syk), intermediate (LAT) and late (PLCγ2) signalling nodes to evaluate the entire GPVI cascade. Both inhibitors impaired GPVI downstream signalling as shown by the decrease in pSyk Y525/6 and pPLCγ2 Y1217 levels (Fig. 4.17A, B, D). Inhibition of Src kinases reduced the phosphorylation of LAT Y200 whereas the Syk inhibitor did not have a major effect (Fig. 4.17A, C). Notably, PP2 or PRT treatment post-spreading impaired full GPVI activation but did not completely abolish the signalling since tyrosine phosphorylation was still detected, suggesting that, once platelets are adhered and spread on collagen, some signalling activation can be maintained even when one of the two kinases is absent.

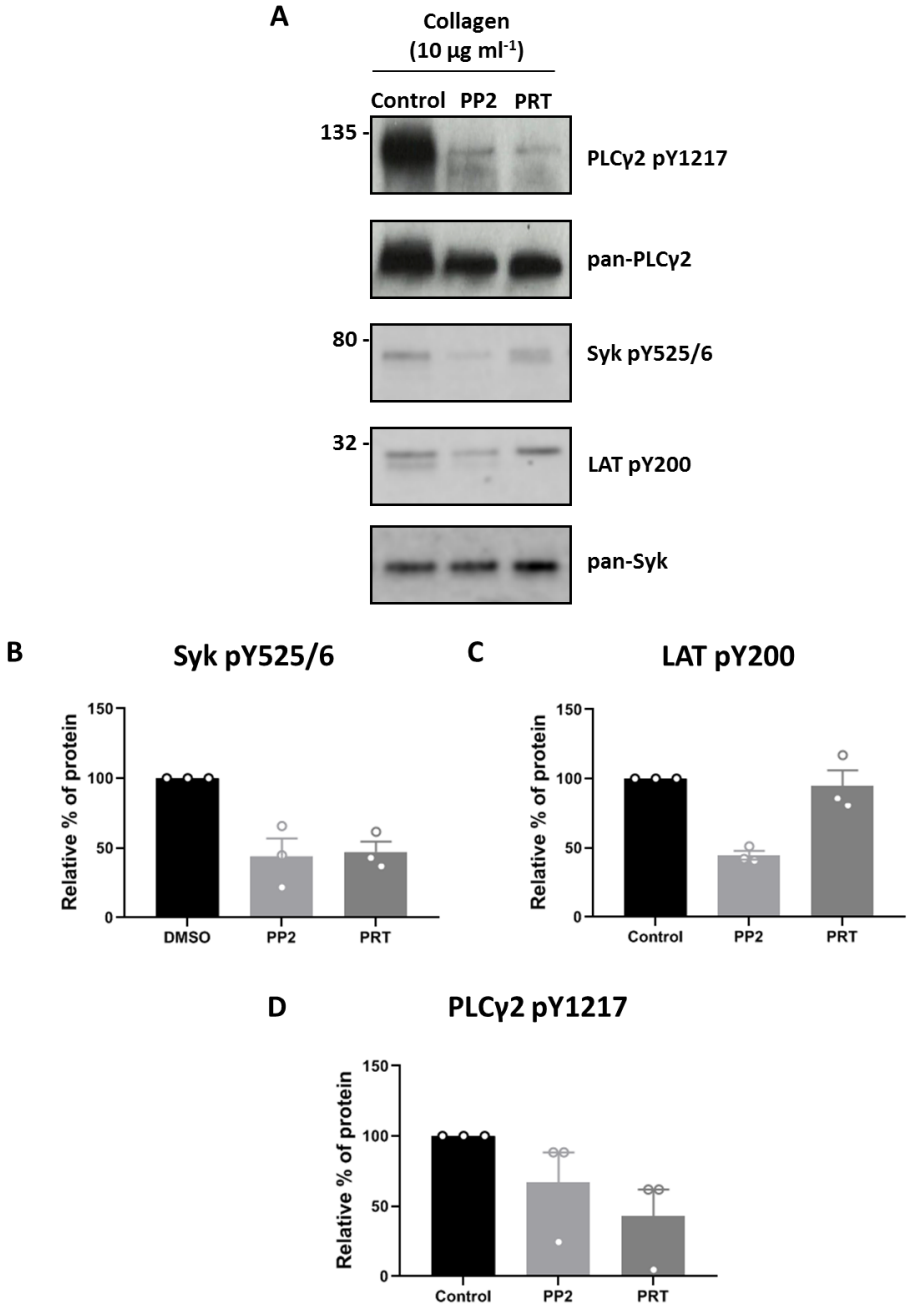

Figure 4.17. Effect of PP2 and PRT post-treatment on tyrosine phosphorylation of Syk, LAT and PLCγ2 in platelets spread on collagen. The effect of PP2 (20 µM) or PRT (10 µM) or DMSO (vehicle control) post-treatment on signalling was evaluated by Western blot analysis. Treated and untreated spread platelet lysates on collagen (10 µg ml^{-1}) were immunoblotted for pSyk (Y525/6) and pLAT (Y200), secondary labelled using anti-rabbit IRDye 800CW conjugated secondary antibodies and fluorescently revealed using the Odyssey Fc system (LI-COR) in the 800 nm channel (A). Lysates, immunoblotted for pPLCγ2 (Y1217) and secondary labelled using anti-rabbit HRP conjugated secondary antibody, were detected using the autoradiographic film (A). Anti-Pan Syk and PLCγ2 antibodies were used as loading controls. The quantitative analysis of the band intensities normalized against the pan signals is shown as mean ± SEM % relative of protein (the control was set at 100%) from three independent experiments (B, C, D).

GPVI-mediated platelet activation culminates with the Ca^{2+} movement from intracellular compartments. Therefore, we examined the effect of Src and Syk inhibition on Ca^{2+} spikes within a 2 min time period in platelets already spread on collagen. Post-treatment with PP2 and PRT reduced the percentage of platelets experiencing the collagen-induced Ca^{2+} elevation with a dramatic drop in the frequency of spikes detected in these cells (Fig. 4.18A, B). The Ca^{2+} spikes in treated platelets were also characterised by a significant decrease in the amplitude and duration in comparison with the control (Fig. 4.18C, D). Together, these data suggest that sustained activation of Src-family and Syk kinases plays a major role in maintaining late signalling events involved in GPVI-mediated platelet activation in response to collagen.

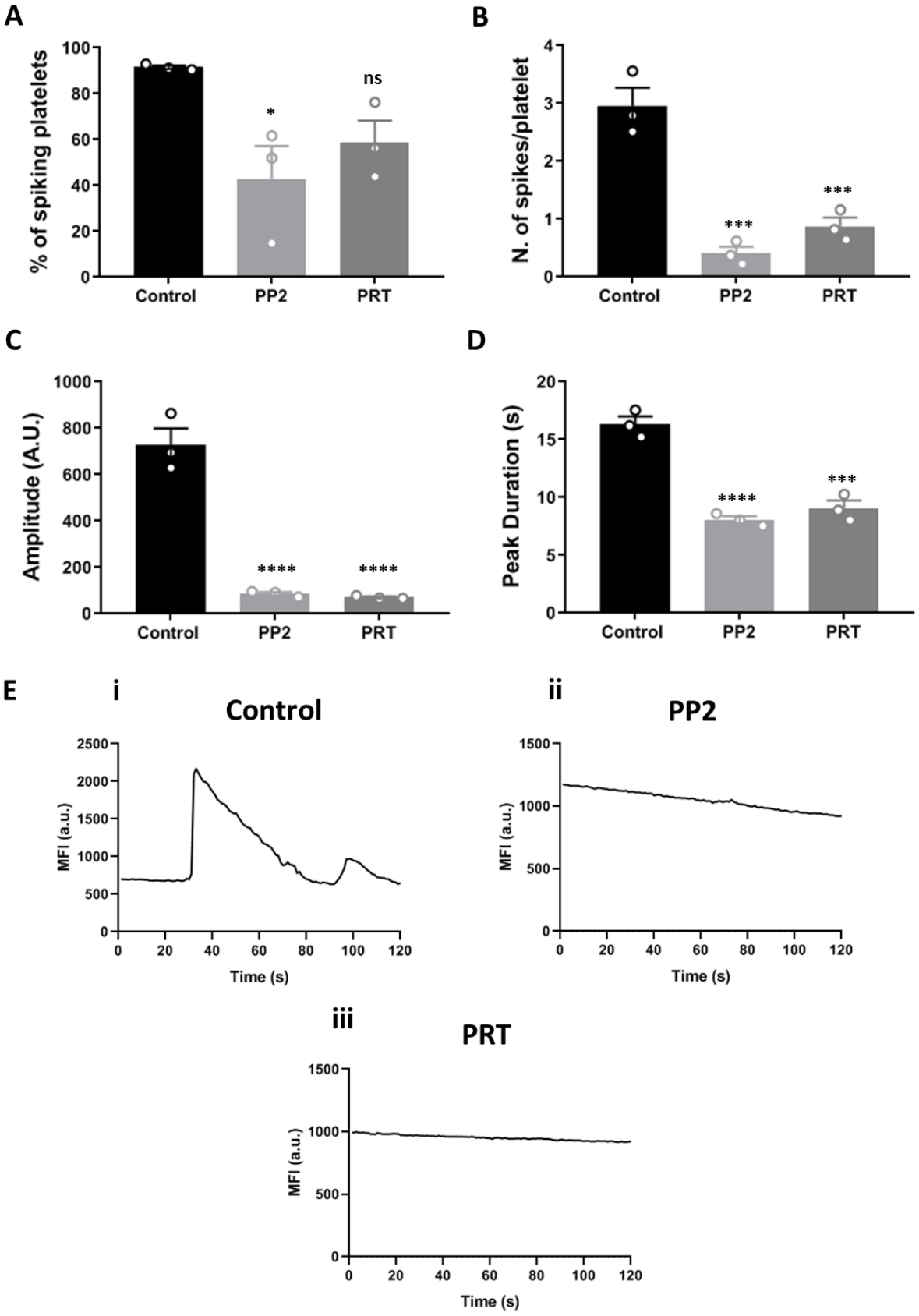
A
% of spiking platelets
100
80
60
40
20
0
*
ns
Control
PP2
PRT
B
N. of spikes/platelet
4
3
2
1
0
***
***
Control
PP2
PRT
C
Amplitude (A.U.)
1000
800
600
400
200
0
****
****
Control
PP2
PRT
D
Peak Duration (s)
20
15
10
5
0
****
***
Control
PP2
PRT
E
i
Control
MFI (a.u.)
2500
2000
1500
1000
500
0
0
20
40
60
80
100
120
Time (s)
ii
PP2
MFI (a.u.)
1500
1000
500
0
0
20
40
60
80
100
120
Time (s)
iii
PRT
MFI (a.u.)
1500
1000
500
0
0
20
40
60
80
100
120
Time (s)

Figure 4.18. PP2 and PRT post-treatment impairs collagen-induced Ca^{2+} mobilisation in spread platelets. Real-time platelet imaging of Ca^{2+} mobilisation in platelets labelled with Oregon green-488 BAPTA-1-AM Ca^{2+} dye, spread on collagen (10 µg ml^{-1}) for 45 min and post-treated with PP2 (20 µM) or PRT (10 µM) or DMSO (vehicle control). Images were acquired every 1 sec for a 2 min time frame using epifluorescence microscopy (1 or 2 movies for each condition were acquired). The quantitative analysis of Ca^{2+} spiking was performed in MATLAB applying a threshold of 20 fluorescent unit. The histograms show a decrease in the mean ± SEM percentage of spiking platelets (A), number of spikes per platelet (B), amplitude (C) and peak duration (D) induced by PP2 or PRT treatment. In total, ~150 platelets within a whole FOV were analysed for each individual experiment (n=3). The significance was measured using one-way ANOVA with Tukey's multiple comparisons test where $P < 0.05$. Representative single-cell Ca^{2+} traces in control and PP2 or PRT-treated platelets are shown in Ei, ii, iii.

4.3.9 Src-family and Syk kinases are not required to maintain GPVI clusters on collagen

We next evaluated the potential feedback exerted by Src-family and Syk kinases on the receptor spatial nanoscale patterning at the platelet plasma membrane. Platelets labelled for GPVI were treated with PP2 and PRT post-spreading and receptor cluster formation was visualised by *d*STORM in TIRF mode. Super-resolution imaging demonstrates that GPVI was still clustered along collagen fibres upon Src-family and Syk kinases inhibition (Fig. 4.19Aii) with neither inhibitor affecting the cluster parameters being measured as confirmed by the Level I clustering analysis (Fig. 4.19Aiii, B, D). Interestingly, Syk, but not Src, inhibition resulted in the appearance of slightly larger individual nanoclusters in comparison with the control as shown in the Level II clustering analysis (Fig. 4.19C). However, despite the size, these nanoclusters were characterised by unchanged density (Fig. 4.19E). Overall, these data suggest that there is no positive feedback exerted by Src-family and Syk kinases on GPVI oligomerisation in platelets once they have adhered to collagen.

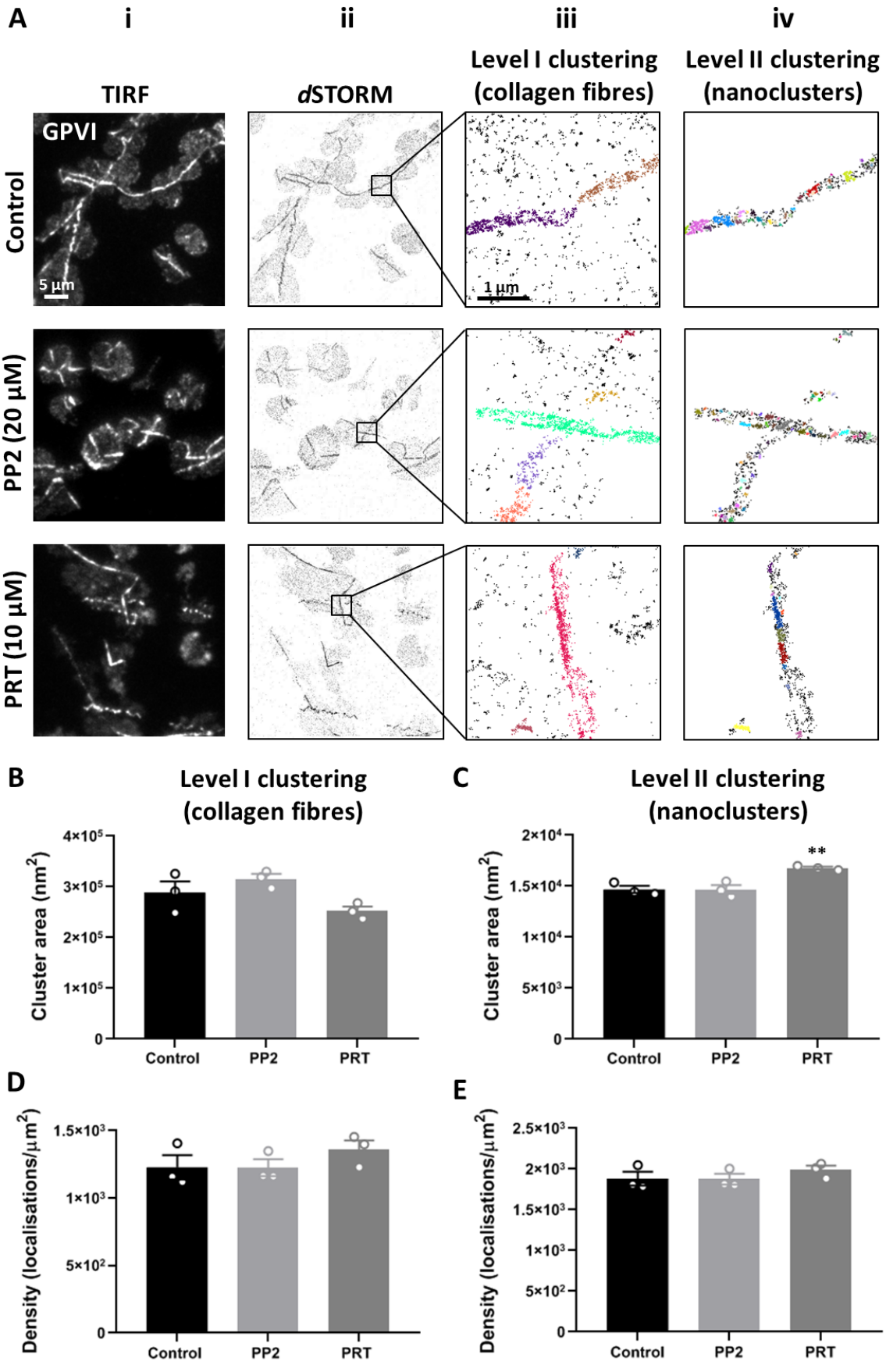
A
i
ii
iii
iv
TIRF
dSTORM
Level I clustering (collagen fibres)
Level II clustering (nanoclusters)
GPVI
Control
PP2 (20 µM)
PRT (10 µM)
5 µm
1 µm
B
Level I clustering (collagen fibres)
Cluster area (nm2)
4×10^5
3×10^5
2×10^5
1×10^5
0
Control
PP2
PRT
C
Level II clustering (nanoclusters)
Cluster area (nm2)
2×10^4
1.5×10^4
1×10^4
5×10^3
0
**
Control
PP2
PRT
D
Density (localisations/µm2)
1.5×10^3
1×10^3
5×10^2
0
Control
PP2
PRT
E
Density (localisations/µm2)
2.5×10^3
2×10^3
1.5×10^3
1×10^3
5×10^2
0
Control
PP2
PRT

Figure 4.19. Effect of PP2 and PRT post-treatment on GPVI clustering in spread platelets. Human washed platelets, stained for GPVI using 1G5-Fab (2 μg ml^{-1}), were spread on collagen (10 μg ml^{-1}) for 45 min and post-incubated with PP2 (20 μM) or PRT (10 μM) or DMSO (vehicle control) for 15 min. *d*STORM imaging of platelets, labelled with anti-mouse Alexa Fluor 647 conjugated, was carried out in TIRF to allow visualisation of GPVI distribution at the cell surface in the presence of PP2 or PRT (Ai, ii). GPVI clusters were quantitatively compared in control and treated platelets using DBSCAN-based two-step cluster analysis (Aiii, iv) with the application of the same settings used in the previous experiments. Mean ± SEM cluster area and density of clusters and nanoclusters are shown in B, C, D, E (n=3). In total, 14, 12 and 13 FOVs were analysed for the control, PP2 and PRT-treated platelets, respectively. Significance was measured using one-way ANOVA with Tukey's multiple comparisons ($P < 0.05$). Scale bar: 5 μm (*d*STORM images) and 1 μm (Level I and II cluster plots).

4.3.10 Inhibition of Syk but not Src-family kinases impairs clustering of integrin α2β1 along collagen fibres

To further address the long-term effect of Src-family and Syk inhibition on collagen-induced platelet spreading and signalling, we investigated the distribution of the other collagen receptor, integrin α2β1, which has been shown to mediate the outside-in regulation of platelet spreading through Src and Syk activation (Inoue et al., 2003). Platelets, completely spread on a collagen surface, were treated with PP2 and PRT for 15 min and the localisation of integrin α2β1 was super-resolved and quantitatively assessed using the two-level cluster analysis. In accordance with previous findings (Poulter et al., 2017), integrin α2β1 aggregated specifically at the collagen fibres in control platelets (Fig. 4.20Ai, ii, iii, iv, first panel). Inhibition of Src kinases had no effect on the integrin location and agglomeration on collagen (Fig. 4.20Ai, ii, iii, iv, second panel). However, in contrast to what was observed for GPVI, Syk inactivation induced the disruption of the long integrin clusters aligned along collagen (Fig. 4.20Ai, ii, third panel). Large and dense clusters were still detected by the Level I cluster analysis (Fig. 4.20B, D) but these were not lined up along collagen fibres (Fig. 4.20Aiii, third panel), probably due to the impairment of the cortical actin cytoskeleton shown above. Once segmented in the Level II clustering analysis (Fig. 4.20Aiv, third panel), these oligomers were made up by slightly smaller nanoclusters in comparison with the control (Fig. 4.20C), suggesting a compromised interaction of the integrin with its ligand which may affect the size of resulting nanoclusters. However, the cluster density was not affected by PRT-treatment (Fig. 4.20E). Therefore these results suggest that, contrarily to GPVI receptors, Syk kinase appears to be fundamental for the maintenance of integrin α2β1 clustering along collagen fibres in spread platelets.

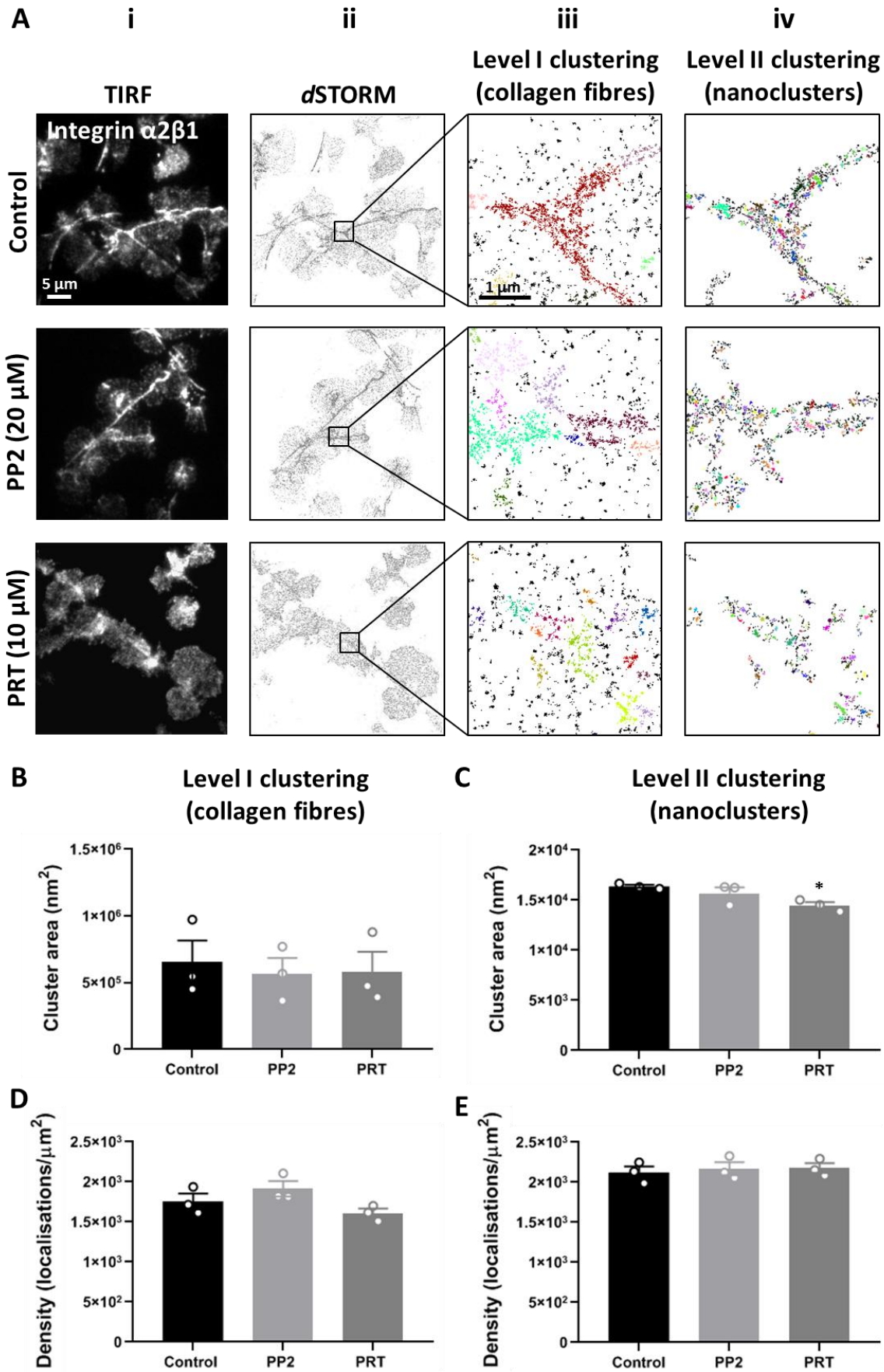
A
i
ii
iii
iv
TIRF
dSTORM
Level I clustering (collagen fibres)
Level II clustering (nanoclusters)
Integrin α2β1
Control
PP2 (20 µM)
PRT (10 µM)
5 µm
1 µm
B
Level I clustering (collagen fibres)
Cluster area (nm²)
1.5×10⁶
1×10⁶
5×10⁵
0
Control
PP2
PRT
C
Level II clustering (nanoclusters)
Cluster area (nm²)
2×10⁴
1.5×10⁴
1×10⁴
5×10³
0
*
Control
PP2
PRT
D
Density (localisations/µm²)
2.5×10³
2×10³
1.5×10³
1×10³
5×10²
0
Control
PP2
PRT
E
Density (localisations/µm²)
2.5×10³
2×10³
1.5×10³
1×10³
5×10²
0
Control
PP2
PRT

Figure 4.20. PRT but not PP2 impairs integrin α2β1 clustering on collagen in spread platelets. Human washed platelets spread on collagen (10 μg ml^{-1}) and post-treated with PP2 (20 μM) or PRT (10 μM) or DMSO (vehicle control) as previously described, were labelled for integrin α2β1 and secondary stained with anti-mouse Alexa Fluor 647 conjugated. TIRFM highlights the lack of enrichment of integrin α2β1 on collagen upon PRT treatment (Ai). The *d*STORM image of the same cells confirms the absence of receptor clustering along collagen fibres (Aii). Receptor clustering was quantitatively determined by the application of two-level cluster analysis based on DBSCAN. Both clustering levels show the absence of continuous clusters along fibrous collagen in comparison with control and PP2-treated platelets (Aiii, iv). The quantification of integrin α2β1 cluster and nanocluster area and density is reported in B, C, D, E as mean ± SEM from three independent experiments (a total of at least 12 FOVs for each condition were analysed). One-way ANOVA with Tukey's multiple comparisons was used to evaluate the statistical significance ($P < 0.05$). Scale bar: 5 μm (*d*STORM images) and 1 μm (Level I and II cluster plots).

4.4 Discussion

In this Chapter, we have used a variety of advanced microscopy, image analysis and biochemical techniques to demonstrate that GPVI-mediated signalling is sustained in platelets adhering to and spreading on an immobilised collagen surface. Our data show that GPVI clustering along collagen fibrils leads to a concentration of the receptor and activated downstream signalling molecules such as pSyk and pLAT. Downstream signalling events, such as Ca^{2+} spiking is also maintained over the 3 h time period. Our epifluorescence and single molecule imaging data show a little overlap of GPVI with its sheddase ADAM10. This is consistent with no significant shedding of GPVI taking place in collagen-adhered platelets over a 3 h time frame. Furthermore, once bound to collagen, GPVI does not require positive feedback from secondary mediators or Src-family and Syk kinases to maintain the clusters. This is in contrast to integrin α2β1 which necessitates continued Syk, but not Src, activity to remain bound to collagen fibrils.

In *Chapter 3*, we have shown that GPVI is enriched along collagen fibres and remains clustered over a 3 h time frame. We hypothesized that clustering of GPVI may support and potentiate signalling at the platelet surface through the recruitment and activation of signalling proteins. Our data support this hypothesis with sustained tyrosine phosphorylation of Syk and LAT and Ca^{2+} mobilisation which maintain platelet spreading on collagen for at least 3 h. This is in line with studies under flow conditions which demonstrated that GPVI activation results in a robust and longer-lasting Ca^{2+} mobilisation under flow which is sufficient to mediate the integrin-dependent firm adhesion of platelets to collagen (Mazzucato et al., 2009, Pugh et al., 2017). However, the signalling dynamics observed in platelets stimulated in suspension were different with downregulation in Syk and LAT phosphorylations over time. This is in contrast to findings from Tomlinson et al. (2007) showing that collagen promotes weak but sustained

signal transduction in platelets and GPVI-expressing cell lines (Tomlinson et al., 2007). This discrepancy is likely due to the different antibodies used to measure the levels of tyrosine phosphorylations; the 4G10 antibody used by Tomlinson et al. (2007) detects whole-cell tyrosine phosphorylations, which also include negative regulations. Syk downregulation within the GPVI signalling pathway has previously been attributed to the phosphatase T-cell ubiquitin ligand-2 (TULA-2) in human platelets stimulated with CVX (Thomas et al., 2010). Furthermore, this regulatory mechanism has recently been mathematically modelled (Dunster et al., 2015); however, the model did not take into account spatial information relating to GPVI within the platelet PM which will undoubtedly affect the signalling transduction.

A major difference between the two stimulations is that, in the spreading experiment, the GPVI ligand (collagen) is immobilised on a surface whereas, in solution, the collagen and the platelets are continuously moving so contact between the two might be more transient and less stable. Signals emanating from smaller, more mobile clusters would be more prone to downregulation from negative regulators such as phosphatases or sheddases as these would have easier access to the receptor and downstream signalling proteins. However, once bound to an immobilised ligand, GPVI would not be able to move within the plane of the platelet PM and as the platelet spread more receptors bind to the collagen increasing the cluster size and facilitating the formation of signalling complexes that may help to exclude negative regulators. These functional advantages of receptor clustering has also been studied in other cell types (Cebecauer et al., 2010). T cells are a good example as an immunological synapse can be experimentally induced by immobilising activating antibodies on a glass slide and allowing T cells (e.g. Jurkat T cells) to interact with them. Studies on this model system have demonstrated the formation of TCR clusters and large signalosomes within the T cell PM which concentrate signalling molecules and exclude phosphatases, thereby facilitating the

signalling transduction (Douglass and Vale, 2005, Furlan et al., 2014, Lin and Weiss, 2003). In spreading platelets we have shown that total phosphotyrosines and particularly phosphorylated LAT and Syk were specifically enriched at the large collagen-bound clusters even after 3 h of spreading, supporting the hypothesis that clustering facilitates sustained signalling. It would be interesting to investigate whether phosphatases known to be involved in downregulation of GPVI signalling such as TULA-2 (Dunster et al., 2015, Thomas et al., 2010) are excluded from these clusters as seen for CD45 (Furlan et al., 2014) and CD148 (Lin and Weiss, 2003) in T cells.

GPVI density at the platelet surface is also modulated by cleavage of the extracellular region by members of the ADAM family of sheddases. It is known that shedding of GPVI can be induced by a number of physiological and non-physiological stimuli (Montague et al., 2018a). Here, we have shown that GPVI is only shed at very low levels in spread platelets but can be cleaved in platelets stimulated in suspension. A recent work by Facey et al. (2016) has shown that ADAM10 activity is not affected by collagen engagement but GPVI shedding occurs (Facey et al., 2016), suggesting the existence of another level of control which could include altered ADAM10 or GPVI localisation within the PM. Our findings have shown that there is no clear colocalisation of GPVI and ADAM10 at collagen fibres and, as the cluster size and density do not decrease over time, little shedding is occurring in these regions, likely due to the exclusion of the sheddase. Other possible components involved in the protection from shedding are tetraspanins, a superfamily of 33 four-transmembrane proteins, which can interact with both ADAM10 and GPVI. Indeed, recent findings from Noy et al. (2016) have demonstrated that Tspan14, which belongs to TspanC8 subgroup and regulates ADAM10 maturation and trafficking, was the only tetraspanin able to inhibit GPVI cleavage by ADAM10 in cell lines (Noy et al., 2016). The authors proposed a model in which the specific

interaction of GPVI and ADAM10 with different tetraspanin partners may drive the activation/blocking of receptor shedding (Noy et al., 2016).

In addition to ADAM10, platelets express and release several metalloproteinases [matrix metalloproteinases (MMPs) and ADAMs] which regulate platelet functions (Montague et al., 2018a), raising also the question whether ADAM10-independent shedding takes place at the platelet surface. Using the broad-spectrum metalloproteinase inhibitor, GM6001 and the ADAM10-specific inhibitor, GI254023, we correlated GPVI clustering pattern and size with the block of shedding. GPVI oligomerisation was not affected when the sheddases, including ADAM10, were blocked further reinforcing our proposed model. Contrarily, NEM, which enhances ADAM10 activity (Facey et al., 2016) and induces ~100% shedding as shown by Western blot, triggered the release of the majority of GPVI receptors from the platelet surface. Only a few localisations were detected by *d*STORM indicating that some receptors may be trapped between platelets and collagen and therefore they are not accessible for release. The thiol-modifying reagent NEM may represent a stronger and/or faster stimulus than the GPVI physiological ligand, collagen, or they may induce shedding through a different mechanism. Indeed, GPVI shedding induced by ligand engagement is thought to require receptor clustering, dissociation of CaM from the intracellular tail and activation of the signalling cascade (Gardiner et al., 2004). Platelet spreading on collagen was impaired upon NEM-induced shedding, suggesting that intact GPVI receptors are fundamental for the initial steps of platelet activation and spreading on a collagen surface. This is in accordance with previous studies conducted in GPVI-deficient patients (Arai et al., 1995, Boylan et al., 2004, Dumont et al., 2009, Matus et al., 2013, Sugiyama et al., 1987, Takahashi and Moroi, 2001) and mouse models (Kato et al., 2003, Lockyer et al., 2006, Nieswandt et al., 2000, Nieswandt et al.,

2001a, Nieswandt et al., 2001b) which all exhibited impaired platelet adhesion and aggregation in response to collagen.

Upon collagen-adhesion, activated platelets release soluble agonists from the storage organelles such as ADP and TxA_2 which act as pro-thrombotic triggers through the amplification of the signalling cascades, ultimately leading to enhanced integrin activation and platelet aggregation (Bye et al., 2016). Despite all these roles in platelet responses, the discharge of secondary mediators is not needed to potentiate platelet spreading on collagen and GPVI signalling or cluster formation, as these events were not altered in the presence of indomethacin and apyrase. This is in contrast to CLEC-2 signalling which requires second messenger as platelets treated with indomethacin and apyrase showed a dramatic impairment of CLEC-2 phosphorylation, whole-cell tyrosine phosphorylation and rhodocytin-induced platelet aggregation (Pollitt et al., 2010). Therefore, these results suggest that soluble agonists do not function as a positive feedback loop of the initial stimulus on collagen in contrast to their fundamental role in supporting collagen-induced platelet aggregation during thrombus growth (Atkinson et al., 2001).

GPVI activation by collagen results in a potent cascade of protein tyrosine phosphorylation initiated by Src-family and Syk kinases and culminating in Ca^{2+} elevation (Watson et al., 2010). The Src-family kinase inhibitor PP2 (Ezumi et al., 1998, Li et al., 2010, Spalton et al., 2009) and Syk inhibitor PRT (Badolia et al., 2017, Jooss et al., 2019, Reilly et al., 2011) have been widely used to investigate the Src and Syk-dependent platelet activation processes mediated by GPVI. At concentrations able to block collagen-induced platelet aggregation, inhibition of either kinases interfered with platelet spreading. The effect was more marked with the Syk inhibitor in accordance with previous findings (Poulter et al., 2017), indicating again that intact GPVI-mediated signalling is crucial for the initial phase of platelet activation

by collagen. On the other hand, when platelets were already spread, Src kinases activity was not needed to support platelet spreading along collagen fibres. Notably, Syk kinase appeared to be important for the maintenance of platelet morphology during spreading with the detection of foci of actin depolymerisation, likely due to the inhibition of downstream targets implicated in the cytoskeletal regulation such as Vav1 and SLP-76 (Judd et al., 2000, Obergfell et al., 2002, Obergfell et al., 2001).

Since receptor cluster formation seems to play a role in sustaining the signalling over time, the signalling itself, once activated, may contribute to the ability of GPVI to coalesce in large clusters in a double-positive loop manner. Our results have demonstrated that Src-family and Syk kinases signalling are fundamental for sustaining full GPVI activation as tyrosine phosphorylation of Syk and PLCγ2 were decreased and Ca^{2+} spiking was severely impaired by PP2 and PRT treatment post-spreading. Notably, phosphorylation of LAT in its Tyr 200 was reduced by Src but not Syk inhibition. This could be related to the specific tyrosine residue investigated which is a docking and not an activation site (Balagopalan et al., 2010) and may be not affected by Syk inhibition. Therefore, other tyrosine residues should be explored to evaluate the effect of Syk inhibition on the adapter LAT.

Despite the effect on GPVI-mediated signalling, inhibition of Src or Syk in spread platelets did not impair receptor cluster formation along collagen fibres, with only a slight increase in GPVI nanocluster area seen upon Syk inhibition. It has previously been shown that disruption of the actin cytoskeleton reduces the formation of GPVI dimers (Poulter et al., 2017). Here, we have found that Syk inhibition triggers the actin depolymerisation which may disrupt GPVI dimers and result in the deposition of slightly larger nanoclusters at the platelet surface. However, this finding is in contrast to work on the FcγR in macrophages where Syk inhibition resulted in the decreased lateral mobility and increased clustering of this receptor (Jaumouillé

et al., 2014). Together, these results suggest that, whereas sustained collagen-induced platelet activation requires intact Src and Syk activity, prolonged GPVI cluster formation does not. This is in line with findings from Poulter et al. (2017) who showed that pre-treatment of platelets with Src and Syk inhibitors does not preclude the formation of GPVI oligomers on collagen (Poulter et al., 2017). On the contrary, only Syk kinase activity was required for maintaining integrin α2β1 clustering along collagen since its inhibition induced the disruption of the long and continuous clusters aligned on collagen fibres. Unlike GPVI whose affinity for collagen is regulated via dimerisation, integrins fluctuate between an 'on' and 'off' state and only the conversion into the active conformation allows the high-affinity ligand binding (Hynes, 2002, Spiess et al., 2018). The F-actin cytoskeleton plays an important role in the up-regulation of integrin activity (Zhu et al., 2008) through the engagement of different adaptor proteins such as kindlin, vinculin and talin which couple integrins to the F-actin (Horton et al., 2015). Syk inhibition using piceatannol has previously been shown to cause a redistribution of the actin cytoskeleton in macrophages (Jaumouillé et al., 2014). Here, we have shown that Syk inhibition via PRT treatment also results in the disruption of the cortical actin cytoskeleton in spread platelets. Integrin α2β1 is linked to the actin cytoskeleton via talin (Beckerle et al., 1989) and we propose that actin disruption causes the inactivation of the integrin and its subsequent dissociation from collagen. Indeed, loss of talin from platelets causes a massive reduction in β1 integrin-mediated platelet adhesion under flow conditions, with no stable adhesion or microthrombi formed (Petrich et al., 2007), demonstrating the importance of this interaction. As GPVI clusters are largely unaffected by the PRT treatment it implies that, once bound to collagen, GPVI remains bound and does not have such a dependence on the actin cytoskeleton, although there is some evidence that actin is involved in GPVI dimer formation (Poulter et al., 2017).

Overall, the findings in this Chapter propose that clustering of GPVI on immobilised collagen protects GPVI from shedding, possibly through the marginalisation of ADAM10, to maintain sustained Src and Syk kinases-dependent signalling, integrin activation and continued adhesion to collagen. The sustained adhesion and signalling is likely to be important for thrombus stability and the prevention of bleeding associated with disrupted vascular integrity driven by inflammation, where GPVI plays a critical role (Boulaftali et al., 2018).

CHAPTER 5

Purification and characterisation of different nanobodies targeting human platelet GPVI

5.1 Aims

The company VIB Nanobody Core (Brussel, Belgium) was contracted to raise nanobodies against a recombinant form of dimeric GPVI (hGPVI-Fcα-His_6). In total, 54 different nanobody sequences, from 33 different families (based on CD3 sequences), were obtained from the immunization of two llamas. VIB provided us with vials of *E. coli* TG1 harbouring recombinant phagemid pMECS containing the nanobody genes. The pMECS vector enabled the addition of an HA tag and a His_6 tag to the nanobodies to allow their purification and further detection. The main aim of this Chapter was to find a nanobody that was suitable for super-resolution imaging of GPVI in platelets. Initially, all 54 nanobodies were produced and screened for reactivity to native GPVI and then 3 of the candidate nanobodies were taken forward to fully characterise for imaging purposes.

5.2 Introduction

Antibodies are fundamental tools in biomedical research and typically share a common structure consisting of a combination of heavy and light chains which are required for the recognition of the target antigen. Simpler antibodies lacking the light chains are naturally found in sera of camelids and sharks. These 'heavy-chain only' antibodies have been widely used for the engineering of nanobodies which are composed of only a single antigen-binding domain, namely the variable region of the heavy chain (camelid VHHs or shark VNARs, Fig. 5.1). They only measure ~4 nm in length (MW: ~15 kDa) and therefore are much smaller than than full-length antibodies (length: ~15 nm and MW: 150 kDa) and Fab fragments (length: ~9 nm and MW: 50 kDa) (Muyldermans, 2013).

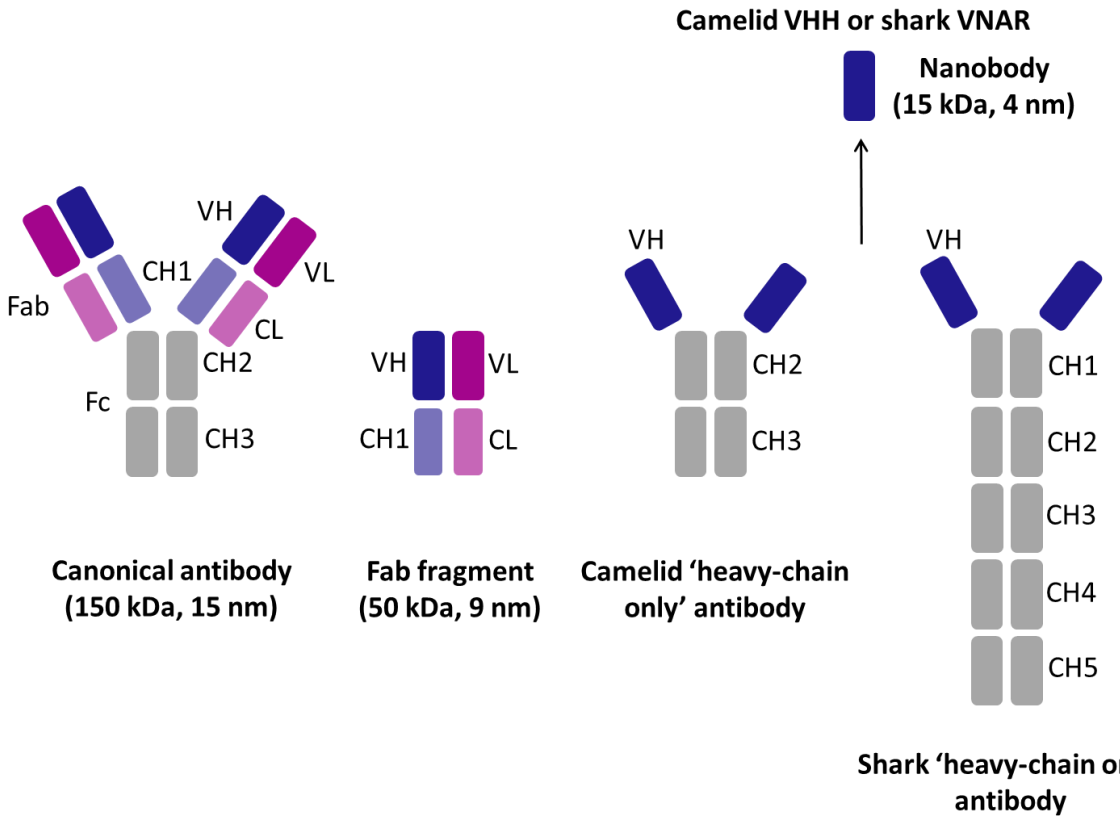

Figure 5.1. Structural properties of canonical antibodies, Fab fragments and camelid 'heavy-chain only' antibodies. The canonical antibody structure (150 kDa, 15 nm) contains two heavy (H) and two light (L) chains, each with variable (V) and constant (C) regions. The Fab fragment (50 kDa, 9 nm) represents the antigen-binding domain of a standard antibody which can be chemically separated from the Fc portion, resulting in a monomeric antibody. Nanobodies (15 kDa, 4 nm) are single antigen-binding domain antibodies corresponding to the variable region of the heavy chain of camelid and shark 'heavy chain only' antibodies (VHHs in camelids and VNARs in sharks). VH: variable domain of the heavy chain; VL: variable domain of the light chain; CH: constant domain of the heavy chain; CL: constant domain of the light chain; VHH: variable domain of the heavy chain of 'heavy-chain only antibodies; VNAR: variable antigen-binding domain. Adapted from (Doshi et al., 2014).

Despite the small dimensions, nanobodies exhibit the same specificity as standard antibodies and provide numerous advantages in biological, diagnostic and therapeutic approaches (Beghein and Gettemans, 2017, Siontorou, 2013). Their small size, in combination with an extended CDR3 loop, allows them to bind hidden or difficult-to-access antigens such as enzyme active sites (De Genst et al., 2006), infectious agents (Stijlemans et al., 2004) and conformational epitopes (Manglik et al., 2017). *In vivo*, this unique property can be exploited for diagnostic and therapeutic applications, due to their efficient tissue penetration, rapid blood clearance, high stability and low immunogenicity (Hu et al., 2017, Siontorou, 2013). In particular, nanobodies targeting tumour markers have been successfully adopted in cancer biology for non-invasive *in vivo* tumour imaging in xenograft cancer models (Kijanka et al., 2013, Oliveira et al., 2012) and for the development of drug delivery strategies, for example using nanobody-coupled liposomes and micelles delivery systems (Talelli et al., 2013, Talelli et al., 2011, Van Der Meel et al., 2012, van der Meel et al., 2013). This is also achieved because they can be easily genetically engineered, allowing the generation of customized constructs, such as bivalent and bispecific nanobodies (Els Conrath et al., 2001, Ulrichts et al., 2011). An interesting example in the platelet biology is represented by the antithrombotic agent ALX-0081, a bivalent anti-vWF nanobody which is currently under clinical trials (Ulrichts et al., 2011). In cellular biology, nanobodies have been successfully used in the purification of native protein complexes by affinity chromatography (Fridy et al., 2015, Pleiner et al., 2015) and in the investigation of protein localisation by super-resolution microscopy (Platonova et al., 2015, Pleiner et al., 2015, Ries et al., 2012, Virant et al., 2018). In addition, nanobodies have been used as crystallization chaperones in structural biology which has aided the structural resolution of transient protein conformations (Pardon et al., 2014).

Despite numerous advantages, nanobodies do have several limitations. They are usually well-expressed in *E. coli* strains and purified from their periplasmic space where they are secreted. However, purification of proteins from the periplasm is much more difficult than from the cytoplasm and can compromise the final yield, due to the limited secretion capacity and the elevated number of proteases which can catalyze the proteolysis of the final recombinant proteins (Rosano and Ceccarelli, 2014). Nanobodies are characterised by a convex shape in comparison with the flat or concave conformation of conventional antibodies. While this feature represents an advantage for the binding to concave-shaped enzyme active sites (De Genst et al., 2006), it also limits the use of nanobodies for the detection of small molecules, since their topology would not be suitable for the binding of targets with limited size (Muyldermans, 2013).

Despite these limitations, there is a growing interest in using nanobodies as alternatives to full-length antibodies and Fab fragments in super-resolution microscopy to exploit the full potential of this cutting-edge technique in localising target proteins to the highest precision (Traenkle and Rothbauer, 2017). In immunofluorescence microscopy, the use of a primary and a fluorescently-conjugated secondary antibody to detect the epitope of interest would displace the fluorophore from the epitope by ~30 nm (Deschout et al., 2014b). Nanobodies have turned out to be the ideal substitute for conventional antibodies since they significantly decrease the label-epitope distance and enhance the achievable spatial resolution of protein localisation by super-resolution microscopy (Platonova et al., 2015, Pleiner et al., 2015, Ries et al., 2012, Virant et al., 2018). However, the direct conjugation of nanobodies with fluorescent dyes represents a critical point which may result in poor labelling, low signal-to-noise ratio or even loss of functionality. Traditional labelling strategies include the conjugation of nanobodies with N-hydroxysuccinimide (NHS) ester fluorophores such as

Alexa Fluor dyes at lysine residues (Platonova et al., 2015, Ries et al., 2012). However, this labelling method is not site-specific and often results in a high background staining (Pleiner et al., 2015, Virant et al., 2018). Alternative site-specific labelling approaches have been proposed and involve the enzymatic coupling of fluorophores to protein tags (Virant et al., 2018) or via cysteines engineering with maleimide fluorophores (Pleiner et al., 2015), resulting in a high-quality super-resolution performance.

In this Chapter, we have produced and initially characterised the first 20 nanobodies against human GPVI expressed in TG1 *E. coli* strain. The remaining 34 nanobodies of the full set were purified, characterised and screened by the research technician Ying Di to select three candidates (two for imaging purposes and one as inhibitory reagent) to express in the WK6 *E. coli* strain to generate pure nanobodies. A full investigation of these three nanobodies, belonging to different CDR3 groups, has been carried out in human platelets with one nanobody being selected as a promising tool for *d*STORM imaging and fluorescently labelled via the genetic fusion with the self-labelling SNAP-tag.

5.3 Results

5.3.1 Expression, purification and initial characterisation of 20 nanobodies targeting human GPVI cloned in pMECS vector by TG1 *E. coli* strain

We have expressed and purified the first subset of 20 nanobodies against human GPVI from the TG1 *E.coli* strain in two consecutive rounds (I and II batches of 10 nanobodies each, as described in *Materials and Methods*). These 20 nanobodies are taken from a number of different CDR3 families, with some families having more than one nanobody associated with it. Those classified in the same CDR3 family recognize the same epitope on GPVI; however, due to small sequence differences, other characteristics such as affinity, potency, stability and expression yield of individual nanobodies may be different. The successful generation of nanobodies is shown in Fig. 5.2 where 1 μg of each nanobody was loaded into a polyacrylamide gel and the purity of the nanobodies was inspected by Coomassie staining under reducing conditions. The bands relating to the pure nanobodies appeared at ~17 kDa whereas the top bands at ~58 kDa correspond to the nanobodies fused with the protein III of the phage (Fig. 5.2A, C). The fused proteins were detected in some clones but not in others, likely due to the different percentage of suppression of the amber stop codon following the His_6 tag in TG1 strains. Western blot confirmed the presence of nanobodies using anti-His_6 tag for the detection (Fig. 5.2B, D). The nanobodies were detected at ~17 kDa as shown previously whereas the fused proteins were undetectable, indicating that the His_6 tag may be covered by the protein III of the phage.

To investigate whether the nanobodies were able to efficiently bind GPVI in human platelets, we performed flow cytometry analysis in resting platelets and platelets activated by CRP-XL, the GPVI-specific ligand. Unstained platelets and platelets labelled only with secondary

antibody were used as negative controls (Fig. 5.3Ai, B). All the nanobodies were able to bind human GPVI as shown by the increase in the mean fluorescence intensity (MFI) in resting and activated platelets in comparison with the negative control (Fig. 5.3Aii, iii, C). However, for all the nanobodies (except nanobody #15), the extent of binding appeared to increase in CRP-stimulated platelets, likely due to the recognition of the dimeric conformation of GPVI which increases upon activation.

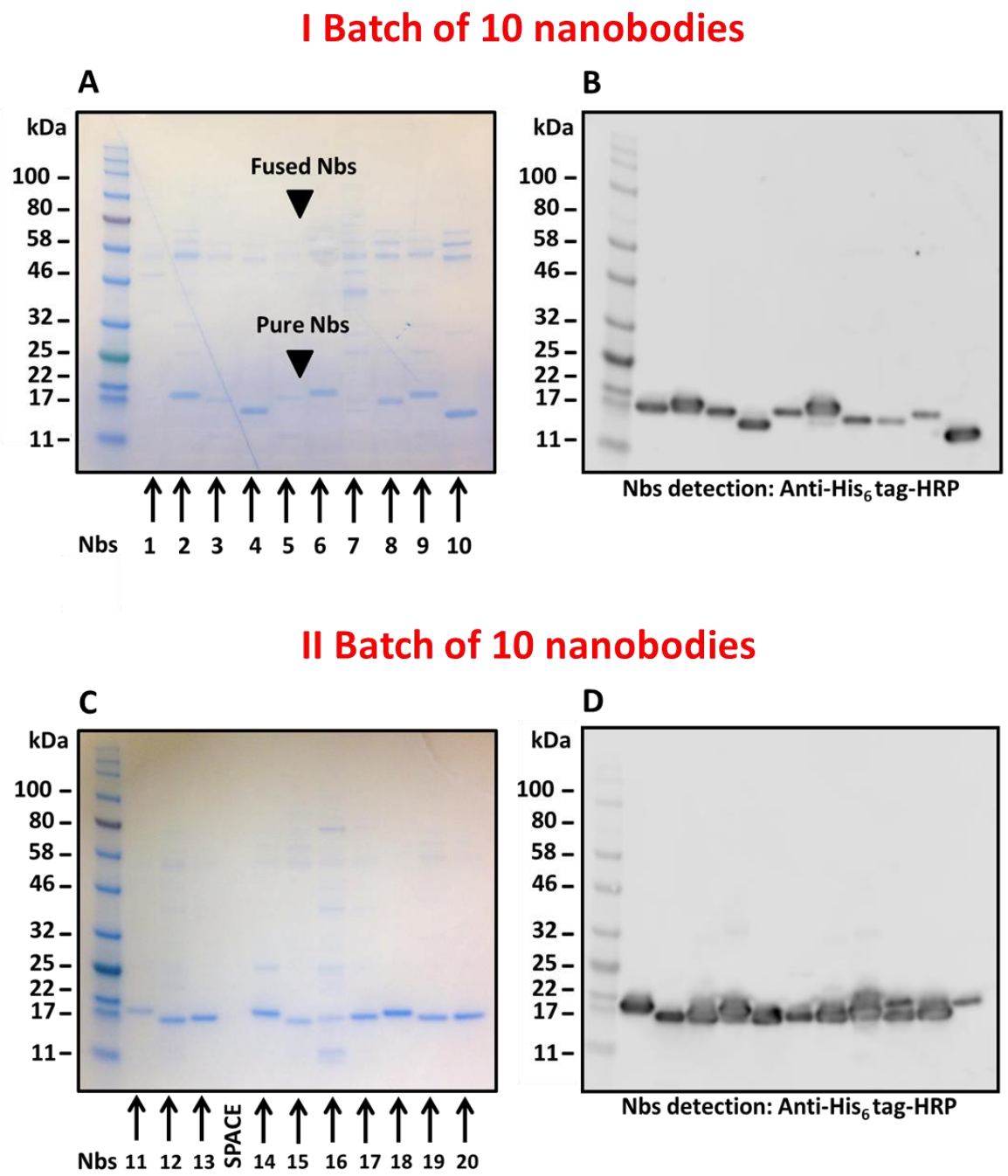

Figure 5.2. Purification of 20 nanobodies against human GPVI cloned in pMECS vector by TG1 *E.coli* strain. Coomassie staining of SDS-PAGE gels under reducing conditions loaded with 1 µg of 20 different nanobodies (Nbs) purified in two consecutive rounds (A, C). The pure Nbs appear at ~17 kDa whereas the Nbs fused with the protein III of the phage become visible at ~58 kDa (indicated by black arrows). Western blot confirms the presence of Nbs detected by anti-His_6 tag HRP conjugated secondary antibody (1/1000) at ~17 kD. The chemiluminescent detection of the Nbs was undertaken using the Odyssey Fc system (LI-COR) (B, D). Technical assistance in expressing and purifying the nanobodies was kindly provided by Ying Di, University of Birmingham, UK.

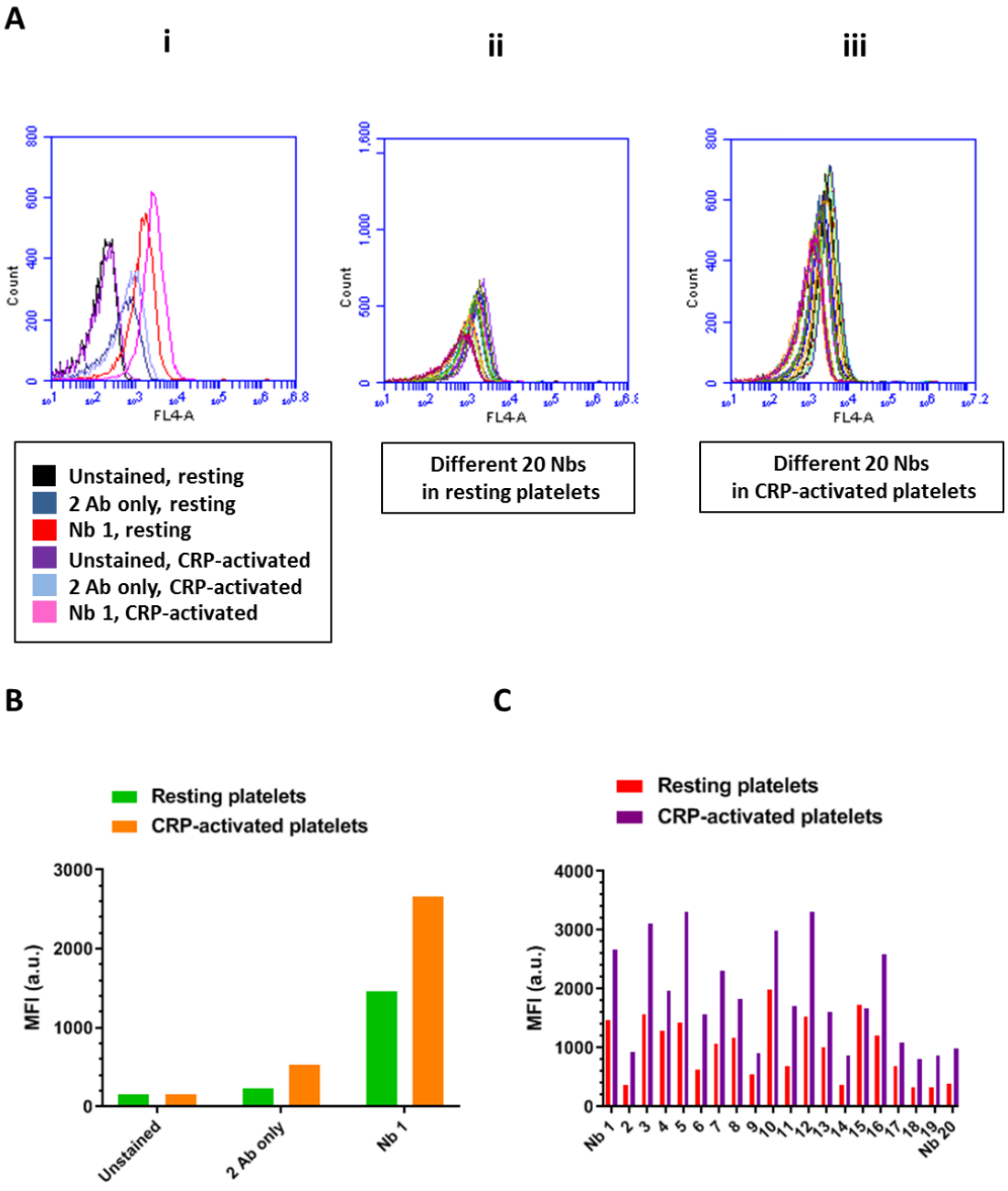

Figure 5.3. Flow cytometry analysis of nanobodies binding in resting and CRP-activated platelets. Human washed platelets, unstimulated (PBS) or stimulated with 10 μg ml^{-1} CRP-XL, were incubated with 1 μg ml^{-1} nanobodies (Nbs), secondary stained with anti-His_6 HRP conjugated (1/500) + anti-Mouse IgG Alexa Fluor 647 conjugated (1/500) and GPVI-binding was assessed by flow cytometry. The fluorescence signal on gated platelets was detected in the FL4 channel and is expressed as MFI (n=1). The flow cytometry traces in Ai and the histogram in B show a representative example (Nb #1) of the increased signal in platelets stained with the Nb in comparison with unstained platelets and platelets labelled only with the secondary antibody (2 Ab only). For all the purified Nbs, the extent of binding in resting and activated platelets is shown in the flow cytometry traces (Aii, iii) and in the histograms (C).

5.3.2 Expression and purification of three nanobodies targeting human GPVI cloned in pMECS vector by WK6 *E. coli* strain

Once the full set of 54 nanobodies had been expressed and purified in TG1 *E. coli* strain, they were further characterised by the research technician Ying Di to select good candidates to express and produce in WK6 *E. coli* strain. The nanobodies extracted from WK6 *E. coli* are pure since the amber stop codon, which follows the His_6 tag in the pMECS vector, is read as a stop codon and therefore the production of the nanobody fused with the protein III of the phage is suppressed. Nanobodies #14 and #27 were chosen as potential good candidates for imaging applications whereas nanobody #21 was selected as a putative blocking reagent. These three nanobodies are classified in different CDR3 families suggesting their epitopes are slightly different.

All the three nanobodies were successfully expressed and purified in WK6 *E. coli* strain as shown by the bands appearing at ~17 kDa in the Coomassie staining of SDS-PAGE gel loaded with 100 μg ml^{-1} nanobodies (Fig. 5.4A). Higher MW bands corresponding to fused proteins did not appear, confirming the nanobody purity. Western blot confirmed that the eluted proteins correspond to the nanobodies since they were detected by antibodies against both His_6 tag and HA tag (Fig. 5.4B, C).

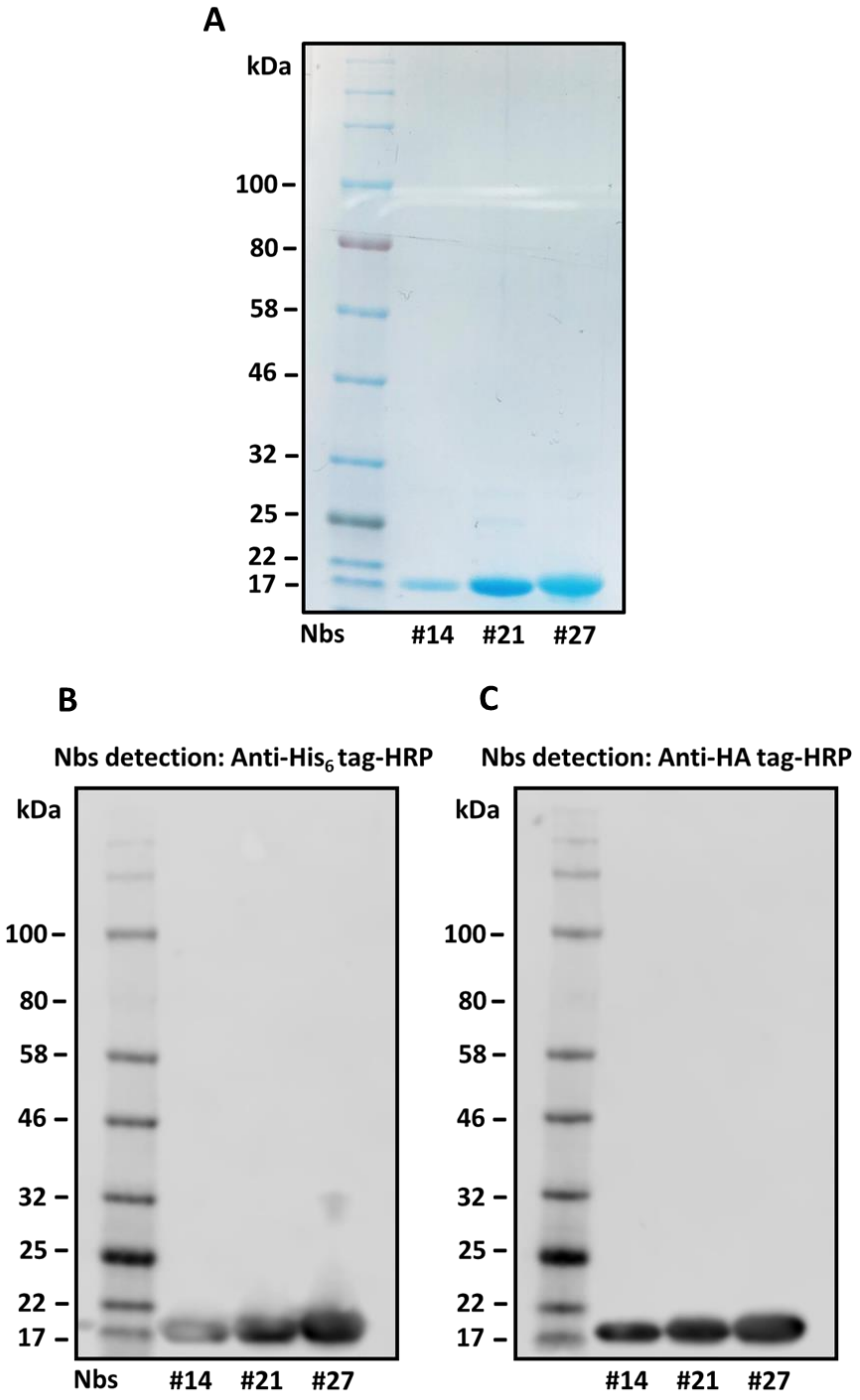

Figure 5.4. Purification of nanobodies #14, #21 and #27 against human GPVI cloned in pMECS vector by WK6 *E.coli* strain. The purity of nanobodies (Nbs) #14, #21 and #27 (100 μg ml^{-1}) extracted from WK6 *E.coli* strain was checked by Coomassie staining of SDS-PAGE gel under reducing conditions. Bands corresponding to the Nbs appear at ~17 kDa (A). Western blot and anti-His_6 tag and HA tag HRP conjugated secondary antibodies (1/1000) were used to confirm the presence of Nbs. The chemiluminescent detection of the Nbs was undertaken using the Odyssey Fc system (LI-COR) (B, C).

5.3.3 Binding of nanobodies #14, #21 and #27 to recombinant GPVI

To investigate whether nanobodies #14, #21 and #27 were functional and able to bind GPVI in a monomeric and/or dimeric conformation, an ELISA binding assay was carried out using recombinant monomeric (mGPVI) and dimeric GPVI (GPVI-Fc/dGPVI) proteins (as described in *Materials and Methods*). The Fc domain and BSA were used as negative controls. Fig. 5.5A, B, C shows that all the nanobodies, at a concentration of 1 μM, bound both monomeric and dimeric GPVI with no selectivity for one of the two receptor conformations.

To further explore the position of the nanobody-binding sites on GPVI, ELISA-based assay using different recombinant proteins corresponding to the monomeric full-length GPVI (GPVI FL) and the D1 and D2 domains of the receptor extracellular region was performed. The protein named CD200 represents the negative control. The linear dose-response plot shows that nanobody #14 bound only GPVI FL with the maximal response obtained at 100 nM (Fig. 5.5D), indicating that it likely binds GPVI at the interface between D1 and D2 domains. Contrarily, nanobodies #21 and #27 were able to bind both GPVI FL and D1 (Fig. 5.5E, F), suggesting that they may interact with the same binding domain as collagen. Like nanobody #14, the highest binding of nanobody #27 to GPVI FL was detected at 100 nM (Fig. 5.5F). Contrarily, nanobody #21 required lower concentration (1.23 nM) to induce the maximal response (Fig. 5.5E). However, this result is representative of only one experiment and further research needs to be done to determine the binding affinity of each nanobody by surface plasma resonance (SPR).

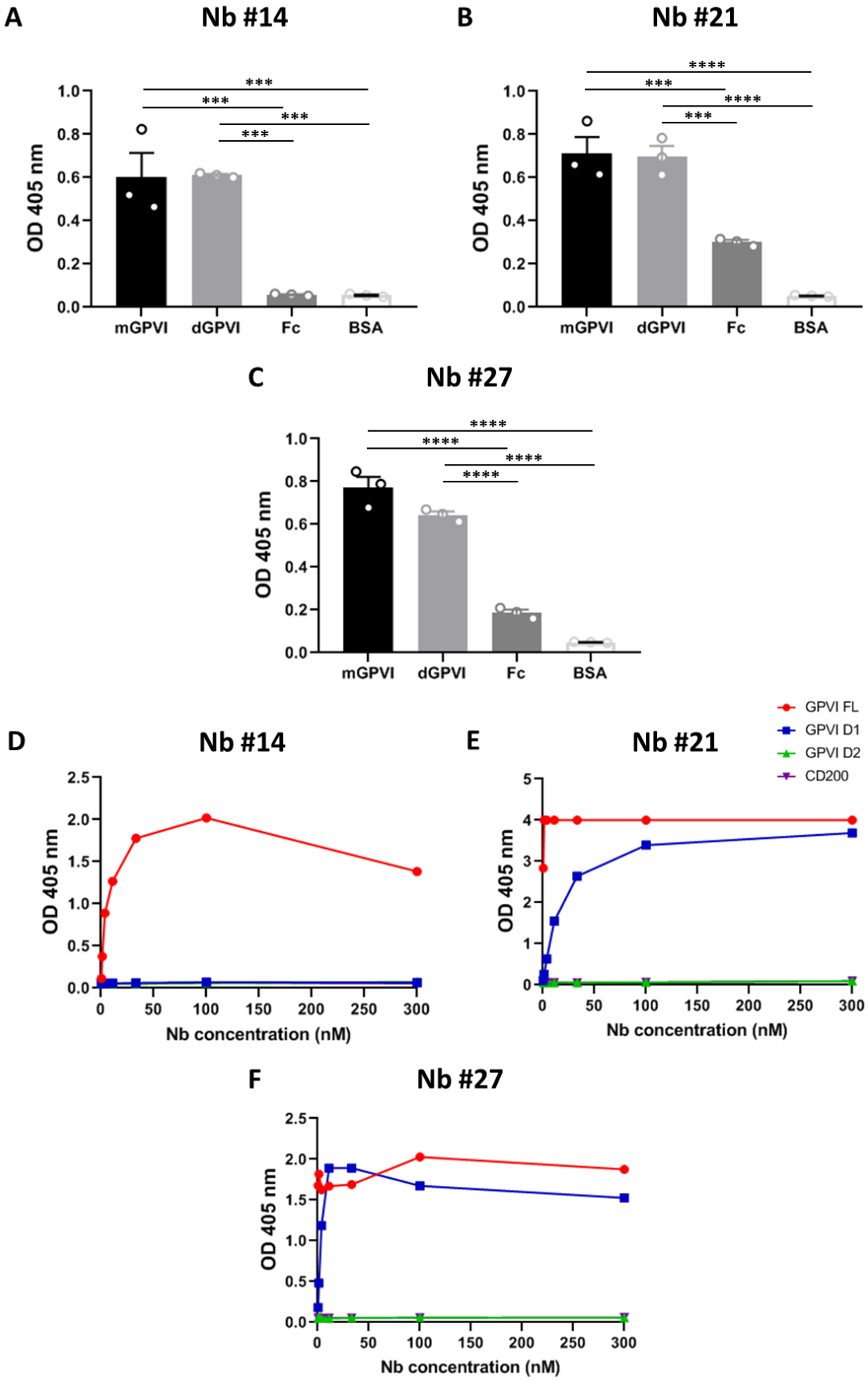
A
Nb #14
B
Nb #21
C
Nb #27
D
Nb #14
E
Nb #21
F
Nb #27
OD 405 nm
mGPVI
dGPVI
Fc
BSA
***
****
Nb concentration (nM)
GPVI FL
GPVI D1
GPVI D2
CD200

Figure 5.5. ELISA assay of nanobodies #14, #21 and #27 binding to recombinant GPVI constructs. The ELISA-based assay was performed in Nunc MaxiSorp® micro-titer 96 well plates coated with 0.1 μM recombinant mGPVI, dGPVI (GPVI-Fc) and Fc domain (negative control) at 4 °C overnight. A 3% BSA-coated well was used as an extra negative control. Nanobodies (Nbs) #14, #21 and #27 (1 μM) were allowed to bind to the recombinant proteins. Bound Nbs were detected using anti-His_6 tag HRP conjugated secondary antibody (1/10,000). The histograms show the mean ± SEM absorbance (OD = 405 nm) for each Nb compared with the controls from three replicates (A, B, C). The significant difference was evaluated using one-way ANOVA with Tukey's multiple comparisons ($P < 0.05$). The ELISA binding assay was also performed on additional recombinant proteins: monomeric GPVI FL, GPVI D1 and D2 domains and CD200 (negative control). The Nbs were used at the initial concentration of 300 nM and then diluted 1:3. Bound Nbs were detected using anti-HA HRP conjugated secondary antibody (1/10,000). The linear dose-response plots (D, E, F) show the specific binding of Nb #14 to GPVI FL and Nbs #21 and #27 to GPVI D1 domain (n=1). The data in parts D-F was kindly provided by Dr Ruben Barroso and Dr Yi Sun, University of Birmingham, UK.

5.3.4 Nanobody #14 but not #21 and #27 binds GPVI in human platelets

To confirm the binding of nanobodies #14, #21 and #27 to endogenous GPVI in human platelets, flow cytometry analysis was carried out in resting platelets and platelets stimulated with different agonists, namely PAR1 peptide and CRP-XL which induce platelet activation in a GPCR and ITAM-dependent manner, respectively. P-selectin exposure was used as a marker of platelet activation (Fig. 5.6Ai, ii). In addition, unspecific binding was monitored by labelling platelets with only the secondary antibody (anti-His_6 Alexa Fluor 647 conjugated, Fig. 5.6B, C, D). At the final concentration of 8 μg ml^{-1}, nanobody #14 was able to bind endogenous GPVI. This is shown by the significant increase in the MFI value induced by nanobody #14 in both resting and activated platelets in comparison with platelets stained only with the secondary antibody (5 different donors, Fig. 5.6Bi, ii). Contrarily, at the same final concentration used for nanobody #14, no binding of nanobodies #21 and #27 was detected (2 of the 5 donors used to test nanobody #14, Fig. 5.6C, D, E, F). Hypothesizing that the concentration of nanobodies #21 and #27 was not sufficient to bind GPVI in human platelets, we have repeated the experiments on other 3 different donors (the same donors used to test nanobody #14) using higher concentrations of both nanobodies (38 and 63 μg ml^{-1} for #21 and #27, respectively). Nanobodies #21 and #27 did not induce a significant increase in the MFI value relative to the negative control even at higher concentrations (Fig. 5.6 G, H), suggesting that they may induce a change in GPVI conformation or localisation, thereby making it unavailable for binding.

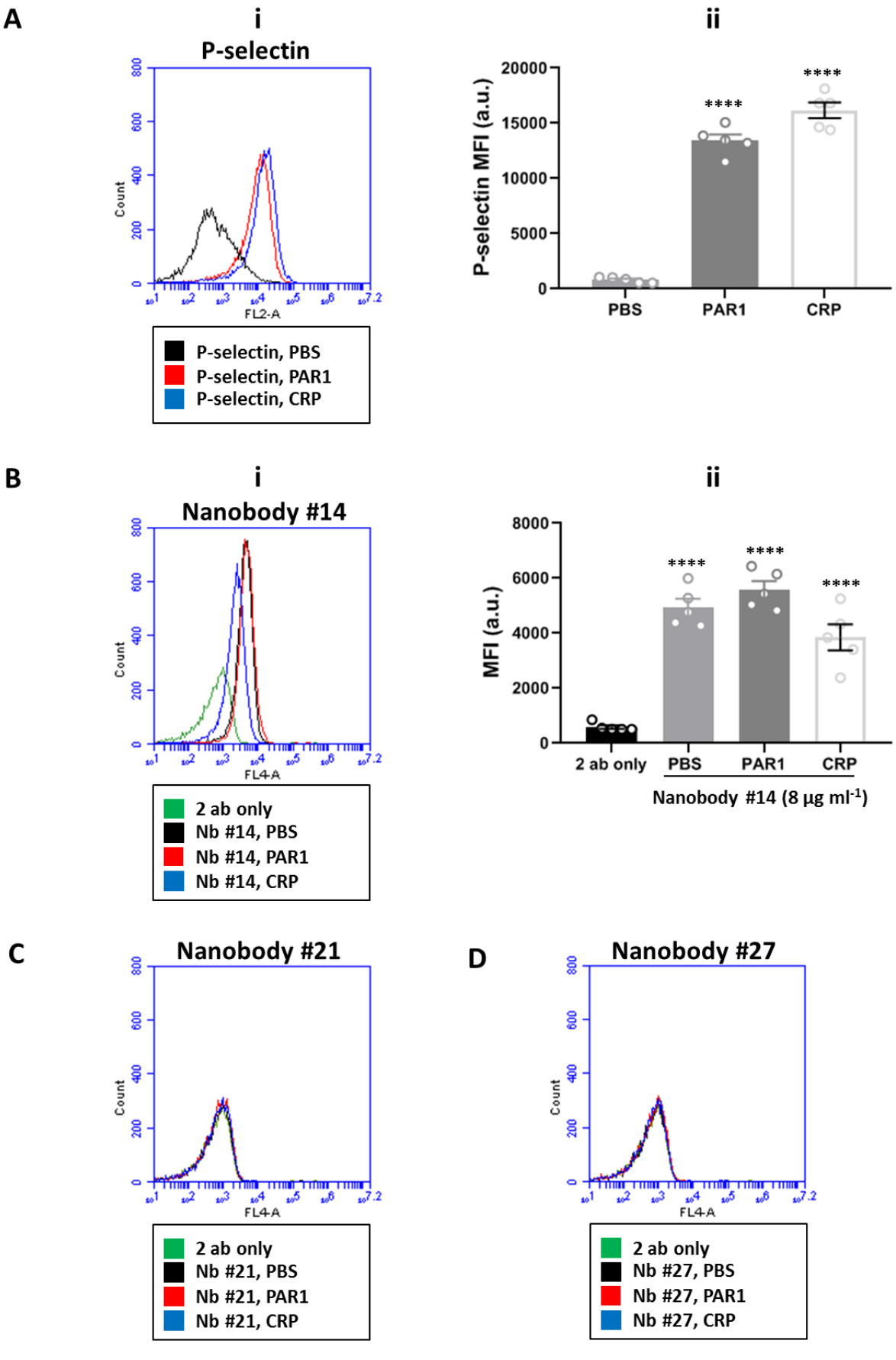
A
i
P-selectin
Count
FL2-A
P-selectin, PBS
P-selectin, PAR1
P-selectin, CRP
ii
P-selectin MFI (a.u.)
20000
15000
10000
5000
0
****
****
PBS
PAR1
CRP
B
i
Nanobody #14
Count
FL4-A
2 ab only
Nb #14, PBS
Nb #14, PAR1
Nb #14, CRP
ii
MFI (a.u.)
8000
6000
4000
2000
0
****
****
****
2 ab only
PBS
PAR1
CRP
Nanobody #14 (8 µg ml-1)
C
Nanobody #21
Count
FL4-A
2 ab only
Nb #21, PBS
Nb #21, PAR1
Nb #21, CRP
D
Nanobody #27
Count
FL4-A
2 ab only
Nb #27, PBS
Nb #27, PAR1
Nb #27, CRP

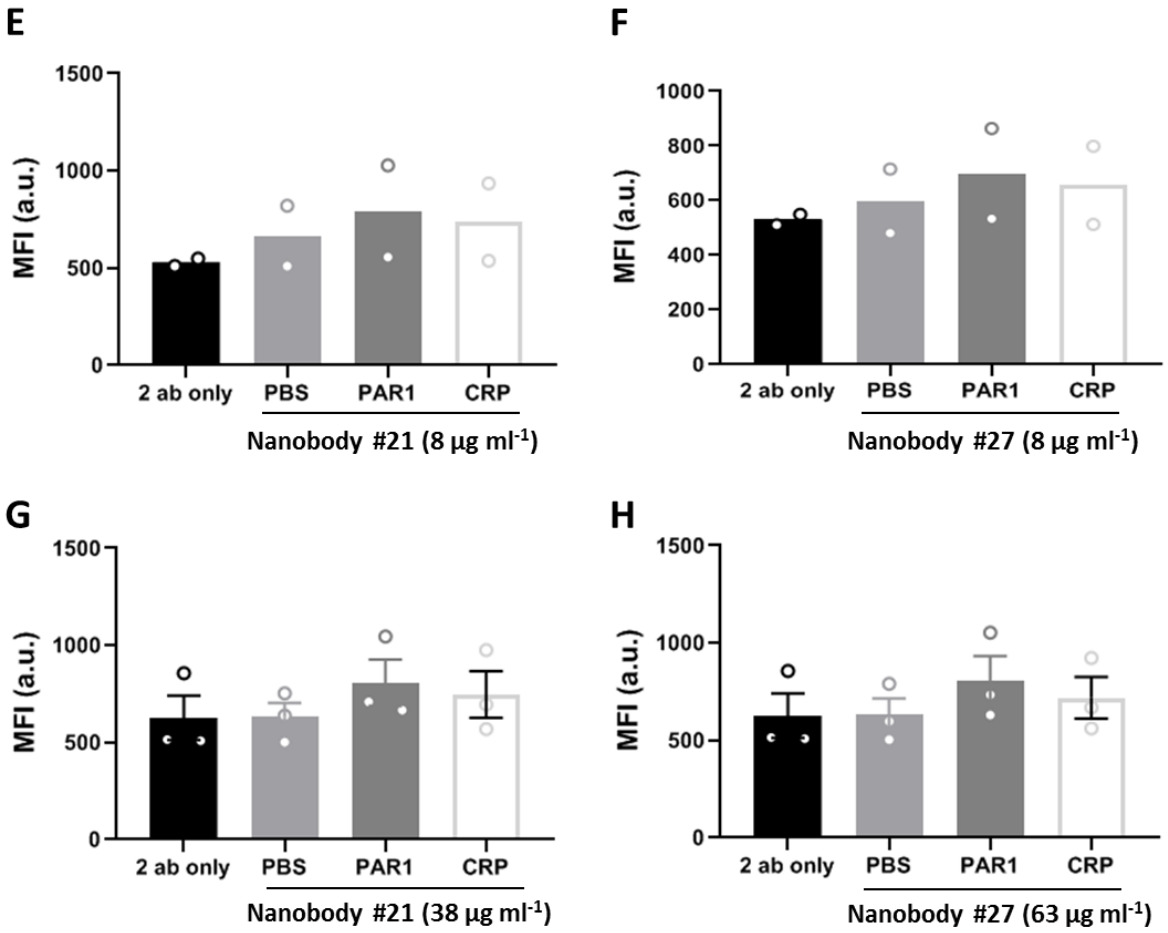

Figure 5.6. Flow cytometry analysis of nanobodies #14, #21 and #27 binding to GPVI in resting and PAR1 and CRP-activated platelets. Unstimulated human platelets (PBS) or platelets stimulated with 200 µM PAR1 peptide or 10 µg ml^{-1} CRP-XL, were labelled with PE anti-human CD62-P to monitor P-selectin exposure as a marker of platelet activation (Ai, ii). Resting and activated platelets were also incubated with 8 µg ml^{-1} nanobody (Nb) #14 and secondary labelled with anti-His_6 Alexa Fluor 647 conjugated (1/80) (Bi, ii, n=5). In the first 2 experiments, Nbs #21 and #27 were used at the same concentration of Nb #14 (8 µg ml^{-1}, C, D, E, F) whereas higher concentrations (38 and 63 µg ml^{-1} for #21 and #27, respectively) were tested on the last 3 donors (G, H). Platelets stained only with the secondary antibody were used as a negative control. On gated samples, positive signals for P-selectin and Nbs were detected in the FL2 and FL4 channels, respectively. The flow cytometry analysis demonstrates that only Nb #14 can bind GPVI in human platelets (Bi, ii). One-way ANOVA with Tukey's multiple comparisons shows a significant increase ($P < 0.05$) in the MFI value induced by Nb #14 in resting and activated platelets compared with platelets labelled only with the secondary antibody.

5.3.5 Nanobodies #21 and #27 but not #14 induce GPVI shedding in human platelets

In addition to the other mechanisms, the antibody-induced shedding has been described as a potent trigger of GPVI shedding in patients and mouse models (Boylan et al., 2006, Boylan et al., 2004, Nieswandt et al., 2001b, Schulte et al., 2003). In light of the lack of binding of nanobodies #21 and #27 in human platelets, we postulated that they may induce the release of GPVI from the platelet surface, thereby preventing the binding. For this purpose, platelets were stimulated with each of the three nanobodies under stirring conditions for 1 h and GPVI cleavage was explored by Western blot using the anti-GPVI-tail antibody. In control platelets (stimulated with PBS) and platelets incubated with nanobody #14, GPVI shedding was not triggered as the band relating to the intracellular tail at ~10 kDa did not appear (Fig. 5.7A). However, nanobodies #21 and #27 caused receptor cleavage from the cell surface with detection of the band relative to the 10 kDa membrane-bound tail (Fig. 5.7A). ~25% of total GPVI receptor underwent proteolytic cleavage after 1 h of stimulation with nanobodies #21 and #27 (Fig. 5.7B). Therefore, this finding could, at least partially, explain the loss of GPVI signal in flow cytometry and proposes a novel, unexplored mode of action of anti-GPVI nanobodies in human platelets.

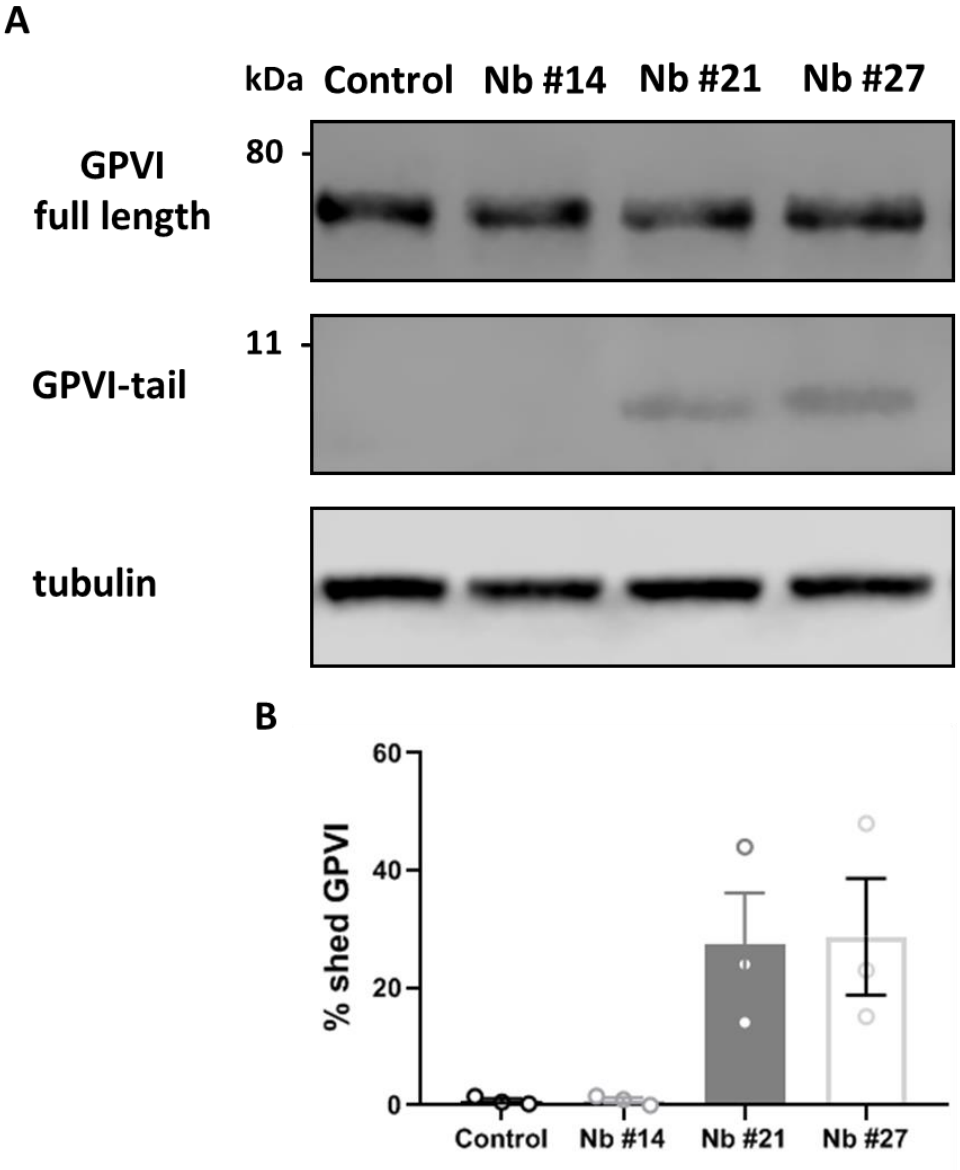

Figure 5.7. GPVI shedding in platelets stimulated with nanobodies #14, #21 and #27. Human washed platelets, pre-incubated with 2 mM $CaCl_2$, were stimulated with 8 μg ml^{-1} nanobodies (Nbs) #14, #21 and #27 or PBS (control) for 1 h under stirring conditions. SDS-PAGE analysis and western blot were carried out on lysates from both control and stimulated platelets. GPVI shedding was evaluated by immunoblotting with the anti-GPVI-tail antibody, secondary labelled with anti-rabbit IRDye 800CW conjugated secondary antibody and fluorescently revealed by Odyssey Fc system (LI-COR). The loading was monitored using the α-tubulin antibody (A). The percentage of shed GPVI was calculated on the fluorescent signal as described in *Chapter 4*. The histogram represents the mean ± SEM from three independent experiments (B).

5.3.6 Nanobodies #21 and #27 but not #14 inhibit platelet aggregation in response to collagen

Previous work performed on recombinant GPVI proteins has demonstrated that nanobody #14 binds full-length GPVI whereas nanobodies #21 and #27 interact specifically with the GPVI D1 domain, the major collagen-binding site. Thus, we hypothesized that nanobodies #21 and #27 could potentially compete with collagen for binding to GPVI and interfere with collagen-induced platelet aggregation. Fig. 5.8A, B shows that collagen at 3 μg ml^{-1} triggered ~70% of the maximal aggregation within a 5 min time in control samples. At 10 μg ml^{-1} nanobody #14 did not significantly affect platelet aggregation in response to collagen (Fig. 5.8A, B). However, there was significant inter-donor variability, with the platelets from some donors aggregating normally to collagen stimulation whilst the platelets from other donors did not aggregate at all. On the contrary, nanobodies #21 and #27 at the same concentration used for nanobody #14, completely blocked platelet aggregation induced by collagen compared with control platelets (Fig. 5.8A, B). Therefore, this result demonstrates that nanobodies #21 and #27 interfere with platelet function in response to collagen and supports previous findings proposing that they may occupy the collagen-binding site of GPVI and induce the proteolytic cleavage from the platelet surface.

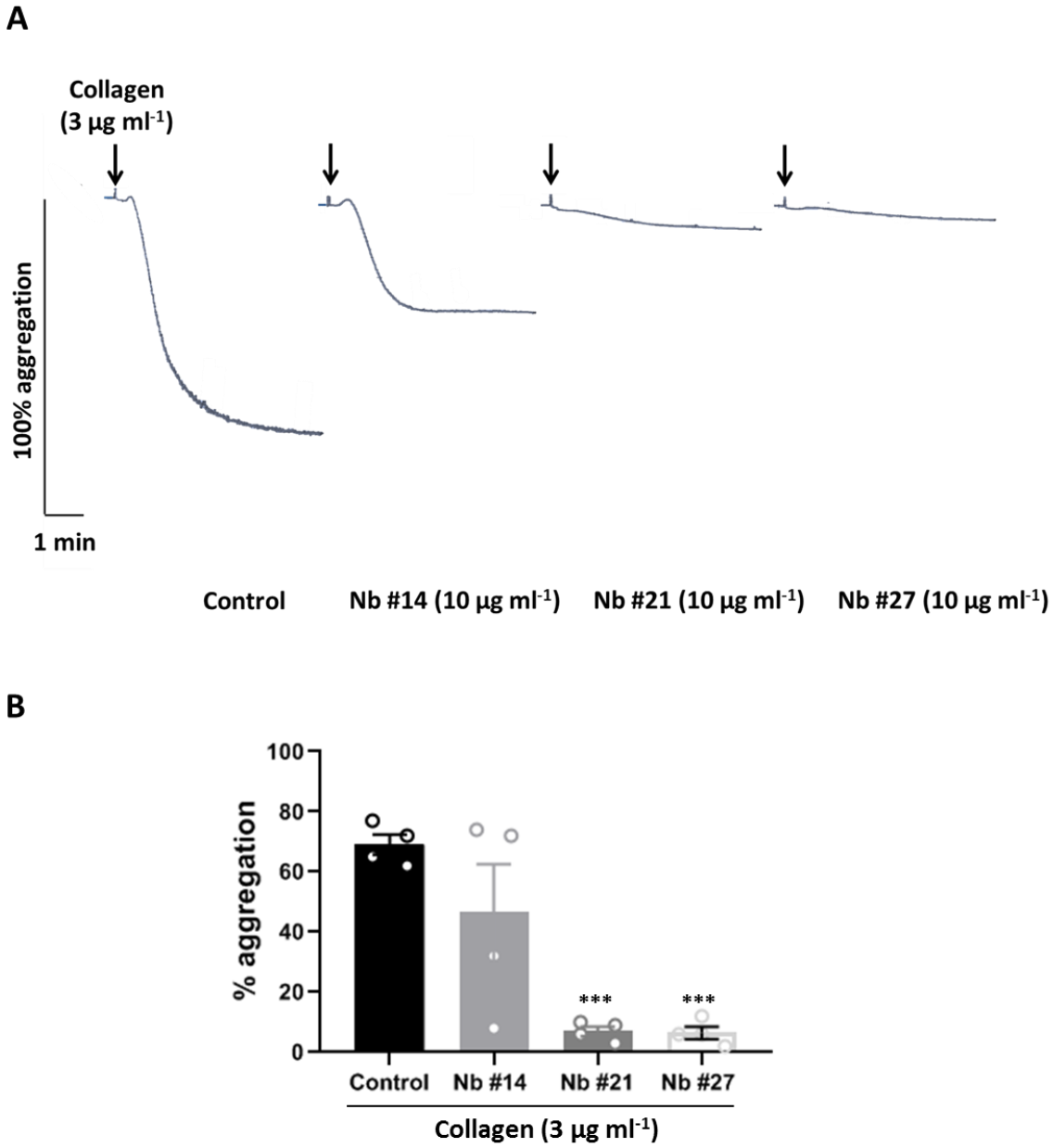

Figure 5.8. Effect of nanobodies #14, #21 and #27 on collagen-induced platelet aggregation. The effect of nanobodies (Nbs) #14, #21 and #27 (10 µg ml^{-1}) or PBS (control vehicle) on platelet aggregation in response to collagen (3 µg ml^{-1}) was monitored by light transmission aggregometry at 37 °C under steady stirring conditions (1200 rpm) within a 5 min time frame. The aggregation traces shown in A are representative of n=4 separate experiments. The histogram reports the mean ± SEM % of aggregation in control platelets and platelets incubated with Nbs (B). One-way ANOVA with Tukey's multiple comparisons shows that Nbs #21 and #27 significantly ($P < 0.05$) inhibit collagen-induced platelet aggregation.

5.3.7 Effect of nanobodies #14, #21 and #27 on platelet spreading on collagen

To further investigate whether the nanobodies compete with collagen for binding to GPVI, we evaluated their effect on platelet adhesion and spreading on immobilised collagen in static conditions. Based on the ELISA and aggregation data, we expect that pre-incubation of platelets with nanobodies #21 and #27 would prevent GPVI-collagen interaction with the subsequent impairment of platelet adhesion and spreading. The platelet count, used as a quantitative parameter of platelet adhesion, was not hampered by nanobodies #14, #21 and #27 (Fig. 5.9B). The spreading of platelets in the presence of the different nanobodies was also not significantly affected in comparison with the control platelets (Fig. 5.9C). However, we again found a high inter-experimental variability with the platelets from some donors showing a normal spreading whilst the platelets from other donors exhibiting a partial reduction in spreading. Therefore, it would be good to test the effect of the nanobodies on collagen-induced platelet aggregation and spreading using the same platelet donor to understand whether the outcomes correlate to each other. In summary, whilst nanobodies #21 and #27 block platelet aggregation in response to collagen, they do not profoundly impair collagen-induced platelet spreading, likely due to the ability of integrin α2β1 to support platelet adhesion and spreading on collagen.

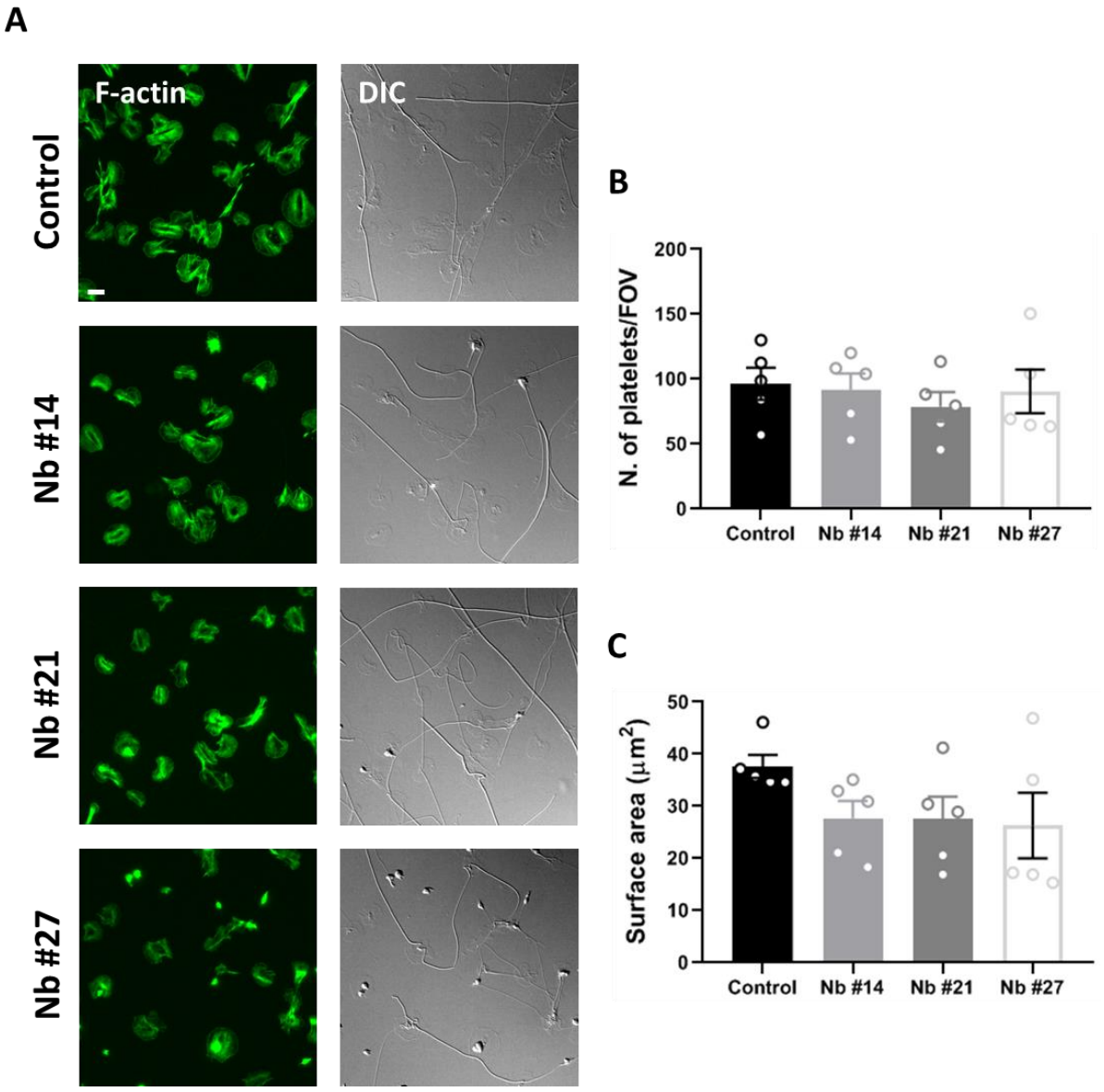

Figure 5.9. Effect of nanobodies #14, #21 and #27 on collagen-induced platelet adhesion and spreading. Human washed platelets, pre-incubated with nanobodies (Nbs) #14, #21 and #27 (5 μg ml^{-1}) or PBS (control vehicle) for 10 min, were spread on an immobilised collagen (10 μg ml^{-1}) surface for 1 h. F-actin was stained with Alexa Fluor phalloidin 488 and imaged by epifluorescence microscopy (A, first column). The DIC images (A, second column) illustrate the adhesion and spreading of platelets on the collagen monolayer. The quantitative analysis of platelets count (B) and surface area (C) was performed in KNIME and is reported as mean ± SEM from 5 independent experiments (in total, 25 FOVs for each condition were analysed). One-way ANOVA with Tukey's multiple comparisons shows non-significant difference ($P < 0.05$) between the control platelets and platelets incubated with the Nbs. Scale bar: 5 μm.

5.3.8 Generation and fluorescent labelling of SNAP-tagged nanobody #14

The full characterisation of nanobodies #14, #21 and #27 enabled the selection of nanobody #14 as the best candidate for imaging applications. For SMLM the ideal protein label would have a single fluorescent tag to enable accurate quantification. For this purpose, we genetically fused the SNAP-tag protein to the N-terminus of the nanobody gene (as described in *Materials and Methods*, Fig. 5.10A) and further purified by FPLC. The FPLC profile illustrates that the eluted protein was collected in the fractions 4-8 (Fig. 5.10B) of which 7 and 8 contained the nanobody with the highest purity, as shown by Coomassie staining of SDS-PAGE gel (Fig. 5.10C). Western blot confirmed that the bands between 46 and 32 kDa correspond to the SNAP-nanobody #14 as detected by anti-His_6 tag (Fig. 5.10D).

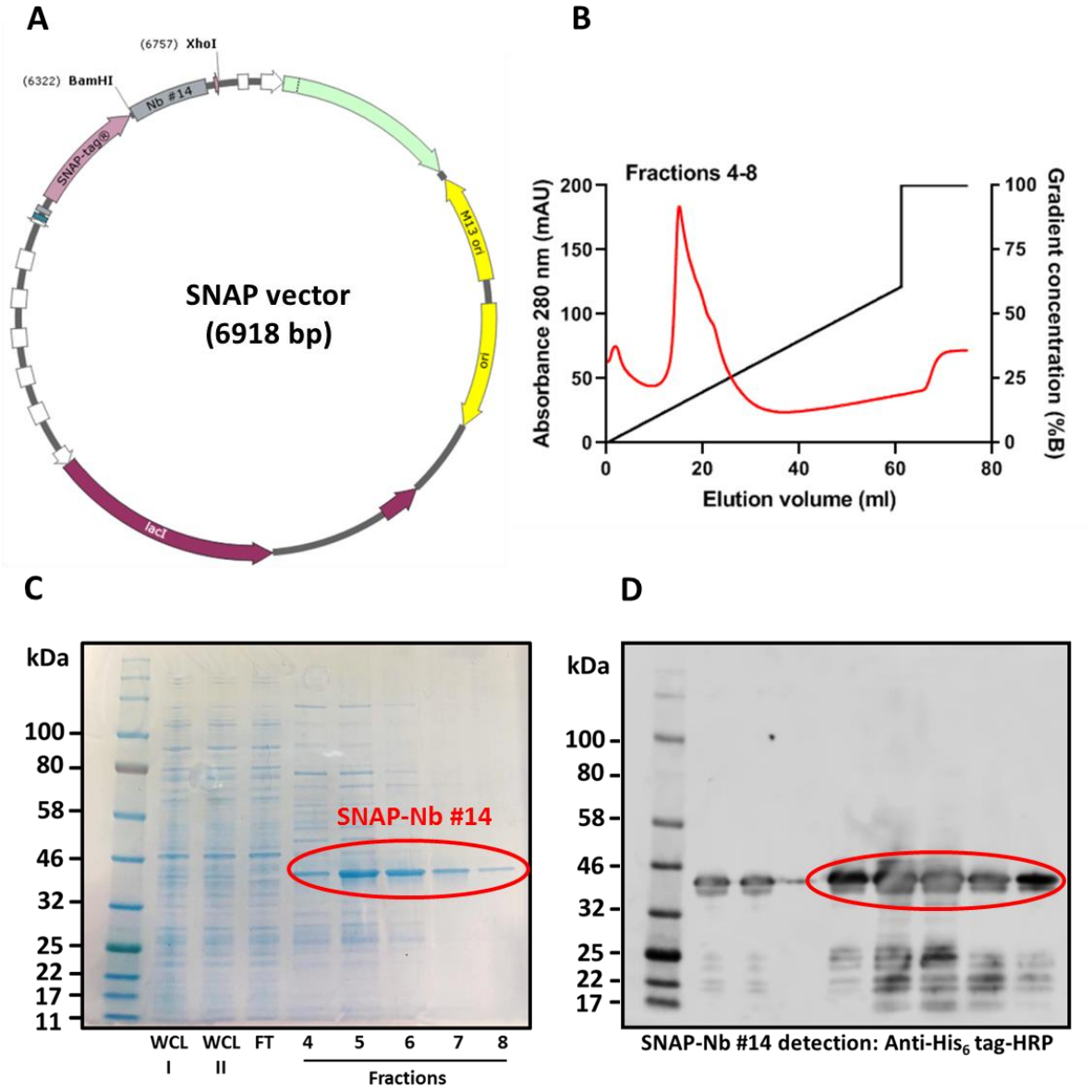

Figure 5.10. Production of SNAP-tagged nanobody #14. Nanobody (Nb) #14 was cloned into the BamHI and Xhol sites of the SNAP-tag vector as described in *Materials and Methods*. The SNAP-tag lies at the N-terminus of the Nb sequence, the PelB signal sequence is lost whereas the HA and His_6 tags are still located at the C-terminus of the Nb gene (A). FPLC elution profile of SNAP-tagged nanobody #14 (SNAP-Nb #14) where absorbance at 280 nM is plotted against the elution volume. The protein was eluted by applying a pump B gradient which was equilibrated in 500 mM imidazole. The eluent was collected in the fractions 4-8 and is represented by a peak (red) in the graph (B). Coomassie staining of SDS-PAGE gel loaded with the whole-cell lysates (WCL) I and II (from the two bacteria colonies harbouring the right insertion of the Nb #14 into the SNAP-tag vector), the flow-through (FT) liquid and the fractions 4-8 correspondent to the eluted Nb. The SNAP-Nb #14 was detected between 46 and 32 kDa (C, circled in red) as confirmed by Western blot using anti-His_6 tag HRP conjugated secondary antibody (D). Dr Alex Slater (University of Birmingham, UK) kindly provided technical help with the cloning and FPLC chromatography.

The advantage of the SNAP-tag protein is its irreversible, site-specific and quantitative self-labelling using commercial *in vitro* kits which covalently attach the fluorophore to the active site cysteine (Cole, 2013). We, therefore, exploited the full potential of the SNAP-tag by directly conjugating the protein with Alexa Fluor 647, resulting in the generation of SNAP-nanobody #14-Alexa Fluor 647. The covalent bond between the fluorescent probe and the SNAP-nanobody #14 allowed its detection by SDS-PAGE and exposure on the Odyssey fluorescence detection system. Fig. 5.11A shows the successful conjugation of the SNAP-tagged nanobody #14 with the Alexa Fluor 647 dye. We then tested the ability of the fluorescently conjugated SNAP-nanobody #14 to efficiently immunolocalise GPVI in platelets spread on immobilised collagen compared with 1G5-Fab which has been shown to successfully label GPVI in all our previous experiments. Fig. 5.11B shows that whereas SNAP-nanobody #14-Alexa Fluor 647 was able to target GPVI as shown by the classical enrichment along collagen fibres, it is characterised by a lower signal-to-noise ratio compared to 1G5-Fab. Furthermore, we detected non-specific binding to the collagen fibres even outside the platelet surface, probably due to the unreacted substrate still present in solution or the SNAP-tag itself may non-specifically interact with the collagen substrate. Therefore, this finding suggests that further optimisation is required to evaluate the fluorescent SNAP-nanobody as a potential imaging tool for targeting GPVI receptors in human platelets.

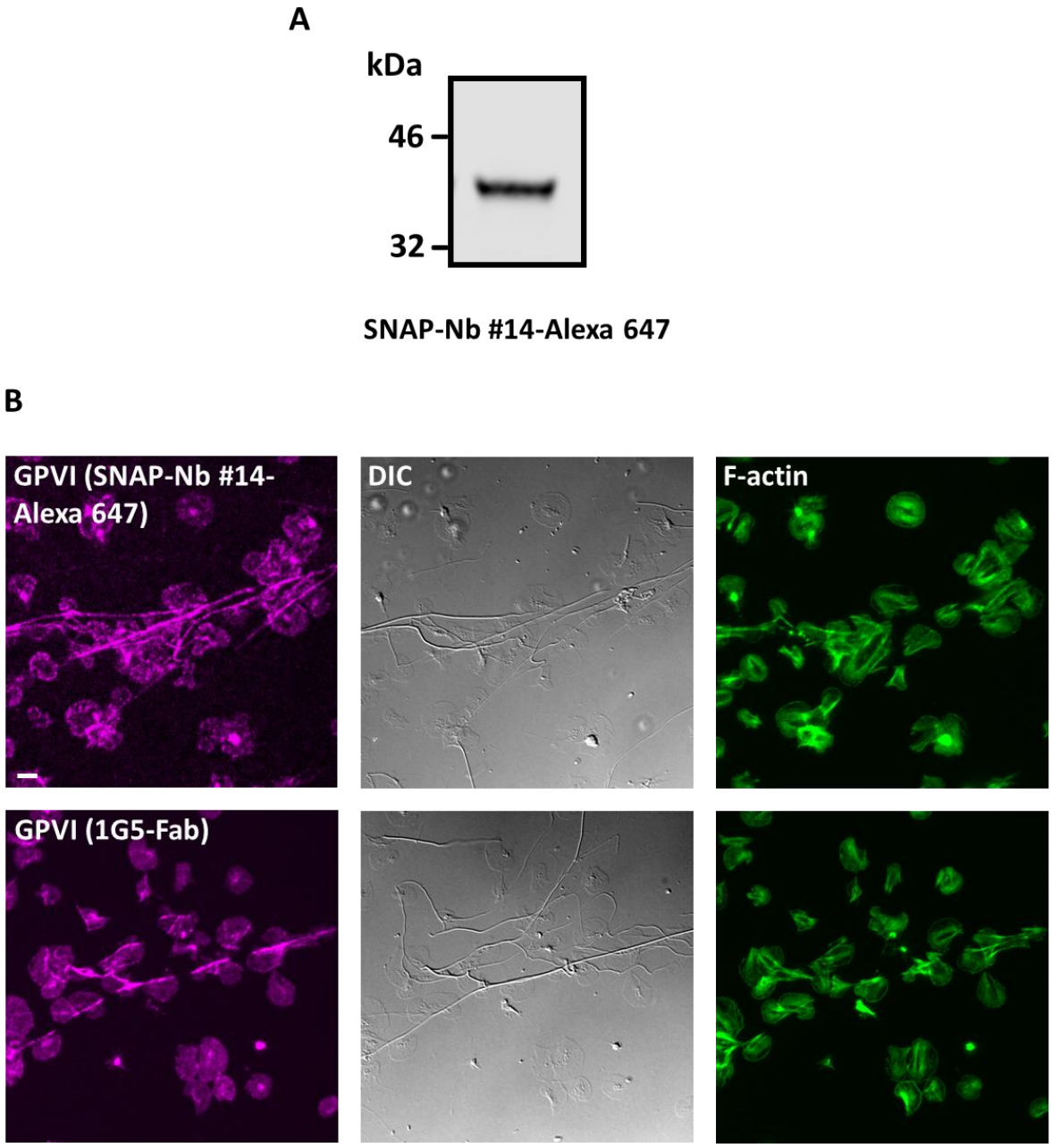

Figure 5.11. Confocal imaging of GPVI labelled with SNAP-nanobody #14-Alexa Fluor 647 or 1G5-Fab in platelets spread on collagen. The SNAP-tagged nanobody #14 conjugated with Alexa Fluor 647 (SNAP-Nb #14-Alexa 647) was run on an SDS-PAGE gel and detected using Odyssey Fc-system in the 700 nm channel (A). Human washed platelets were spread on an immobilised collagen (10 μg ml^{-1}) monolayer for 1 h and GPVI was labelled with SNAP-Nb #14-Alexa 647 (5 μg ml^{-1}, post-spreading) or 1G5-Fab (2 μg ml^{-1}, pre-spreading) and secondary stained with anti-mouse Alexa Fluor 647 conjugated. Confocal imaging shows the comparison between the labelling efficiency of SNAP-Nb #14 and 1G5-Fab (B, left-hand side). The presence of platelets was confirmed by Alexa Fluor phalloidin 488 staining of F-actin (B, right-hand side) whereas the collagen distribution was visualised by DIC (B, middle). The images are representative of n=1 experiment. Scale bar: 5 μm.

5.4 Discussion

Nanobodies are promising experimental tools in a variety of biological applications, including super-resolution microscopy for the interrogation of surface receptors localisation (Manglik et al., 2017, Traenkle and Rothbauer, 2017). In this Chapter we present the first toolset of 54 nanobodies generated against the human platelet GPVI receptor. The initial characterisation of a subset of 20 impure nanobodies shows high specificity of binding to GPVI in human platelets. Ultimately, the full validation of three selected nanobodies, which recognise different epitopes of GPVI, highlights their diversity in a variety of biological assays.

Our ELISA binding assay shows that they were able to specifically bind both recombinant monomeric and dimeric GPVI which may represent an advantage for the accurate detection of GPVI in activated platelets which is predominantly found in a dimeric conformation (Jung et al., 2012, Loyau et al., 2012). The identification of the specific binding site of nanobodies #21 and #27 in the D1 domain, which represents the major collagen-binding loop (Smethurst et al., 2004), gave rise to the hypothesis that they may interfere with GPVI-collagen interaction. On the contrary, nanobody #14 only bound the full-length GPVI protein, suggesting that it interacts with a different site compared to #21 and #27, probably located at the interface between the D1 and D2 loops and therefore not competing with collagen. Surprisingly, flow cytometry of GPVI failed to detect binding of nanobodies #21 and #27 to human GPVI whereas nanobody #14 successfully labelled GPVI with a large shift in fluorescence detected, proposing a compromised presence of GPVI at the platelet surface upon stimulation with the first two nanobodies. GPVI surface expression within the PM can be controlled by different regulatory mechanisms, most importantly receptor endocytosis and receptor shedding. Shedding of GPVI can be induced by a number of physiological/non-physiological stimuli in *in vitro* and *in vivo* systems, including ligand engagement (Facey et al., 2016, Gardiner et al.,

2004), synthetic compounds (Bergmeier et al., 2004, Facey et al., 2016, Gardiner et al., 2004, Gardiner et al., 2007), coagulation factors (Al-Tamimi et al., 2011b), shear stress (Al-Tamimi et al., 2012, Facey et al., 2016), activation of (hem)ITAM receptors (Gardiner et al., 2008, Gitz et al., 2014) and anti-GPVI antibodies (Nieswandt et al., 2001b, Schulte et al., 2003). Here, we found that nanobodies #21 and #27 induced ~25% shedding of GPVI, a phenomenon that has previously been proposed for conventional antibodies in immunodepletion strategies in mouse models (Nieswandt et al., 2001b, Schulte et al., 2003) or in patients affected by immune thrombocytopenia as a result of autoimmune processes (Boylan et al., 2004, Sugiyama et al., 1987, Takahashi and Moroi, 2001). However, this does not explain the total lack of GPVI signal detected by flow cytometry, suggesting that additional mechanisms may be involved in affecting the GPVI expression levels at the platelet surface. One possibility is that the nanobodies also induce internalisation of GPVI, rendering it unavailable to be bound by the fluorescently tagged secondary antibody. It is known that CLEC-2 can be internalised following antibody-binding (Lorenz et al., 2015, May et al., 2009) whereas there is a rudimentary knowledge of whether GPVI can be endocytosed. One study has demonstrated the efficacy of an engineered anti-hGPVI antibody, labelled with a fluorescent endocytosis probe, to induce a cAMP-dependent GPVI internalisation in both *in vitro* and *in vivo* systems using cynomolgus monkeys as a model (Takayama et al., 2008). Therefore, it would be interesting to investigate whether the anti-GPVI nanobodies can also deplete GPVI through endocytosis as described by Takayama et al. (2008). The block of platelet aggregation in response to collagen induced by nanobodies #21 and #27 is also in line with their putative interaction with the collagen-binding site and the loss/reduction of GPVI receptors available to bind collagen and induce aggregation. However, the mechanisms underlying the nanobodies-induced shedding remain to be elucidated. They may trigger a

conformational change and interfere with receptor dimerisation and clustering, allowing the exposure of the cleavage site for metalloproteinases. Alternatively, they may prevent binding of a protective protein, for example, a member of the tetraspanin superfamily as proposed by the model from (Noy et al., 2016). In addition, whether they induce shedding through ADAM10 remains to be verified. The hypothetical change in GPVI distribution relative to e.g. ADAM10 and tetraspanins would be revealed by super-resolution microscopy. Taken together, these findings propose nanobodies #21 and #27 as potential inhibitory reagents to limit platelet activation.

Nanobody #14 did not induce GPVI shedding or block platelet aggregation. However, the aggregation data in the presence of nanobody #14 were characterised by high inter-experimental variability using platelets from different donors (different gender, age and nationality). The same issue was detected in the platelet spreading assay, making the result inconclusive. This inter-donor variability may be associated with the expression of a different GPVI haplotype (*GP6a* or *GP6b*) as platelets homozygous for *GP6b* express GPVI at a lower level and are less able to aggregate compared to homozygous for *GP6a* (Joutsi-Korhonen et al., 2003). One approach to address this issue would be to use the same donor for all the assays to verify if the results correlate.

Taken together, the experimental observations propose nanobody #14 as a non-blocking nanobody making it the most promising candidate for SMLM imaging. In our standard staining procedure for SMLM imaging of GPVI (*Chapter 3* and *4*), the epitope is displaced from the fluorophore by ~24 nm, interfering with the effective spatial resolution of the receptor achieved during imaging. In a previous attempt, the labelling of a nanobody with standard NHS ester fluorophores (data not shown) resulted in a poor staining and low signal-to-noise ratio, in accordance with recent reports from different groups (Pleiner et al., 2015,

Virant et al., 2018). This labelling procedure is also not site-specific and may compromise the epitope-binding. Here, we genetically fused nanobody #14 with the SNAP-tag to obtain an irreversible, site-specific and quantitative labelling of the nanobody using a commercial *in vitro* kit (Cole, 2013). This way, we successfully immunolocalised GPVI by epifluorescence microscopy. Unfortunately, the fluorescent SNAP-nanobody #14 performed worse than the anti-GPVI Fab detected by a fluorescently-conjugated secondary antibody as shown by the lower signal-to-background ratio and some unspecific binding to the collagen fibres outside the platelet surface. This may be caused by the inefficacy of the dialysis in removing the unreacted substrate or the high reactivity of the SNAP-tag. Furthermore, the SNAP-tag is a quite large molecule (~20 kDa) and therefore, despite the advantages in specific tagging with fluorophores, it is not the ideal solution for SMLM applications.

Overall, findings from this Chapter represent the first generation and characterisation of nanobodies targeting human platelet GPVI and highlight their heterogeneity and suitability for many different applications, from anti-platelet approaches to super-resolution imaging. Future work is needed to confirm the inhibitory effect of nanobodies #21 and #27 in flow assays and in *in vivo* and *ex vivo* studies. Moreover, other labelling strategies need to be contemplated to adopt and optimise nanobody #14 as a tool for the spatial investigation of GPVI receptor by super-resolution imaging. The array of assays reported in this Chapter should be taken as an example for the future characterisation of the other unexplored anti-GPVI nanobodies.

CHAPTER 6

General Discussion

6.1 Summary of results

The platelet collagen receptor GPVI is a current antithrombotic drug target due to its platelet (and MK)-specific expression profile and its minimal role in haemostasis. Despite there being extensive data on the components of the GPVI signalling cascade, there is negligible understanding of how the spatial organisation of GPVI at the platelet PM regulates the intracellular signalling. Recent advances in super-resolution microscopy and accompanying analysis methods have the potential to address this lack of understanding and it is this which has driven the work of this PhD project. The 3 main points addressed in this research are: 1) identifying the clustering approach suitable for the analysis of different cluster shapes; 2) elucidating the mechanisms of clustering, signalling and shedding in human platelets adhered to collagen; 3) employing the nanobody technology to construct a more accurate map of GPVI nanoscale organisation via single molecule super-resolution microscopy.

6.2 Challenges in quantitative analysis of GPVI clustering in platelets

The work in this thesis presents the application of the most widely used clustering methods, namely Ripley's K-function, DBSCAN and Voronoï tessellation, for the quantitative study of GPVI nanoscopic distribution in the form of *d*STORM pointillistic dataset. The main aim was to identify the most appropriate approach for quantitative interrogation of elongated clusters such as those formed by GPVI when bound to fibrous collagen. All the cluster analyses investigated show that the higher-order clustering of GPVI on collagen is maintained for up to 3 h of spreading. The first characterisation of GPVI clustering on fibrillar collagen was carried out by Poulter et al. (2017) employing Ripley's K-function-based cluster analysis (Poulter et al., 2017). In our study, the same clustering method adopted by Poulter et al. (2017) allowed us to discriminate between GPVI clusters formed on collagen-rich and -poor areas. However, following our investigations, Ripley's K-function was not deemed to be the

most appropriate analysis method for these elongated clusters due to its dependence on square ROIs. Based on its statistical nature, this method is more often used for global distribution analyses to identify the presence of clusters within the localisation dataset. For example, it allowed mapping the localisation of phosphoproteins and integrin clusters at the platelet actin nodules (Poulter et al., 2015b). Ripley's K-function also enabled the identification of the presence of receptor clusters in different types of cells as has been described for CLEC-2 in platelets (Pollitt et al., 2014), TCR-CD3 in T cells (Pageon et al., 2016) and the GPCR β2-adrenergic receptor in cardiomyocytes (Scarselli et al., 2012). Additionally, Ripley's K-function has been applied as a quantitative method for the analysis of circular clusters such as those formed by the adapter LAT and the kinase Lck in T cells (Owen et al., 2010, Rossy et al., 2013, Williamson et al., 2011). User bias can be introduced by the selection of a limited number of representative areas. This drawback is bypassed by DBSCAN which takes into account the entire density map of spatial localisations within the super-resolved image. The benefits of DBSCAN as a clustering approach have been highlighted in a variety of biological systems (Endesfelder et al., 2013, Nan et al., 2013, Pageon et al., 2016), including platelets (Clark et al., 2019, Onselaer et al., 2019), since it is not sensitive to cluster size and morphology like Ripley's K-function. In our study, DBSCAN also proved to be powerful in separating different types of cluster shapes such as those induced by collagen and the other substrates investigated, providing important quantitative information on individual clusters and allowing further relative comparisons. In Chapter 3, the finding that fibrinogen induced larger GPVI clusters than Horm collagen was surprising. However, this may be attributed to a variety of factors associated with the experimental and analysis procedures such as: 1) activation-induced deposition of fibrinogen on the glass surface which may induce the receptors to coalesce into clusters; 2) underestimation of the size of collagen-induced clusters

due to the inclusion of small clusters outside the visible collagen fibres; 3) lack of correction for multiblinking artifacts; 4) cluster detection hampered by varying local density. The latter point could be addressed by the application of novel clustering methods based on topological data analysis (TDA) such as persistence based clustering and persistence homology (Pike et al., 2019). These analysis tools have been proposed to be superior over the conventional cluster algorithms since they also take into account topological information relative to nanostructures and nanoclusters unknown *a priori*. The Topological Mode Analysis Tool (ToMATo) has already been used to analyse the integrin α2β1 clustering on collagen (Pike et al., 2019), providing the same result as the two-layer DBSCAN method presented in this thesis. Therefore, it would be interesting to employ these new cluster analyses for the study of GPVI clustering induced by the heterogeneous repertoire of ligands to allow us to confirm our results and conclusions.

SR-Tessler, based on Voronoï tessellation, has been demonstrated to perform robustly in a number of biological samples and is able to overcome the drawbacks introduced by Ripley's K-function (sensitivity to cellular morphology) and DBSCAN (sensitivity to background and noise) (Levet et al., 2015). It has been applied to both *d*STORM and PALM biological datasets and allowed segmentation of cell bodies such as in neurons and fibroblasts as well as provided quantitative insights into the nanoscopic organisation of receptors (e.g. neuronal glutamate receptor) and structures (e.g. microtubules) (Andronov et al., 2016, Levet et al., 2015). In our study, SR-Tesseler allowed the successful segmentation of GPVI clusters along collagen fibres in some *d*STORM datasets but it failed in others. Where SR-Tesseler fails, the extended two-layer cluster analysis based on DBSCAN demonstrates its robustness and consistency in isolating the large and continuous GPVI clusters along visible collagen fibres and restricting the analysis of nanoclusters specifically to those regions, which was the first

aim of the study. This method, which also accounts for multiblinking artifacts, enables a more accurate quantification of GPVI nanocomplexes lined up along the fibrous structure of Horm collagen over the other clustering approaches investigated. The two-step DBSCAN-based cluster analysis, detailed for the first time in this thesis, can be applied to a variety of biological models where the investigation of cellular components or signalling receptors/mediators that coalesce in elongated macromolecular complexes is required. Future work is needed to integrate this novel clustering tool with an automatic thresholding function such as that implemented in SR-Tesseler (Monte-Carlo simulations) (Andronov et al., 2016), to allow an unbiased segmentation of the SMLM dataset of interest. Additionally, since DIC imaging only detects the big collagen fibrils, an important extension of this work would be the fluorescently labelling of Horm collagen to allow the segmentation of platelet areas corresponding to the collagen fibres and the further analysis of bound GPVI clusters. Ultimately, a significant step forward would be the development of *in vivo* models and iPSC to generate platelets (Thon et al., 2017) which express CRISPR-Cas9-tagged PALM fluorophores (Khan et al., 2017) to enable the real-time visualisation of endogenous GPVI cluster formation and extend the relative comparisons to absolute quantitative analyses. The CRISPR-Cas9 genome editing methodology would allow genetically expressing PALM fluorescent tags under the control of endogenous promoters without encountering the issues relative to plasmid transfection such as the experimental variation and the over-expression of fusion proteins. This way a direct correlation between the cellular expression of tagged GPVI and its fluorescent detection can be achieved, allowing to fully exploit the quantitative nature of SMLM (Khan et al., 2017). Dynamic analysis of GPVI clustering in platelets spread on collagen could be performed by PALM imaging and single-particle tracking using a fluorescently labelled 1G5-Fab. Such microscopy tool, in combination with actin-

depolymerizing drugs, would also provide further insights into the involvement of the actin cytoskeleton in the diffusion of GPVI clusters at the platelet surface.

6.3 GPVI clustering as a mechanism to enhance the signalling transduction

Receptor clustering has been proposed as a key mechanism to potentiate the quantitative and qualitative features of the signalling transduction and limit the signal downregulation emanated by negative regulators (Cebecauer et al., 2010). Experimental evidence has suggested that GPVI cluster formation at the plasma membrane plays a central role in regulating the signalling intensity in platelets and cell lines (Berlanga et al., 2007, Horii et al., 2009, Poulter et al., 2017). However, studies performed in human platelets activated in suspension have shown that GPVI surface expression is negatively regulated by ectodomain shedding mediated predominantly by ADAM10 (Facey et al., 2016, Gardiner et al., 2004). This gives rise to the question of whether a platelet suspension is the appropriate experimental model to mimic the signalling dynamics underlying GPVI-collagen interaction within the vasculature. Findings from this thesis demonstrate that the dynamics of GPVI signalling remarkably differ between platelets adhered to an immobile collagen substrate and those stimulated with the agonist in suspension. In the first experimental condition, GPVI signalling machinery remains active for up to 3 h of spreading in tandem with minimal shedding occurring in these platelets. On the contrary, the signalling is markedly downregulated along with up to ~70% of GPVI receptors being cleaved from the cell surface when platelets are stimulated in suspension. The results support a model (Fig. 6.1) in which GPVI clustering induced by immobilised collagen triggers the assembly of signalling complexes at the platelet surface via the engagement of downstream signalling proteins, increasing the avidity for ligand-binding and strengthening the signal. This way the sheddase ADAM10 would be excluded from tight clusters due to steric hindrance, preventing its access to the cleavage site

on individual GPVI molecules and enhancing the duration of signalling (Fig. 6.1 A). Contrarily, in platelets stimulated with collagen in suspension, the stirring forces would lead to the formation of smaller clusters and more volatile signalling complexes which are more susceptible to the negative regulation mediated by ADAM10 (Fig. 6.1 B).

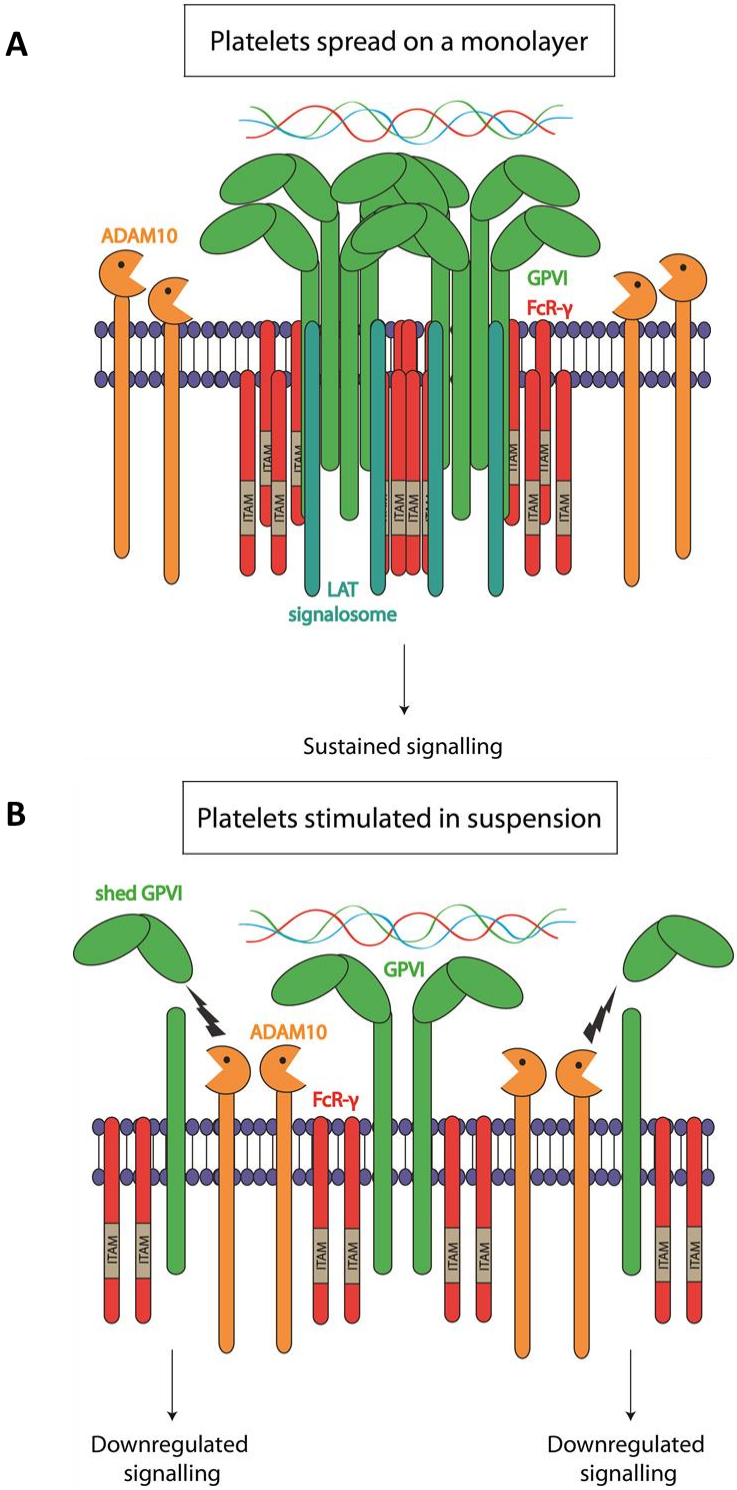

Figure 6.1. Model of GPVI signalling in platelets adhered to an immobilised collagen monolayer and stimulated with collagen in suspension. We propose that immobilised collagen initiates the signalling cascade via GPVI clustering and organisation of signalling complexes which hinder the GPVI cleavage-site for ADAM10, allowing sustained signalling (A). Contrarily, stimulation of platelets with collagen in suspension triggers GPVI downregulation through the formation of unstable clusters and signalling systems and activation of ADAM10-dependent ectodomain shedding (B).

In addition to protection from ADAM10 activity, stable signalling complexes may also be insensitive to phosphatase-mediated downregulation such as that exerted by TULA-2, which has been shown to target Syk in platelet suspensions stimulated with CVX (Thomas et al., 2010). Therefore, an interesting topic for future investigation would be mapping the location of TULA-2 relative to GPVI at the platelet surface. A similar signalling mode has already been described in T cells where the TCR coalesces in large clusters at the cell surface which traps signalling proteins such as LAT and Lck (Douglass and Vale, 2005) and marginalises phosphatases such as CD45 (Furlan et al., 2014) and CD148 (Lin and Weiss, 2003). The employment of super-resolution microscopy in combination with newly-discovered DNA-based approaches such as DNA-PAINT for the simultaneous labelling of multiple targets and qPAINT to extract numerical information (Jungmann et al., 2016, Jungmann et al., 2014), will enable the construction of a qualitative and quantitative map of GPVI receptor, signalling mediators and negative regulators at the platelet PM. However, these techniques require a long and laborious optimisation process which did not fit with the duration of my PhD.

The sustained GPVI signalling observed in platelets adhered to a static collagen monolayer is corroborated by studies performed under flow conditions (Mazzucato et al., 2009, Pugh et al., 2017), which would be the ideal experimental model to mimic the vasculature system *in vivo*. Notably, a significant difference between platelets stimulated in suspension and spread on a monolayer is the shear stress. The shear forces present in platelet suspensions may prevent the formation of robust and longer-lasting clusters and induce shedding. Indeed, a compelling study using an ADAM10-specific substrate, which becomes fluorescent when cleaved, has shown that shear stress and NEM are the only stimuli able to induce shedding increasing ADAM10 activity, representing stronger triggers than GPVI agonists (Facey et al., 2016).

Therefore, extending our study to a flow model of haemostasis will be fundamental to verify the advanced hypotheses and confirm our conclusions.

The importance of GPVI-collagen interaction in spreading and aggregation has been reported in a variety of studies performed in GPVI-deficient patients (Arai et al., 1995, Boylan et al., 2004, Dumont et al., 2009, Matus et al., 2013, Sugiyama et al., 1987, Takahashi and Moroi, 2001) and mouse models (Kato et al., 2003, Lockyer et al., 2006, Nieswandt et al., 2000, Nieswandt et al., 2001a, Nieswandt et al., 2001b). In our study, the relevance of GPVI shedding in limiting platelet activation in response to collagen is highlighted by the effect of NEM. NEM triggers ~100% of GPVI shedding from the platelet surface which remarkably impaired platelet spreading on collagen. Therefore, the main conclusion of this work is that the negligible level of GPVI shedding and the sustained clustering and signalling induced by immobilised collagen function to maintain integrin-dependent platelet adhesion and spreading on collagen. Current anti-thrombotic strategies targeting GPVI aim to interfere with the receptor-collagen interaction via fusion proteins or anti-GPVI monoclonal antibodies and these have had positive functional outcomes in clinical trials and animal models (Goebel et al., 2013, Lebozec et al., 2017, Li et al., 2007, Massberg et al., 2004, Ohlmann et al., 2008). The development of novel agents targeting collagen-induced GPVI clustering combined with *in vivo* and *ex vivo* studies will be pivotal in determining whether this mechanism has (patho)physiological relevance to prevent bleeding and maintain vascular integrity during inflammation (Boulaftali et al., 2018). This would also be of pharmacological interest in the treatment of atherosclerotic plaque rupture-driven thrombus formation where GPVI-collagen interaction plays a key role (Kuijpers et al., 2009, Penz et al., 2005). Losartan, an angiotensin II receptor antagonist, has been proposed to inhibit platelet responses to collagen via the blockade of GPVI clustering *in vitro* using a Duolink imaging technique. However, Losartan

did not inhibit platelet activation *ex vivo*, ruling out its potential as an antiplatelet agent (Jiang et al., 2015). Indeed, whilst Onselaer et al. (2019) confirmed the inhibitory effect of Losartan and that of another compound, Honokiol, on collagen-induced platelet aggregation, they did not find any impairment of GPVI clustering by super-resolution microscopy, which is undoubtedly more reliable than the Duolink methodology (Onselaer et al., 2019). To our knowledge, chemical agents able to block collagen-induced GPVI clustering have not been developed yet, due to the lack of crystallography and cryo-electron microscopy studies of GPVI in combination with the agonist.

The finding that fibrinogen and fibrin are also able to cluster GPVI highlights the importance of receptor oligomerisation in the later stages of platelet aggregation and thrombus growth and stabilisation, where these ligands have been shown to play a critical role (Alshehri et al., 2015a, Induruwa et al., 2018, Mammadova-Bach et al., 2015, Mangin et al., 2018, Onselaer et al., 2017). Fibrin, but not fibrinogen, also induces GPVI shedding in platelet suspensions (Montague et al., 2018b); whether these two ligands can trigger the receptor cleavage under static conditions remains to be investigated. The fibrin-induced GPVI shedding has been used as a marker of platelet activation in inflammatory settings characterised by unregulated fibrin formation such as thermal injury, sepsis and inflammatory bowel disease (IBD) (Montague et al., 2018b). Furthermore, the binding sites between GPVI and fibrin(ogen) have been mapped to a different location to that for collagen (Induruwa et al., 2018, Onselaer et al., 2017). Therefore, specifically targeting GPVI clustering triggered by fibrinogen and fibrin could have therapeutical applications in inflammatory conditions characterised by minimal activation by collagen.

6.4 How does GPVI cluster at the platelet surface?

Whether GPVI is pre-clustered in resting platelets remains to be established. Previous attempts from members of the Watson laboratory (University of Birmingham, UK) using polylysine-coated coverslips and fixed platelets in solution have been made to answer this question. However, the comparison between resting platelets characterised by a 3D geometry and spread platelets with a 2D conformation resulted to be technically difficult and therefore the project was not pursued further. As discussed by Jung et al. (2012), the early formation of GPVI dimers in resting platelets may serve to prime GPVI for activation when the subendothelial collagens, which are located in the interstitial layers of the vessel wall, will be exposed upon vascular injury. Platelet activation will then increase the dimer formation as it has been shown in thrombin and CRP-XL-stimulated platelets (Jung et al., 2012) and induce further clustering to ensure sustained signalling and stable adhesion of platelets to collagen. In this context, integrin α2β1 synergizes with GPVI in supporting firm adhesion to collagen (Auger et al., 2005, Lecut et al., 2004, Mazzucato et al., 2009, Pugh et al., 2017) but it does not contribute to GPVI cluster formation as our findings and those reported by (Poulter et al., 2017) show that GPVI clusters on collagen and CRP-XL to the same extent. However, as *d*STORM uses fixed material it does not give any information on the dynamics of the clustering. Therefore, we can not rule out the possibility that the integrin may aid faster formation of the clusters and this is something that could be verified in future experiments using single-particle tracking.

The work from this thesis also establishes a negligible role of second messengers, signalling kinases and actin cytoskeletal dynamics in maintaining GPVI clustering on collagen. However, the cytoskeleton may play a crucial role in facilitating GPVI dimer formation and further clustering before full platelet spreading on collagen (Poulter et al., 2017). Therefore, it

appears clear that further research is required to investigate the driving forces behind this process. GPVI has been localised in membrane lipid rafts at the platelet surface, although it is not clear whether it is constitutively associated with these microdomains or if it translocates upon activation (Ezumi et al., 2002, Locke et al., 2002, Wonerow et al., 2002). A recent proteomic study proposed that platelet activation through GPVI or CLEC-2 induces a change in the lipid rafts as well as cytoskeleton proteins composition, suggesting a cooperative role (Izquierdo et al., 2019). Such concerted regulation may drive GPVI clustering at the platelet surface. Super-resolution microscopy and the design of specific probes to directly image lipid rafts components will be vital to establish their role in GPVI clustering and signalling in platelets.

GPVI is also organised into tetraspanins microdomains within the platelet PM which may represent key players in modulating its lateral mobility and oligomerisation, as has been reported for Tspan9 whose deficiency in a mouse model impaired GPVI lateral diffusion within the membrane (Haining et al., 2017b). This study proposed a role for Tspan9 in the 'fine-tuning' of GPVI signalling. The development of further Tspan knockout mice will be pivotal in identifying additional tetraspanins involved in the regulation of GPVI clustering and signalling at the platelet surface.

Of considerable interest in this thesis is the finding that, contrarily to GPVI, integrin α2β1 clustering is found to be dependent on Syk kinase activity. This has been attributed to the effect of the kinase inhibitor on the actin cytoskeleton disruption which would block the integrin in the inactive state (Zhu et al., 2008). Integrin α2β1 is linked to F-actin through the adapter protein talin (Horton et al., 2015) which is fundamental in mediating platelet adhesion under flow (Petrich et al., 2007). Therefore, the investigation of the effect of Syk inhibition on

the binding of α2β1 to talin or other cytoskeletal adaptors such as kindlin and vinculin will be crucial to verify our hypothesis.

6.5 Anti-GPVI nanobodies as promising tools for the study of platelet biology

The work discussed at the end of this thesis presents the first generation and validation of nanobodies targeting human platelet GPVI. The project revealed to be challenging due to the large repertoire of nanobody genes provided by the VIB Nanobody Core (Brussel, Belgium) and the wide range of paratopes generated, resulting in different final yields and modes of action in *in vitro* assays. However, the characterisation of the three candidate nanobodies for imaging applications generated fascinating and unexpected data. Two of them (#21 and #27) appears to be anti-GPVI blocking nanobodies since they interact with the same binding domain of collagen and induce the proteolytic cleavage of GPVI from the platelet surface. These findings correlate with the block of collagen-induced platelet aggregation detected upon nanobody stimulation. Such mechanisms are not novel and have already been proposed for canonical antibodies. For example, the monoclonal antibody JAQ1 targeting the major collagen-binding site of mouse GPVI has been shown to immunodeplete GPVI from circulating platelets *in vivo* and completely block platelet responses to collagen and CRP-XL *ex vivo*, generating a long-term antithrombotic effect (Nieswandt et al., 2001b). Further antibodies against different epitopes of mouse GPVI (JAQ2 and JAQ3) were then developed and showed the same properties of JAQ1 (Schulte et al., 2003). However, the inhibitory effects were negligible in *in vitro* systems, suggesting the presence of additional stimuli *in vivo* (Nieswandt et al., 2001b, Schulte et al., 2003, Schulte et al., 2001). A similar phenomenon has been found in patients affected by immune thrombocytopenia who develop autoantibodies against GPVI (Boylan et al., 2004, Sugiyama et al., 1987, Takahashi and

Moroi, 2001). In all these studies, the mechanisms underlying GPVI clearing from the platelet surface have not been investigated. As suggested by our findings, it can be a combination of receptor shedding and receptor endocytosis. Although the data from this thesis represent only the starting point of a long-term project, they propose these two nanobodies as potential candidates in anti-thrombotic approaches whose inhibitory effect would need to be confirmed in flow assays, *in vivo* and *ex vivo* studies and in experimental thrombosis models before potentially introducing them into clinical trials.

Due to the different performance in the *in vitro* assays, the last nanobody (#14) was exploited as an imaging tool and therefore genetically fused with the SNAP-tag to allow a site-specific and quantitative nanobody labelling (Cole, 2013). The SNAP-tag was chosen for its easy self-labelling by commercial *in vitro* kits but, on the other hand, its large size and high reactivity represent a disadvantage for super-resolution imaging. Indeed, the labelling procedure appears to be unsuccessful due to the lower signal-to-background ratio compared with the 1G5-Fab and the unspecific binding to the collagen outside the boundary of the platelets. Alternative small peptide-tags genetically fused to nanobodies have shown to allow the quantitative and site-specific labelling via a Sortase A system, resulting in high-quality *d*STORM imaging (Virant et al., 2018). Another successful method, involving the labelling of nanobodies with maleimides at engineered cysteines, has been demonstrated to be site-specific, does not perturb the epitope recognition and displaces the label from the target by only ~1-2 nm (Pleiner et al., 2015). These are just a few solutions that could be considered to render the nanobody into a powerful tool for the qualitative and quantitative investigation of platelet GPVI receptor by super-resolution microscopy.

6.6 Concluding remarks

Findings from this thesis provide novel insights into the signalling mechanisms initiate by the GPVI-collagen interaction in human platelets. GPVI clustering helps to potentiate the signalling and prevent negative regulation mediated by the sheddase ADAM10 to maintain platelet activation and adhesion to collagen. Due to the restricted role of GPVI in haemostasis, the selective inhibition of the receptor clustering induced by collagen, fibrinogen and fibrin provides an interesting target for the development of novel therapeutic approaches to improve the functional outcomes of a variety of thrombotic and inflammatory conditions and reduce the bleeding risk associated with the current antiplatelet drugs.

References

ABBE, E. 1873. Beiträge zur Theorie des Mikroskops und der mikroskopischen Wahrnehmung. *Archiv für mikroskopische Anatomie,* 9**,** 413-418.

AGBANI, E. O. & POOLE, A. W. 2017. Procoagulant platelets: generation, function, and therapeutic targeting in thrombosis. *Blood,* 130**,** 2171-2179.

AKBAR, H., SHANG, X., PERVEEN, R., BERRYMAN, M., FUNK, K., JOHNSON, J. F., TANDON, N. N. & ZHENG, Y. 2011. Gene targeting implicates Cdc42 GTPase in GPVI and non-GPVI mediated platelet filopodia formation, secretion and aggregation. *PloS one,* 6**,** e22117.

AL-TAMIMI, M., GARDINER, E. E., THOM, J. Y., SHEN, Y., COOPER, M. N., HANKEY, G. J., BERNDT, M. C., BAKER, R. I. & ANDREWS, R. K. 2011a. Soluble glycoprotein VI is raised in the plasma of patients with acute ischemic stroke. *Stroke,* 42**,** 498-500.

AL-TAMIMI, M., GRIGORIADIS, G., TRAN, H., PAUL, E., SERVADEI, P., BERNDT, M. C., GARDINER, E. E. & ANDREWS, R. K. 2011b. Coagulation-induced shedding of platelet glycoprotein VI mediated by factor Xa. *Blood,* 117**,** 3912-3920.

AL-TAMIMI, M., MU, F. T., ARTHUR, J. F., SHEN, Y., MOROI, M., BERNDT, M. C., ANDREWS, R. K. & GARDINER, E. E. 2009. Anti-glycoprotein VI monoclonal antibodies directly aggregate platelets independently of FcgammaRIIa and induce GPVI ectodomain shedding. *Platelets,* 20**,** 75-82.

AL-TAMIMI, M., TAN, C. W., QIAO, J., PENNINGS, G. J., JAVADZADEGAN, A., YONG, A. S., ARTHUR, J. F., DAVIS, A. K., JING, J., MU, F. T., HAMILTON, J. R., JACKSON, S. P., LUDWIG, A., BERNDT, M. C., WARD, C. M., KRITHARIDES, L., ANDREWS, R. K. & GARDINER, E. E. 2012. Pathologic shear triggers shedding of vascular receptors: a novel mechanism for down-regulation of platelet glycoprotein VI in stenosed coronary vessels. *Blood,* 119**,** 4311-20.

ALLEN, J. R., ROSS, S. T. & DAVIDSON, M. W. 2013. Single molecule localization microscopy for superresolution. *Journal of Optics,* 15**,** 094001.

ALSHEHRI, O. M., HUGHES, C. E., MONTAGUE, S., WATSON, S. K., FRAMPTON, J., BENDER, M. & WATSON, S. P. 2015a. Fibrin activates GPVI in human and mouse platelets. *Blood,* 126**,** 1601-8.

ALSHEHRI, O. M., MONTAGUE, S., WATSON, S., CARTER, P., SARKER, N., MANNE, B. K., MILLER, J. L., HERR, A. B., POLLITT, A. Y., O'CALLAGHAN, C. A., KUNAPULI, S., ARMAN, M., HUGHES, C. E. & WATSON, S. P. 2015b. Activation of glycoprotein VI (GPVI) and C-type lectin-like receptor-2 (CLEC-2) underlies platelet activation by diesel exhaust particles and other charged/hydrophobic ligands. *Biochem J,* 468**,** 459-73.

ANDERS, A., GILBERT, S., GARTEN, W., POSTINA, R. & FAHRENHOLZ, F. 2001. Regulation of the alpha-secretase ADAM10 by its prodomain and proprotein convertases. *Faseb j,* 15**,** 1837-9.

ANDREWS, R. K., GARDINER, E. E., ASAZUMA, N., BERLANGA, O., TULASNE, D., NIESWANDT, B., SMITH, A. I., BERNDT, M. C. & WATSON, S. P. 2001. A novel viper venom metalloproteinase, alborhagin, is an agonist at the platelet collagen receptor GPVI. *J Biol Chem,* 276**,** 28092-7.

ANDREWS, R. K., KARUNAKARAN, D., GARDINER, E. E. & BERNDT, M. C. 2007. Platelet receptor proteolysis: a mechanism for downregulating platelet reactivity. *Arterioscler Thromb Vasc Biol,* 27**,** 1511-20.

ANDREWS, R. K., SUZUKI-INOUE, K., SHEN, Y., TULASNE, D., WATSON, S. P. & BERNDT, M. C. 2002. Interaction of calmodulin with the cytoplasmic domain of platelet glycoprotein VI. *Blood,* 99**,** 4219-21.

ANDRONOV, L., MICHALON, J., OUARARHNI, K., ORLOV, I., HAMICHE, A., VONESCH, J. L. & KLAHOLZ, B. P. 2018. 3DClusterViSu: 3D clustering analysis of super-resolution microscopy data by 3D Voronoi tessellations. *Bioinformatics,* 34**,** 3004-3012.

ANDRONOV, L., ORLOV, I., LUTZ, Y., VONESCH, J.-L. & KLAHOLZ, B. P. 2016. ClusterViSu, a method for clustering of protein complexes by Voronoi tessellation in super-resolution microscopy. *Scientific reports,* 6**,** 24084.

ANNIBALE, P., VANNI, S., SCARSELLI, M., ROTHLISBERGER, U. & RADENOVIC, A. 2011. Identification of clustering artifacts in photoactivated localization microscopy. *Nature methods,* 8**,** 527.

ARAI, M., YAMAMOTO, N., MOROI, M., AKAMATSU, N., FUKUTAKE, K. & TANOUE, K. 1995. Platelets with 10% of the normal amount of glycoprotein VI have an impaired response to collagen that results in a mild bleeding tendency. *British journal of haematology,* 89**,** 124-130.

ARMAN, M. & KRAUEL, K. 2015. Human platelet IgG Fc receptor FcgammaRIIA in immunity and thrombosis. *J Thromb Haemost,* 13**,** 893-908.

ARMAN, M., KRAUEL, K., TILLEY, D. O., WEBER, C., COX, D., GREINACHER, A., KERRIGAN, S. W. & WATSON, S. P. 2014. Amplification of bacteria-induced platelet activation is triggered by FcγRIIA, integrin αIIbβ3, and platelet factor 4. *Blood,* 123**,** 3166-3174.

ARTHUR, J. F., GARDINER, E. E., MATZARIS, M., TAYLOR, S. G., WIJEYEWICKREMA, L., OZAKI, Y., KAHN, M. L., ANDREWS, R. K. & BERNDT, M. C. 2005. Glycoprotein VI is associated with GPIb-IX-V on the membrane of resting and activated platelets. *Thromb Haemost,* 93**,** 716-23.

ARTHUR, J. F., SHEN, Y., KAHN, M. L., BERNDT, M. C., ANDREWS, R. K. & GARDINER, E. E. 2007. Ligand binding rapidly induces disulfide-dependent dimerization of glycoprotein VI on the platelet plasma membrane. *Journal of Biological Chemistry,* 282**,** 30434-30441.

ARYA, M., LOPEZ, J. A., ROMO, G. M., CRUZ, M. A., KASIRER-FRIEDE, A., SHATTIL, S. J. & ANVARI, B. 2003. Glycoprotein Ib-IX-mediated activation of integrin alpha(IIb)beta(3): effects of receptor clustering and von Willebrand factor adhesion. *J Thromb Haemost,* 1**,** 1150-7.

ASAI, J., HIRAKAWA, S., SAKABE, J., KISHIDA, T., WADA, M., NAKAMURA, N., TAKENAKA, H., MAZDA, O., URANO, T., SUZUKI-INOUE, K., TOKURA, Y. & KATOH, N. 2016. Platelets Regulate the Migration of Keratinocytes via Podoplanin/CLEC-2 Signaling during Cutaneous Wound Healing in Mice. *Am J Pathol,* 186**,** 101-8.

ASAZUMA, N., WILDE, J. I., BERLANGA, O., LEDUC, M., LEO, A., SCHWEIGHOFFER, E., TYBULEWICZ, V., BON, C., LIU, S. K. & MCGLADE, C. J. 2000. Interaction of linker for activation of T cells with multiple adapter proteins in platelets activated by the glycoprotein VI-selective ligand, convulxin. *Journal of Biological Chemistry,* 275**,** 33427-33434.

ASLAN, J. E., ITAKURA, A., HALEY, K. M., TORMOEN, G. W., LOREN, C. P., BAKER, S. M., PANG, J., CHERNOFF, J. & MCCARTY, O. J. 2013. P21 activated kinase signaling coordinates glycoprotein receptor VI–mediated platelet aggregation, lamellipodia formation, and aggregate stability under shear. *Arteriosclerosis, thrombosis, and vascular biology,* 33**,** 1544-1551.

ASLAN, J. E. & MCCARTY, O. J. 2013. Rho GTPases in platelet function. *Journal of Thrombosis and Haemostasis,* 11**,** 35-46.

ASSELIN, J., GIBBINS, J. M., ACHISON, M., LEE, Y. H., MORTON, L. F., FARNDALE, R. W., BARNES, M. J. & WATSON, S. P. 1997. A collagen-like peptide stimulates tyrosine phosphorylation of syk and phospholipase C gamma2 in platelets independent of the integrin alpha2beta1. *Blood,* 89**,** 1235-42.

ASSELIN, J., KNIGHT, C. G., FARNDALE, R. W., BARNES, M. J. & WATSON, S. P. 1999. Monomeric (glycine-proline-hydroxyproline)10 repeat sequence is a partial agonist of the platelet collagen receptor glycoprotein VI. *Biochem J,* 339 (Pt 2)**,** 413-8.

ATKINSON, B. T., ELLMEIER, W. & WATSON, S. P. 2003. Tec regulates platelet activation by GPVI in the absence of Btk. *Blood,* 102**,** 3592-3599.

ATKINSON, B. T., STAFFORD, M. J., PEARS, C. J. & WATSON, S. P. 2001. Signalling events underlying platelet aggregation induced by the glycoprotein VI agonist convulxin. *European journal of biochemistry,* 268**,** 5242-5248.

AUGER, J. M., KUIJPERS, M. J., SENIS, Y. A., WATSON, S. P. & HEEMSKERK, J. W. 2005. Adhesion of human and mouse platelets to collagen under shear: a unifying model. *The FASEB journal,* 19**,** 825-827.

BADDELEY, A. J., MØLLER, J. & WAAGEPETERSEN, R. 2000. Non-and semi-parametric estimation of interaction in inhomogeneous point patterns. *Statistica Neerlandica,* 54**,** 329-350.

BADOLIA, R., KOSTYAK, J. C., DANGELMAIER, C. & KUNAPULI, S. P. 2017. Syk Activity Is Dispensable for Platelet GP1b-IX-V Signaling. *Int J Mol Sci,* 18.

BALAGOPALAN, L., COUSSENS, N. P., SHERMAN, E., SAMELSON, L. E. & SOMMERS, C. L. 2010. The LAT story: a tale of cooperativity, coordination, and choreography. *Cold Spring Harbor perspectives in biology,* 2**,** a005512.

BATES, M., HUANG, B., DEMPSEY, G. T. & ZHUANG, X. 2007. Multicolor super-resolution imaging with photo-switchable fluorescent probes. *Science,* 317**,** 1749-53.

BEARER, E. L., PRAKASH, J. M. & LI, Z. 2002. Actin dynamics in platelets. *Int Rev Cytol,* 217**,** 137-82.

BECKERLE, M. C., MILLER, D. E., BERTAGNOLLI, M. E. & LOCKE, S. J. 1989. Activation-dependent redistribution of the adhesion plaque protein, talin, in intact human platelets. *The Journal of cell biology,* 109**,** 3333-3346.

BEGHEIN, E. & GETTEMANS, J. 2017. Nanobody Technology: A Versatile Toolkit for Microscopic Imaging, Protein-Protein Interaction Analysis, and Protein Function Exploration. *Front Immunol,* 8**,** 771.

BEHNKE, O. 1967. Electron microscopic observations on the membrane systems of the rat blood platelet. *The Anatomical Record,* 158**,** 121-137.

BENDER, M., HAGEDORN, I. & NIESWANDT, B. 2011. Genetic and antibody-induced glycoprotein VI deficiency equally protects mice from mechanically and FeCl3-induced thrombosis. *Journal of Thrombosis and Haemostasis,* 9**,** 1423-1426.

BENDER, M., HOFMANN, S., STEGNER, D., CHALARIS, A., BÖSL, M., BRAUN, A., SCHELLER, J., ROSE-JOHN, S. & NIESWANDT, B. 2010. Differentially regulated GPVI ectodomain shedding by multiple platelet–expressed proteinases. *Blood,* 116**,** 3347-3355.

BENDER, M., MAY, F., LORENZ, V., THIELMANN, I., HAGEDORN, I., FINNEY, B. A., VÖGTLE, T., REMER, K., BRAUN, A. & BÖSL, M. 2013. Combined in vivo depletion of glycoprotein VI and C-type lectin-like receptor 2 severely compromises hemostasis and abrogates arterial thrombosis in mice. *Arteriosclerosis, thrombosis, and vascular biology,* 33**,** 926-934.

BÉNÉZECH, C., NAYAR, S., FINNEY, B. A., WITHERS, D. R., LOWE, K., DESANTI, G. E., MARRIOTT, C. L., WATSON, S. P., CAAMAÑO, J. H. & BUCKLEY, C. D. 2014. CLEC-2 is required for development and maintenance of lymph nodes. *Blood,* 123**,** 3200-3207.

BENNETT, J. S. 2005. Structure and function of the platelet integrin α IIb β 3. *The Journal of clinical investigation,* 115**,** 3363-3369.

BERGMEIER, W., RABIE, T., STREHL, A., PIFFATH, C. L., PROSTREDNA, M., WAGNER, D. D. & NIESWANDT, B. 2004. GPVI down-regulation in murine platelets through metalloproteinase-dependent shedding. *Thrombosis and haemostasis,* 91**,** 951-958.

BERLANGA, O., BOBE, R., BECKER, M., MURPHY, G., LEDUC, M., BON, C., BARRY, F. A., GIBBINS, J. M., GARCIA, P., FRAMPTON, J. & WATSON, S. P. 2000. Expression of the collagen receptor glycoprotein VI during megakaryocyte differentiation. *Blood,* 96**,** 2740-5.

BERLANGA, O., BORI-SANZ, T., JAMES, J. R., FRAMPTON, J., DAVIS, S. J., TOMLINSON, M. G. & WATSON, S. P. 2007. Glycoprotein VI oligomerization in cell lines and platelets. *Journal of Thrombosis and Haemostasis,* 5**,** 1026-1033.

BERLANGA, O., TULASNE, D., BORI, T., SNELL, D. C., MIURA, Y., JUNG, S., MOROI, M., FRAMPTON, J. & WATSON, S. P. 2002. The Fc receptor γ-chain is necessary and sufficient to initiate signalling through glycoprotein VI in transfected cells by the snake C-type lectin, convulxin. *European journal of biochemistry,* 269**,** 2951-2960.

BERTHOLD, M. R., CEBRON, N., DILL, F., GABRIEL, T. R., KÖTTER, T., MEINL, T., OHL, P., THIEL, K. & WISWEDEL, B. 2009. KNIME-the Konstanz information miner: version 2.0 and beyond. *AcM SIGKDD explorations Newsletter,* 11**,** 26-31.

BERTOZZI, C. C., HESS, P. R. & KAHN, M. L. 2010. Platelets: covert regulators of lymphatic development. *Arteriosclerosis, thrombosis, and vascular biology,* 30**,** 2368-2371.

BETHANI, I., SKANLAND, S. S., DIKIC, I. & ACKER-PALMER, A. 2010. Spatial organization of transmembrane receptor signalling. *Embo j,* 29**,** 2677-88.

BETZIG, E., PATTERSON, G. H., SOUGRAT, R., LINDWASSER, O. W., OLENYCH, S., BONIFACINO, J. S., DAVIDSON, M. W., LIPPINCOTT-SCHWARTZ, J. & HESS, H. F. 2006. Imaging intracellular fluorescent proteins at nanometer resolution. *Science,* 313**,** 1642-1645.

BIGALKE, B., STELLOS, K., GEISLER, T., LINDEMANN, S., MAY, A. E. & GAWAZ, M. 2010. Glycoprotein VI as a prognostic biomarker for cardiovascular death in patients with symptomatic coronary artery disease. *Clinical research in cardiology,* 99**,** 227-233.

BIZZOZERO, G. 1882. Ueber einen neuen Formbestandtheil des Blutes und dessen Rolle bei der Thrombose und der Blutgerinnung. *Archiv für pathologische Anatomie und Physiologie und für klinische Medicin, 90, 261-332*.

BODIN, S., TRONCHÈRE, H. & PAYRASTRE, B. 2003. Lipid rafts are critical membrane domains in blood platelet activation processes. *Biochimica et Biophysica Acta (BBA)-Biomembranes,* 1610**,** 247-257.

BOESZE-BATTAGLIA, K., CLAYTON, S. T. & SCHIMMEL, R. J. 1996. Cholesterol redistribution within human platelet plasma membrane: evidence for a stimulus-dependent event. *Biochemistry,* 35**,** 6664-6673.

BOILARD, E., NIGROVIC, P. A., LARABEE, K., WATTS, G. F., COBLYN, J. S., WEINBLATT, M. E., MASSAROTTI, E. M., REMOLD-O'DONNELL, E., FARNDALE, R. W. & WARE, J. 2010. Platelets amplify inflammation in arthritis via collagen-dependent microparticle production. *Science,* 327**,** 580-583.

BOILARD, E., PARE, G., ROUSSEAU, M., CLOUTIER, N., DUBUC, I., LEVESQUE, T., BORGEAT, P. & FLAMAND, L. 2014. Influenza virus H1N1 activates platelets through FcgammaRIIA signaling and thrombin generation. *Blood,* 123**,** 2854-63.

BORGES, I., SENA, I., AZEVEDO, P., ANDREOTTI, J., ALMEIDA, V., PAIVA, A., SANTOS, G., GUERRA, D., PRAZERES, P., MESQUITA, L. L., SILVA, L. S. B., LEONEL, C., MINTZ, A. & BIRBRAIR, A. 2017. Lung as a Niche for Hematopoietic Progenitors. *Stem Cell Rev,* 13**,** 567-574.

BOULAFTALI, Y., HESS, P. R., GETZ, T. M., CHOLKA, A., STOLLA, M., MACKMAN, N., OWENS, A. P., 3RD, WARE, J., KAHN, M. L. & BERGMEIER, W. 2013. Platelet ITAM signaling is critical for vascular integrity in inflammation. *J Clin Invest,* 123**,** 908-16.

BOULAFTALI, Y., MAWHIN, M. A., JANDROT-PERRUS, M. & HO-TIN-NOÉ, B. 2018. Glycoprotein VI in securing vascular integrity in inflamed vessels. *Research and practice in thrombosis and haemostasis,* 2**,** 228-239.

BOYLAN, B., BERNDT, M. C., KAHN, M. L. & NEWMAN, P. J. 2006. Activation-independent, antibody-mediated removal of GPVI from circulating human platelets: development of a novel NOD/SCID mouse model to evaluate the in vivo effectiveness of anti–human platelet agents. *Blood,* 108**,** 908-914.

BOYLAN, B., CHEN, H., RATHORE, V., PADDOCK, C., SALACZ, M., FRIEDMAN, K. D., CURTIS, B. R., STAPLETON, M., NEWMAN, D. K. & KAHN, M. L. 2004. Anti-GPVI–associated ITP: an acquired platelet disorder caused by autoantibody-mediated clearance of the GPVI/FcRγ-chain complex from the human platelet surface. *Blood,* 104**,** 1350-1355.

BOYLAN, B., GAO, C., RATHORE, V., GILL, J. C., NEWMAN, D. K. & NEWMAN, P. J. 2008. Identification of FcgammaRIIa as the ITAM-bearing receptor mediating alphaIIbbeta3 outside-in integrin signaling in human platelets. *Blood,* 112**,** 2780-6.

BOYLES, J., FOX, J., PHILLIPS, D. R. & STENBERG, P. E. 1985. Organization of the cytoskeleton in resting, discoid platelets: preservation of actin filaments by a modified fixation that prevents osmium damage. *The Journal of cell biology,* 101**,** 1463-1472.

BRASS, L. 1984. Ca2+ homeostasis in unstimulated platelets. *Journal of Biological Chemistry,* 259**,** 12563-12570.

BRIDDELL, R. A., BRANDT, J. E., STRANEVA, J. E., SROUR, E. F. & HOFFMAN, R. 1989. Characterization of the human burst-forming unit-megakaryocyte. *Blood,* 74**,** 145-151.

BURGER, P. C. & WAGNER, D. D. 2003. Platelet P-selectin facilitates atherosclerotic lesion development. *Blood,* 101**,** 2661-6.

BURKHART, J. M., VAUDEL, M., GAMBARYAN, S., RADAU, S., WALTER, U., MARTENS, L., GEIGER, J., SICKMANN, A. & ZAHEDI, R. P. 2012. The first comprehensive and quantitative analysis of human platelet protein composition allows the comparative analysis of structural and functional pathways. *Blood,* 120**,** e73-82.

BUSYGINA, K., JAMASBI, J., SEILER, T., DECKMYN, H., WEBER, C., BRANDL, R., LORENZ, R. & SIESS, W. 2018. Oral Bruton tyrosine kinase inhibitors selectively block atherosclerotic plaque–triggered thrombus formation in humans. *blood,* 131**,** 2605-2616.

BYE, A. P., UNSWORTH, A. J. & GIBBINS, J. M. 2016. Platelet signaling: a complex interplay between inhibitory and activatory networks. *J Thromb Haemost,* 14**,** 918-30.

BYNAGARI-SETTIPALLI, Y. S., CORNELISSEN, I., PALMER, D., DUONG, D., CONCENGCO, C., WARE, J. & COUGHLIN, S. R. 2014. Redundancy and interaction of thrombin-and collagen-mediated platelet activation in tail bleeding and carotid thrombosis in mice. *Arteriosclerosis, thrombosis, and vascular biology,* 34**,** 2563-2569.

CALAMINUS, S. D., THOMAS, S., MCCARTY, O., MACHESKY, L. & WATSON, S. 2008. Identification of a novel, actin-rich structure, the actin nodule, in the early stages of platelet spreading. *Journal of Thrombosis and Haemostasis,* 6**,** 1944-1952.

CAREY, F., MENASHI, S. & CRAWFORD, N. 1982. Localization of cyclo-oxygenase and thromboxane synthetase in human platelet intracellular membranes. *Biochemical Journal,* 204**,** 847-851.

CASELLA, J. F., FLANAGAN, M. D. & LIN, S. 1981. Cytochalasin D inhibits actin polymerization and induces depolymerization of actin filaments formed during platelet shape change. *Nature,* 293**,** 302.

CEBECAUER, M., SPITALER, M., SERGE, A. & MAGEE, A. I. 2010. Signalling complexes and clusters: functional advantages and methodological hurdles. *J Cell Sci,* 123**,** 309-20.

CHACKO, G. W., DUCHEMIN, A.-M., COGGESHALL, K. M., OSBORNE, J. M., BRANDT, J. T. & ANDERSON, C. L. 1994. Clustering of the platelet Fc gamma receptor induces noncovalent association with the tyrosine kinase p72syk. *Journal of Biological Chemistry,* 269**,** 32435-32440.

CHARRIN, S., JOUANNET, S., BOUCHEIX, C. & RUBINSTEIN, E. 2014. Tetraspanins at a glance. *J Cell Sci,* 127**,** 3641-3648.

CHELI, Y., JENSEN, D., MARCHESE, P., HABART, D., WILTSHIRE, T., COOKE, M., FERNANDEZ, J. A., WARE, J., RUGGERI, Z. M. & KUNICKI, T. J. 2008. The Modifier of hemostasis (Mh) locus on chromosome 4 controls in vivo hemostasis of Gp6−/− mice. *Blood,* 111**,** 1266-1273.

CHEN, H., LOCKE, D., LIU, Y., LIU, C. & KAHN, M. L. 2002. The platelet receptor GPVI mediates both adhesion and signaling responses to collagen in a receptor density-dependent fashion. *Journal of Biological Chemistry,* 277**,** 3011-3019.

CHEN, Y., RUGGERI, Z. M. & DU, X. 2018. 14-3-3 proteins in platelet biology and glycoprotein Ib-IX signaling. *Blood,* 131**,** 2436-2448.

CHUNG, I. & LIP, G. Y. H. 2006. Platelets and heart failure. *European Heart Journal,* 27**,** 2623-2631.

CLARK, J. C., KAVANAGH, D. M., WATSON, S., PIKE, J. A., ANDREWS, R. K., GARDINER, E. E., POULTER, N. S., HILL, S. J. & WATSON, S. P. 2019. Adenosine and Forskolin Inhibit Platelet Aggregation by Collagen but not the Proximal Signalling Events. *Thromb Haemost,* 119**,** 1124-1137.

CLAUSHUIS, T. A. M., DE VOS, A. F., NIESWANDT, B., BOON, L., ROELOFS, J., DE BOER, O. J., VAN 'T VEER, C. & VAN DER POLL, T. 2018. Platelet glycoprotein VI aids in local immunity during pneumonia-derived sepsis caused by gram-negative bacteria. *Blood,* 131**,** 864-876.

CLEMETSON, J. M., POLGAR, J., MAGNENAT, E., WELLS, T. N. & CLEMETSON, K. J. 1999. The platelet collagen receptor glycoprotein VI is a member of the immunoglobulin superfamily closely related to FcαR and the natural killer receptors. *Journal of Biological Chemistry,* 274**,** 29019-29024.

CLEMETSON, K. J. & CLEMETSON, J. M. 2019. Platelet receptors. *Platelets.* Elsevier.

COLE, N. B. 2013. Site-Specific Protein Labeling with SNAP-Tags. *Current protocols in protein science,* 73**,** 30.1. 1-30.1. 16.

COVIC, L., GRESSER, A. L. & KULIOPULOS, A. 2000. Biphasic kinetics of activation and signaling for PAR1 and PAR4 thrombin receptors in platelets. *Biochemistry,* 39**,** 5458-67.

COXON, C. H., GEER, M. J. & SENIS, Y. A. 2017. ITIM receptors: more than just inhibitors of platelet activation. *Blood,* 129**,** 3407-3418.

CRUZ, M. A., YUAN, H., LEE, J. R., WISE, R. J. & HANDIN, R. I. 1995. Interaction of the von Willebrand factor (vWF) with collagen Localization of the primary collagen-binding site by analysis of recombinant vWF a domain polypeptides. *Journal of Biological Chemistry,* 270**,** 10822-10827.

DAI, K., BODNAR, R., BERNDT, M. C. & DU, X. 2005. A critical role for 14-3-3zeta protein in regulating the VWF binding function of platelet glycoprotein Ib-IX and its therapeutic implications. *Blood,* 106**,** 1975-81.

DALY, M. E. 2011. Determinants of platelet count in humans. *Haematologica,* 96**,** 10-3.

DE GENST, E., SILENCE, K., DECANNIERE, K., CONRATH, K., LORIS, R., KINNE, J., MUYLDERMANS, S. & WYNS, L. 2006. Molecular basis for the preferential cleft recognition by dromedary heavy-chain antibodies. *Proc Natl Acad Sci U S A,* 103**,** 4586-91.

DEMPSEY, G. T., VAUGHAN, J. C., CHEN, K. H., BATES, M. & ZHUANG, X. 2011. Evaluation of fluorophores for optimal performance in localization-based super-resolution imaging. *Nature methods,* 8**,** 1027.

DESCHOUT, H., SHIVANANDAN, A., ANNIBALE, P., SCARSELLI, M. & RADENOVIC, A. 2014a. Progress in quantitative single-molecule localization microscopy. *Histochem Cell Biol,* 142**,** 5-17.

DESCHOUT, H., ZANACCHI, F. C., MLODZIANOSKI, M., DIASPRO, A., BEWERSDORF, J., HESS, S. T. & BRAECKMANS, K. 2014b. Precisely and accurately localizing single emitters in fluorescence microscopy. *Nature methods,* 11**,** 253.

DEUTSCH, V. R. & TOMER, A. 2006. Megakaryocyte development and platelet production. *Br J Haematol,* 134**,** 453-66.

DEWITTE, A., LEPREUX, S., VILLENEUVE, J., RIGOTHIER, C., COMBE, C., OUATTARA, A. & RIPOCHE, J. 2017. Blood platelets and sepsis pathophysiology: A new therapeutic prospect in critical ill patients? *Ann Intensive Care,* 7**,** 115.

DORNIER, E., COUMAILLEAU, F., OTTAVI, J.-F., MORETTI, J., BOUCHEIX, C., MAUDUIT, P., SCHWEISGUTH, F. & RUBINSTEIN, E. 2012. TspanC8 tetraspanins regulate ADAM10/Kuzbanian trafficking and promote Notch activation in flies and mammals. *J Cell Biol,* 199**,** 481-496.

DORSAM, R. T. & KUNAPULI, S. P. 2004. Central role of the P2Y12 receptor in platelet activation. *J Clin Invest,* 113**,** 340-5.

DOSHI, R., CHEN, B. R., VIBAT, C. R. T., HUANG, N., LEE, C.-W. & CHANG, G. 2014. In vitro nanobody discovery for integral membrane protein targets. *Scientific reports,* 4**,** 6760.

DOUGLASS, A. D. & VALE, R. D. 2005. Single-molecule microscopy reveals plasma membrane microdomains created by protein-protein networks that exclude or trap signaling molecules in T cells. *Cell,* 121**,** 937-50.

DUBOIS, C., PANICOT-DUBOIS, L., MERRILL-SKOLOFF, G., FURIE, B. & FURIE, B. C. 2006. Glycoprotein VI–dependent and–independent pathways of thrombus formation in vivo. *Blood,* 107**,** 3902-3906.

DUMONT, B., LASNE, D., ROTHSCHILD, C., BOUABDELLI, M., OLLIVIER, V., OUDIN, C., AJZENBERG, N., GRANDCHAMP, B. & JANDROT-PERRUS, M. 2009. Absence of collagen-induced platelet activation caused by compound heterozygous GPVI mutations. *Blood,* 114**,** 1900-1903.

DUNSTER, J. L., MAZET, F., FRY, M. J., GIBBINS, J. M. & TINDALL, M. J. 2015. Regulation of early steps of GPVI signal transduction by phosphatases: a systems biology approach. *PLoS computational biology,* 11**,** e1004589.

DÜTTING, S., BENDER, M. & NIESWANDT, B. 2012. Platelet GPVI: a target for antithrombotic therapy?! *Trends in pharmacological sciences,* 33**,** 583-590.

DYKSTRA, M., CHERUKURI, A., SOHN, H. W., TZENG, S.-J. & PIERCE, S. K. 2003. Location is everything: lipid rafts and immune cell signaling. *Annual review of immunology,* 21**,** 457-481.

ELASKALANI, O., KHAN, I., MORICI, M., MATTHYSEN, C., SABALE, M., MARTINS, R. N., VERDILE, G. & METHAROM, P. 2018. Oligomeric and fibrillar amyloid beta 42 induce platelet aggregation partially through GPVI. *Platelets,* 29**,** 415-420.

ELS CONRATH, K., LAUWEREYS, M., WYNS, L. & MUYLDERMANS, S. 2001. Camel single-domain antibodies as modular building units in bispecific and bivalent antibody constructs. *J Biol Chem,* 276**,** 7346-50.

ENDESFELDER, U., FINAN, K., HOLDEN, S. J., COOK, P. R., KAPANIDIS, A. N. & HEILEMANN, M. 2013. Multiscale spatial organization of RNA polymerase in Escherichia coli. *Biophys J,* 105**,** 172-81.

ESTER, M., KRIEGEL, H.-P., SANDER, J. & XU, X. A density-based algorithm for discovering clusters in large spatial databases with noise. Kdd, 1996. 226-231.

EZUMI, Y., KODAMA, K., UCHIYAMA, T. & TAKAYAMA, H. 2002. Constitutive and functional association of the platelet collagen receptor glycoprotein VI–Fc receptor γ-chain complex with membrane rafts. *Blood,* 99**,** 3250-3255.

EZUMI, Y., SHINDOH, K., TSUJI, M. & TAKAYAMA, H. 1998. Physical and functional association of the Src family kinases Fyn and Lyn with the collagen receptor glycoprotein VI-Fc receptor γ chain complex on human platelets. *Journal of Experimental Medicine,* 188**,** 267-276.

EZUMI, Y., UCHIYAMA, T. & TAKAYAMA, H. 2000. Molecular cloning, genomic structure, chromosomal localization, and alternative splice forms of the platelet collagen receptor glycoprotein VI. *Biochemical and biophysical research communications,* 277**,** 27-36.

FACEY, A., PINAR, I., ARTHUR, J. F., QIAO, J., JING, J., MADO, B., CARBERRY, J., ANDREWS, R. K. & GARDINER, E. E. 2016. A-Disintegrin-And-Metalloproteinase (ADAM) 10 Activity on Resting and Activated Platelets. *Biochemistry,* 55**,** 1187-94.

FAGER, A. M., WOOD, J. P., BOUCHARD, B. A., FENG, P. & TRACY, P. B. 2010. Properties of procoagulant platelets: defining and characterizing the subpopulation binding a functional prothrombinase. *Arteriosclerosis, thrombosis, and vascular biology,* 30**,** 2400-2407.

FAVALORO, E. J. 2000. Collagen binding assay for von Willebrand factor (VWF: CBA): detection of von Willebrands Disease (VWD), and discrimination of VWD subtypes, depends on collagen source. *Thrombosis and haemostasis,* 83**,** 127-135.

FENG, J., GARRITY, D., CALL, M. E., MOFFETT, H. & WUCHERPFENNIG, K. W. 2005. Convergence on a distinctive assembly mechanism by unrelated families of activating immune receptors. *Immunity,* 22**,** 427-438.

FINNEY, B. A., SCHWEIGHOFFER, E., NAVARRO-NÚÑEZ, L., BÉNÉZECH, C., BARONE, F., HUGHES, C. E., LANGAN, S. A., LOWE, K. L., POLLITT, A. Y. & MOURAO-SA, D. 2012. CLEC-2 and Syk in the megakaryocytic/platelet lineage are essential for development. *Blood,* 119**,** 1747-1756.

FLAUMENHAFT, R. & SHARDA, A. 2019. Platelet secretion. *Platelets.* Elsevier.

FRIDY, P. C., THOMPSON, M. K., KETAREN, N. E. & ROUT, M. P. 2015. Engineered high-affinity nanobodies recognizing staphylococcal Protein A and suitable for native isolation of protein complexes. *Anal Biochem,* 477**,** 92-4.

FURLAN, G., MINOWA, T., HANAGATA, N., KATAOKA-HAMAI, C. & KAIZUKA, Y. 2014. Phosphatase CD45 both positively and negatively regulates T cell receptor phosphorylation in reconstituted membrane protein clusters. *Journal of Biological Chemistry,* 289**,** 28514-28525.

GARDINER, E. E., ARTHUR, J. F., KAHN, M. L., BERNDT, M. C. & ANDREWS, R. K. 2004. Regulation of platelet membrane levels of glycoprotein VI by a platelet-derived metalloproteinase. *Blood,* 104**,** 3611-3617.

GARDINER, E. E., KARUNAKARAN, D., ARTHUR, J. F., MU, F.-T., POWELL, M. S., BAKER, R. I., HOGARTH, P. M., KAHN, M. L., ANDREWS, R. K. & BERNDT, M. C. 2008. Dual ITAM-mediated proteolytic pathways for irreversible inactivation of platelet receptors: de-ITAM-izing FcγRIIa. *Blood,* 111**,** 165-174.

GARDINER, E. E., KARUNAKARAN, D., SHEN, Y., ARTHUR, J. F., ANDREWS, R. K. & BERNDT, M. C. 2007. Controlled shedding of platelet glycoprotein (GP) VI and GPIb–IX–V by ADAM family metalloproteinases. *Journal of Thrombosis and Haemostasis,* 5**,** 1530-1537.

GIBBINS, J. M., BRIDDON, S., SHUTES, A., VAN VUGT, M. J., VAN DE WINKEL, J. G., SAITO, T. & WATSON, S. P. 1998. The p85 subunit of phosphatidylinositol 3-kinase associates with the Fc receptor γ-chain and linker for activitor of T cells (LAT) in platelets stimulated by collagen and convulxin. *Journal of Biological Chemistry,* 273**,** 34437-34443.

GIBBINS, J. M., OKUMA, M., FARNDALE, R., BARNES, M. & WATSON, S. P. 1997. Glycoprotein VI is the collagen receptor in platelets which underlies tyrosine phosphorylation of the Fc receptor γ-chain. *FEBS letters,* 413**,** 255-259.

GITZ, E., POLLITT, A. Y., GITZ-FRANCOIS, J. J., ALSHEHRI, O., MORI, J., MONTAGUE, S., NASH, G. B., DOUGLAS, M. R., GARDINER, E. E. & ANDREWS, R. K. 2014. CLEC-2 expression is maintained on activated platelets and on platelet microparticles. *Blood,* 124**,** 2262-2270.

GOEBEL, S., LI, Z., VOGELMANN, J., HOLTHOFF, H.-P., DEGEN, H., HERMANN, D. M., GAWAZ, M., UNGERER, M. & MÜNCH, G. 2013. The GPVI-Fc fusion protein Revacept improves cerebral infarct volume and functional outcome in stroke. *PloS one,* 8**,** e66960.

GOERGE, T., HO-TIN-NOE, B., CARBO, C., BENARAFA, C., REMOLD-O'DONNELL, E., ZHAO, B. Q., CIFUNI, S. M. & WAGNER, D. D. 2008. Inflammation induces hemorrhage in thrombocytopenia. *Blood,* 111**,** 4958-64.

GOLEBIEWSKA, E. M. & POOLE, A. W. 2015. Platelet secretion: From haemostasis to wound healing and beyond. *Blood Rev,* 29**,** 153-62.

GOSCHNICK, M. W., LAU, L.-M., WEE, J. L., LIU, Y. S., HOGARTH, P. M., ROBB, L. M., HICKEY, M. J., WRIGHT, M. D. & JACKSON, D. E. 2006. Impaired "outside-in" integrin αIIbβ3 signaling and thrombus stability in TSSC6-deficient mice. *Blood,* 108**,** 1911-1918.

GOYETTE, J., NIEVES, D. J., MA, Y. & GAUS, K. 2019. How does T cell receptor clustering impact on signal transduction? *J Cell Sci,* 132.

GRATACAP, M.-P., MARTIN, V., VALÉRA, M.-C., ALLART, S., GARCIA, C., SIÉ, P., RECHER, C. & PAYRASTRE, B. 2009. The new tyrosine-kinase inhibitor and anticancer drug dasatinib reversibly affects platelet activation in vitro and in vivo. *Blood,* 114**,** 1884-1892.

GROS, A., SYVANNARATH, V., LAMRANI, L., OLLIVIER, V., LOYAU, S., GOERGE, T., NIESWANDT, B., JANDROT-PERRUS, M. & HO-TIN-NOE, B. 2015. Single platelets seal neutrophil-induced vascular breaches via GPVI during immune-complex-mediated inflammation in mice. *Blood,* 126**,** 1017-26.

GRYKA, R. J., BUCKLEY, L. F. & ANDERSON, S. M. 2017. Vorapaxar: The current role and future directions of a novel protease-activated receptor antagonist for risk reduction in atherosclerotic disease. *Drugs in R&D,* 17**,** 65-72.

HAINING, E. J., CHERPOKOVA, D., WOLF, K., BECKER, I. C., BECK, S., EBLE, J. A., STEGNER, D., WATSON, S. P. & NIESWANDT, B. 2017a. CLEC-2 contributes to hemostasis independently of classical hemITAM signaling in mice. *Blood,* 130**,** 2224-2228.

HAINING, E. J., MATTHEWS, A. L., NOY, P. J., ROMANSKA, H. M., HARRIS, H. J., PIKE, J., MOROWSKI, M., GAVIN, R. L., YANG, J. & MILHIET, P.-E. 2017b. Tetraspanin Tspan9 regulates platelet collagen receptor GPVI lateral diffusion and activation. *Platelets,* 28**,** 629-642.

HAINING, E. J., YANG, J., BAILEY, R. L., KHAN, K., COLLIER, R., TSAI, S., WATSON, S. P., FRAMPTON, J., GARCIA, P. & TOMLINSON, M. G. 2012. The TspanC8 subgroup of tetraspanins interacts with A disintegrin and metalloprotease 10 (ADAM10) and regulates its maturation and cell surface expression. *J Biol Chem,* 287**,** 39753-65.

HAMILTON, J. R., CORNELISSEN, I. & COUGHLIN, S. R. 2004. Impaired hemostasis and protection against thrombosis in protease-activated receptor 4-deficient mice is due to lack of thrombin signaling in platelets. *J Thromb Haemost,* 2**,** 1429-35.

HARTWIG, J. H. 2006. The platelet: form and function. *Semin Hematol,* 43**,** S94-100.

HARTWIG, J. H., BARKALOW, K., AZIM, A. & ITALIANO, J. 1999. The elegant platelet: signals controlling actin assembly. *Thrombosis and haemostasis,* 82**,** 392-398.

HARTWIG, J. H. & DESISTO, M. 1991. The cytoskeleton of the resting human blood platelet: structure of the membrane skeleton and its attachment to actin filaments. *J Cell Biol,* 112**,** 407-25.

HEILEMANN, M., VAN DE LINDE, S., SCHÜTTPELZ, M., KASPER, R., SEEFELDT, B., MUKHERJEE, A., TINNEFELD, P. & SAUER, M. 2008. Subdiffraction-resolution fluorescence imaging with conventional fluorescent probes. *Angewandte Chemie International Edition,* 47**,** 6172-6176.

HERR, A. B. & FARNDALE, R. W. 2009. Structural insights into the interactions between platelet receptors and fibrillar collagen. *Journal of Biological Chemistry,* 284**,** 19781-19785.

HO-TIN-NOE, B., BOULAFTALI, Y. & CAMERER, E. 2018. Platelets and vascular integrity: how platelets prevent bleeding in inflammation. *Blood,* 131**,** 277-288.

HORII, K., BROOKS, M. T. & HERR, A. B. 2009. Convulxin forms a dimer in solution and can bind eight copies of glycoprotein VI: implications for platelet activation. *Biochemistry,* 48**,** 2907-2914.

HORII, K., KAHN, M. L. & HERR, A. B. 2006. Structural basis for platelet collagen responses by the immune-type receptor glycoprotein VI. *Blood,* 108**,** 936-942.

HORTON, E. R., BYRON, A., ASKARI, J. A., NG, D. H. J., MILLON-FREMILLON, A., ROBERTSON, J., KOPER, E. J., PAUL, N. R., WARWOOD, S., KNIGHT, D., HUMPHRIES, J. D. & HUMPHRIES, M. J. 2015. Definition of a consensus integrin adhesome and its dynamics during adhesion complex assembly and disassembly. *Nat Cell Biol,* 17**,** 1577-1587.

HOTTZ, E. D., BOZZA, F. A. & BOZZA, P. T. 2018. Platelets in Immune Response to Virus and Immunopathology of Viral Infections. *Front Med (Lausanne),* 5**,** 121.

HU, Y., LIU, C. & MUYLDERMANS, S. 2017. Nanobody-based delivery systems for diagnosis and targeted tumor therapy. *Frontiers in immunology,* 8**,** 1442.

HUANG, B., BABCOCK, H. & ZHUANG, X. 2010. Breaking the diffraction barrier: super-resolution imaging of cells. *Cell,* 143**,** 1047-58.

HUANG, B., WANG, W., BATES, M. & ZHUANG, X. 2008. Three-dimensional super-resolution imaging by stochastic optical reconstruction microscopy. *Science,* 319**,** 810-3.

HUANG, M. M., INDIK, Z., BRASS, L. F., HOXIE, J. A., SCHREIBER, A. D. & BRUGGE, J. S. 1992. Activation of Fc gamma RII induces tyrosine phosphorylation of multiple proteins including Fc gamma RII. *J Biol Chem,* 267**,** 5467-73.

HUGHES, C. E., NAVARRO-NUNEZ, L., FINNEY, B. A., MOURAO-SA, D., POLLITT, A. Y. & WATSON, S. P. 2010a. CLEC-2 is not required for platelet aggregation at arteriolar shear. *J Thromb Haemost,* 8**,** 2328-2332.

HUGHES, C. E., POLLITT, A. Y., MORI, J., EBLE, J. A., TOMLINSON, M. G., HARTWIG, J. H., O'CALLAGHAN, C. A., FUTTERER, K. & WATSON, S. P. 2010b. CLEC-2 activates Syk through dimerization. *Blood,* 115**,** 2947-55.

HYNES, R. O. 2002. Integrins: bidirectional, allosteric signaling machines. *cell,* 110**,** 673-687.
INDURUWA, I., MOROI, M., BONNA, A., MALCOR, J. D., HOWES, J. M., WARBURTON, E., FARNDALE, R. & JUNG, S. 2018. Platelet collagen receptor Glycoprotein VI-dimer recognizes fibrinogen and fibrin through their D-domains, contributing to platelet adhesion and activation during thrombus formation. *Journal of Thrombosis and Haemostasis,* 16**,** 389-404.
INOUE, O., SUZUKI-INOUE, K., DEAN, W. L., FRAMPTON, J. & WATSON, S. P. 2003. Integrin alpha2beta1 mediates outside-in regulation of platelet spreading on collagen through activation of Src kinases and PLCgamma2. *J Cell Biol,* 160**,** 769-80.
INOUE, O., SUZUKI-INOUE, K., MCCARTY, O. J., MOROI, M., RUGGERI, Z. M., KUNICKI, T. J., OZAKI, Y. & WATSON, S. P. 2006. Laminin stimulates spreading of platelets through integrin α6β1–dependent activation of GPVI. *Blood,* 107**,** 1405-1412.
ISAKOV, N. 1997. Immunoreceptor tyrosine-based activation motif (ITAM), a unique module linking antigen and Fc receptors to their signaling cascades. *J Leukoc Biol,* 61**,** 6-16.
ITO, T., ISHIDA, Y., KASHIWAGI, R. & KURIYA, S. 1996. Recombinant human c-Mpl ligand is not a direct stimulator of proplatelet formation in mature human megakaryocytes. *Br J Haematol,* 94**,** 387-90.
IZQUIERDO, I., BARRACHINA, M. N., HERMIDA-NOGUEIRA, L., CASAS, V., EBLE, J. A., CARRASCAL, M., ABIAN, J. & GARCIA, A. 2019. Platelet membrane lipid rafts protein composition varies following GPVI and CLEC-2 receptors activation. *J Proteomics,* 195**,** 88-97.
JAIN, S., RUSSELL, S. & WARE, J. 2009. Platelet glycoprotein VI facilitates experimental lung metastasis in syngenic mouse models. *Journal of Thrombosis and Haemostasis,* 7**,** 1713-1717.
JANDROT-PERRUS, M., BUSFIELD, S., LAGRUE, A.-H., XIONG, X., DEBILI, N., CHICKERING, T., LE COUEDIC, J.-P., GOODEARL, A., DUSSAULT, B. & FRASER, C. 2000. Cloning, characterization, and functional studies of human and mouse glycoprotein VI: a platelet-specific collagen receptor from the immunoglobulin superfamily. *Blood,* 96**,** 1798-1807.
JANOWSKA-WIECZOREK, A., WYSOCZYNSKI, M., KIJOWSKI, J., MARQUEZ-CURTIS, L., MACHALINSKI, B., RATAJCZAK, J. & RATAJCZAK, M. Z. 2005. Microvesicles derived from activated platelets induce metastasis and angiogenesis in lung cancer. *International journal of cancer,* 113**,** 752-760.
JAQAMAN, K. & GRINSTEIN, S. 2012. Regulation from within: the cytoskeleton in transmembrane signaling. *Trends in cell biology,* 22**,** 515-526.
JAUMOUILLÉ, V., FARKASH, Y., JAQAMAN, K., DAS, R., LOWELL, C. A. & GRINSTEIN, S. 2014. Actin cytoskeleton reorganization by Syk regulates Fcγ receptor responsiveness by increasing its lateral mobility and clustering. *Developmental cell,* 29**,** 534-546.
JIANG, P., LOYAU, S., TCHITCHINADZE, M., ROPERS, J., JONDEAU, G. & JANDROT-PERRUS, M. 2015. Inhibition of glycoprotein VI clustering by collagen as a mechanism of inhibiting collagen-induced platelet responses: the example of losartan. *PloS one,* 10**,** e0128744.
JOOSS, N. J., DE SIMONE, I., PROVENZALE, I., FERNANDEZ, D. I., BROUNS, S. L. N., FARNDALE, R. W., HENSKENS, Y. M. C., KUIJPERS, M. J. E., TEN CATE, H., VAN DER MEIJDEN, P. E. J., CAVILL, R. & HEEMSKERK, J. W. M. 2019. Role of Platelet Glycoprotein VI and Tyrosine Kinase Syk in Thrombus Formation on Collagen-Like Surfaces. *Int J Mol Sci,* 20.
JOUTSI-KORHONEN, L., SMETHURST, P. A., RANKIN, A., GRAY, E., IJSSELDIJK, M., ONLEY, C. M., WATKINS, N. A., WILLIAMSON, L. M., GOODALL, A. H. & DE GROOT, P. G. 2003. The low-frequency allele of the platelet collagen signaling receptor glycoprotein VI is associated with reduced functional responses and expression. *Blood,* 101**,** 4372-4379.
JUDD, B. A., MYUNG, P. S., LENG, L., OBERGFELL, A., PEAR, W. S., SHATTIL, S. J. & KORETZKY, G. A. 2000. Hematopoietic reconstitution of SLP-76 corrects hemostasis and platelet signaling through alpha IIb beta 3 and collagen receptors. *Proc Natl Acad Sci U S A,* 97**,** 12056-61.

JUNG, S., TSUJI, K. & MOROI, M. 2009. Glycoprotein (GP) VI dimer as a major collagen-binding site of native platelets: direct evidence obtained with dimeric GPVI-specific Fabs. *Journal of Thrombosis and Haemostasis,* 7**,** 1347-1355.

JUNG, S. M., MOROI, M., SOEJIMA, K., NAKAGAKI, T., MIURA, Y., BERNDT, M. C., GARDINER, E. E., HOWES, J.-M., PUGH, N. & BIHAN, D. 2012. Constitutive dimerization of glycoprotein VI (GPVI) in resting platelets is essential for binding to collagen and activation in flowing blood. *Journal of Biological Chemistry,* 287**,** 30000-30013.

JUNG, S. M., TAKEMURA, Y., IMAMURA, Y., HAYASHI, T., ADACHI, E. & MOROI, M. 2008. Collagen-type specificity of glycoprotein VI as a determinant of platelet adhesion. *Platelets,* 19**,** 32-42.

JUNGMANN, R., AVENDANO, M. S., DAI, M., WOEHRSTEIN, J. B., AGASTI, S. S., FEIGER, Z., RODAL, A. & YIN, P. 2016. Quantitative super-resolution imaging with qPAINT. *Nat Methods,* 13**,** 439-42.

JUNGMANN, R., AVENDAÑO, M. S., WOEHRSTEIN, J. B., DAI, M., SHIH, W. M. & YIN, P. 2014. Multiplexed 3D cellular super-resolution imaging with DNA-PAINT and Exchange-PAINT. *Nature methods,* 11**,** 313.

KANAJI, S., FAHS, S. A., SHI, Q., HABERICHTER, S. L. & MONTGOMERY, R. R. 2012. Contribution of platelet vs. endothelial VWF to platelet adhesion and hemostasis. *J Thromb Haemost,* 10**,** 1646-52.

KANNAN, M., AHMAD, F., YADAV, B. K., KUMAR, R., CHOUDHRY, V. P. & SAXENA, R. 2009. Molecular defects in ITGA2B and ITGB3 genes in patients with Glanzmann thrombasthenia. *J Thromb Haemost,* 7**,** 1878-85.

KAPLAN, Z. S. & JACKSON, S. P. 2011. The role of platelets in atherothrombosis. *Hematology Am Soc Hematol Educ Program,* 2011**,** 51-61.

KASIRER-FRIEDE, A., KAHN, M. L. & SHATTIL, S. J. 2007. Platelet integrins and immunoreceptors. *Immunological reviews,* 218**,** 247-264.

KATO, K., KANAJI, T., RUSSELL, S., KUNICKI, T. J., FURIHATA, K., KANAJI, S., MARCHESE, P., REININGER, A., RUGGERI, Z. M. & WARE, J. 2003. The contribution of glycoprotein VI to stable platelet adhesion and thrombus formation illustrated by targeted gene deletion. *Blood,* 102**,** 1701-7.

KHAN, A. O., SIMMS, V. A., PIKE, J. A., THOMAS, S. G. & MORGAN, N. V. 2017. CRISPR-Cas9 Mediated Labelling Allows for Single Molecule Imaging and Resolution. *Sci Rep,* 7**,** 8450.

KIJANKA, M., WARNDERS, F. J., EL KHATTABI, M., LUB-DE HOOGE, M., VAN DAM, G. M., NTZIACHRISTOS, V., DE VRIES, L., OLIVEIRA, S. & VAN BERGEN EN HENEGOUWEN, P. M. 2013. Rapid optical imaging of human breast tumour xenografts using anti-HER2 VHHs site-directly conjugated to IRDye 800CW for image-guided surgery. *Eur J Nucl Med Mol Imaging,* 40**,** 1718-29.

KLEINSCHNITZ, C., POZGAJOVA, M., PHAM, M., BENDSZUS, M., NIESWANDT, B. & STOLL, G. 2007. Targeting platelets in acute experimental stroke: impact of glycoprotein Ib, VI, and IIb/IIIa blockade on infarct size, functional outcome, and intracranial bleeding. *Circulation,* 115**,** 2323-30.

KNIGHT, C. G., MORTON, L. F., ONLEY, D. J., PEACHEY, A. R., MESSENT, A. J., SMETHURST, P. A., TUCKWELL, D. S., FARNDALE, R. W. & BARNES, M. J. 1998. Identification in collagen type I of an integrin alpha2 beta1-binding site containing an essential GER sequence. *J Biol Chem,* 273**,** 33287-94.

KUIJPERS, M. J., GILIO, K., REITSMA, S., NERGIZ-UNAL, R., PRINZEN, L., HEENEMAN, S., LUTGENS, E., VAN ZANDVOORT, M. A., NIESWANDT, B. & OUDE EGBRINK, M. G. 2009. Complementary roles of platelets and coagulation in thrombus formation on plaques acutely ruptured by targeted ultrasound treatment: a novel intravital model. *Journal of Thrombosis and Haemostasis,* 7**,** 152-161.

LAGRUE-LAK-HAL, A.-H., DEBILI, N., KINGBURY, G., LECUT, C., LE COUEDIC, J.-P., VILLEVAL, J.-L., JANDROT-PERRUS, M. & VAINCHENKER, W. 2001. Expression and function of the collagen

receptor GPVI during megakaryocyte maturation. *Journal of Biological Chemistry,* 276**,** 15316-15325.

LAM, W. A., CHAUDHURI, O., CROW, A., WEBSTER, K. D., LI, T. D., KITA, A., HUANG, J. & FLETCHER, D. A. 2011. Mechanics and contraction dynamics of single platelets and implications for clot stiffening. *Nat Mater,* 10**,** 61-6.

LEBOZEC, K., JANDROT-PERRUS, M., AVENARD, G., FAVRE-BULLE, O. & BILLIALD, P. Design, development and characterization of ACT017, a humanized Fab that blocks platelet's glycoprotein VI function without causing bleeding risks. MAbs, 2017. Taylor & Francis, 945-958.

LECUT, C., SCHOOLMEESTER, A., KUIJPERS, M. J., BROERS, J. L., VAN ZANDVOORT, M. A., VANHOORELBEKE, K., DECKMYN, H., JANDROT-PERRUS, M. & HEEMSKERK, J. W. 2004. Principal role of glycoprotein VI in alpha2beta1 and alphaIIbbeta3 activation during collagen-induced thrombus formation. *Arterioscler Thromb Vasc Biol,* 24**,** 1727-33.

LEE, F. A., VAN LIER, M., RELOU, I. A., FOLEY, L., AKKERMAN, J. W., HEIJNEN, H. F. & FARNDALE, R. W. 2006. Lipid rafts facilitate the interaction of PECAM-1 with the glycoprotein VI-FcR gamma-chain complex in human platelets. *J Biol Chem,* 281**,** 39330-8.

LEE, R. H., STEFANINI L. AND BERGMEIER W. 2019. Chapter 18 - Platelet Signal Transduction. *In: MICHELSON, A. D. (ed.) Platelets (Fourth Edition)*.

LEFRANCAIS, E., ORTIZ-MUNOZ, G., CAUDRILLIER, A., MALLAVIA, B., LIU, F., SAYAH, D. M., THORNTON, E. E., HEADLEY, M. B., DAVID, T., COUGHLIN, S. R., KRUMMEL, M. F., LEAVITT, A. D., PASSEGUE, E. & LOONEY, M. R. 2017. The lung is a site of platelet biogenesis and a reservoir for haematopoietic progenitors. *Nature,* 544**,** 105-109.

LEIVA, O., LEON, C., KAH NG, S., MANGIN, P., GACHET, C. & RAVID, K. 2018. The role of extracellular matrix stiffness in megakaryocyte and platelet development and function. *Am J Hematol,* 93**,** 430-441.

LEVET, F., HOSY, E., KECHKAR, A., BUTLER, C., BEGHIN, A., CHOQUET, D. & SIBARITA, J.-B. 2015. SR-Tesseler: a method to segment and quantify localization-based super-resolution microscopy data. *Nature methods,* 12**,** 1065.

LI, H., LOCKYER, S., CONCEPCION, A., GONG, X., TAKIZAWA, H., GUERTIN, M., MATSUMOTO, Y., KAMBAYASHI, J., TANDON, N. N. & LIU, Y. 2007. The Fab fragment of a novel anti-GPVI monoclonal antibody, OM4, reduces in vivo thrombosis without bleeding risk in rats. *Arterioscler Thromb Vasc Biol,* 27**,** 1199-205.

LI, R. 2019. The Glycoprotein Ib-IX-V Complex. *Platelets.* Elsevier.

LI, Z., ZHANG, G., LIU, J., STOJANOVIC, A., RUAN, C., LOWELL, C. A. & DU, X. 2010. An important role of the SRC family kinase Lyn in stimulating platelet granule secretion. *Journal of Biological Chemistry,* 285**,** 12559-12570.

LICKERT, S., SORRENTINO, S., STUDT, J. D., MEDALIA, O., VOGEL, V. & SCHOEN, I. 2018. Morphometric analysis of spread platelets identifies integrin alphaIIbbeta3-specific contractile phenotype. *Sci Rep,* 8**,** 5428.

LIN, J. & WEISS, A. 2003. The tyrosine phosphatase CD148 is excluded from the immunologic synapse and down-regulates prolonged T cell signaling. *J Cell Biol,* 162**,** 673-82.

LOCKE, D., CHEN, H., LIU, Y., LIU, C. & KAHN, M. L. 2002. Lipid rafts orchestrate signaling by the platelet receptor glycoprotein VI. *Journal of Biological Chemistry,* 277**,** 18801-18809.

LOCKYER, S., OKUYAMA, K., BEGUM, S., LE, S., SUN, B., WATANABE, T., MATSUMOTO, Y., YOSHITAKE, M., KAMBAYASHI, J. & TANDON, N. N. 2006. GPVI-deficient mice lack collagen responses and are protected against experimentally induced pulmonary thromboembolism. *Thromb Res,* 118**,** 371-80.

LORENZ, V., STEGNER, D., STRITT, S., VOGTLE, T., KIEFER, F., WITKE, W., SCHYMEINSKY, J., WATSON, S. P., WALZOG, B. & NIESWANDT, B. 2015. Targeted downregulation of platelet CLEC-2 occurs through Syk-independent internalization. *Blood,* 125**,** 4069-77.

LOWE, K. L., FINNEY, B. A., DEPPERMANN, C., HÄGERLING, R., GAZIT, S. L., FRAMPTON, J., BUCKLEY, C., CAMERER, E., NIESWANDT, B. & KIEFER, F. 2015a. Podoplanin and CLEC-2 drive cerebrovascular patterning and integrity during development. *Blood,* 125**,** 3769-3777.

LOWE, K. L., NAVARRO-NUNEZ, L., BENEZECH, C., NAYAR, S., KINGSTON, B. L., NIESWANDT, B., BARONE, F., WATSON, S. P., BUCKLEY, C. D. & DESANTI, G. E. 2015b. The expression of mouse CLEC-2 on leucocyte subsets varies according to their anatomical location and inflammatory state. *Eur J Immunol,* 45**,** 2484-93.

LOYAU, S., DUMONT, B., OLLIVIER, V., BOULAFTALI, Y., FELDMAN, L., AJZENBERG, N. & JANDROT-PERRUS, M. 2012. Platelet glycoprotein VI dimerization, an active process inducing receptor competence, is an indicator of platelet reactivity. *Arteriosclerosis, thrombosis, and vascular biology,* 32**,** 778-785.

MACHLUS, K. R., THON, J. N. & ITALIANO, J. E., JR. 2014. Interpreting the developmental dance of the megakaryocyte: a review of the cellular and molecular processes mediating platelet formation. *Br J Haematol,* 165**,** 227-36.

MACRAE, F. L., DUVAL, C., PAPAREDDY, P., BAKER, S. R., YULDASHEVA, N., KEARNEY, K. J., MCPHERSON, H. R., ASQUITH, N., KONINGS, J. & CASINI, A. 2018. A fibrin biofilm covers blood clots and protects from microbial invasion. *Journal of Clinical Investigation,* 128**,** 3356-3368.

MAMMADOVA-BACH, E., OLLIVIER, V., LOYAU, S., SCHAFF, M., DUMONT, B., FAVIER, R., FREYBURGER, G., LATGER-CANNARD, V., NIESWANDT, B., GACHET, C., MANGIN, P. H. & JANDROT-PERRUS, M. 2015. Platelet glycoprotein VI binds to polymerized fibrin and promotes thrombin generation. *Blood,* 126**,** 683-91.

MANGIN, P., YAP, C. L., NONNE, C., STURGEON, S. A., GONCALVES, I., YUAN, Y., SCHOENWAELDER, S. M., WRIGHT, C. E., LANZA, F. & JACKSON, S. P. 2006. Thrombin overcomes the thrombosis defect associated with platelet GPVI/FcRγ deficiency. *Blood,* 107**,** 4346-4353.

MANGIN, P. H., ONSELAER, M.-B., RECEVEUR, N., LE LAY, N., HARDY, A. T., WILSON, C., SANCHEZ, X., LOYAU, S., DUPUIS, A. & BABAR, A. K. 2018. Immobilized fibrinogen activates human platelets through glycoprotein VI. *haematologica,* 103**,** 898-907.

MANGLIK, A., KOBILKA, B. K. & STEYAERT, J. 2017. Nanobodies to study G protein–coupled receptor structure and function. *Annual review of pharmacology and toxicology,* 57**,** 19-37.

MASSBERG, S., KONRAD, I., BÜLTMANN, A., SCHULZ, C., MÜNCH, G. T., PELUSO, M., LORENZ, M., SCHNEIDER, S., BESTA, F. & MÜLLER, I. 2004. Soluble glycoprotein VI dimer inhibits platelet adhesion and aggregation to the injured vessel wall in vivo. *The FASEB journal,* 18**,** 397-399.

MATUS, V., VALENZUELA, G., SÁEZ, C., HIDALGO, P., LAGOS, M., ARANDA, E., PANES, O., PEREIRA, J., PILLOIS, X. & NURDEN, A. 2013. An adenine insertion in exon 6 of human GP 6 generates a truncated protein associated with a bleeding disorder in four C hilean families. *Journal of Thrombosis and Haemostasis,* 11**,** 1751-1759.

MAY, F., HAGEDORN, I., PLEINES, I., BENDER, M., VÖGTLE, T., EBLE, J., ELVERS, M. & NIESWANDT, B. 2009. CLEC-2 is an essential platelet-activating receptor in hemostasis and thrombosis. *Blood,* 114**,** 3464-3472.

MAYR, S., HAUSER, F., PETERBAUER, A., TAUSCHER, A., NADERER, C., AXMANN, M., PLOCHBERGER, B. & JACAK, J. 2018. Localization Microscopy of Actin Cytoskeleton in Human Platelets. *International journal of molecular sciences,* 19**,** 1150.

MAZZUCATO, M., COZZI, M. R., BATTISTON, M., JANDROT-PERRUS, M., MONGIAT, M., MARCHESE, P., KUNICKI, T. J., RUGGERI, Z. M. & DE MARCO, L. 2009. Distinct spatio-temporal Ca2+ signaling elicited by integrin α2β1 and glycoprotein VI under flow. *Blood,* 114**,** 2793-2801.

MCARTHUR, K., CHAPPAZ, S. & KILE, B. T. 2018. Apoptosis in megakaryocytes and platelets: the life and death of a lineage. *Blood,* 131**,** 605-610.

METCALF, D. J., EDWARDS, R., KUMARSWAMI, N. & KNIGHT, A. E. 2013. Test samples for optimizing STORM super-resolution microscopy. *J Vis Exp*.

MIURA, S., LI, C. Q., CAO, Z., WANG, H., WARDELL, M. R. & SADLER, J. E. 2000. Interaction of von Willebrand Factor Domain A1 with Platelet Glycoprotein Ibα-(1–289) SLOW INTRINSIC BINDING KINETICS MEDIATE RAPID PLATELET ADHESION. *Journal of Biological Chemistry,* 275**,** 7539-7546.

MIURA, Y., TAKAHASHI, T., JUNG, S. M. & MOROI, M. 2002. Analysis of the interaction of platelet collagen receptor glycoprotein VI (GPVI) with collagen A dimeric form of GPVI, but not the monomeric form, shows affinity to fibrous collagen. *Journal of Biological Chemistry,* 277**,** 46197-46204.

MONROE, D. M. & HOFFMAN, M. 2006. What does it take to make the perfect clot? *Arterioscler Thromb Vasc Biol,* 26**,** 41-8.

MONTAGUE, S. J., ANDREWS, R. K. & GARDINER, E. E. 2018a. Mechanisms of receptor shedding in platelets. *Blood,* 132**,** 2535-2545.

MONTAGUE, S. J., DELIERNEUX, C., LECUT, C., LAYIOS, N., DINSDALE, R. J., LEE, C. S.-M., POULTER, N. S., ANDREWS, R. K., HAMPSON, P. & WEARN, C. M. 2018b. Soluble GPVI is elevated in injured patients: shedding is mediated by fibrin activation of GPVI. *Blood advances,* 2**,** 240-251.

MORALES, L. D., MARTIN, C. & CRUZ, M. A. 2006. The interaction of von Willebrand factor-A1 domain with collagen: mutation G1324S (type 2M von Willebrand disease) impairs the conformational change in A1 domain induced by collagen. *J Thromb Haemost,* 4**,** 417-25.

MORTON, L., HARGREAVES, P., FARNDALE, R., YOUNG, R. & BARNES, M. 1995. Integrin α2β1-independent activation of platelets by simple collagen-like peptides: collagen tertiary (triple-helical) and quaternary (polymeric) structures are sufficient alone for α2β1-independent platelet reactivity. *Biochemical Journal,* 306**,** 337-344.

MURANYI, W., MALKUSCH, S., MULLER, B., HEILEMANN, M. & KRAUSSLICH, H. G. 2013. Super-resolution microscopy reveals specific recruitment of HIV-1 envelope proteins to viral assembly sites dependent on the envelope C-terminal tail. *PLoS Pathog,* 9**,** e1003198.

MUYLDERMANS, S. 2013. Nanobodies: natural single-domain antibodies. *Annual review of biochemistry,* 82**,** 775-797.

NAGY, Z. & SMOLENSKI, A. 2018. Cyclic nucleotide-dependent inhibitory signaling interweaves with activating pathways to determine platelet responses. *Res Pract Thromb Haemost,* 2**,** 558-571.

NAN, X., COLLISSON, E. A., LEWIS, S., HUANG, J., TAMGÜNEY, T. M., LIPHARDT, J. T., MCCORMICK, F., GRAY, J. W. & CHU, S. 2013. Single-molecule superresolution imaging allows quantitative analysis of RAF multimer formation and signaling. *Proc Natl Acad Sci U S A,* 110**,** 18519-24.

NEWMAN, P. J. 2010. GPVI and the not so eager cleaver. *Blood,* 116**,** 3124-3126.

NICOLSON, P. L., HUGHES, C. E., WATSON, S., NOCK, S. H., HARDY, A. T., WATSON, C. N., MONTAGUE, S. J., CLIFFORD, H., HUISSOON, A. P. & MALCOR, J.-D. 2018. Inhibition of Btk by Btk-specific concentrations of ibrutinib and acalabrutinib delays but does not block platelet aggregation mediated by glycoprotein VI. *haematologica,* 103**,** 2097-2108.

NICOVICH, P. R., OWEN, D. M. & GAUS, K. 2017. Turning single-molecule localization microscopy into a quantitative bioanalytical tool. *Nature protocols,* 12**,** 453.

NIESWANDT, B., BERGMEIER, W., SCHULTE, V., RACKEBRANDT, K., GESSNER, J. E. & ZIRNGIBL, H. 2000. Expression and function of the mouse collagen receptor glycoprotein VI is strictly dependent on its association with the FcRγ chain. *Journal of Biological Chemistry,* 275**,** 23998-24002.

NIESWANDT, B., BRAKEBUSCH, C., BERGMEIER, W., SCHULTE, V., BOUVARD, D., MOKHTARI-NEJAD, R., LINDHOUT, T., HEEMSKERK, J. W., ZIRNGIBL, H. & FÄSSLER, R. 2001a. Glycoprotein VI but not α2β1 integrin is essential for platelet interaction with collagen. *The EMBO journal,* 20**,** 2120-2130.

NIESWANDT, B., KLEINSCHNITZ, C. & STOLL, G. 2011. Ischaemic stroke: a thrombo-inflammatory disease? *J Physiol,* 589**,** 4115-23.

NIESWANDT, B., SCHULTE, V., BERGMEIER, W., MOKHTARI-NEJAD, R., RACKEBRANDT, K., CAZENAVE, J.-P., OHLMANN, P., GACHET, C. & ZIRNGIBL, H. 2001b. Long-term antithrombotic protection by in vivo depletion of platelet glycoprotein VI in mice. *Journal of Experimental Medicine,* 193**,** 459-470.

NIESWANDT, B. & WATSON, S. P. 2003. Platelet-collagen interaction: is GPVI the central receptor? *Blood,* 102**,** 449-61.

NORDING, H. M., SEIZER, P. & LANGER, H. F. 2015. Platelets in inflammation and atherogenesis. *Front Immunol,* 6**,** 98.

NOY, P. J., YANG, J., REYAT, J. S., MATTHEWS, A. L., CHARLTON, A. E., FURMSTON, J., ROGERS, D. A., RAINGER, G. E. & TOMLINSON, M. G. 2016. TspanC8 Tetraspanins and A Disintegrin and Metalloprotease 10 (ADAM10) Interact via Their Extracellular Regions EVIDENCE FOR DISTINCT BINDING MECHANISMS FOR DIFFERENT TspanC8 PROTEINS. *Journal of Biological Chemistry,* 291**,** 3145-3157.

NURDEN, A. T., NURDEN, P., SANCHEZ, M., ANDIA, I. & ANITUA, E. 2008. Platelets and wound healing. *Front Biosci,* 13**,** 3532-48.

OBERGFELL, A., ETO, K., MOCSAI, A., BUENSUCESO, C., MOORES, S. L., BRUGGE, J. S., LOWELL, C. A. & SHATTIL, S. J. 2002. Coordinate interactions of Csk, Src, and Syk kinases with [alpha]IIb[beta]3 initiate integrin signaling to the cytoskeleton. *J Cell Biol,* 157**,** 265-75.

OBERGFELL, A., JUDD, B. A., DEL POZO, M. A., SCHWARTZ, M. A., KORETZKY, G. A. & SHATTIL, S. J. 2001. The molecular adapter SLP-76 relays signals from platelet integrin αIIbβ3 to the actin cytoskeleton. *Journal of Biological Chemistry,* 276**,** 5916-5923.

OFOSU, F. A. 2003. Protease activated receptors 1 and 4 govern the responses of human platelets to thrombin. *Transfusion and apheresis science,* 28**,** 265-268.

OHLMANN, P., HECHLER, B., RAVANAT, C., LOYAU, S., HERRENSCHMIDT, N., WANERT, F., JANDROT-PERRUS, M. & GACHET, C. 2008. Ex vivo inhibition of thrombus formation by an anti-glycoprotein VI Fab fragment in non-human primates without modification of glycoprotein VI expression. *J Thromb Haemost,* 6**,** 1003-11.

OLIVEIRA, S., VAN DONGEN, G. A., WALSUM, M. S.-V., ROOVERS, R. C., STAM, J. C., MALI, W., VAN DIEST, P. J. & VAN BERGEN EN HENEGOUWEN, P. M. 2012. Rapid visualization of human tumor xenografts through optical imaging with a near-infrared fluorescent anti–epidermal growth factor receptor nanobody. *Molecular imaging,* 11**,** 7290.2011. 00025.

ONSELAER, M.-B., HARDY, A. T., WILSON, C., SANCHEZ, X., BABAR, A. K., MILLER, J. L., WATSON, C. N., WATSON, S. K., BONNA, A. & PHILIPPOU, H. 2017. Fibrin and D-dimer bind to monomeric GPVI. *Blood advances,* 1**,** 1495-1504.

ONSELAER, M. B., NAGY, M., PALLINI, C., PIKE, J. A., PERRELLA, G., QUINTANILLA, L. G., EBLE, J. A., POULTER, N. S., HEEMSKERK, J. W. M. & WATSON, S. P. 2019. Comparison of the GPVI inhibitors losartan and honokiol. *Platelets***,** 1-11.

ORLOWSKI, E., CHAND, R., YIP, J., WONG, C., GOSCHNICK, M. W., WRIGHT, M. D., ASHMAN, L. K. & JACKSON, D. 2009. A platelet tetraspanin superfamily member, CD151, is required for regulation of thrombus growth and stability in vivo. *Journal of Thrombosis and Haemostasis,* 7**,** 2074-2084.

OVESNÝ, M., KŘÍŽEK, P., BORKOVEC, J., ŠVINDRYCH, Z. & HAGEN, G. M. 2014. ThunderSTORM: a comprehensive ImageJ plug-in for PALM and STORM data analysis and super-resolution imaging. *Bioinformatics,* 30**,** 2389-2390.

OWEN, D. M., RENTERO, C., ROSSY, J., MAGENAU, A., WILLIAMSON, D., RODRIGUEZ, M. & GAUS, K. 2010. PALM imaging and cluster analysis of protein heterogeneity at the cell surface. *Journal of biophotonics,* 3**,** 446-454.

PAGEON, S. V., TABARIN, T., YAMAMOTO, Y., MA, Y., NICOVICH, P. R., BRIDGEMAN, J. S., COHNEN, A., BENZING, C., GAO, Y., CROWTHER, M. D., TUNGATT, K., DOLTON, G., SEWELL, A. K., PRICE, D. A., ACUTO, O., PARTON, R. G., GOODING, J. J., ROSSY, J., ROSSJOHN, J. & GAUS, K. 2016.

Functional role of T-cell receptor nanoclusters in signal initiation and antigen discrimination. *Proc Natl Acad Sci U S A,* 113**,** E5454-63.

PAKNIKAR, A. K., ELTZNER, B. & KÖSTER, S. 2019. Direct characterization of cytoskeletal reorganization during blood platelet spreading. *Progress in biophysics and molecular biology,* 144**,** 166-176.

PARDON, E., LAEREMANS, T., TRIEST, S., RASMUSSEN, S. G., WOHLKONIG, A., RUF, A., MUYLDERMANS, S., HOL, W. G., KOBILKA, B. K. & STEYAERT, J. 2014. A general protocol for the generation of Nanobodies for structural biology. *Nat Protoc,* 9**,** 674-93.

PARETI, F. I., NIIYA, K., MCPHERSON, J. & RUGGERI, Z. 1987. Isolation and characterization of two domains of human von Willebrand factor that interact with fibrillar collagen types I and III. *Journal of Biological Chemistry,* 262**,** 13835-13841.

PASQUET, J.-M., GROSS, B., QUEK, L., ASAZUMA, N., ZHANG, W., SOMMERS, C. L., SCHWEIGHOFFER, E., TYBULEWICZ, V., JUDD, B. & LEE, J. R. 1999. LAT is required for tyrosine phosphorylation of phospholipase Cγ2 and platelet activation by the collagen receptor GPVI. *Molecular and cellular biology,* 19**,** 8326-8334.

PATEL-HETT, S., RICHARDSON, J. L., SCHULZE, H., DRABEK, K., ISAAC, N. A., HOFFMEISTER, K., SHIVDASANI, R. A., BULINSKI, J. C., GALJART, N. & HARTWIG, J. H. 2008. Visualization of microtubule growth in living platelets reveals a dynamic marginal band with multiple microtubules. *Blood,* 111**,** 4605-4616.

PATEL-HETT, S., WANG, H., BEGONJA, A. J., THON, J. N., ALDEN, E. C., WANDERSEE, N. J., AN, X., MOHANDAS, N., HARTWIG, J. H. & ITALIANO, J. E. 2011. The spectrin-based membrane skeleton stabilizes mouse megakaryocyte membrane systems and is essential for proplatelet and platelet formation. *Blood,* 118**,** 1641-1652.

PATEL, S. R., HARTWIG, J. H. & ITALIANO, J. E. 2005a. The biogenesis of platelets from megakaryocyte proplatelets. *The Journal of clinical investigation,* 115**,** 3348-3354.

PATEL, S. R., RICHARDSON, J. L., SCHULZE, H., KAHLE, E., GALJART, N., DRABEK, K., SHIVDASANI, R. A., HARTWIG, J. H. & ITALIANO, J. E., JR. 2005b. Differential roles of microtubule assembly and sliding in proplatelet formation by megakaryocytes. *Blood,* 106**,** 4076-85.

PEARCE, A. C., SENIS, Y. A., BILLADEAU, D. D., TURNER, M., WATSON, S. P. & VIGORITO, E. 2004. Vav1 and vav3 have critical but redundant roles in mediating platelet activation by collagen. *Journal of Biological Chemistry,* 279**,** 53955-53962.

PENNINGS, G. J., YONG, A. S., WONG, C., AL-TAMIMI, M., GARDINER, E. E., ANDREWS, R. K. & KRITHARIDES, L. 2014. Circulating levels of soluble EMMPRIN (CD147) correlate with levels of soluble glycoprotein VI in human plasma. *Platelets,* 25**,** 639-42.

PENZ, S., REININGER, A. J., BRANDL, R., GOYAL, P., RABIE, T., BERNLOCHNER, I., ROTHER, E., GOETZ, C., ENGELMANN, B., SMETHURST, P. A., OUWEHAND, W. H., FARNDALE, R., NIESWANDT, B. & SIESS, W. 2005. Human atheromatous plaques stimulate thrombus formation by activating platelet glycoprotein VI. *Faseb j,* 19**,** 898-909.

PETRICH, B. G., MARCHESE, P., RUGGERI, Z. M., SPIESS, S., WEICHERT, R. A., YE, F., TIEDT, R., SKODA, R. C., MONKLEY, S. J. & CRITCHLEY, D. R. 2007. Talin is required for integrin-mediated platelet function in hemostasis and thrombosis. *Journal of Experimental Medicine,* 204**,** 3103-3111.

PIKE, J. A., KHAN, A. O., PALLINI, C., THOMAS, S. G., MUND, M., RIES, J., POULTER, N. S. & STYLES, I. B. 2019. Topological data analysis quantifies biological nano-structure from single molecule localization microscopy. *Bioinformatics*.

PLATONOVA, E., WINTERFLOOD, C. M., JUNEMANN, A., ALBRECHT, D., FAIX, J. & EWERS, H. 2015. Single-molecule microscopy of molecules tagged with GFP or RFP derivatives in mammalian cells using nanobody binders. *Methods,* 88**,** 89-97.

PLEINER, T., BATES, M., TRAKHANOV, S., LEE, C.-T., SCHLIEP, J. E., CHUG, H., BÖHNING, M., STARK, H., URLAUB, H. & GÖRLICH, D. 2015. Nanobodies: site-specific labeling for super-resolution imaging, rapid epitope-mapping and native protein complex isolation. *Elife,* 4**,** e11349.

PLEINES, I., ELVERS, M., STREHL, A., POZGAJOVA, M., VARGA-SZABO, D., MAY, F., CHROSTEK-GRASHOFF, A., BRAKEBUSCH, C. & NIESWANDT, B. 2009. Rac1 is essential for phospholipase C-γ2 activation in platelets. *Pflügers Archiv-European Journal of Physiology,* 457**,** 1173-1185.

PODOLNIKOVA, N. P., YAKOVLEV, S., YAKUBENKO, V. P., WANG, X., GORKUN, O. V. & UGAROVA, T. P. 2014. The interaction of integrin αIIbβ3 with fibrin occurs through multiple binding sites in the αIIb β-propeller domain. *Journal of Biological Chemistry,* 289**,** 2371-2383.

POLGÁR, J., CLEMETSON, J. M., KEHREL, B. E., WIEDEMANN, M., MAGNENAT, E. M., WELLS, T. N. & CLEMETSON, K. J. 1997. Platelet activation and signal transduction by convulxin, a C-type lectin from Crotalus durissus terrificus (tropical rattlesnake) venom via the p62/GPVI collagen receptor. *Journal of Biological Chemistry,* 272**,** 13576-13583.

POLLITT, A. Y., GRYGIELSKA, B., LEBLOND, B., DÉSIRÉ, L., EBLE, J. A. & WATSON, S. P. 2010. Phosphorylation of CLEC-2 is dependent on lipid rafts, actin polymerization, secondary mediators, and Rac. *Blood,* 115**,** 2938-2946.

POLLITT, A. Y., POULTER, N. S., GITZ, E., NAVARRO-NUNEZ, L., WANG, Y. J., HUGHES, C. E., THOMAS, S. G., NIESWANDT, B., DOUGLAS, M. R., OWEN, D. M., JACKSON, D. G., DUSTIN, M. L. & WATSON, S. P. 2014. Syk and Src family kinases regulate C-type lectin receptor 2 (CLEC-2)-mediated clustering of podoplanin and platelet adhesion to lymphatic endothelial cells. *J Biol Chem,* 289**,** 35695-710.

POULTER, N., POLLITT, A. Y., OWEN, D., GARDINER, E., ANDREWS, R., SHIMIZU, H., ISHIKAWA, D., BIHAN, D., FARNDALE, R. W. & MOROI, M. 2017. Clustering of glycoprotein VI (GPVI) dimers upon adhesion to collagen as a mechanism to regulate GPVI signaling in platelets. *Journal of Thrombosis and Haemostasis,* 15**,** 549-564.

POULTER, N. S., KHAN, A. O., PALLINI, C. & THOMAS, S. G. 2018. Single-Molecule Localization and Structured Illumination Microscopy of Platelet Proteins. *Methods Mol Biol,* 1812**,** 33-54.

POULTER, N. S., PITKEATHLY, W. T., SMITH, P. J. & RAPPOPORT, J. Z. 2015a. The physical basis of total internal reflection fluorescence (TIRF) microscopy and its cellular applications. *Methods Mol Biol,* 1251**,** 1-23.

POULTER, N. S., POLLITT, A. Y., DAVIES, A., MALINOVA, D., NASH, G. B., HANNON, M. J., PIKRAMENOU, Z., RAPPOPORT, J. Z., HARTWIG, J. H., OWEN, D. M., THRASHER, A. J., WATSON, S. P. & THOMAS, S. G. 2015b. Platelet actin nodules are podosome-like structures dependent on Wiskott-Aldrich syndrome protein and ARP2/3 complex. *Nat Commun,* 6**,** 7254.

PROTTY, M. B., WATKINS, N. A., COLOMBO, D., THOMAS, S. G., HEATH, V. L., HERBERT, J. M., BICKNELL, R., SENIS, Y. A., ASHMAN, L. K. & BERDITCHEVSKI, F. 2009. Identification of Tspan9 as a novel platelet tetraspanin and the collagen receptor GPVI as a component of tetraspanin microdomains. *Biochemical Journal,* 417**,** 391-401.

PROX, J., WILLENBROCK, M., WEBER, S., LEHMANN, T., SCHMIDT-ARRAS, D., SCHWANBECK, R., SAFTIG, P. & SCHWAKE, M. 2012. Tetraspanin15 regulates cellular trafficking and activity of the ectodomain sheddase ADAM10. *Cell Mol Life Sci,* 69**,** 2919-32.

PUGH, N., MADDOX, B. D., BIHAN, D., TAYLOR, K. A., MAHAUT-SMITH, M. P. & FARNDALE, R. W. 2017. Differential integrin activity mediated by platelet collagen receptor engagement under flow conditions. *Thromb Haemost,* 117**,** 1588-1600.

QIU, Y., BROWN, A. C., MYERS, D. R., SAKURAI, Y., MANNINO, R. G., TRAN, R., AHN, B., HARDY, E. T., KEE, M. F. & KUMAR, S. 2014. Platelet mechanosensing of substrate stiffness during clot formation mediates adhesion, spreading, and activation. *Proceedings of the National Academy of Sciences,* 111**,** 14430-14435.

RAYES, J., JADOUI, S., LAX, S., GROS, A., WICHAIYO, S., OLLIVIER, V., DENIS, C. V., WARE, J., NIESWANDT, B. & JANDROT-PERRUS, M. 2018. The contribution of platelet glycoprotein receptors to inflammatory bleeding prevention is stimulus and organ dependent. *haematologica,* 103**,** e256-e258.

RAYES, J., WATSON, S. P. & NIESWANDT, B. 2019. Functional significance of the platelet immune receptors GPVI and CLEC-2. *The Journal of clinical investigation,* 129**,** 12-23.

REILLY, M. P., SINHA, U., ANDRE, P., TAYLOR, S. M., PAK, Y., DEGUZMAN, F. R., NANDA, N., PANDEY, A., STOLLA, M., BERGMEIER, W. & MCKENZIE, S. E. 2011. PRT-060318, a novel Syk inhibitor, prevents heparin-induced thrombocytopenia and thrombosis in a transgenic mouse model. *Blood,* 117**,** 2241-6.

REILLY, M. P., TAYLOR, S. M., HARTMAN, N. K., AREPALLY, G. M., SACHAIS, B. S., CINES, D. B., PONCZ, M. & MCKENZIE, S. E. 2001. Heparin-induced thrombocytopenia/thrombosis in a transgenic mouse model requires human platelet factor 4 and platelet activation through FcgammaRIIA. *Blood,* 98**,** 2442-7.

REININGER, A. J. 2008. Function of von Willebrand factor in haemostasis and thrombosis. *Haemophilia,* 14 Suppl 5**,** 11-26.

RENZ, M. 2013. Fluorescence microscopy—A historical and technical perspective. *Cytometry Part A,* 83**,** 767-779.

RIBA, R., HUGHES, C., GRAHAM, A., WATSON, S. & NASEEM, K. 2008. Globular adiponectin induces platelet activation through the collagen receptor GPVI-Fc receptor γ chain complex. *Journal of Thrombosis and Haemostasis,* 6**,** 1012-1020.

RIES, J., KAPLAN, C., PLATONOVA, E., EGHLIDI, H. & EWERS, H. 2012. A simple, versatile method for GFP-based super-resolution microscopy via nanobodies. *Nature methods,* 9**,** 582.

RIPLEY, B. 1977. Modelling spatial patterns (with discussion). JR Statist. Soc. B 39,172-212. Ripley17239J. R. *Statist. Soc B,* 1977.

ROSANO, G. L. & CECCARELLI, E. A. 2014. Recombinant protein expression in Escherichia coli: advances and challenges. *Frontiers in microbiology,* 5**,** 172.

ROSSY, J., OWEN, D. M., WILLIAMSON, D. J., YANG, Z. & GAUS, K. 2013. Conformational states of the kinase Lck regulate clustering in early T cell signaling. *Nature immunology,* 14**,** 82.

RUBIN-DELANCHY, P., BURN, G. L., GRIFFIE, J., WILLIAMSON, D. J., HEARD, N. A., COPE, A. P. & OWEN, D. M. 2015. Bayesian cluster identification in single-molecule localization microscopy data. *Nat Methods,* 12**,** 1072-6.

SAKURAI, Y., FITCH-TEWFIK, J. L., QIU, Y., AHN, B., MYERS, D. R., TRAN, R., FAY, M. E., DING, L., SPEARMAN, P. W. & MICHELSON, A. D. 2015. Platelet geometry sensing spatially regulates α-granule secretion to enable matrix self-deposition. *Blood,* 126**,** 531-538.

SARRATT, K. L., CHEN, H., ZUTTER, M. M., SANTORO, S. A., HAMMER, D. A. & KAHN, M. L. 2005. GPVI and alpha2beta1 play independent critical roles during platelet adhesion and aggregate formation to collagen under flow. *Blood,* 106**,** 1268-77.

SAVOIA, A., KUNISHIMA, S., DE ROCCO, D., ZIEGER, B., RAND, M. L., PUJOL-MOIX, N., CALISKAN, U., TOKGOZ, H., PECCI, A., NORIS, P., SRIVASTAVA, A., WARD, C., MOREL-KOPP, M. C., ALESSI, M. C., BELLUCCI, S., BEURRIER, P., DE MAISTRE, E., FAVIER, R., HEZARD, N., HURTAUD-ROUX, M. F., LATGER-CANNARD, V., LAVENU-BOMBLED, C., PROULLE, V., MEUNIER, S., NEGRIER, C., NURDEN, A., RANDRIANAIVO, H., FABRIS, F., PLATOKOUKI, H., ROSENBERG, N., HADJKACEM, B., HELLER, P. G., KARIMI, M., BALDUINI, C. L., PASTORE, A. & LANZA, F. 2014. Spectrum of the mutations in Bernard-Soulier syndrome. *Hum Mutat,* 35**,** 1033-45.

SCARSELLI, M., ANNIBALE, P. & RADENOVIC, A. 2012. Cell type-specific beta2-adrenergic receptor clusters identified using photoactivated localization microscopy are not lipid raft related, but depend on actin cytoskeleton integrity. *J Biol Chem,* 287**,** 16768-80.

SCHINDELIN, J., ARGANDA-CARRERAS, I., FRISE, E., KAYNIG, V., LONGAIR, M., PIETZSCH, T., PREIBISCH, S., RUEDEN, C., SAALFELD, S. & SCHMID, B. 2012. Fiji: an open-source platform for biological-image analysis. *Nature methods,* 9**,** 676.

SCHLESINGER, M. 2018. Role of platelets and platelet receptors in cancer metastasis. *Journal of hematology & oncology,* 11**,** 125.

SCHMAIER, A. A., ZOU, Z., KAZLAUSKAS, A., EMERT-SEDLAK, L., FONG, K. P., NEEVES, K. B., MALONEY, S. F., DIAMOND, S. L., KUNAPULI, S. P. & WARE, J. 2009. Molecular priming of Lyn by GPVI enables an immune receptor to adopt a hemostatic role. *Proceedings of the National Academy of Sciences,* 106**,** 21167-21172.

SCHMITT, A., GUICHARD, J., MASSE, J. M., DEBILI, N. & CRAMER, E. M. 2001. Of mice and men: comparison of the ultrastructure of megakaryocytes and platelets. *Exp Hematol,* 29**,** 1295-302.

SCHOONOOGHE, S., LAOUI, D., VAN GINDERACHTER, J. A., DEVOOGDT, N., LAHOUTTE, T., DE BAETSELIER, P. & RAES, G. 2012. Novel applications of nanobodies for in vivo bio-imaging of inflamed tissues in inflammatory diseases and cancer. *Immunobiology,* 217**,** 1266-1272.

SCHULTE, V., RABIE, T., PROSTREDNA, M., AKTAS, B., GRÜNER, S. & NIESWANDT, B. 2003. Targeting of the collagen-binding site on glycoprotein VI is not essential for in vivo depletion of the receptor. *Blood,* 101**,** 3948-3952.

SCHULTE, V., SNELL, D., BERGMEIER, W., ZIRNGIBL, H., WATSON, S. P. & NIESWANDT, B. 2001. Evidence for two distinct epitopes within collagen for activation of murine platelets. *J Biol Chem,* 276**,** 364-8.

SELVADURAI, M. V. & HAMILTON, J. R. 2018. Structure and function of the open canalicular system - the platelet's specialized internal membrane network. *Platelets,* 29**,** 319-325.

SENGUPTA, P., JOVANOVIC-TALISMAN, T., SKOKO, D., RENZ, M., VEATCH, S. L. & LIPPINCOTT-SCHWARTZ, J. 2011. Probing protein heterogeneity in the plasma membrane using PALM and pair correlation analysis. *Nature methods,* 8**,** 969.

SÉVERIN, S., NASH, C., MORI, J., ZHAO, Y., ABRAM, C., LOWELL, C., SENIS, Y. & WATSON, S. 2012. Distinct and overlapping functional roles of Src family kinases in mouse platelets. *Journal of Thrombosis and Haemostasis,* 10**,** 1631-1645.

SÉVERIN, S., POLLITT, A. Y., NAVARRO-NUÑEZ, L., NASH, C. A., MOURÃO-SÁ, D., EBLE, J. A., SENIS, Y. A. & WATSON, S. P. 2011. Syk-dependent phosphorylation of CLEC-2 a novel mechanism of hem-immunoreceptor tyrosine-based activation motif signaling. *Journal of Biological Chemistry,* 286**,** 4107-4116.

SIONTOROU, C. G. 2013. Nanobodies as novel agents for disease diagnosis and therapy. *International journal of nanomedicine,* 8**,** 4215.

SLATER, A., PERRELLA, G., ONSELAER, M.-B., MARTIN, E. M., GAUER, J. S., XU, R.-G., HEEMSKERK, J. W., ARIËNS, R. A. & WATSON, S. P. 2019. Does fibrin (ogen) bind to monomeric or dimeric GPVI, or not at all? *Platelets,* 30**,** 281-289.

SMETHURST, P. A., JOUTSI-KORHONEN, L., O'CONNOR, M. N., WILSON, E., JENNINGS, N. S., GARNER, S. F., ZHANG, Y., KNIGHT, C. G., DAFFORN, T. R. & BUCKLE, A. 2004. Identification of the primary collagen-binding surface on human glycoprotein VI by site-directed mutagenesis and by a blocking phage antibody. *Blood,* 103**,** 903-911.

SMETHURST, P. A., ONLEY, D. J., JARVIS, G. E., O'CONNOR, M. N., KNIGHT, C. G., HERR, A. B., OUWEHAND, W. H. & FARNDALE, R. W. 2007. Structural Basis for the Platelet-Collagen Interaction THE SMALLEST MOTIF WITHIN COLLAGEN THAT RECOGNIZES AND ACTIVATES PLATELET GLYCOPROTEIN VI CONTAINS TWO GLYCINE-PROLINE-HYDROXYPROLINE TRIPLETS. *Journal of Biological Chemistry,* 282**,** 1296-1304.

SOMMER, C., STRAEHLE, C., KOETHE, U. & HAMPRECHT, F. A. Ilastik: Interactive learning and segmentation toolkit. 2011 IEEE international symposium on biomedical imaging: From nano to macro, 2011. IEEE, 230-233.

SPALTON, J. C., MORI, J., POLLITT, A. Y., HUGHES, C. E., EBLE, J. A. & WATSON, S. P. 2009. The novel Syk inhibitor R406 reveals mechanistic differences in the initiation of GPVI and CLEC-2 signaling in platelets. *Journal of Thrombosis and Haemostasis,* 7**,** 1192-1199.

SPEICH, H. E., GRGUREVICH, S., KUETER, T. J., EARHART, A. D., SLACK, S. M. & JENNINGS, L. K. 2008. Platelets undergo phosphorylation of Syk at Y525/526 and Y352 in response to

pathophysiological shear stress. *American Journal of Physiology-Cell Physiology,* 295**,** C1045-C1054.

SPIESS, M., HERNANDEZ-VARAS, P., ODDONE, A., OLOFSSON, H., BLOM, H., WAITHE, D., LOCK, J. G., LAKADAMYALI, M. & STRÖMBLAD, S. 2018. Active and inactive β1 integrins segregate into distinct nanoclusters in focal adhesions. *J Cell Biol,* 217**,** 1929-1940.

STALKER, T. J., WELSH, J. D., TOMAIUOLO, M., WU, J., COLACE, T. V., DIAMOND, S. L. & BRASS, L. F. 2014. A systems approach to hemostasis: 3. Thrombus consolidation regulates intrathrombus solute transport and local thrombin activity. *Blood,* 124**,** 1824-31.

STIJLEMANS, B., CONRATH, K., CORTEZ-RETAMOZO, V., VAN XONG, H., WYNS, L., SENTER, P., REVETS, H., DE BAETSELIER, P., MUYLDERMANS, S. & MAGEZ, S. 2004. Efficient targeting of conserved cryptic epitopes of infectious agents by single domain antibodies. African trypanosomes as paradigm. *J Biol Chem,* 279**,** 1256-61.

SUGIYAMA, T., OKUMA, M., USHIKUBI, F., SENSAKI, S., KANAJI, K. & UCHINO, H. 1987. A novel platelet aggregating factor found in a patient with defective collagen-induced platelet aggregation and autoimmune thrombocytopenia. *Blood,* 69**,** 1712-1720.

SUZUKI-INOUE, K., FULLER, G. L., GARCIA, A., EBLE, J. A., POHLMANN, S., INOUE, O., GARTNER, T. K., HUGHAN, S. C., PEARCE, A. C., LAING, G. D., THEAKSTON, R. D., SCHWEIGHOFFER, E., ZITZMANN, N., MORITA, T., TYBULEWICZ, V. L., OZAKI, Y. & WATSON, S. P. 2006. A novel Syk-dependent mechanism of platelet activation by the C-type lectin receptor CLEC-2. *Blood,* 107**,** 542-9.

SUZUKI-INOUE, K., INOUE, O., DING, G., NISHIMURA, S., HOKAMURA, K., ETO, K., KASHIWAGI, H., TOMIYAMA, Y., YATOMI, Y. & UMEMURA, K. 2010. Essential in Vivo Roles of the C-type Lectin Receptor CLEC-2 embryonic/neonatal lethality of CLEC-2-deficient mice by blood/lymphatic misconnections and impaired thrombus formation of CLEC-2-deficient platelets. *Journal of Biological Chemistry,* 285**,** 24494-24507.

SUZUKI-INOUE, K., KATO, Y., INOUE, O., KANEKO, M. K., MISHIMA, K., YATOMI, Y., YAMAZAKI, Y., NARIMATSU, H. & OZAKI, Y. 2007. Involvement of the snake toxin receptor CLEC-2, in podoplanin-mediated platelet activation, by cancer cells. *J Biol Chem,* 282**,** 25993-6001.

SUZUKI-INOUE, K., TSUKIJI, N., SHIRAI, T., OSADA, M., INOUE, O. & OZAKI, Y. Platelet CLEC-2: Roles beyond hemostasis. Seminars in thrombosis and hemostasis, 2018. Thieme Medical Publishers, 126-134.

SUZUKI-INOUE, K., TULASNE, D., SHEN, Y., BORI-SANZ, T., INOUE, O., JUNG, S. M., MOROI, M., ANDREWS, R. K., BERNDT, M. C. & WATSON, S. P. 2002. Association of Fyn and Lyn with the proline-rich domain of glycoprotein VI regulates intracellular signaling. *Journal of Biological Chemistry,* 277**,** 21561-21566.

TAKAHASHI, H. & MOROI, M. 2001. Antibody against platelet membrane glycoprotein VI in a patient with systemic lupus erythematosus. *American journal of hematology,* 67**,** 262-267.

TAKAYAMA, H., HOSAKA, Y., NAKAYAMA, K., SHIRAKAWA, K., NAITOH, K., MATSUSUE, T., SHINOZAKI, M., HONDA, M., YATAGAI, Y., KAWAHARA, T., HIROSE, J., YOKOYAMA, T., KURIHARA, M. & FURUSAKO, S. 2008. A novel antiplatelet antibody therapy that induces cAMP-dependent endocytosis of the GPVI/Fc receptor gamma-chain complex. *J Clin Invest,* 118**,** 1785-95.

TALELLI, M., OLIVEIRA, S., RIJCKEN, C. J., PIETERS, E. H., ETRYCH, T., ULBRICH, K., VAN NOSTRUM, R. C., STORM, G., HENNINK, W. E. & LAMMERS, T. 2013. Intrinsically active nanobody-modified polymeric micelles for tumor-targeted combination therapy. *Biomaterials,* 34**,** 1255-1260.

TALELLI, M., RIJCKEN, C. J., OLIVEIRA, S., VAN DER MEEL, R., VAN BERGEN EN HENEGOUWEN, P. M., LAMMERS, T., VAN NOSTRUM, C. F., STORM, G. & HENNINK, W. E. 2011. Reprint of "Nanobody--shell functionalized thermosensitive core-crosslinked polymeric micelles for active drug targeting". *J Control Release,* 153**,** 93-102.

THACHIL, J. & WARKENTIN, T. E. 2017. How do we approach thrombocytopenia in critically ill patients? *Br J Haematol,* 177**,** 27-38.

THOMAS, D. H., GETZ, T. M., NEWMAN, T. N., DANGELMAIER, C. A., CARPINO, N., KUNAPULI, S. P., TSYGANKOV, A. Y. & DANIEL, J. L. 2010. A novel histidine tyrosine phosphatase, TULA-2, associates with Syk and negatively regulates GPVI signaling in platelets. *Blood,* 116**,** 2570-8.

THON, J. N., DYKSTRA, B. J. & BEAULIEU, L. M. 2017. Platelet bioreactor: accelerated evolution of design and manufacture. *Platelets,* 28**,** 472-477.

THON, J. N., MONTALVO, A., PATEL-HETT, S., DEVINE, M. T., RICHARDSON, J. L., EHRLICHER, A., LARSON, M. K., HOFFMEISTER, K., HARTWIG, J. H. & ITALIANO, J. E., JR. 2010. Cytoskeletal mechanics of proplatelet maturation and platelet release. *J Cell Biol,* 191**,** 861-74.

TOMLINSON, M., CALAMINUS, S., BERLANGA, O., AUGER, J., BORI-SANZ, T., MEYAARD, L. & WATSON, S. 2007. Collagen promotes sustained glycoprotein VI signaling in platelets and cell lines. *Journal of Thrombosis and Haemostasis,* 5**,** 2274-2283.

TOT PANNERDEN, H. V. N., DE HAAS, F., GEERTS, W., POSTHUMA, G., VAN DIJK, S. & HEIJNEN, H. F. 2010. The platelet interior revisited: Electron tomography reveals tubular α-granule subtypes. *Blood,* 116**,** 1147-1156.

TRAENKLE, B. & ROTHBAUER, U. 2017. Under the microscope: Single-domain antibodies for live-cell imaging and super-resolution microscopy. *Frontiers in immunology,* 8**,** 1030.

TSUJI, M., EZUMI, Y., ARAI, M. & TAKAYAMA, H. 1997. A novel association of Fc receptor γ-chain with glycoprotein VI and their co-expression as a collagen receptor in human platelets. *Journal of Biological Chemistry,* 272**,** 23528-23531.

UGORSKI, M., DZIEGIEL, P. & SUCHANSKI, J. 2016. Podoplanin - a small glycoprotein with many faces. *Am J Cancer Res,* 6**,** 370-86.

ULRICHTS, H., SILENCE, K., SCHOOLMEESTER, A., DE JAEGERE, P., ROSSENU, S., ROODT, J., PRIEM, S., LAUWEREYS, M., CASTEELS, P., VAN BOCKSTAELE, F., VERSCHUEREN, K., STANSSENS, P., BAUMEISTER, J. & HOLZ, J. B. 2011. Antithrombotic drug candidate ALX-0081 shows superior preclinical efficacy and safety compared with currently marketed antiplatelet drugs. *Blood,* 118**,** 757-65.

VAN DE LINDE, S., WOLTER, S., HEILEMANN, M. & SAUER, M. 2010. The effect of photoswitching kinetics and labeling densities on super-resolution fluorescence imaging. *J Biotechnol,* 149**,** 260-6.

VAN DER MEEL, R., OLIVEIRA, S., ALTINTAS, I., HASELBERG, R., VAN DER VEEKEN, J., ROOVERS, R. C., EN HENEGOUWEN, P. M. V. B., STORM, G., HENNINK, W. E. & SCHIFFELERS, R. M. 2012. Tumor-targeted Nanobullets: Anti-EGFR nanobody-liposomes loaded with anti-IGF-1R kinase inhibitor for cancer treatment. *Journal of controlled release,* 159**,** 281-289.

VAN DER MEEL, R., OLIVEIRA, S., ALTINTAS, I., HEUKERS, R., PIETERS, E. H., VAN BERGEN EN HENEGOUWEN, P. M., STORM, G., HENNINK, W. E., KOK, R. J. & SCHIFFELERS, R. M. 2013. Inhibition of tumor growth by targeted anti-EGFR/IGF-1R nanobullets depends on efficient blocking of cell survival pathways. *Molecular pharmaceutics,* 10**,** 3717-3727.

VINCKE, C., GUTIÉRREZ, C., WERNERY, U., DEVOOGDT, N., HASSANZADEH-GHASSABEH, G. & MUYLDERMANS, S. 2012. Generation of single domain antibody fragments derived from camelids and generation of manifold constructs. *Antibody Engineering.* Springer.

VIRANT, D., TRAENKLE, B., MAIER, J., KAISER, P. D., BODENHÖFER, M., SCHMEES, C., VOJNOVIC, I., PISAK-LUKÁTS, B., ENDESFELDER, U. & ROTHBAUER, U. 2018. A peptide tag-specific nanobody enables high-quality labeling for dSTORM imaging. *Nature communications,* 9**,** 930.

WALSH, T. G., METHAROM, P. & BERNDT, M. C. 2015. The functional role of platelets in the regulation of angiogenesis. *Platelets,* 26**,** 199-211.

WARNER, T. D., NYLANDER, S. & WHATLING, C. 2011. Anti-platelet therapy: cyclo-oxygenase inhibition and the use of aspirin with particular regard to dual anti-platelet therapy. *British journal of clinical pharmacology,* 72**,** 619-633.

WATSON, S., HERBERT, J. & POLLITT, A. Y. 2010. GPVI and CLEC-2 in hemostasis and vascular integrity. *Journal of Thrombosis and Haemostasis,* 8**,** 1456-1467.

WEIS, W. I., TAYLOR, M. E. & DRICKAMER, K. 1998. The C-type lectin superfamily in the immune system. *Immunological reviews,* 163**,** 19-34.

WEISS, E. J., HAMILTON, J. R., LEASE, K. E. & COUGHLIN, S. R. 2002. Protection against thrombosis in mice lacking PAR3. *Blood,* 100**,** 3240-4.

WESTMORELAND, D., SHAW, M., GRIMES, W., METCALF, D. J., BURDEN, J. J., GOMEZ, K., KNIGHT, A. E. & CUTLER, D. F. 2016. Super-resolution microscopy as a potential approach to diagnosis of platelet granule disorders. *J Thromb Haemost,* 14**,** 839-49.

WHITE, J. G. & RAO, G. 1998. Microtubule coils versus the surface membrane cytoskeleton in maintenance and restoration of platelet discoid shape. *The American journal of pathology,* 152**,** 597.

WICHAIYO, S., LAX, S., MONTAGUE, S. J., LI, Z., GRYGIELSKA, B., PIKE, J. A., HAINING, E. J., BRILL, A., WATSON, S. P. & RAYES, J. 2019. Platelet glycoprotein VI and C-type lectin-like receptor 2 deficiency accelerates wound healing by impairing vascular integrity in mice. *Haematologica*.

WIJEYEWICKREMA, L. C., GARDINER, E. E., MOROI, M., BERNDT, M. C. & ANDREWS, R. K. 2007. Snake venom metalloproteinases, crotarhagin and alborhagin, induce ectodomain shedding of the platelet collagen receptor, glycoprotein VI. *Thrombosis and haemostasis,* 98**,** 1285-1290.

WILLIAMSON, D. J., OWEN, D. M., ROSSY, J., MAGENAU, A., WEHRMANN, M., GOODING, J. J. & GAUS, K. 2011. Pre-existing clusters of the adaptor Lat do not participate in early T cell signaling events. *Nature immunology,* 12**,** 655.

WONEROW, P., OBERGFELL, A., WILDE, J. I., RÉGIS, B., ASAZUMA, N., BRDIČKA, T., ALBRECHT, L., SCHRAVEN, B., HOŘEJŠÍ, V. & SHATTIL, S. J. 2002. Differential role of glycolipid-enriched membrane domains in glycoprotein VI-and integrin-mediated phospholipase Cγ2 regulation in platelets. *Biochemical Journal,* 364**,** 755-765.

WOOLTHUIS, C. M. & PARK, C. Y. 2016. Hematopoietic stem/progenitor cell commitment to the megakaryocyte lineage. *Blood,* 127**,** 1242-8.

WOULFE, D. S. 2005. Platelet G protein-coupled receptors in hemostasis and thrombosis. *J Thromb Haemost,* 3**,** 2193-200.

XU, J., MA, H. & LIU, Y. 2017. Stochastic Optical Reconstruction Microscopy (STORM). *Curr Protoc Cytom,* 81**,** 12.46.1-12.46.27.

ZAHN, A., JENNINGS, N., OUWEHAND, W. H. & ALLAIN, J.-P. 2006. Hepatitis C virus interacts with human platelet glycoprotein VI. *Journal of general virology,* 87**,** 2243-2251.

ZHU, J., LUO, B. H., XIAO, T., ZHANG, C., NISHIDA, N. & SPRINGER, T. A. 2008. Structure of a complete integrin ectodomain in a physiologic resting state and activation and deactivation by applied forces. *Mol Cell,* 32**,** 849-61.

APPENDIX

Appendix I - Matlab code for the single-cell Ca^{2+} mobilisation analysis

(Christopher O'Shea, University of Birmingham, UK)

```
function [amp,dur,no_of_peaks,alll] = plat_analysis(x);

x=table2cell(x); %x is the datafile containing ROIs and
fluorescent signals
[tlen ylen]=size(x);
rcount=0;
for j=2:ylen
    y=x(:,j);
    if strcmp(class(y(Rayes et al.)),'double') == 1
        if y ~= 0
            rcount=rcount+1;
            for t=1:tlen
                vals(t,rcount)=y(Abbe);
            end
        end
    end
end

tim=x(:,1);
tim=cell2mat(tim);

se = strel('line', 30, 90); %Baseline correction settings
Threshold=20; %Amplitude of Peak thresholds
Prominence=20; %Minimum prominence of Peaks to remove
double peaks
tp=1;

for i = 1:size(vals,2) %Loop through all ROIs in the image
    sig=squeeze(vals(:,i))

%% Baseline Correction
    BL = imopen(sig, se);
    sig=sig-BL;
    sig=smooth(sig);
    ssig=zeros(numel(sig),1);

%% Find areas of amplitude greater than threshold
    for n=1:numel(sig)
        if sig(n) > Threshold
            ssig(n)=sig(n);
        end
```

```
    end

%% Find maximum fluorescent value of ROI
    amp(i,tp)=max(ssig);

%% Find other peaks in the signal
    [pks1
locs1]=findpeaks(ssig,'MinPeakHeight',Threshold,'MinPeakPr
ominence',Prominence);
    pks(1:numel(pks1),i,tp)=pks1; %Peak amplitudes
    locs(1:numel(locs1),i,tp)=locs1; %Peak times
    no_of_peaks(i,tp)=numel(pks1); %Total number of peaks


%% Count number of peaks where amplitude drops below
threshold
    gaps=find(ssig==0);
    gcount1=0;

    for c=2:numel(gaps);
        if gaps(c)-gaps(c-1)>1
            gcount1=gcount1+1; % if non consecutive
integers, there is a peak between the two timepoints
        end
    end

%% Check to account for peaks that happen at the start or
end of the recording
    if isempty(gaps) == 0
        check1=gaps(1)==1
        check2=gaps(end)==numel(ssig);
        if check1 == 1 && check2 == 1
            check=0;
        else
            check=1;
        end
    end

%% Save number of peaks, amplitude and duration
    gcount(i,tp)=gcount1+check;
    dur(i,tp)=[121-numel(gaps)]*(tim(4)-
tim(3))*(1/gcount(i,tp));
    if numel(gaps) > 120
        gcount(i,tp)=NaN;
        dur(i,tp)=NaN;
        no_of_peaks(i,tp)=NaN;
```

```
    end
end

amp(amp==0)=NaN
alll=[amp,dur,no_of_peaks] %%collect all parameters
```

Appendix II - Workflows of DBSCAN-based cluster analyses in KNIME

(Dr Jeremy Pike, University of Birmingham, UK)

Single-layer analysis

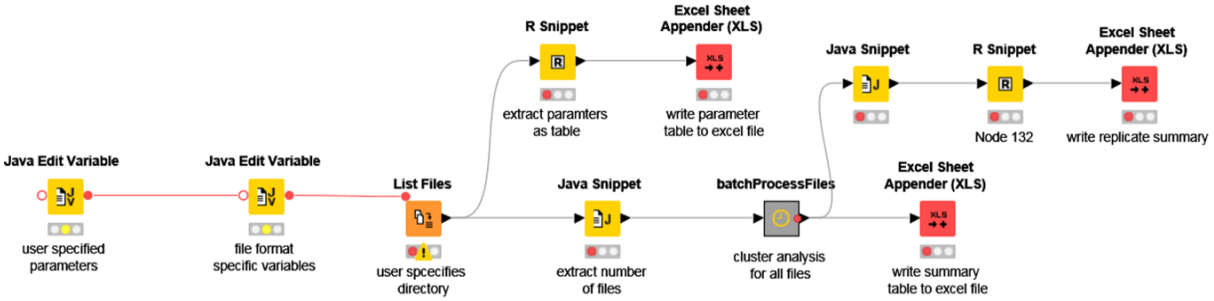

Two-layer analysis